Alkyl and Fluoroalkyl Manganese Pentacarbonyl Complexes as Models of OMRP Dormant Species

Roberto Morales Cerrada

THÈSE

En vue de l'obtention du

DOCTORAT DE L'UNIVERSITÉ DE TOULOUSE

Délivré par :

Institut National Polytechnique de Toulouse (Toulouse INP)

Discipline ou spécialité :

Chimie Organométallique et de Coordination

Présentée et soutenue par :

M. ROBERTO MORALES CERRADA

le jeudi 15 novembre 2018

Titre :

Complexes de manganèse pentacarbonyle alkyle et fluoroalkyle comme modèles d'espèces dormantes de l'OMRP

Ecole doctorale :

Sciences de la Matière (SDM)

Unité de recherche :

Laboratoire de Chimie de Coordination (L.C.C.)

Directeur(s) de Thèse :

MME FLORENCE GAYET

M. BRUNO AMEDURI

Rapporteurs :

M. GERARD JAOUEN, UNIVERSITE PARIS 6

Mme SOPHIE GUILLAUME, CNRS

Membre(s) du jury :

M. MATHIAS DESTARAC, UNIVERSITE TOULOUSE 3, Président

M. BRUNO AMEDURI, CNRS, Membre

M. HENRI CRAMAIL, INP BORDEAUX, Membre

Mme FLORENCE GAYET, INP TOULOUSE, Membre

A mi abuelo Antonio

Remerciements

Ce travail a été réalisé dans deux unités de recherche du CNRS : le laboratoire de Chimie de Coordination (LCC) à Toulouse, au sein de l'équipe LAC_2, et l'Institut Charles Gerhardt de Montpellier (ICGM), au sein de l'équipe IAM. Il a été codirigé par Dr. Florence Gayet et Dr. Bruno Améduri.

Je tiens tout d'abord à remercier Dr. Azzedine Bousseksou, directeur du LCC, et Dr. Patrick Lacroix-Desmazes, directeur de l'équipe IAM à l'ICGM, pour avoir accepté de m'accueillir au sein de ses laboratoires.

Je remercie tout particulièrement mes directeurs de thèse, Dr. Florence Gayet et Dr. Bruno Améduri, pour m'avoir encadré durant ces trois années de doctorat. Un immense merci à tous les deux pour tous leurs conseils, leur patience et leurs connaissances qui m'ont apporté et qui m'ont permis de mener à bien ce travail.

Je suis très honoré que Dr. Sophie Guillaume et Prof. Gérald Jaouen aient accepté d'être rapporteurs. Qu'ils trouvent ici l'expression de ma profonde reconnaissance et mes sincères remerciements.

J'exprime également ma gratitude au Prof. Mathias Destarac et au Prof. Henri Cramail, qui ont bien voulu être examinateurs.

Un très grand merci également au Prof. Rinaldo Poli pour toute son aide apportée pendant ces trois années de thèse et de son expertise en chimie qui m'a permis de résoudre un grand nombre de questions et problèmes auxquels j'ai dû faire face. Qu'il soit aussi remercié pour sa gentillesse, sa disponibilité permanente et pour les nombreux encouragements qu'il m'a prodigués.

Je remercie Dr. Vincent Ladmiral et Dr. Christophe Fliedel pour leur aide et leurs conseils, Dr. Antoine Debuigne et Dr. Christophe Detrembleur pour leurs conseils lors des réunions d'avancement du projet, ainsi que l'ensemble de personnes qui ont participé à ce travail. Merci au Dr. Jean-Claude Daran pour son expertise à déterminer la plupart des structures DRX de ce travail. Mme Dominique Granier et Dr. Arie Van der

Lee pour leur aide en DRX, ainsi que M. Cédric Totée, Prof. Gilles Silly et M. Francis Lacassin pour leur aide et grande expertise en spectroscopie RMN. Dr. Claire Negrell pour son aide en caractérisation des polymères par chromatographie d'exclusion stérique.

Je tiens à remercier l'ensemble du personnel du LCC et de l'ICGM, avec une mention spéciale à Sandrine Vincendeau pour toute son aide pour mettre en place un grand nombre d'expériences, ainsi que de m'avoir accueilli au laboratoire toujours avec un grand sourire, Dr. Eric Manoury pour son aide dans le domaine de la chimie organique et sa bonne humeur, Dr. Agnès Labande pour ses conseils et gentillesse et Dr. Abdellatif Manseri pour son support technique et son humour.

Je remercie également l'ensemble des personnes que j'ai côtoyé tout au long de la thèse, notamment Dr. Ekaterina Bellan, Maxime Colpaert, Dr. Gérald Lopez, Marc Guerre, Dr. Qizhi Yang, Mohammad Wehbi, Dr. Panagiotis Falireas, Erinque Folgado et Kazuki Komoda.

Je remercie l'Agence Nationale de la Recherche (ANR) pour avoir financé ces recherches dans le cadre du projet FLUPOL.

Je tiens également à remercier très chaleureusement toute ma famille qui m'a soutenu et motivé pendant ces trois ans.

Enfin, je tiens à remercier ma compagne María José pour sa patience et son soutien tout au long de ce travail.

“Once you stop learning, you start dying.”

Albert Einstein

Abbreviations list

acac	Acetylacetonate
Acetone-d_6	Deuterated acetone
AFCT	Addition-Fragmentation Chain Transfer
ATRP	Atom Transfer Radical Polymerization
b. p.	Boiling Point
BDE	Bond Dissociation Enthalpy
Benzene-d_6	Deuterated benzene
BrTFE	Bromotrifluoroethylene
CMRP	Cobalt-Mediated Radical Polymerization
CRP	Controlled Radical Polymerization
CSIRO	Commonwealth Scientific and Industrial Research Organization
CTA	Control Transfer Agent
CTFE	Chlorotrifluoroethylene
D.P.	Degree of Polymerization
DCM	Dichloromethane
DFAA	Difluoroacetic anhydride
DFT	Density Functional Theory
DMC	Dimethyl Carbonate
DMF-d_6	Deuterated dimethylformamide
DMSO-d_6	Deuterated dimethyl sulfoxide
DSC	Differential Scanning Calorimetry
Đ	Dispersity
FEVE	Fluoroethylenevinylether
FTIR	Fourier-Transform Infrared spectroscopy
HF	Hydrogen Fluoride
HOAO	Highest Occupied Atomic Orbital
ITP	Iodine Transfer Polymerization
k_a	Activation rate constant
k_d	Deactivation rate constant
L	Ligand

LUMO	Lowest Unoccupied Molecular Orbital
MADIX	Macromolecular Design by Interchange of Xanthates
MAF-TBE	*tert*-butyl-2-trifluoromethacrylate
MMA	Methyl Methacrylate
Mt	Metal
NaK	Sodium-potassium metallic liquid alloy
NMP	Nitroxide-Mediated Polymerization
NMR	Nuclear Magnetic Resonance
OMRP	Organometallic-Mediated Radical Polymerization
OMRP-DT	Organometallic-Mediated Radical Polymerization – Degenerative Transfer
OMRP-RT	Organometallic-Mediated Radical Polymerization – Reversible Termination
ORD	Optical Rotatory Dispersion
PMA	Poly(Methyl acrylate)
PMMA	Poly(Methyl Methacrylate)
ppm	Parts-Per-Million (10^{-6})
PPN^+	Bis(triphenylphosphine)iminium
PS	Poly(Styrene)
PTFE	Poly(Tetrafluoroethylene)
PVAc	Poly(Vinyl Acetate)
PVDF or PVF_2	Poly(Vinylidene Fluoride)
$PVDF_H$	PVDF-(CF_2CH_2)-
$PVDF_T$	PVDF-(CH_2CF_2)-
PVF	Poly(Vinyl Fluoride)
R	Alkyl chain
RAFT	Reversible Addition-Fragmentation chain Transfer
RDRP	Reversible-Deactivation Radical Polymerization
R_F	Fluoroalkyl chain
S	Styrene
SEC	Size exclusion chromatography
TFAA	Trifluoroacetic anhydride
TFE	Tetrafluoroethylene
TFP	3,3,3-Trifluoropropene
TGA	Thermogravimetric Analysis

THF	Tetrahydrofuran
TrFE	Trifluoroethylene
UV	Ultraviolet
VDF or VF_2	Vinylidene Fluoride
VF	Vinyl Fluoride

Complexes abbreviations

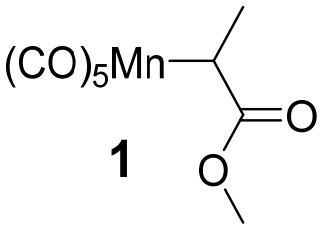

1

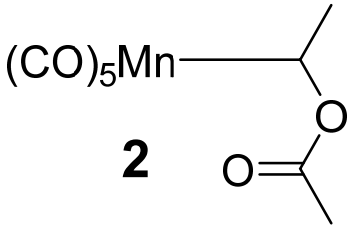

2

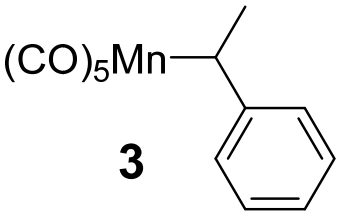

3

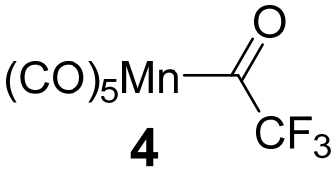

4

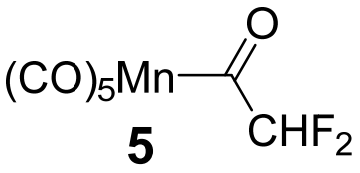

5

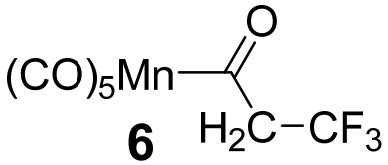

6

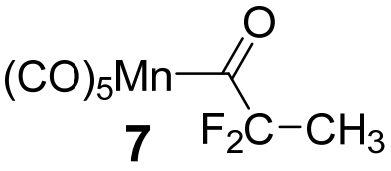

7

8

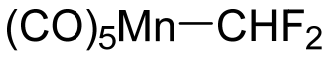

9

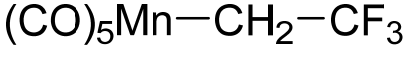

10

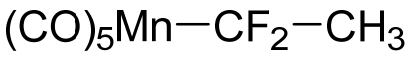

11

Table of contents

General introduction

General introduction

Controlled radical polymerization (CRP and also called reversible-deactivation radical polymerization or RDRP) makes possible to synthesize innovative architectures inaccessible by any other method. The first controlled radical polymerization, the iodine transfer polymerization (ITP), was described for the very first time by researchers at Daikin Company (Japan) in 1979,[1] but it was not until the mid-1990s that RDRP methods were exceptionally well-developed.

Macromolecular engineering concerns well-defined architectures such as block copolymers, grafted, star-shaped, hyperbranched or dendrimers. Among the various RDRP techniques, the most common are nitroxide mediated polymerization (NMP),[2-5] atom transfer radical polymerization (ATRP),[6-8] reversible addition-fragmentation chain-transfer polymerization (RAFT),[9-11] ITP,[12] organometallic mediated radical polymerization (OMRP)[13] or telluride-mediated polymerizartion (TERP).[14] ITP is the oldest RDRP method that has led to the first industrial developments (fluorinated thermoplastic elastomers).[15] It is applicable to fluorinated olefins such as tetrafluoroethylene (TFE), vinylidene fluoride (VDF) and TFE/VDF copolymers, VDF/HFP (HFP: hexafluoropropene), VDF/CTFE (CTFE: chlorotrifluoroethylene), etc.[11,16]

Fluoropolymers are macromolecules which possess remarkable properties (hydrophobicity, oleophobicity, thermostability, low refractive index, low dielectric constant, etc.)[17] finding applications in high-tech fields (thermostable, high performance elastomers, gaskets and O-rings for aerospace sealing, sheaths and cores of optical fibers, wires, paints, coatings, etc.).[17] These polymers are generally synthesized by radical (co)polymerization and industrially manufactured by large American companies (EI du Pont of Nemours and Company, Chemours, 3M, Dyneon, Gore, Honeywell, Halocarbon), Japanese (Daikin, Asahi Glass Chemical, Mitsue, Showa Denko, Kureha), Chinese (F & F, Juhua, Dongyue) and European (Arkema, Solvay Specific Polymers), etc.

Historically, the first fluoropolymer was discovered in 1934 by IG Farbenindustrie AG[18], then Plunkett[19] (at E. I. du Pont de Nemours and Co.) accidentally obtained PTFE but it was not until the late 1970s that it carried out the first work on the RDRP of fluorinated monomers.[1] Although many studies on the RDRP of styrenic and (meth)acrylic monomers are reported in the literature, the RDRP of fluorinated olefins remains a real scientific challenge.[20] Only ITP[16,21-23] and RAFT polymerization have proven effective, for instance RAFT homopolymerization of VDF[24-26] or copolymerization of VDF with 3,3,3-trifluoropropene,[27] with perfluoromethylvinylether[28] or with *tert*-butyl 2-trifluoromethylacrylate.[29]

Both techniques have led to block copolymers,[30] nevertheless they suffer a loss of control because the CF_2CH_2X (with X = I or SC(S)OEt) chain-ends are generated by the inverse (head-to-head) addition of the monomer, which are more difficult to reactivate under thermal conditions, leading to an accumulation of PVDF having such terminations.

However, these disadvantages could be overpassed by the presence of decacarbonyl dimanganese, $[Mn_2(CO)_{10}]$, under the effect of a visible irradiation.[31,32] This strategy of ITP allowed to improve the control of the polymerization of VDF obtaining long polymer chains and to synthesize block copolymers. More recently, the polymerization of VDF has been effectively controlled by cobalt complexes (CMRP) leading to original PVDF-b-PVAc block copolymers and PVDF-*b*-PVAc-*b*-PVDF triblocks. We therefore found it interesting to continue this study of the OMRP and to synthesize organometallic complexes based on manganese.

The aim of this thesis is therefore the study of the use of $[Mn(CO)_5R]$ organometallic complexes of the in the polymerization of fluorinated and nonfluorinated monomers. This thesis is composed of five parts: a first chapter will focus on a non-exhaustive state-of-the-art on fluorinated polymers and organometallic complexes based on manganese. The second and third chapters will describe the synthesis, structure and spectroscopic characterization of $[Mn(CO)_5R]$ complexes, with R = alkyl and fluoroalkyl chain respectively. In a third chapter, we will study theoretically and experimentally the dissociation enthalpy of the Mn-C bond for some of these complexes. A final part will concern the study of the radical polymerization initiated by the complexes synthesized

in this work. The polymers obtained will be characterized to check if there is any control on the polymerization, before ending with the general conclusion.

References

[1] M. Tatemoto In *First Regular Meeting of Soviet-Japanese Fluorine Chemists* Tokyo, 1979.
[2] C. J. Hawker; A. W. Bosman; E. Harth *Chem. Rev.* **2001**, *101*, 3661-3688.
[3] V. Sciannamea; R. Jérôme; C. Detrembleur *Chem. Rev.* **2008**, *108*, 1104-1126.
[4] D. Gigmes *Nitroxide Mediated Polymerization: From Fundamentals to Applications in Materials Science. [In: RSC Polym. Chem. Ser., 2016; 19]*; RSC, 2016.
[5] J. Nicolas; Y. Guillaneuf; C. Lefay; D. Bertin; D. Gigmes; B. Charleux *Prog. Polym. Sci.* **2013**, *38*, 63-235.
[6] K. Matyjaszewski; J. Xia *Chem. Rev.* **2001**, *101*, 2921-2990.
[7] W. A. Braunecker; K. Matyjaszewski *Prog. Polym. Sci.* **2007**, *32*, 93-146.
[8] M. Kamigaito; T. Ando; M. Sawamoto *Chem. Rev.* **2001**, *101*, 3689-3745.
[9] S. Perrier *Macromolecules* **2017**, *50*, 7433-7447.
[10] C. Barner-Kowollik *Handbook of RAFT Polymerization*; Wiley-VCH Verlag GmbH & Co. KGaA, 2008.
[11] M. R. Hill; R. N. Carmean; B. S. Sumerlin *Macromolecules* **2015**, *48*, 5459-5469.
[12] G. David; C. Boyer; J. Tonnar; B. Ameduri; P. Lacroix-Desmazes; B. Boutevin *Chem. Rev.* **2006**, *106*, 3936-3962.
[13] A. Debuigne; R. Poli; C. Jerome; R. Jerome; C. Detrembleur *Prog. Polym. Sci.* **2009**, *34*, 211-239.
[14] S. Yamago *Chem. Rev.* **2009**, *109*, 5051-5068.
[15] M. Tatemoto (Daikin Industries). Fluorine-containing elastomer composition. EP 0399543 A2, 1990.
[16] M. Oka; M. Tatemoto In *Contemporary Topics in Polymer Science: Volume 4*; Bailey, W. J., Tsuruta, T., Eds.; Springer: Boston, 1984, p 763-777.
[17] B. Ameduri; H. Sawada *Fluorinated polymers*; Royal Society of Chemistry, 2017; Vol. 1&2.
[18] IG Farbenindustrie AG. GB 465520, 1937.
[19] R. J. Plunkett (Kinetic Chemicals, Inc.). Tetrafluoroethylene polymers. US 2230654, 1941.
[20] B. Ameduri *Macromolecules* **2010**, *43*, 10163-10184.
[21] C. Boyer; D. Valade; L. Sauguet; B. Ameduri; B. Boutevin *Macromolecules* **2005**, *38*, 10353-10362.
[22] C. Boyer; D. Valade; P. Lacroix-Desmazes; B. Ameduri; B. Boutevin *J. Polym. Sci., Part A: Polym. Chem.* **2006**, *44*, 5763-5777.
[23] C. Boyer; B. Ameduri; M. H. Hung *Macromolecules* **2010**, *43*, 3652-3663.
[24] M. Guerre; B. Campagne; O. Gimello; K. Parra; B. Ameduri; V. Ladmiral *Macromolecules* **2015**, *48*, 7810-7822.
[25] M. Guerre; S. M. W. Rahaman; B. Ameduri; R. Poli; V. Ladmiral *Macromolecules* **2016**, *49*, 5386-5396.
[26] M. Guerre; M. Semsarilar; F. Godiard; B. Ameduri; V. Ladmiral *Polym. Chem.* **2017**, *8*, 1477-1487.

[27] G. Kostov; F. Boschet; J. Buller; L. Badache; S. Brandsadter; B. Ameduri *Macromolecules* **2011**, *44*, 1841-1855.
[28] E. Girard; J.-D. Marty; B. Ameduri; M. Destarac *ACS Macro Letters* **2012**, *1*, 270-274.
[29] Y. Patil; B. Ameduri *Polym. Chem.* **2013**, *4*, 2783-2799.
[30] M. Guerre; J. Schmidt; Y. Talmon; B. Ameduri; V. Ladmiral *Polym. Chem.* **2017**, *8*, 1125-1128.
[31] A. D. Asandei; O. I. Adebolu; C. P. Simpson *J. Am. Chem. Soc.* **2012**, *134*, 6080-6083.
[32] A. D. Asandei *Chem. Rev.* **2016**, *116*, 2244-2274.

Chapter 1

State-of-the-art

Outline:

1. State-of-the-art

1.1. Fluorinated polymers

1.1.1. Introduction

Fluorine and fluorinated compounds are very present in our daily lives. Fluorine is unique because it is possible to substitute hydrogen by fluorine in organic compounds without a great distortion of the geometry of the system but, surprisingly, compounds containing carbon-fluorine bonds are rare in nature.[1,2] However, many synthetic products contain fluorine such as fluoridated water, fluorinated drugs (e.g. Ciprofloxacin®, Prozac®), anesthetics, agrochemical products, refrigerants, fluoride toothpaste, as well as fluoride additives in lithium batteries.[3-6] Even though the use of fluorine in organic and inorganic chemistry dates from the 17th century,[7] the great development of fluorine chemistry has occurred in the early-to-mid 20th century (e.g. synthesis of trifluoroacetic acid in 1920 by Swartz, isolation of carbon tetrafluoride by Lebeau and Damien in 1926).[8,9]

Fluorine chemistry has an important impact in materials chemistry, especially with the fluorinated polymers and copolymers.[5,10-14] They are niche and specialty polymers with a high production cost and a low production scale (around 4.5% of the World polymer production) contrary to commodity polymers, which are unexpensive and synthesized on a large scale. These materials have attracted wide attention in both industry and academia due to the low polarizability and the very strong electronegativity of fluorine. This induces a short (1.32 Å) and strong (485 kJ·mol^{-1}) C-F bond. The morphologies of fluoropolymers can be either thermoplastic, elastomeric,[15] plastomeric, or even thermoplastic elastomeric, and they can be either semicrystalline or totally amorphous. All these specific characteristics confer outstanding properties to the fluorinated polymers,[16] such as high thermal, chemical, aging and weather

resistance, excellent inertness to solvents, to hydrocarbons, to acids, and to alkalis, low surface energy (oil and water repellency), low dielectric constants, low flammability, low refractive index, and low moisture absorption. Moreover, the presence of the strong C-F bond has a decisive impact on the high resistance to oxidation and other kinds of degradation.

The aforementioned extraordinary properties make fluoropolymers advantageous materials, involved in many products such as paints and coatings (Figure 1), optical fibers, fuel cell membranes, gaskets and O-rings for use in extreme temperatures, textile and microelectronics among others. They are also used in many industrial sectors such as petrochemical, automotive, aeronautics, aerospace, building treatments, etc. However, fluoropolymers have several drawbacks such as their low solubility in the most common organic solvents due to their high crystallinity. Nevertheless, this property can be an advantage in terms of chemical resistance. In addition, fluorinated copolymers[12,13,17] possess a higher solubility in organic solvents, because the presence of a comomoner (bearing side groups) creates a certain disorder in the structure that reduces the degree of crystallinity.

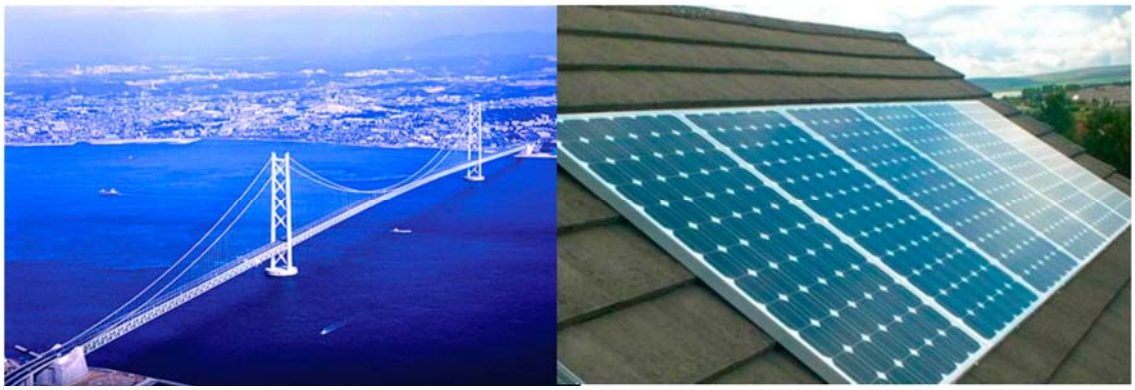

Figure 1. Left picture: fluoroethylenevinylether (FEVE)-based paints are used to coat exposed constructions such as the Akashi-Kaikyo Bridge in Japan, one of the world's longest suspension bridges.[18] Right picture: solar panels are coated with fluoropolymers such as polyvinylfluoride (PVF) to impart photoresistance and weather durability.[18]

1.1.2. Vinylidene fluoride and poly(vinylidene fluoride)

1,1-Difluoroethylene, also called vinylidene fluoride (VDF or VF_2), is a hydrofluoroolefin with the chemical formula $F_2C=CH_2$. The CF_2 extremity is usually named the "head" and the CH_2 the "tail". It is a colorless, flammable, and nearly odorless gas that boils at -82 °C and it melts at -144 °C. VDF exhibits several advantages: it is a non-toxic fluorinated gas in contrast to chlorotrifluoroethylene (CTFE) and bromotrifluoroethylene (BrTFE), non-explosive contrarily to tetrafluoroethylene (TFE) or trifluoroethylene (TrFE), and can easily homopolymerize and copolymerize by radical initiation.[17,19]

VDF can be prepared by various methods. The principal industrial process consists of the chlorination of 1,1-difluoroethane to lead to 1-chloro-1,1-difluoroethane, followed by a dehydrochlorination at about 700-900 °C.[17]

The resulting polymer, the poly(vinylidene fluoride), also called PVDF or PVF_2, is a specialty thermoplastic belonging to the fluoropolymer family. After polytetrafluoroethylene (PTFE), it is the second most produced and consumed fluoropolymer in the world market (Figure 2).

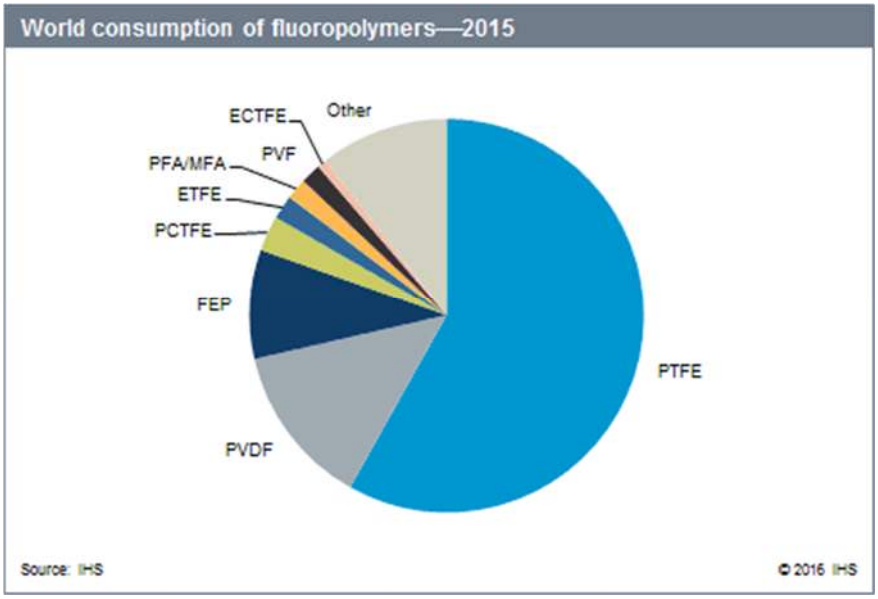

Figure 2. World consumption of fluoropolymers. Source: IHS Markit Ltd.[20]

PVDF is a thermoplastic and non-reactive fluoropolymer (except against strong bases, producing HF). It is primarily involved in applications that require high resistance to solvents, acids and heat. It is also employed as an important component in high-end paints for metal roofing in commercial and residential applications, as well as for separators and binders in lithium-ion batteries.[21] Membranes of PVDF are extensively consumed for the purpose of immobilizing proteins, as well as for water purification[22] and ferro- and piezoelectrical devices.[23] PVDF is also used widely in sheets, films, membranes and coatings in various end-user industries such as chemical processing, oil and gas, construction and energy.[21] The high demand from different industries such as coatings, photovoltaic films, oil and gas, and electrical appliances are expected to grow the PVDF market.[24,25] Arkema, Daikin Industries Ltd., Dyneon GmbH, Shanghai Ofluorine Chemical Technology Co. Ltd., Shanghai 3F New Materials Co. Ltd., Solvay S.A., Zhuzhou Hongda Polymer Materials Co. Ltd., Zhejiang Fotech International Co. Ltd., Kureha Corporation and Quadrant Engineering Plastics Products Inc. are some of the main manufacturers of PVDF dominating the market.

1.1.3. Polymerization of fluoromonomers

1.1.3.1. Conventional radical polymerization

Conventional radical polymerization is the oldest method to synthesize polymers and this technique is well suited to fluoroolefins. The process takes place in three main steps. The first one is the initiation where a radical is generated from a stable molecule called initiator (which can be activated by a stimulus such as thermal, UV or visible irradiation, ionization, electrolysis, etc.). Then, during the propagation, the radical reacts with a monomer generating a C-C bond and transferring to it the radical function, which then reacts again with another monomer and so on. Finally, the last step is the termination by recombination (with another macroradical or with an initiator radical) or by the reaction of the active radical chain with an inhibitor such as oxygen or any molecule that reacts with a radical. Another possibility to deactivate the growing chain

is the hydrogen transfer from the solvent or other molecule able to transfer a proton, killing the active chain (Scheme 1).

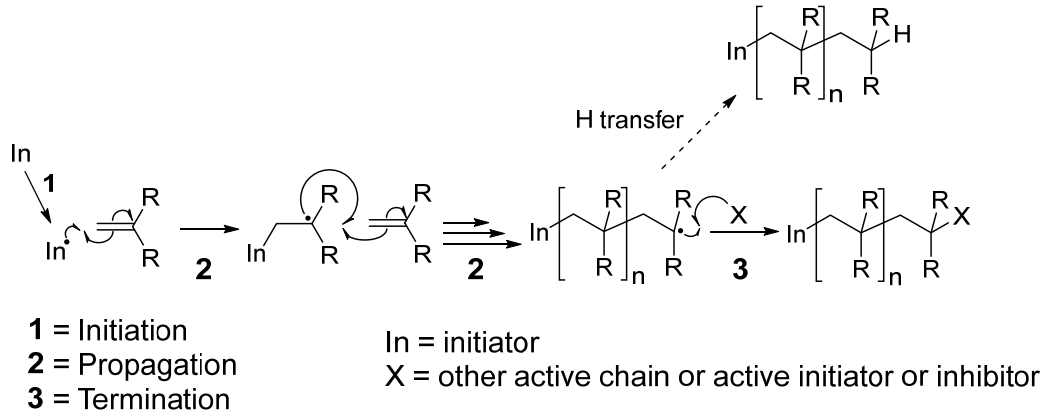

Scheme 1. Example of the general mechanism of the free radical polymerization.

Conventional radical polymerization is the most employed method to obtain fluorinated polymers (95% of the World production).[16] Most of fluoropolymers are synthesized by this method,[10,12,13,26] notwithstanding a few fluorinated monomers are polymerized by anionic (hexafluoropropylene oxide) or cationic (oxetanes, oxazoline or vinyl ethers; $H_2C=CHOR_F$) mechanisms. In fact, certain fluorinated monomers such as hexafluoropropylene or perfluoroalkyl vinyl ethers cannot homopolymerize by conventional radical polymerization.

1.1.3.2. Cationic polymerization

Cationic polymerization is a polymerization in which a cationic initiator adds to a monomer which is then transformed into a reactive carbocation and then reacts with other monomers to form the polymer.[27] This polymerization is limited to monomers such as olefins with electron-donating substituents and heterocycles.

The first step is the initiation, where a carbenium ion is generated with a non-nucleophilic (or weakly nucleophilic) counterion to avoid the recombination. This carbenium ion can be generated by a strong acid (Lewis or Brønsted), by a stable

carbenium ion salts or by an ionizing radiation.[28] Then, the propagation consists in the addition of the monomer to the carbenium ion, linking the monomer to the chain *via* a carbon-carbon bond and regenerating the carbenium ion at the end of the chain. Finally, termination occurs when the counterion reacts with the carbenium ion *via* a unimolecular rearrangement or when other nucleophilic reagents irreversibly add to quench the cationic reaction center (Scheme 2).

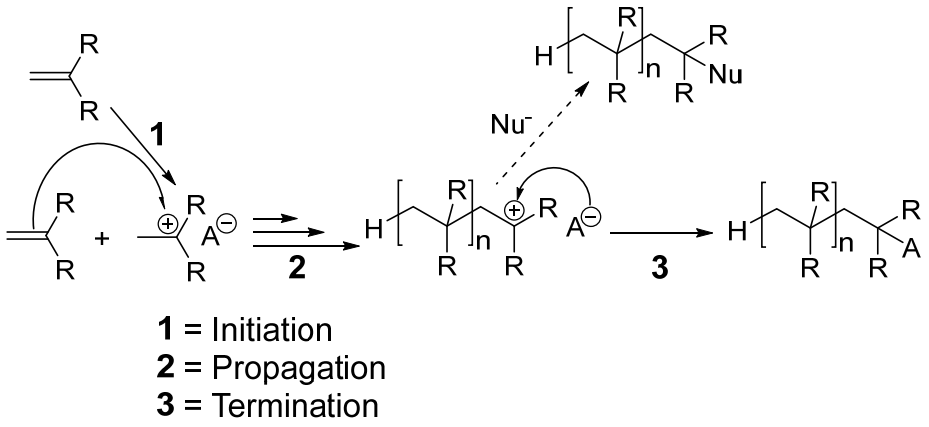

Scheme 2. Example of the general mechanism of cationic polymerization.

Moreover, cationic polymerization can be a living polymerization to control the growth and obtain well-defined polymers.[29] For this, the termination step should be reduced or eliminated, stopping the reaction when all the monomer is consumed.

Only a few fluorinated monomers can polymerize by this way. For instance, the fluorinated monomers that have been used in cationic polymerization are fluorinated oxetanes,[30-32] oxazolines,[33-35] and vinyl ethers bearing a fluorinated group (Scheme 3).[36-39]

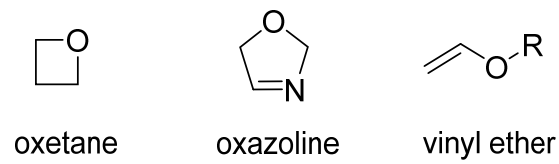

Scheme 3. Chemical structure of oxetane, oxazoline and vinyl ether.

1.1.3.3. Anionic polymerization

The anionic polymerization[40] of vinyl monomers involves a carbanionic species. To stabilize the negative charge of the carbanion, the vinyl monomer should bear a high electronegative group or stabilize the charge by mesomeric effects. For instance, monomers like styrene, diene, methacrylate and vinyl pyridine among others can react by this way.

The initiation occurs by the generation of a carbanion in the monomer. This can be produced by an electron transfer from an alkali metal or by strong anions such as alkyllithium compounds. Propagation in anionic radical polymerization is a very fast process and occurs until total consumption of the monomer, even at low temperatures. Then, termination only takes place by quenching due to impurity traces or by intentional addition of quenching agents such as water, alcohols, oxygen or carbon dioxide (Scheme 4).

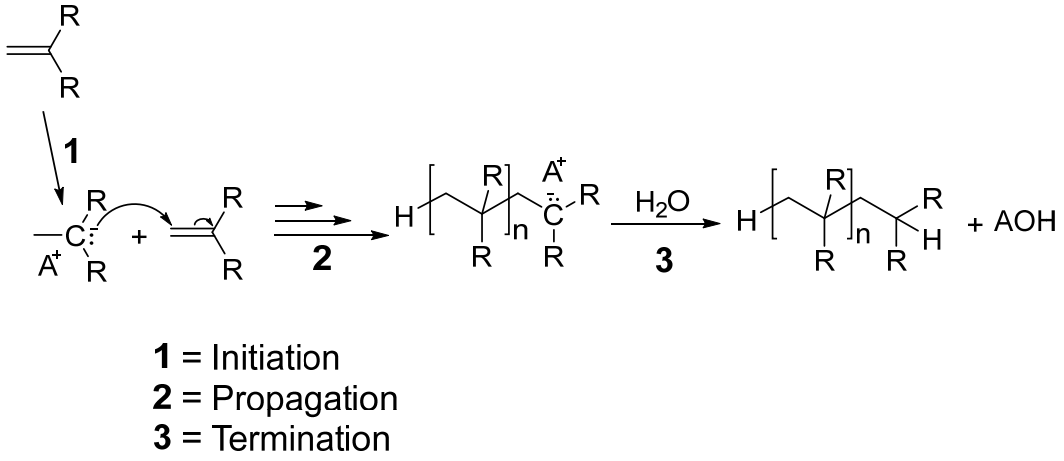

Scheme 4. Example of the general mechanism of anionic polymerization.

In the absence of impurities, the carbanion would still be active and capable of adding another monomer, giving place to a living radical polymerization. The chains will remain active indefinitely unless there is a termination or a chain transfer. Like the cationic polymerization, only a few fluorinated monomers can react by anionic polymerization such as α-trifluoromethacrylic acid.[41,42]

1.1.4. Coordination-insertion polymerization of fluoromonomers

Coordination-insertion polymerization (or coordination polymerization) is a kind of polymerization catalyzed by complexes or transitions metal salts. Ziegler[43,44] and Natta[45,46] were pioneered in the mid-1950s in this technique with the use of heterogeneous catalyst based on an organoaluminium and titanium or vanadium tetrachloride to polymerize ethylene and propylene. These studies led them to win the Nobel Prize in Chemistry in 1963.[47] Other homogeneous catalysts were developed at the end of 1950s by Breslow *et al.*,[48] based on titanium metallocenes and aluminum complexes, however the polymerization mechanism was not well-known at this time. At the beginning of 1970s, Meyer *et al.*[49] carried out kinetic studies on alkylaluminum activated metallocene catalysts, revealing that polymer growth alternated between dormant and active states.

In the last 40 years, there has been a great development in the use of homogeneous catalysts for polymerization *via* insertion-coordination, especially to make polyethylene and polypropylene. Additionally, this polymerization method allow synthesizing copolymers with polar and non-polar functions such as polar vinyl monomers and non-polar olefins.[50]

Concerning the fluoromonomers, some recent studies about the copolymerization of ethylene and vinyl fluoride (VF) have been reported by Jordan *et al.*[51] using palladium phospine-sulfonate complexes. The obtained copolymers have molar masses of 4500-14500 $g \cdot mol^{-1}$ and a high content in ethylene and thus low content in VF (< 0.5 mol %). This was produced by the weak ability of VF to coordinate to the palladium(II) catalyst compare to ethylene. More recent studies of this research group reported with a similar system the way to increase the proportion of VF in the polymer,[52] and the introduction of fluorine atoms in this copolymer by a β-F elimination.[53]

1.1.5. Controlled radical polymerization of fluoromonomers

The history of controlled radical copolymerization (CRP) or reversible-deactivation radical polymerization (RDRP) started in the late 1970s when Tatemoto pioneered the concept on the iodine transfer (co)polymerization (ITP) of fluoroalkenes, especially on vinylidene fluoride.[54]

Since then, and especially in the 1990s, RDRP methods have undergone an extraordinary development by the improvement of the known methods or the discovery of new ones.[55] All these methods are based on the formation of a dormant species (or capped chains), which cannot react with another monomer, in a fast equilibrium with active chains (Scheme 5). This reaction should be fast, reversible and with a large majority of dormant species. The dormant chains may be alkyl halides (typically chlorides or bromides for atom transfer radical polymerization or ATRP[56,57] or iodide for ITP),[58] thioesters (reversible addition-fragmentation chain transfer polymerization or RAFT polymerization),[59-61] alkoxyamines (nitroxide-mediated polymerization or NMP),[62,63] or an organometallic species (organometallic-mediated radical polymerization or OMRP).[64,65] Free radicals may be generated by the spontaneous thermal process (NMP), *via* a catalyzed reaction (ATRP) or reversibly *via* the degenerative exchange process with dormant species (RAFT and ITP).

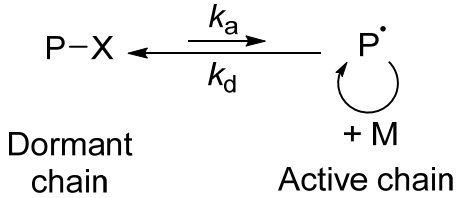

Scheme 5. Equilibrium between the active chain and the dormant chain in RDRP.

1.1.5.1. ITP

As mentioned above, ITP was the first RDRP technique used in the late 1970s by Tatemoto[54,66,67] to control the (co)polymerization of fluoroolefins, even before the findings of CRP or RDRP in the mid-1990s. Various fluorinated monomers such as VDF and TFE have been successfully used in ITP within Daikin Industries. From that advance, this company has been producing by ITP many fluorinated thermoplastic elastomers (based on thermoplastic-*b*-elastomers-*b*-thermoplastic block copolymers) for more than 20 years.[13,67,68] Other companies such as Ausimont S.p.A.[69] and E.I. du Pont de Nemours and Co[70] have been inspired from this RDRP method to produce other fluorinated block copolymers.

The general mechanism of ITP consists of six main steps as shown in Scheme 6. The first one deals with initiation (**1**) where the initiator is activated. The second step is the propagation (**2**) where the activated initiator reacts with a monomer which can propagate. Then, the control transfer agent (CTA) transfers an iodine atom onto the growing chain (**3**), generating a dormant chain and a new radical which is able to react with a monomer (**4**). Then, iodine is exchanged between the different polymer chains by an iodine degenerative transfer (IDT, step **5**). Finally, the termination (**6**) occurs when two active chains react together or by a hydrogen transfer.

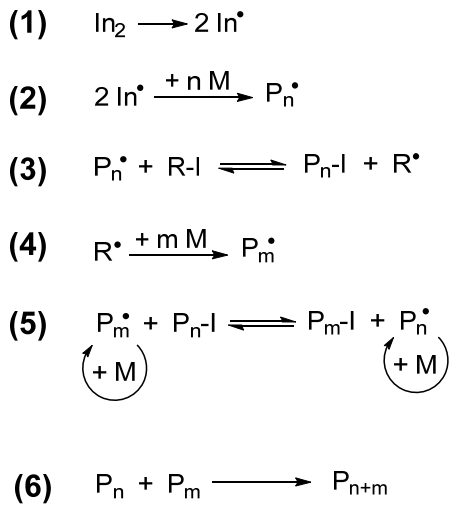

Scheme 6. General mechanism of Iodine Transfer Polymerization (ITP).

Nevertheless, the evidence of the controlled radical polymerization behavior was reported in 2005 by Boyer *et al.*,[71] through the polymerization of VDF with $C_6F_{13}I$. Conversely, the same polymerization using $HC_2F_4CH_2I$ gave much worse results and led to telomerization (a radical polymerization where a chain-transfer reaction restricts the size of the obtained oligomer, usually called telomer, see Scheme 7). A more in-depth mechanistic approach was reported in a later work,[72] concluding that the presence of $-CF_2-CH_2-I$ end-group is the primary cause of the poor results in the case of $HC_2F_4CH_2I$. These chains cannot be reactivated and their accumulation led to high dispersities.

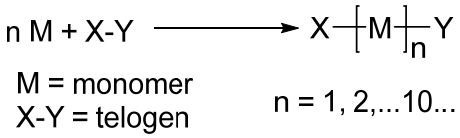

Scheme 7. General scheme of telomerization process.

Nonetheless, this problem can be solved by the reactivation of the reverse dormant chains with the $[(CO)_5Mn^\bullet]$ radical generated from the dimanganese decacarbonyl under visible light irradiation at 40 °C.[73,74] Dimanganese decacarbonyl is known to generate $[(CO)_5Mn^\bullet]$ under both thermal and photochemical conditions, but the free $[(CO)_5Mn^\bullet]$ radicals are not capable to add onto VDF to initiate the polymerization. These results confirm previous studies by Bamford *et al.*[75] and by Asandei *et al.*,[73] where $[(CO)_5Mn^\bullet]$ photoproduced from $[Mn_2(CO)_{10}]$ was shown unable to initiate the radical polymerization of VDF (although it can initiate those of C_2F_4 and C_2F_3Cl). However, $[(CO)_5Mn^\bullet]$ can abstract an iodine atom from the dormant chain-ends, including from the more recalcitrant $PVDF_T$-I (PVDF-CH_2-CF_2-I), to form $[Mn(CO)_5I]$ irreversibly and to regenerate the reactive radical chain. Recently, a similar procedure was employed by Golzari *et al.*[76] activating the dimanganese decacarbonyl by UV irradiation, and finally obtaining VDF/methyl methacrylate (MMA) or VDF/styrene (S) block copolymers. However the possible direct radical chain trapping to yield PVDF-$Mn(CO)_5$ was not reported, which would correspond to the dormant species of a putative OMRP process.

Despite the possibility to reactivate the $PVDF_T$-I dormant chain by the manganese pentacarbonyl radical, the polymerization is not so well-controlled because the iodine

atom is removed irreversibly, decreasing the amount of controlling agent in the system. Other polymerization methods may be the solution to produce a well-defined PVDF.

1.1.5.2. RAFT/MADIX

The first radical addition-fragmentation processes were reported in the early 1970s.[77] Nevertheless, the process initially involved non-degenerate and therefore irreversible radical exchanges, so the transfer reagents could not be used to control radical polymerization at that time. RAFT polymerization was discovered in 1986 by researchers at the Commonwealth Scientific and Industrial Research Organization (CSIRO). They reported the use of poly(methyl methacrylate) (PMMA) macromonomers as chain transfer agents in radical polymerization and described how a propagating radical would add onto a PMMA macromonomer by a chain-transfer reaction.[78,79] This mechanism was initially called addition-fragmentation chain transfer (AFCT). Several other AFCT agents[78,80,81] were later synthesized, however the polymers obtained by this method showed high dispersities, until the use of thiocarbonyl-thio groups by the CSIRO scientists to obtain narrow dispersities for a variety of monomers (Đ = 1.05 to 1.40),[82] concluding that thiocarbonyl-thio groups are the most efficient chain transfer agents. This system was then renamed “reversible addition-fragmentation chain transfer” (RAFT).

RAFT and MADIX (macromolecular design by interchange of xanthates) follow the same mechanism and differ only by the polymerization mediator used. This mechanism is based on six main steps as shown in Scheme 8. The first one consists in the activation of the initiator during the initiation (**1**). The second step is the propagation (**2**), where a free-radical source reacts with a single monomer to yield a propagating polymeric radical $P_n^{\bullet}$. Then, the propagating radical adds to the thiocarbonyl-thio compound to form the radical intermediate, which subsequently fragments to give another thiocarbonyl-thio group and a new radical $R^{\bullet}$. This equilibrium is usually called the RAFT pre-equilibrium (**3**). The next step is the re-initiation (**4**) and consists in the reaction of the radical $R^{\bullet}$ with a new monomer to form a new propagating radical $P_m^{\bullet}$. Then, after

consumption of the initially added CTA (completion of step **3**), the main RAFT equilibrium (**5**) is established by degenerative chain transfer between propagating and dormant chains. Finally, termination (**6**) may occur by the reaction of two active chains or by other reactions with the active chain (proton transfer, etc.). A key parameter is the right choice of the Z and R group of the CTA. The Z group primarily affects the stability of the S=C bond and the stability of the adduct radical, while the R group must be able to stabilize the radical ($R^{\bullet}$) of step **3**, but it must be unstable enough to initiate the growth of a new polymer chain.

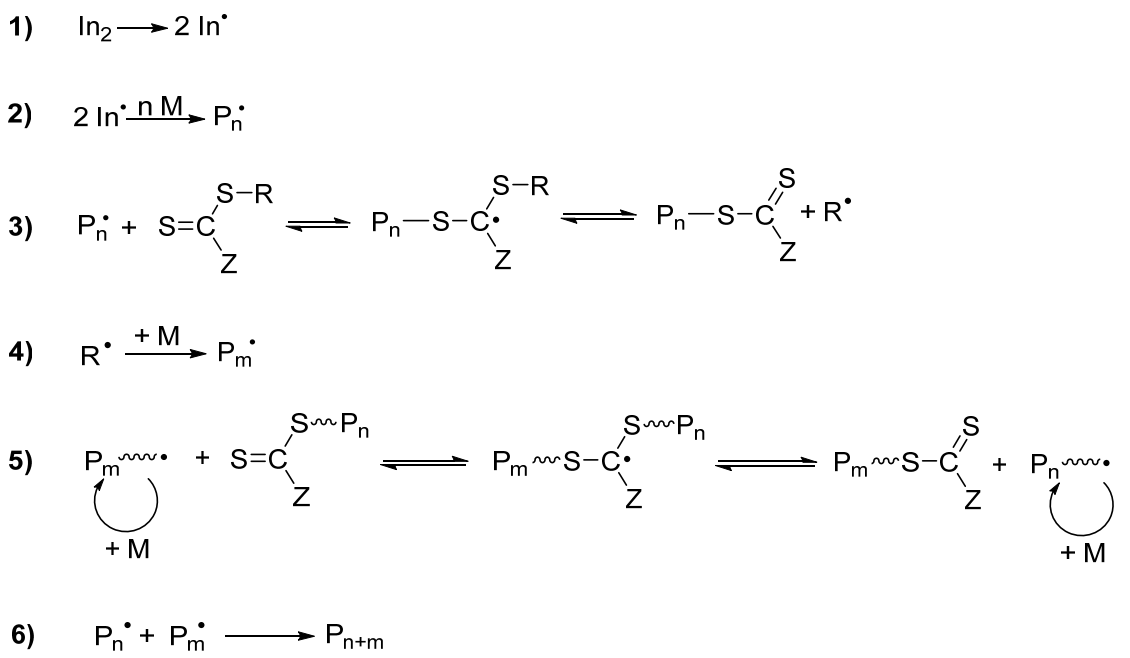

Scheme 8. General mechanism of the RAFT/MADIX polymerization.

The RAFT polymerization was used with fluorinated monomers successfully in 2011 by Kostov et *al.*[83] to carry out the copolymerization of VDF and 3,3,3-trifluoropropene (TFP) using xanthates as CTAs (RAFT/MADIX polymerization). Subsequently, the RAFT/MADIX copolymerizations of other fluorinated monomers were reported, such as chlorotrifluoroethylene/*tert*-butyl vinyl ether,[84] VDF/perfluoro(methyl vinyl ether),[85] hexafluoropropene/butyl vinyl ether,[86] VDF/*tert*-butyl 2-trifluoromethacrylate,[87] tetrafluoroethylene/isobutyl vinyl ether.[88]

The controlled radical homopolymerization of VDF by RAFT/MADIX was more carefully studied by Guerre *et al.*,[89,90] showing that some degree of control can be obtained using *O*-ethyl-*S*-(1-methoxycarbonyl)ethyldithiocarbonate as CTA. The loss of control is essentially due to the accumulation of the reverse dormant chains, $-CF_2-CH_2$-Xanthate, which are reactivated much slower than the normal chain ends, $-CH_2-CF_2$-Xanthate,[90,91] and a trick to reactivate them such as the use of $[Mn_2(CO)_{10}]$ in ITP has not yet been found. In addition, a loss of CTA was discovered,[89] which is caused by irreversible transfer from the dimethyl carbonate (as the solvent).[89] However, despite the reverse additions and the side reactions, PVDF with 90% chain-end functionality, with a degree of polymerization (D.P.) of 250 and a dispersity (Đ) of 1.49 was obtained, further leading to block copolymers.[89-92] A cyclic xanthate was also able to control the RAFT polymerization of VDF further leading to block copolymers, as above.[92]

In conclusion, chain defects provoked by reverse additions are intrinsic to radical polymerization and RAFT/MADIX polymerization could not solve the consequences of this phenomenon.

1.1.5.3. Boron-initiated and regulated CRP

Another possible and more recent method to (co)polymerize fluoroolefins involves alkylboron compounds activated by oxygen. First employed by Natta *et al.*[93] in 1965, and then revisited and more deeply investigated by Chung's group,[94-96] alkylboranes turn out to be efficient initiators and controlling agents for radical polymerization. The mechanism is based on the reaction of the alkylborane BR_3 with oxygen to generate $RO-OBR_2$ in which the O-O bond undergoes a homolytic cleavage to produce $RO^{\bullet}$ and $^{\bullet}OBR_2$ radicals. $RO^{\bullet}$ can initiate the homopolymerization of VDF (or the copolymerization of VDF with various other comonomers). In contrast, the $^{\bullet}$OBR2 radical is too stabilized and, consequently, is not able to initiate any polymerization. However, it is an effective counter radical which can trap the macroradical by recombination and thus controls the polymerization through a fast equilibrium between the active chain and the dormant

ones. This method was developed for piezoelectric polymers[96] after the selective reduction of chlorine atoms of CTFE units in poly(VDF-co-CTFE) copolymers to yield poly(VDF-*ter*-CTFE-*ter*-TrFE) or poly-(VDF-*co*-TrFE) copolymers.

1.1.5.4. Organometallic-mediated radical polymerization OMRP

Organometallic-mediated radical polymerization (OMRP) is a more recent technique of controlled radical polymerization (or RDRP) method based on the formation of an organometallic dormant species. The equilibrium between the free radicals of growing chains and the organometallic dormant species must be fast and reversible. Two mechanisms are possible: dissociative (reversible termination, OMRP-RT, Scheme 9) where the transition metal of a complex plays the role of a spin-trap with the generation of the reduced complex, or associative (degenerative transfer, OMRP-DT, Scheme 10). The two modes of action may also interplay.

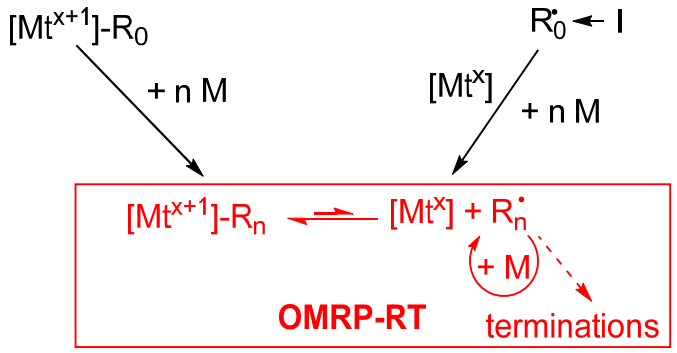

Scheme 9. General mechanism of the reversible termination in an OMRP process.

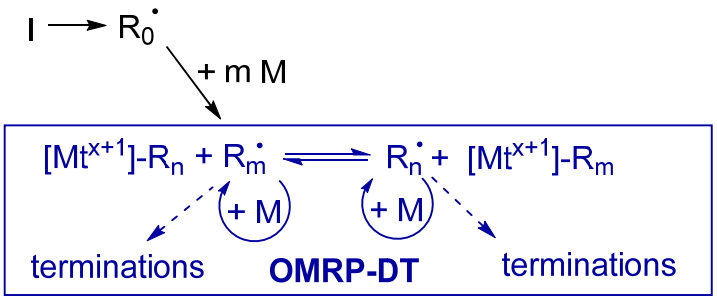

Scheme 10. General mechanism of the degenerative transfer in an OMRP process.

Several suitable reduced [Mt^x/L] complexes and/or organometallic initiators [Mt^{x+1}/L]-R_0 that are capable to regulate the controlled propagation of a variety of monomers have been designed, synthesized and tested.[64,97-100] A key is the appropriate tuning of the Mt-R_n homolytic bond strength while avoiding harmful side reactivity. The reactive fluorinated radicals lead to strong bonds with transition metals, thus the generation of metal complexes with suitably weak Mt-R_F bonds is necessary.

The first OMRP process was reported in 1992 by Wayland *et al.*[101] using rhodium(II) porphyrins. Two molecules of tetramesitylporphyrinatorhodium(II) reacted with an excess of acrylate monomer to form a dirhodium species bridged by an alkyl chain. Exposure of this complex to visible light cleaved homolytically one of the rhodium-acrylate bonds, resulting in the formation of two rhodium species, one with the alkyl chain and the other one without. The one possessing the alkyl chain could initiate the polymerization of acrylic acid, methyl acrylate and ethyl acrylate successfully. Then the growing radical chain was reversibly trapped by rhodium radical without the alkyl chain, with the exchange between dormant and active species leading to some control of the polymerization. Nevertheless, the trapping species could also reinitiate polymerization, through the formation of the bridged dirhodium initiator, resulting in the generation of new growing chains. This uncontrolled initiation, coupled with self-termination reactions between the growing chains, resulted in broadened dispersities (1.75–2.76) and high molar masses (from 144000 to 268000 g·mol^{-1}).

More recent studies developed the use of cobalt complexes as controlling agents.[65] This system is usually called cobalt-mediated radical polymerization (CMRP). Early systems were based on porphyrins[102] and cobaloximines,[103] leading to a linear increase of the molar masses with conversion and to a polydispersity > 1.5. More recent works used cobalt(II) acetylacetonate in the homopolymerization of vinyl acetate,[104] which has two reactive sides like VDF (head and tail), and led to a well-controlled polymer (Đ < 1.2). No accumulation of the less reactive dormant chain was observed, meaning that this complex is able to reactivate the normal and reverse chain. Moreover, this study was accompanied by DFT calculations which predict similar enthalpic stabilizations for the secondary head-to-tail cobalt and primary head-to-head cobalt dormant species. Cobalt(II) acetylacetonate has also been employed in the

copolymerization of *tert*-butyl-2-trifluoromethacrylate with vinyl acetate to synthesized block copolymers.[105] Recently, the homopolymerization of VDF by CMRP using cobalt(II) acetylacetonate was carried out by Banerjee *et al.*,[106] yielding a well-defined PVDF with a molar mass of 14500 g·mol^{-1} (D.P. = 225) and a low dispersity (≤ 1.32). The presence of the organometallic chain-end functionality was proven by the successful chain extension and synthesis of di- and triblock copolymer with PVAc. Besides, this study was accompanied by DFT calculations rationalizing the efficient reactivation of both head and tail chain-end dormant species.

Therefore, OMRP can be the solution to overcome the reverse dormant chain reactivation of PVDF. To the best of our knowledge, pentacarbonyl manganese complexes have not been reported as OMRP mediators, but recent computational studies of the Mn-C bond in some fluoroalkylpentacarbonylmanganese(I) complexes may suggest this possibility.[107] The trend for these complexes is similar to that for the cobalt(II) acetylacetonate, although the Mn-C bond dissociation enthalpy (BDE) are higher (42 to 54 kcal·mol^{-1} for manganese(I) family *vs.* 22 to 31 kcal·mol^{-1} for the cobalt(II) family). One of the objectives of this thesis deals with the preparation of pentacarbonyl manganese complexes that are models of the dormant chains obtained by the OMRP of VDF with these manganese systems, and to measure experimentally their bond dissociation energies. It is therefore of interest to review the synthesis and properties of alkylpentacarbonylmanganese(I) complexes.

1.2. Metal carbonyl complexes

Metal carbonyls are coordination complexes of transition metals which bear carbon monoxide ligands. The family of metal carbonyls has been known for more than one century and is an important one in inorganic and organometallic chemistry. This is due to the interest in the structures, applications to organic and organometallic synthesis and indispensable role of these compounds as catalysts or catalyst precursors, such as in hydroformylation[108], in Reppe chemistry[109] and in the Mond process[110]. The

stability of metal carbonyls with oxidation states that are nil (neutral metal carbonyls) or even negative (anions) is produced by the notable ability of CO to give π-backbonding. A wide diversity of mixed complexes bearing carbonyls and other ligands such as phosphines, cyclopentadienyls, arenes or other unsaturated hydrocarbon ligands are also accessible.

Metal carbonyl complexes are not present in nature, except for a few curious examples such as in the Galactic Center where monoxide vibrations of iron carbonyls in interstellar dust clouds were detected.[111] Iron carbonyl clusters were also observed in Jiange H5 chondrites, a non-metallic stony meteorites that have not been altered due to melting or differentiation of the parent body identified by Fourier-transform infrared spectroscopy (FTIR). Four infrared bands were identified as the terminal and bridging carbon monoxide ligands.[112]

1.2.1. Structure and bonding

The low-nuclearity binary metal carbonyls complexes obey the 18-electron rule if one electron pair is counted from each CO, conferring a certain stability, except for the 17-electron radical $[V(CO)_6]$, the structure of which is stabilized by the octahedral geometry and steric crowding that contributes to prevent radical-type reactions and dimerization. Other complexes such as $[Mn(CO)_6]^+$ complex obey the 18-electron rule and is stabilized for the same structural reasons, metal carbonyl cations being otherwise unstable. The transition metal-carbon bond can be explained by the Dewar-Chatt-Duncanson model.[113-115] The bond strength is attributed to the π-backbonding, which is possible by the mixing of the highest occupied atomic orbital (HOAO) of the metal atom with the lowest unoccupied molecular orbital (LUMO) of CO, see Scheme 11.[116] This kind of bonding requires that the metal possesses d-electrons and is in a relatively low oxidation state. A σ-bond originates from an overlap of the C-O nonbonding (or weakly anti-bonding) sp-hybridized electron pair that is mostly localized on the carbon atom of the CO ligand with a blend of d-, s-, and p-orbitals of the metal atom.

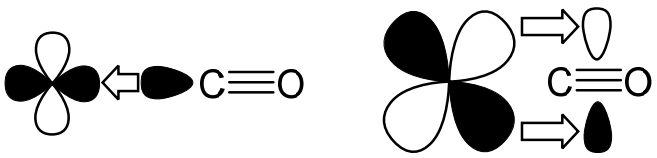

Scheme 11. Sigma bond (left) and "π-backbonding" (right) in metal carbonyl complexes.

The high-nuclearity metal-carbonyl clusters $[M_6(CO)_{16}]$ and beyond often escape the 18-electron rule to obey Wade's rules.[117] Thus, mononuclear neutral metal carbonyls are known for the metals that have an even number of d electrons, whereas neutral dimers with a single metal-metal bond are known for metals that have an odd number of d electrons. Metal-carbonyl clusters are mainly known in the iron, cobalt and nickel groups. They are all the more stable as one goes down in the columns of the periodic table because the strength of the metal-metal bond increases in this direction.

1.2.2. Physical characteristics

Mononuclear carbonyl complexes are usually colorless or pale-yellow volatile liquids or solids that are flammable and toxic. However, vanadium hexacarbonyl, the uniquely stable 17-electron metal carbonyl, is a blue-black solid. Di- and polymetallic carbonyls usually are more intensely colored. For instance, triiron dodecacarbonyl $[Fe_3(CO)_{12}]$ forms dark green crystals. The crystalline metal carbonyls can be normally purified under vacuum, although this process is rarely accompanied by degradation. Metal carbonyls are generally soluble in non-polar and polar organic solvents such as carbon tetrachloride, benzene, diethyl ether, acetone or glacial acetic acid and some cationic or anionic salts of metal carbonyls are soluble in water or alcohols.

1.2.3. Applications

In organometallic chemistry, metal carbonyls are precursors for the preparation of other organometallic complexes, commonly from their anionic derivatives. Numerous anionic derivatives of metal carbonyl have been synthesized for almost a century, allowing to make some alkyl metal carbonyl complexes *via* nucleophilic substitution or another reaction involving an electrophilic molecule (e.g. reaction of a nucleophile with an acid derivate). Metal carbonyl anions are generally used as sodium salts in a tetrahydrofuran solution. They are usually prepared by reduction of binuclear or trinuclear (depending on the metal) metal carbonyl derivatives. In this work, we will focus on manganese carbonyl derivatives synthesized from manganese carbonyl.

1.2.4. Techniques of characterization

Because the carbonyl ligands are firmly bonded to transition metals, the variations of the frequency of the strong infrared carbonyl absorption (around 2000 cm^{-1} for terminal CO) allow to measure the electronic effects of the other ligands. The C-O vibration frequency is related to the strength of carbon-oxygen bond, and also related inversely to the strength of the π-backbonding between the metal and carbon, depending on numerous factors such as the nature of metal, the coordination number or the oxidation state. In addition, the number of vibrational modes can be predicted by group theory. Carbonyl compounds can also be characterized by elemental analysis, NMR (^{13}C, ^{17}O and the metal nuclei if their nuclear spin is non-zero), mass spectroscopy and single-crystal X-Ray diffraction.

1.2.5. Manganese carbonyl complexes

The history of organometallic chemistry of manganese is not particularly extensive, unlike the organometallic chemistry of most other transition metals. There are only some incomplete and unproven reports of phenylmanganese species in the late 1930s and early 1940s, but the real development of the organometallic chemistry of manganese occurred during the 1950s. Hence, the origins of organomanganese chemistry are found in the time following the discovery of ferrocene, and expansion of this area has been in step with the rapid development of modern organometallic chemistry.[118] Dimanganese decacarbonyl was the first organometallic compound of manganese to be isolated and characterized.[119]

1.2.6. Dimanganese decacarbonyl

Dimanganese decacarbonyl, $[Mn_2(CO)_{10}]$, is a metal carbonyl cluster composed of two manganese atoms and ten carbonyl ligands with a manganese-manganese bond between these two metallic atoms. It obeys the 18-electron rule with ten electrons that come from the carbonyl ligands, and eight electrons coming from the two metal centers ($3d^7$ and the shared electron of the Mn-Mn bond).

1.2.6.1. Structure, physical and chemical properties

$[Mn_2(CO)_{10}]$ is a volatile yellow compound, stable as a solid at room temperature in the dark. It decomposes at room temperature over several months in contact with atmospheric oxygen giving a dark solid (manganese oxide). It is soluble in all common organic solvents, but not in water. In solution, it is more sensitive and it reacts quickly with oxygen to give manganese oxide. It can also easily dissociates under an inert atmosphere both thermally (~60–90 °C)[120] and photolytically in solution, even at room temperature (Scheme 12) to generate two manganese pentacarbonyl radicals.

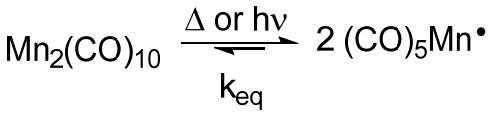

Scheme 12. Thermal or photolytical manganese carbonyl dissociation.

The molecular structure of manganese carbonyl was determined by Churchill *et al.* in 1981 by single-crystal X-ray diffraction.[121] It is composed of two square pyramidal $Mn(CO)_5$ groups linked with a metal-metal bond. The overall molecule thus belongs to the point group D_4d, which is an uncommon symmetry shared with S_2F_{10}.[122] The Mn−Mn bond dissociation enthalpy (BDE) is rather low (36.7±0.4 kcal·mol^{-1}) and decreased upon substitution of CO with other ligands.[123,124]

1.2.6.2. Synthesis

This compound was first obtained by the reduction of manganese iodide with a Grignard reagent and under a carbon monoxide atmosphere in 1949 by Hurd *et al.*,[119] however it was first isolated by reducing manganese iodide using magnesium in the presence of copper and under a carbon monoxide atmosphere by Brimm *et al*.[125] allowing to report the full characterization of this compound. Nevertheless, a meager yield (1%) was obtained by this synthetic pathway. Previously, Mond *et al.*[126] tried to obtain $[Mn_2(CO)_{10}]$ from pyrophoric manganese under a carbon monoxide atmosphere (500 bar) and 450 °C but without any results. In 1958 it was shown that it can be synthesized through reaction of manganese chloride, a phenylmagnesium halide and CO in diethyl ether with 10% yield.[127]

The best method of synthesis of $[Mn_2(CO)_{10}]$ was described by Podall *et al.*[128] employing an aluminum alkyl as the reducing agent leading to 55% yield. Then, Calderazzo[129] proposed a simplified procedure for this process which produced $[Mn_2(CO)_{10}]$ in 48% yield. Another efficient synthetic pathway (but leading to 30% yield) was proposed in 1965 employing manganese(II) chloride with sodium benzophenone ketyl with carbon monoxide under pressure (200 bar).[130]

It is also possible to synthesize manganese carbonyl by a low-pressure route starting from (methylcyclopentadienyl)tricarbonylmanganese with sodium metal in diglyme (dimethyl ether of diethylene glycol) solution under a carbon monoxide atmosphere.[131] Although this synthetic pathway does not lead to a high yield (15-20%), it is easy to implement, does not use high pressures of carbon monoxide, and the starting materials are inexpensive. In fact, this is the synthetic pathway most used for commercially available manganese carbonyl.

1.2.6.3. Reactivity

$[Mn_2(CO)_{10}]$ reacts directly with halogens, X_2, through the scission of metal-metal bond to lead to $[Mn(CO)_5X]$,[132] but the main reactivity patterns involve the manganese pentacarbonyl radical or the pentacarbonylmanganate ion, generally obtained in contact with an alkali metal.

As shown before, manganese pentacarbonyl radical can be formed by thermolysis or photolysis. In contrast to thermolysis, photolysis involves two competitive processes: the cleavage of manganese-manganese bond, as well as loss of CO.[133] The radicals formed by thermolysis are efficient abstractors of halide from $RCCl_3$ compounds,[134] and hence serve to initiate selective hydrogenolysis of such halides in the presence of good hydrogen donors[135] or addition to activated alkenes.[136]

The pentacarbonylmanganate ion, $[Mn(CO)_5]^-$, is usually obtained by reduction of manganese carbonyl with a sodium amalgam in THF as shown in Scheme 13.[130,132,137,138] However, the resulting solution is contaminated with approximately 10% $[(CO)_5Mn\text{-}Hg\text{-}Mn(CO)_5]$.[137] Other reagents can be used to obtain clean pentacarbonylmanganate ion such as a sodium-potassium metallic liquid alloy (NaK) in THF, providing mostly $K[Mn(CO)_5]$,[139] potassium tri-*sec*-butylborohydride, or lithium triethylborohydride, which affords clean $Li[Mn(CO)_5]$.[140]

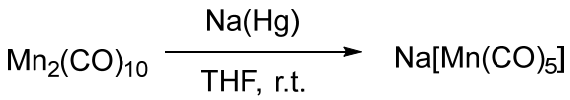

Scheme 13. Reaction of manganese carbonyl with sodium and mercury amalgam.

$[Mn(CO)_5]^-$ is a versatile and strong nucleophile employed in organometallic chemistry. However, other metal carbonyls anions are much stronger nucleophiles such as $[Re(CO)_5]^-$ or $[Fe(CO)_2(C_5H_5)]$ as shown Dessy *et al.*[141] in a study of the rates of reaction of this substance with various alkyl halides. It can react with a variety of electrophiles such as alkyl, acyl or silyl halides[140,142-146] leading to organomanganese complexes. It also reacts with elemental iodine,[132,138] tin and germanium halides,[147] thallium(I) nitrate[148,149] and strongly electron-deficient vinyl halides.[150,151] It can also be protonated giving the corresponding hydride $[Mn(CO)_5H]$.[152]

1.2.7. Manganese carbonyl derivates

1.2.7.1. Alkylpentacarbonylmanganese(I) complexes

Alkylpentacarbonylmanganese(I) complexes are landmark compounds in organometallic chemistry. The first attempts to prepare compounds involving manganese-carbon σ-bonds were carried out approximately 80 years ago by Gilman *et al.*[153,154], using $[MnI_2]$ and phenylmagnesium bromide. $[MnPh_2]$ and [MnPhI] were identified as products but characterization of these species was inconclusive. The first original syntheses of the simplest acyl and alkylpentacarbonylmanganese(I) complexes, the acetylpentacarbonylmanganese(I) and methylpentacarbonylmanganese(I) respectively, were reported by Closson and Coffield in 1957.[155,156] They also reported the syntheses of benzoyl and benzylpentacarbonylmanganese(I) as shown in Scheme 14. Previously, other authors reported the synthesis of cyclopentadienyl metal carbonyls[157,158] and their alkyl derivates[159], as well as acetylene[160] and allene[161] complexes of metal carbonyls.

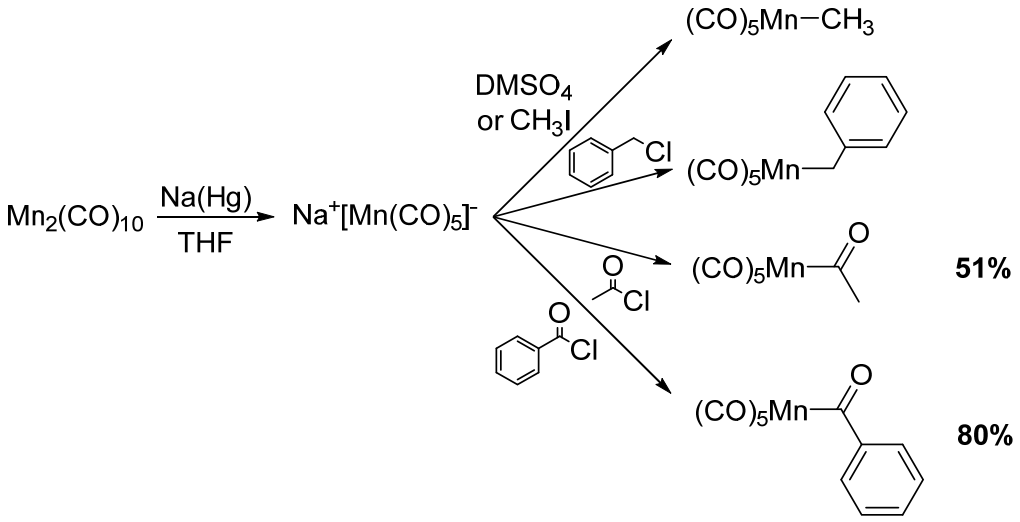

Scheme 14. First alkyl and acyl derivates synthetic pathway of a metal carbonyl prepared by Coffield and Closson.[155,156]

Shortly after these contributions, Hieber *et al.*[162] reported the synthesis of ethyl and *n*-propylpentacarbonylmanganese(I) complexes, however this research group subsequently reported that these compounds were in fact respectively the acyl derivates (propionyl and butanoylpentacarbonylmanganese(I).[163] In fact, the first original *n*-propylpentacarbonylmanganese(I) complex was reported by Calderazzo *et al.* in 1962.[164] However is was noted that these compounds are extremely unstable, decomposing even in the dark under vacuum at -10 °C.[165] $[Mn(CO)_5(CH_3)]$ has been studied as a model for the ubiquitous migratory insertion reaction leading to acyl derivatives,[166] which is a fundamental step in many catalytic cycles.[167]

In the literature, it is possible to find some discrepancy about the stability of the ethyl and *n*-propylpentacarbonylmanganese(I) complexes. Several authors support the possibility that these compounds decompose via β-hydride alkene elimination (e.g. $[Mn(CO)_5(C_2H_5)]$ gives $[Mn(CO)_5H]$ and ethylene).[168-170] Nevertheless, the acyl complex, $[Mn(CO)_5(COC_2H_5)]$, was also observed during the spontaneous decomposition of $[Mn(CO)_5(C_2H_5)]$,[165,171,172] so one of the decomposition mechanisms may involve a carbonyl insertion.[173] The high rate constant value measured for the carbonylation of $[Mn(CO)_5(C_2H_5)]$[164] strengthen this hypothesis. Moreover, the rate constant measured for the carbonylation of $[Mn(CO)_5(n\text{-}C_3H_7)]$[164] is even larger than the one measured for the ethyl derivate, and in fact *n*-propylpentacarbonylmanganese(I) is even less stable than ethylpentacarbonylmanganese(I), favoring this hypothesis.

Several studies have been carried out concerning the rate of migratory carbonyl insertion and decarbonylation of this kind of compounds,[172,174-181] all of them concluding that the rates increase with the chain length and that the carbonyl insertion occurs by the migration of the alkyl group onto an adjacent carbonyl group rather than a direct carbonyl insertion. In addition, the presence of a coordinating ligand from the solvent or other source stimulates the migration of the alkyl group because of the direct coordination to the manganese, yielding $[Mn(CO)_4(L)(R)]$.[182] However, alkylpenta-carbonylmanganese(I) complexes with a long linear alkyl chain (until *n*-$C_{18}H_{37}$) have been obtained and characterized,[183] concluding that the stability of these compounds depends on a subtle balance between the electronic and steric effects exerted by the alkyl chain. It was also proven that complexes containing β-hydrogens are less stable than those that not contain hydrogens at this position, due to the β-elimination reaction (e.g. $[Mn(CO)_5(CH_2Si(CH_3)_3)]$ is much more stable than $[Mn(CO)_5(C_2H_5)]$).[168]

To synthesize alkylpentacarbonylmanganese(I) complexes, one of the synthetic strategies consists in reducing the manganese carbonyl dimer to get the highly nucleophilic pentacarbonyl manganate, which can react with an electrophile such as an alkyl halide or an acid chloride to lead the alkyl or acyl manganese pentacarbonyl complexes respectively (Scheme 15).

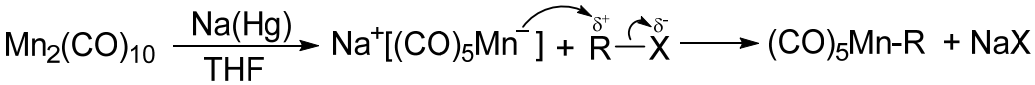

Scheme 15. General synthetic pathway for the synthesis of alkylpentacarbonylmanganese(I) complexes by nucleophilic substitution.

Sodium pentacarbonylmanganate is the most common salt employed in this reaction. However, pentacarbonyl manganate anion with other electropositive metals can be also used; such as the Li^+ and K^+ salts, as well as $[Mn(CO)_5MgBr]$[184], $Tl[Mn(CO)_5]_3$, $In[Mn(CO)_5]_3$, $Hg[Mn(CO)_5]_2$ and $Cd[Mn(CO)_5]_2$[149] species have been found to react with alkyl halides to give alkylmanganese carbonyls. Salts with other organic cations such as bis(triphenylphosphine)iminium (PPN^+) are also employed.[185]

Another possible synthetic pathway consists in synthesizing the acyl intermediate via an acyl chloride (or anhydride) followed by the decarbonylation of the acyl complex[183], but this involved one more step in the synthetic pathway. It is also possible to synthesized these compounds using $[Mn(CO)_5X]$ (X = Cl, Br, I) and an organolithium by a nucleophilic substitution yielding the alkylpentacarbonylmanganese(I) complex and lithium bromide. However, this synthetic pathway is usually reserved for substituted alkyl chains or more complex structures such as silanes or arenes.[186-188]

1.2.7.2. Fluoroalkylmanganese pentacarbonyl complexes

Among the alkylpentacarbonylmanganese(I) complexes, those containing a fluoroalkyl group have received special attention because of their enhanced thermal stability. At the beginning of the 1960s, only a few fluoroalkyl complexes had been described.[189] Unlike the simple alkylpentacarbonylmanganese(I) compounds, which are easily accessible by nucleophilic substitution of the halide in R-X by $[Mn(CO)_5]^-$, the corresponding derivatives with fluorine-containing alkyl ligands are not reachable by this way because the inverted polarity of the C-X bond leads instead to the formation of $[Mn(CO)_5X]$ with release of R_F^-, with $[Mn_2(CO)_{10}]$ and R_F-R_F resulting from further side reactions as described by both Beck[190] and McClellan[191] simultaneously (Scheme 16).

$$Na[Mn(CO)_5] \xrightarrow[THF]{CF_3I} [Mn(CO)_5I] + NaI + C_2F_6$$

Scheme 16. Reaction of sodium pentacarbonylmanganate with trifluoroiodomethane.[190,191]

However, this obstacle can be overcome by carrying out the nucleophilic substitution on the acyl chloride, R_FCOCl, or the corresponding anhydride, $R_FCOOCOR_F$, to obtain an acyl intermediate $[Mn(CO)_5(COR_F)]$, which can then be thermally decarbonylated. Coffield *et al.*[192] reported the first synthesis of two fluorinated manganese pentacarbonyl derivatives: the trifluoroacylmanganese pentacarbonyl complex obtained from the trifluoroacetyl chloride, and the trifluoromethylmanganese

pentacarbonyl by decarbonylation of trifluoroacetylmanganese pentacarbonyl (Scheme 17). Kaesz *et al.*[193-195] and Clark *et al.*[196] synthesized several perfluoroacyl and perfluoroalkyl derivates of tin and lead, and then reported some physical and analytical properties of a few fluoroacyl and fluoroalkyl pentacarbonyl manganese and rhenium complexes.[194]

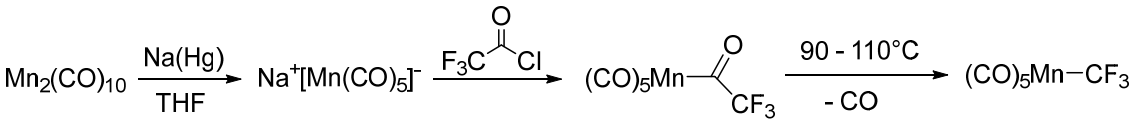

Scheme 17. Synthesis of trifluoroacetylpentacarbonylmanganese(I) by Coffield *et al.*[192]

The pentacarbonyl manganate ion cannot react with a aryl or vinyl halides or to displace a fluoride ion from alkyl fluorides.[143] To prepare these compounds it is necessary to use a two-step sequence, first preparing the appropriate acyl compound from an acyl halide and $[Mn(CO)_5]^-$, and then decarbonylating these intermediates either thermally or photolytically.[197] For instance, it is not possible to prepare (pentafluorophenyl)pentacarbonylmanganese(I) from $Na[Mn(CO)_5]$ and C_6F_6, whereas the corresponding reaction takes place for the analogous pentacarbonylrhenate, leading to (pentafluorophenyl)pentacarbonylrhenium(I). The synthesis of $[Mn(CO)_5(C_6F_6)]$ could be achieved using $[Mn(CO)_5Br]$ and C_6F_5Li.[198] Other possibilities to prepare directly the perfluoroalkylpentacarbonylmanganese(I) compounds is through the reaction of $[Cd(R_F)_2]$[199,200] with $[Mn(CO)_5Br]$ activated by $Ag[BF_4]$ or catalyzed with CuI.[201]

Perfluoroalcylpentacarbonylmanganese(I) complexes were generally described as white to pale-yellow crystalline solids, very volatile and air-stable. Perfluoroalkylmanganese(I) complexes can be obtained from acyl complexes by decarbonylation in high yields (80-100%) as shown Coffield *et al.*[155] This process needs different temperatures and times to be completed, depending mainly on the nature of the alkyl group. It also possible to obtain trifluoroacetylpentacarbonylmanganese(I) from trifluoroacetic anhydride (liquid at room temperature) instead of trifluoroacetyl chloride (gas at room temperature), forming the trifluoroacetylsodium(I) organic salt (Scheme 15).[190,202]

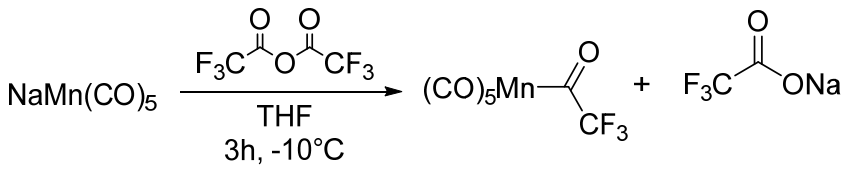

Scheme 15. Synthesis of trifluoroacylmanganese pentacarbonyl from trifluoroacetic anhydride by Beck *et al.*[190]

Thus, trifluoroacetylpentacarbonylmanganese(I), $[Mn(CO)_5(COCF_3)]$, resulting from the addition of $Na[Mn(CO)_5]$ to either trifluoroacetyl chloride[192,194] or trifluoroacetic anhydride[190,202] was used to yield $[Mn(CO)_5(CF_3)]$. Later, other $[Mn(CO)_5R_F]$ complexes have also been reported with $R_F = CFH_2$,[203,204] CF_2H,[203,204] and C_nF_{2n+1} (n = 1-4, 6).[205] These complexes do not appear to have found direct use in catalysis, whereas many other organomanganese complexes are now intensively investigated as precatalysts for various transformations such as hydrosilylation,[206-208] dehydrogenative coupling,[208-211] C-H[212] and C-F[213] activation, etc.

1.3. Conclusion

Fluorinated polymers are attractive materials because of their unique combination of properties that lead to many applications. Among them, PVDF has found interesting applications in a wide range of high-tech fields.[18] However, synthesizing well-defined molar mass PVDF remains a challenge by common RDRP techniques. This is due to the formation of the reverse PVDF-CF_2-$CH_2^\bullet$ chain-end in addition to the normal one (PVDF-CH_2-$CF_2^\bullet$). The reverse one leads to dormant chains that are reactivated less readily in ITP and RAFT, leading to their accumulation and therefore to the increasing of the dispersity. Asandei *et al.*[73] found the solution to such an issue adding dimanganese decacarbonyl in the visible light irradiation, generating the manganese pentacarbonyl radical. UV irradiation can also be used to generate this radical.[76] This species can abstract the iodine from the reverse dormant chain in ITP, reactivating the chain, but the formation of the PVDF-$Mn(CO)_5$ was not reported under these conditions. In addition, organometallic cobalt(II) compounds such as cobalt(II) acetylacetonate have

proven to be very efficient for controlling the polymerization of VDF due to the easy reactivation of the reverse dormant chain,[106] even easier than the normal one according to DFT calculations.[107] Moreover, the same computational study has shown the possibility of the formation of PVDF-$Mn(CO)_5$ and has suggested that the BDE values of the complexes modeling the normal and reverse PVDF-$Mn(CO)_5$ dormant chains are very similar.

The primary objective of this thesis was to investigate the role of manganese pentacarbonyl radical in the polymerizations of VDF and of other non-fluorinated monomers. For this purpose, the synthesis and full characterization of several alkyl and fluoroalkylmanganesepentacarbonyl(I) complexes has been carried out by the standard literature methods described above.[156,190,202] A key control parameter is the bond energy between the manganese and the normal and reverse chain-ends. Hence, new complexes modeling the PVDF and other non-fluorinated polymers chain-ends have been synthesized with the purpose of experimentally measuring their Mn-C bond dissociation enthalpy and verify whether the above-mentioned computational estimations are correct. Then, these complexes have been tested as initiators and as possible controlling agents in the polymerizations of VDF and other non-fluorinated monomers by thermal and photochemical activation (visible light and UV irradiation).

1.4. References

[1] D. B. Harper; D. O'Hagan *Nat. Prod. Rep.* **1994**, *11*, 123-133.
[2] D. O'Hagan; D. B. Harper *J. Fluorine Chem.* **1999**, *100*, 127-133.
[3] R. D. Chambers *Fluorine in Organic Chemistry*; 1st Ed. ed.; Blackwell Publishing Ltd: Oxford, 2004.
[4] S. Purser; P. R. Moore; S. Swallow; V. Gouverneur *Chem. Soc. Rev.* **2008**, *37*, 320-330.
[5] P. Kirsch *Modern Fluoroorganic Chemistry*; 1st Ed. ed.; Wiley VCH: Darmstadt, 2013.
[6] W. R. Dolbier *J. Fluorine Chem.* **2005**, *126*, 157-163.
[7] V. S. D. Voet; G. ten Brinke; K. Loos *J. Polym. Sci., Part A: Polym. Chem.* **2014**, *52*, 2861-2877.
[8] M. P. Krafft; J. G. Riess *Chemosphere* **2015**, *129*, 4-19.
[9] R. E. Banks *J. Fluorine Chem.* **1986**, *33*, 3-26.
[10] L. A. Wall *Fluoropolymers*; Wiley-Interscience: New York, 1971.
[11] S. Ebnesajjad *Fluoroplastics*; William Andrew Publishing: New York, 2003; Vol. Vol. 2.
[12] B. Ameduri; B. Boutevin; G. Kostov *Prog. Polym. Sci.* **2001**, *26*, 105-187.

[13] B. Ameduri; B. Boutevin *Well Architectured Fluoropolymers: Synthesis, Properties and Applications*; Elsevier: Amsterdam, 2004.
[14] B. Ameduri; H. Sawada *Fluorinated polymers*; Royal Society of Chemistry, 2017; Vol. 1&2.
[15] A. L. Moore *Fluoroelastomers Handbook; the DefinitiVe User's Guide and Data Book*; William Andrew Publishing: Norwich, New York, 2006.
[16] B. Ameduri *Macromolecules* **2010**, *43*, 10163-10184.
[17] B. Ameduri *Chem. Rev.* **2009**, *109*, 6632-6686.
[18] J. Gardiner *Aust. J. Chem.* **2015**, *68*, 13-22.
[19] D. A. Seiler; Scheirs, J., Ed.; Wiley: 1997, p 487-506.
[20] Fluoropolymers; Chemical Economics Handbook. HIS Markit Ltd. https://ihsmarkit.com/products/fluoropolymers-chemical-economics-handbook.html (accessed September 7, 2018).
[21] J. T. Goldbach; R. Amin-Sanayei; W. He; J. Henry; W. Kosar; A. Lefebvre; G. O'Brien; D. Vaessen; K. Wood; S. Zerafati In *Fluorinated Polymers: Volume 2: Applications*; Ameduri, B., Sawada, H., Eds.; The Royal Society of Chemistry: 2017; Vol. 2, p 127-157.
[22] Z. Cui; E. Drioli; Y. M. Lee *Prog. Polym. Sci.* **2014**, *39*, 164-198.
[23] T. Soulestin; V. Ladmiral; F. D. Dos Santos; B. Améduri *Prog. Polym. Sci.* **2017**, *72*, 16-60.
[24] B. Ameduri In *Science of Synthesis*; Ernst Schaumann, E., Nielsen, M. B., Eds.; Thieme Chemistry: 2014; Vol. 24, p 317-352.
[25] *Global Fluoropolymers Market - Products, Technologies & Applications*; ReportLinker: Lyon, 2016.
[26] J. Scheirs *Modern Fluoropolymers: High Performance Polymers for Diverse Applications*; Wiley: New York, 1997.
[27] G. Odian *Principles of Polymerization*; Wiley, 2004.
[28] K. Matyjaszewski *Cationic Polymerizations: Mechanisms, Synthesis & Applications*; Taylor & Francis, 1996.
[29] M. Sawamoto *Prog. Polym. Sci.* **1991**, *16*, 111-172.
[30] B. Ameduri; B. Boutevin; L. Karam *J. Fluorine Chem.* **1993**, *65*, 43-47.
[31] C. M. Kausch; J. E. Leising; R. E. Medsker; V. M. Russell; R. R. Thomas; A. A. Malik *Langmuir* **2002**, *18*, 5933-5938.
[32] C. Wesdemiotis; F. Pingitore; M. J. Polce; V. M. Russell; Y. Kim; C. M. Kausch; T. H. Connors; R. E. Medsker; R. R. Thomas *Macromolecules* **2006**, *39*, 8369-8378.
[33] M. Miyamoto; K. Aoi; T. Saegusa *Macromolecules* **1988**, *21*, 1880-1883.
[34] M. Miyamoto; K. Aoi; T. Saegusa *Macromolecules* **1991**, *24*, 11-16.
[35] J. M. Rodriguez-Parada; M. Kaku; D. Y. Sogah *Macromolecules* **1994**, *27*, 1571-1577.
[36] W. O. Choi; M. Sawamoto; T. Higashimura *Polym. J.* **1988**, *20*, 201-206.
[37] J. Hopken; M. Moller; M. S. Lee; V. Percec *Macromol. Chem. Phys.* **1992**, *193*, 275-284.
[38] M. R. Clark; J. L. Kendall; J. M. DeSimone *Macromolecules* **1997**, *30*, 6011-6014.
[39] A. Meskini; M. Raihane; B. Ameduri *Macromolecules* **2009**, *42*, 3532-3539.
[40] H. Hsieh; R. P. Quirk *Anionic Polymerization: Principles and Practical Applications*; Taylor & Francis, 1996.
[41] T. Narita *Macromol. Rapid Commun.* **2000**, *21*, 613-627.
[42] T. Narita *J. Fluorine Chem.* **2010**, *131*, 812-828.
[43] K. Ziegler; E. Holzkamp; H. Breil; H. Martin *Angew. Chem.* **1955**, *67*, 541-547.
[44] K. Ziegler; H. G. Gellert; K. Zosel; W. Lehmkuhl; W. Pfohl *Angew. Chem.* **1955**, *67*, 424-424.
[45] G. Natta *J. Polym. Sci.* **1955**, *16*, 143-154.
[46] G. Natta; P. Pino; P. Corradini; F. Danusso; E. Mantica; G. Mazzanti; G. Moraglio *J. Am. Chem. Soc.* **1955**, *77*, 1708-1710.

[47] NobelPrize.org. The Nobel Prize in Chemistry 1963. Nobel Media AB 2018. https://www.nobelprize.org/prizes/chemistry/1963/summary/ (accessed September 20, 2018).
[48] D. S. Breslow; N. R. Newburg *J. Am. Chem. Soc.* **1959**, *81*, 81-86.
[49] V. K. Meyer; K. H. Reichert *Angew. Makromol. Chem.* **1970**, *12*, 175-183.
[50] A. Nakamura; S. Ito; K. Nozaki *Chem. Rev.* **2009**, *109*, 5215-5244.
[51] W. Weng; Z. Shen; R. F. Jordan *J. Am. Chem. Soc.* **2007**, *129*, 15450-15451.
[52] Z. L. Shen; R. F. Jordan *Macromolecules* **2010**, *43*, 8706-8708.
[53] S. Wada; R. F. Jordan *Angew. Chem.* **2017**, *129*, 1846-1850.
[54] M. Tatemoto In *First Regular Meeting of Soviet-Japanese Fluorine Chemists* Tokyo, 1979.
[55] K. Matyjaszewski *Controlled Radical Polymerization*; American Chemical Society: Washington, DC, 1998; Vol. 685.
[56] K. Matyjaszewski; J. Xia *Chem. Rev.* **2001**, *101*, 2921-2990.
[57] M. Kamigaito; T. Ando; M. Sawamoto *Chem. Rev.* **2001**, *101*, 3689-3745.
[58] G. David; C. Boyer; J. Tonnar; B. Ameduri; P. Lacroix-Desmazes; B. Boutevin *Chem. Rev.* **2006**, *106*, 3936-3962.
[59] M. R. Hill; R. N. Carmean; B. S. Sumerlin *Macromolecules* **2015**, *48*, 5459-5469.
[60] S. Perrier *Macromolecules* **2017**, *50*, 7433-7447.
[61] S. Perrier; P. Takolpuckdee *J. Polym. Sci., Part A: Polym. Chem.* **2005**, *43*, 5347-5393.
[62] J. Nicolas; Y. Guillaneuf; C. Lefay; D. Bertin; D. Gigmes; B. Charleux *Prog. Polym. Sci.* **2013**, *38*, 63-235.
[63] V. Sciannamea; R. Jérôme; C. Detrembleur *Chem. Rev.* **2008**, *108*, 1104-1126.
[64] L. E. N. Allan; M. R. Perry; M. P. Shaver *Prog. Polym. Sci.* **2012**, *37*, 127-156.
[65] A. Debuigne; R. Poli; C. Jerome; R. Jerome; C. Detrembleur *Prog. Polym. Sci.* **2009**, *34*, 211-239.
[66] M. Oka; M. Tatemoto In *Contemporary Topics in Polymer Science: Volume 4*; Bailey, W. J., Tsuruta, T., Eds.; Springer: Boston, 1984, p 763-777.
[67] M. Tatemoto *Int. Polym. Sci. Technol.* **1985**, *12*, 85-98.
[68] T. Yagi; N. Tsuda; T. Noguchi; K. Sakaguchi; Y. Tanaka; M. Tatemoto (Daikin Industries). Fluorine-containing block copolymer and artificial lens comprising the same. EP 0422644 A2, 1990.
[69] V. Arcella; G. Brinati; M. Albano; V. Tortelli (Ausimont S.p.A.). Fluorinated thermoplastic elastomers having superior mechanical and elastic properties. EP 0661312 A1, 1995.
[70] D. P. Carlson (E. I. du Pont de Nemours and Co.). Fluorinated thermoplastic elastomers with improved base stability. EP 0444700 B1 and US 5284920 A, 1991 and 1994.
[71] C. Boyer; D. Valade; L. Sauguet; B. Ameduri; B. Boutevin *Macromolecules* **2005**, *38*, 10353-10362.
[72] C. Boyer; D. Valade; P. Lacroix-Desmazes; B. Ameduri; B. Boutevin *J. Polym. Sci., Part A: Polym. Chem.* **2006**, *44*, 5763-5777.
[73] A. D. Asandei; O. I. Adebolu; C. P. Simpson *J. Am. Chem. Soc.* **2012**, *134*, 6080-6083.
[74] C. P. Simpson; O. I. Adebolu; J.-S. Kim; V. Vasu; A. D. Asandei *Macromolecules* **2015**, *48*, 6404-6420.
[75] S. M. Aliwi; C. H. Bamford; S. U. Mullik *J. Polym. Sci., Polym. symp.* **1975**, 33-50.
[76] N. Golzari; J. Adams; S. Beuermann *Polymers* **2017**, *9*, 306.
[77] G. Moad; E. Rizzardo; S. H. Thang *Polymer* **2008**, *49*, 1079-1131.
[78] P. Cacioli; D. G. Hawthorne; R. L. Laslett; E. Rizzardo; D. H. Solomon *J. Macromol. Sci. Chem.* **1986**, *A23*, 839-852.
[79] L. Hutson; J. Krstina; C. L. Moad; G. Moad; G. R. Morrow; A. Postma; E. Rizzardo; S. H. Thang *Macromolecules* **2004**, *37*, 4441-4452.
[80] G. F. Meijs; E. Rizzardo; S. H. Thang *Polym. Bull.* **1990**, *24*, 501-505.

[81] B. Yamada; T. Otsu *Macromol. Rapid Commun.* **1990**, *11*, 513-518.
[82] J. Chiefari; Y. K. Chong; F. Ercole; J. Krstina; J. Jeffery; T. P. T. Le; R. T. A. Mayadunne; G. F. Meijs; C. L. Moad; G. Moad; E. Rizzardo; S. H. Thang *Macromolecules* **1998**, *31*, 5559-5562.
[83] G. Kostov; F. Boschet; J. Buller; L. Badache; S. Brandsadter; B. Ameduri *Macromolecules* **2011**, *44*, 1841-1855.
[84] L. Liu; D. Lu; H. Wang; Q. Dong; P. Wang; R. Bai *Chem. Commun.* **2011**, *47*, 7839-7841.
[85] E. Girard; J.-D. Marty; B. Ameduri; M. Destarac *ACS Macro Lett.* **2012**, *1*, 270-274.
[86] P. Wang; J. Dai; L. Liu; Q. Dong; B. Jin; R. Bai *Polym. Chem.* **2013**, *4*, 1760-1764.
[87] Y. Patil; B. Ameduri *Polym. Chem.* **2013**, *4*, 2783-2799.
[88] G. Puts; V. Venner; B. Améduri; P. Crouse *Macromolecules* **2018**, *51*, 6724-6739.
[89] M. Guerre; B. Campagne; O. Gimello; K. Parra; B. Ameduri; V. Ladmiral *Macromolecules* **2015**, *48*, 7810-7822.
[90] M. Guerre; S. M. W. Rahaman; B. Ameduri; R. Poli; V. Ladmiral *Macromolecules* **2016**, *49*, 5386-5396.
[91] M. Guerre; S. M. Wahidur Rahaman; B. Ameduri; R. Poli; V. Ladmiral *Polym. Chem.* **2016**, *7*, 6918-6933.
[92] S. Banerjee; Y. Patil; O. Gimello; B. Ameduri *Chem. Commun.* **2017**, *53*, 10910-10913.
[93] G. Natta; G. Allegra; I. W. Bassi; D. Sianesi; G. Caporiccio; E. Torti *J. Polym. Sci., Part A* **1965**, *3*, 4263-4278.
[94] T. C. Chung; A. Petchsuk *Macromolecules* **2002**, *35*, 7678-7684.
[95] T. C. Chung; A. Petchsuk (Foundation, P. S. R.). 2002.
[96] Z. C. Zhang; Z. M. Wang; T. C. M. Chung *Macromolecules* **2007**, *40*, 5235-5240.
[97] K. M. Smith; W. S. McNeil; A. S. Abd-El-Aziz *Macromol Chem Physic* **2010**, *211*, 10-16.
[98] R. Poli In *Organometallic Mediated Radical Polymerization*; Matyjaszewski, K., Möller, M., Eds.; Elsevier BV: Amsterdam, 2012; Vol. 3, p 351-375.
[99] R. Poli *Chem. Eur. J.* **2015**, *21*, 6988-7001.
[100] A. Debuigne; C. Jerome; C. Detrembleur *Polymer* **2017**, *115*, 285-307.
[101] B. B. Wayland; G. Poszmik; M. Fryd *Organometallics* **1992**, *11*, 3534-3542.
[102] B. B. Wayland; G. Poszmik; S. L. Mukerjee; M. Fryd *J. Am. Chem. Soc.* **1994**, *116*, 7943-7944.
[103] L. D. Arvanitopoulos; M. P. Greuel; H. J. Harwood *Abstr Pap Am Chem S* **1994**, *208*, 402.
[104] A. N. Morin; C. Detrembleur; C. Jerome; P. De Tullio; R. Poli; A. Debuigne *Macromolecules* **2013**, *46*, 4303-4312.
[105] S. Banerjee; V. Ladmiral; A. Debuigne; C. Detrembleur; S. M. W. Rahaman; R. Poli; B. Ameduri *Macromol. Rapid Commun.* **2017**, *38*, 1700203.
[106] S. Banerjee; V. Ladmiral; A. Debuigne; C. Detrembleur; R. Poli; B. Améduri *Angew. Chem., Int. Ed.* **2018**, *57*, 2934-2937.
[107] R. Poli; S. M. W. Rahaman; V. Ladmiral; B. Ameduri *J. Organomet. Chem.* **2018**, *864*, 12-18.
[108] I. Ojima; C.-Y. Tsai; M. Tzamarioudaki; D. Bonafoux In *Organic Reactions*; John Wiley & Sons, Inc.: 2004.
[109] W. Bertleff; M. Roeper; X. Sava In *Ullmann's Encyclopedia of Industrial Chemistry*; Wiley-VCH Verlag GmbH & Co. KGaA: 2000.
[110] L. Mond; C. Langer; F. Quincke *J. Chem. Soc., Trans.* **1890**, *57*, 749-753.
[111] A. G. G. M. Tielens; D. H. Wooden; L. J. Allamandola; J. Bregman; F. C. Witteborn *The Astrophysical Journal* **1996**, *461*, 210-222.
[112] Y. Xu; X. Xiao; S. Sun; Z. Ouyang *Lunar and Planetary Science* **1996**, *27*, 1457-1458.
[113] M. J. S. Dewar *Bull. Soc. Chim. Fr.* **1951**, C71-C79.
[114] J. Chatt; L. A. Duncanson *J. Chem. Soc.* **1953**, 2939-2947.
[115] G. J. Leigh; N. Winterton *Modern Coordination Chemistry: The Legacy of Joseph Chatt*; Royal Society of Chemistry, 2002.

[116] E. R. Davidson; K. L. Kunze; F. B. C. Machado; S. J. Chakravorty *Acc. Chem. Res.* **1993**, *26*, 628-635.
[117] K. Wade *J. Chem. Soc., Chem. Commun.* **1971**, 792-793.
[118] P. M. Treichel In *Comprehensive Organometallic Chemistry*; Stone, F. G. A., Abel, E. W., Eds.; Pergamon: Oxford, 1982, p 1-159.
[119] D. T. Hurd; G. W. Sentell; F. J. Norton *J. Am. Chem. Soc.* **1949**, *71*, 1899-1899.
[120] J. P. Fawcett; A. Poe; K. R. Sharma *J. Am. Chem. Soc.* **1976**, *98*, 1401-1407.
[121] M. R. Churchill; K. N. Amoh; H. J. Wasserman *Inor. Chem.* **1981**, *20*, 1609-1611.
[122] L. F. Dahl; E. Ishishi; R. E. Rundle *J. Chem. Phys.* **1957**, *26*, 1750-1751.
[123] D. M. Chowdhury; A. Poe; K. R. Sharma *J Chem Soc Dalton* **1977**, 2352-2355.
[124] J. L. Hughey; C. P. Anderson; T. J. Meyer *J. Organomet. Chem.* **1977**, *125*, C49-C52.
[125] E. O. Brimm; M. A. Lynch; W. J. Sesny *J. Am. Chem. Soc.* **1954**, *76*, 3831-3835.
[126] L. Mond; H. Hirtz; M. D. Cowap *J. Chem. Soc., Trans.* **1910**, *97*, 798-810.
[127] V. Hnizda (Ethyl Corp). Process for the synthesis of manganese carbonyl US 2822247 A, 1958.
[128] H. E. Podall; J. H. Dunn; H. Shapiro *J. Am. Chem. Soc.* **1960**, *82*, 1325-1330.
[129] F. Calderazzo *Inor. Chem.* **1965**, *4*, 293-296.
[130] J. J. Eisch; R. B. King *Organometallic syntheses*; Academic Press, 1965.
[131] R. B. King; J. C. Stokes; T. F. Korenowski *J. Organomet. Chem.* **1968**, *11*, 641-643.
[132] K. J. Reimer; A. Shaver; M. H. Quick; R. J. Angelici In *Inorganic Syntheses*; John Wiley & Sons, Inc.: 2007, p 154-159.
[133] P. L. Pauson; G. K. Friestad In *Encyclopedia of Reagents for Organic Synthesis*; John Wiley & Sons, Ltd: 2001.
[134] N. A. Kuz'mina; N. P. Zhiryukhina; E. T. Chukovskaya; R. K. Freidlina *Bull. Acad. Sci. USSR, Div. Chem. Sci.* **1981**, *30*, 1715-1719.
[135] L. N. Kiseleva; N. A. Rybakova; R. K. Freidlina *Bull. Acad. Sci. USSR, Div. Chem. Sci.* **1983**, *32*, 2171-2173.
[136] E. T. Chukovskaya; M. A. Rozhkova; R. K. Freidlina *Bull. Acad. Sci. USSR, Div. Chem. Sci.* **1982**, *31*, 1406-1409.
[137] R. B. King *J. Inorg. Nucl. Chem.* **1963**, *25*, 1296-1298.
[138] R. B. King; F. G. A. Stone In *Inorganic Syntheses*; Kleinberg, J., Ed.; McGraw-Hill Book Company, Inc.: 1963; Vol. VII, p 196-201.
[139] J. E. Ellis; E. A. Flom *J. Organomet. Chem.* **1975**, *99*, 263-268.
[140] J. A. Gladysz; G. M. Williams; W. Tam; D. L. Johnson; D. W. Parker; J. C. Selover *Inor. Chem.* **1979**, *18*, 553-558.
[141] R. E. Dessy; R. L. Pohl; R. B. King *J. Am. Chem. Soc.* **1966**, *88*, 5121-5124.
[142] J. E. Ellis *J. Organomet. Chem.* **1975**, *86*, 1-56.
[143] R. B. King *Acc. Chem. Res.* **1970**, *3*, 417-427.
[144] M. I. Bruce; M. J. Liddell; G. N. Pain; M. A. Bennett; H. Neumann In *Inorganic Syntheses*; John Wiley & Sons, Inc.: 2007, p 171-180.
[145] B. D. Dombek *J. Am. Chem. Soc.* **1979**, *101*, 6466-6468.
[146] P. DeShong; G. A. Slough; V. Elango; G. L. Trainor *J. Am. Chem. Soc.* **1985**, *107*, 7788-7790.
[147] D. N. Duffy; B. K. Nicholson *J. Organomet. Chem.* **1979**, *164*, 227-234.
[148] A. T. T. Hsieh; M. J. Mays; J. S. Kristoff; D. F. Shriver In *Inorganic Syntheses*; John Wiley & Sons, Inc.: 2007, p 61-63.
[149] A. T. T. Hsieh; M. J. Mays *J. Organomet. Chem.* **1970**, *22*, 23-28.
[150] R. Robinson; K. Rudolf; T. Koenig *J. Org. Chem.* **1985**, *50*, 5871-5873.
[151] R. B. King; J. W. Howard *J. Org. Chem.* **1977**, *42*, 2335-2337.
[152] W. Hieber; G. Wagner *znb* **1957**, *12*, 478-479.
[153] H. Gilman; J. C. Bailie *J. Org. Chem.* **1937**, *2*, 84-94.
[154] H. Gilman; R. H. Kirby *J. Am. Chem. Soc.* **1941**, *63*, 2046-2048.

[155] T. H. Coffield; J. Kozikowski; R. D. Closson *J. Org. Chem.* **1957**, *22*, 598.
[156] R. D. Closson; J. Kozikowski; T. H. Coffield *J. Org. Chem.* **1957**, *22*, 598.
[157] E. O. Fischer *Angew. Chem.* **1955**, *67*, 475-482.
[158] T. S. Piper; F. A. Cotton; G. Wilkinson *J. Inorg. Nucl. Chem.* **1955**, *1*, 165-174.
[159] T. S. Piper; G. Wilkinson *J. Inorg. Nucl. Chem.* **1956**, *3*, 104-124.
[160] H. W. Sternberg; H. Greenfield; R. A. Friedel; J. Wotiz; R. Markby; I. Wender *J. Am. Chem. Soc.* **1954**, *76*, 1457-1458.
[161] H. Greenfield; I. Wender; J. H. Wotiz *J. Org. Chem.* **1956**, *21*, 875-878.
[162] W. Hieber; G. Wagner *Justus Liebigs Annalen der Chemie* **1958**, *618*, 24-30.
[163] W. Hieber; G. Braun; W. Beck *Ber.* **1960**, *93*, 901-908.
[164] F. Calderazzo; F. A. Cotton In *Proc. Int. Conf. Coord. Chem., 7th* 1962, p 296.
[165] M. L. H. Green; P. L. I. Nagy *J. Organomet. Chem.* **1963**, *1*, 58-69.
[166] F. Calderazzo; F. A. Cotton *Inorg. Chem.* **1962**, *1*, 30-36.
[167] R. H. Crabtree *The Organometallic Chemistry of the Transition Metals*; 4th ed.; Wiley-Interscience: New York, 2005.
[168] B. Wozniak; J. D. Ruddick; G. Wilkinson *Journal of the Chemical Society A: Inorganic, Physical, Theoretical* **1971**, 3116-3120.
[169] P. M. Treichel In *Comprehensive Organometallic Chemistry*; Stone, F. G. A., Abel, E. W., Eds.; Pergamon Press: Oxford, 1982; Vol. 4, p 92.
[170] F. A. Cotton; 4th ed.; John Wiley: New York, 1980.
[171] T. E. Gismondi; M. D. Rausch *J. Organomet. Chem.* **1985**, *284*, 59-71.
[172] T. L. Bent; J. D. Cotton *Organometallics* **1991**, *10*, 3156-3160.
[173] R. B. King In *Advances in Organometallic Chemistry*; Stone, F. G. A., West, R., Eds.; Academic Press: 1965; Vol. 2, p 157-256.
[174] J. N. Cawse; R. A. Fiato; R. L. Pruett *J. Organomet. Chem.* **1979**, *172*, 405-413.
[175] C. P. Casey; C. A. Bunnell *J. Am. Chem. Soc.* **1976**, *98*, 436-440.
[176] C. S. Kraihanzel; P. K. Maples *Inor. Chem.* **1968**, *7*, 1806-1815.
[177] K. Noack; Calderaz.F *J. Organomet. Chem.* **1967**, *10*, 101-104.
[178] F. Calderazzo; K. Noack *Coord. Chem. Rev.* **1966**, *1*, 118-125.
[179] K. Noack; M. Ruch; F. Calderazzo *Inor. Chem.* **1968**, *7*, 345-349.
[180] R. W. Johnson; R. G. Pearson *Inor. Chem.* **1971**, *10*, 2091-2095.
[181] F. Calderazzo; F. A. Cotton *Inorg. Chem.* **1962**, *1*, 30-36.
[182] J.-A. M. Andersen; J. R. Moss *J. Organomet. Chem.* **1992**, *439*, C25-C27.
[183] J.-A. M. Andersen; J. R. Moss *Organometallics* **1994**, *13*, 5013-5020.
[184] J. M. Burlitch; S. W. Ulmer *J. Organomet. Chem.* **1969**, *19*, P21-P23.
[185] A. P. Masters; T. S. Sorensen *Can. J. Chem.* **1990**, *68*, 492-501.
[186] G. D. Vaughn; K. A. Krein; J. A. Gladysz *Organometallics* **1986**, *5*, 936-942.
[187] J. Dubarle Offner; F. Rose-Munch; E. Rose; N. Elgrishi; H. Rousselière *Organometallics* **2010**, *29*, 4643-4646.
[188] H. G. Raubenheimer; A. Neveling; S. Cronje; D. G. Billing *Polyhedron* **2001**, *20*, 1089-1095.
[189] J. J. Lagowski *Quarterly Reviews, Chemical Society* **1959**, *13*, 233-264.
[190] W. Beck; W. Hieber; H. Tengler *Ber.* **1961**, *94*, 862-872.
[191] W. R. McClellan *J. Am. Chem. Soc.* **1961**, *83*, 1598-1600.
[192] T. H. Coffield; J. Kozikowski; R. D. Closson In *Abstracts of the International Conference on Coordination Chemistry* London, 1959, p 126.
[193] H. D. Kaesz; J. R. Phillips; F. G. A. Stone *Chem. Ind.* **1959**, 1409-1410.
[194] H. D. Kaesz; R. B. King; F. G. A. Stone *Z. Naturforsch.* **1960**, *15b*, 763-764.
[195] H. D. Kaesz; J. R. Phillips; F. G. A. Stone *J. Am. Chem. Soc.* **1960**, *82*, 6228-6232.
[196] H. C. Clark; C. J. Willis *J. Am. Chem. Soc.* **1960**, *82*, 1888-1891.
[197] R. B. King; M. B. Bisnette *J. Organomet. Chem.* **1964**, *2*, 15-37.
[198] P. M. Treichel; M. A. Chaudhari; F. G. A. Stone *J. Organomet. Chem.* **1963**, *1*, 98-100.

[199] H. Lange; D. Naumann *J. Fluorine Chem.* **1984**, *26*, 1-18.
[200] R. Eujen; B. Hoge; D. J. Brauer *J. Organomet. Chem.* **1996**, *519*, 7-20.
[201] D. Naumann; M. Kaiser *Z. Anorg. Allg. Chem.* **1995**, *621*, 812-816.
[202] R. B. King In *Organometallic synthesis* 1965; Vol. 1, p 149-151.
[203] F. Calderazzo; K. Noack; U. Schaerer *J. Organomet. Chem.* **1966**, *6*, 265-271.
[204] K. Noack; U. Schaerer; F. Calderazzo *J. Organometal. Chem.* **1967**, *8*, 517-526.
[205] D. Naumann; M. Kaiser *Z. Anorg. Allg. Chem.* **1995**, *621*, 812-816.
[206] X. Ma; Z. Zuo; G. Liu; Z. Huang *ACS Omega* **2017**, *2*, 4688-4692.
[207] D. A. Valyaev; D. Wei; S. Elangovan; M. Cavailles; V. Dorcet; J.-B. Sortais; C. Darcel; N. Lugan *Organometallics* **2016**, *35*, 4090-4098.
[208] S. Vijjamarri; V. K. Chidara; G. Du *ACS Omega* **2017**, *2*, 582-591.
[209] N. Duc Hanh; X. Trivelli; F. Capet; J.-F. Paul; F. Dumeignil; R. M. Gauvin *ACS Catal.* **2017**, *7*, 2022-2032.
[210] B. Dutta; V. Sharma; N. Sassu; Y. Dang; C. Weerakkody; J. Macharia; R. Miao; A. R. Howell; S. L. Suib *Green Chem.* **2017**, *19*, 5350-5355.
[211] N. A. Espinosa-Jalapa; A. Kumar; G. Leitus; Y. Diskin-Posner; D. Milstein *J. Am. Chem. Soc.* **2017**, *139*, 11722-11725.
[212] W. Liu; L. Ackermann *ACS Catal.* **2016**, *6*, 3743-3752.
[213] D. Zell; U. Dhawa; V. Mueller; M. Bursch; S. Grimme; L. Ackermann *ACS Catal.* **2017**, *7*, 4209-4213.

Chapter 2

Alkylpentacarbonyl-manganese(I) complexes

Outline:

2. Alkylpentacarbonylmanganese(I) complexes

2.1. Introduction

This chapter describes the synthesis and characterization of several alkylpentacarbonylmanganese(I) complexes. These complexes model the dormant chains of a few polymers such as poly(methyl acrylate) (PMA), poly(vinyl acetate) (PVAc) and polystyrene (PS) in a putative controlled process by OMRP with the $[Mn(CO)_5]$ controlling agent. The Mn-C BDE in these systems are expected to be much lower than in the fluoroalkylpentacarbonylmanganese(I) complexes as will be shown in Chapter 4.

Three alkylpentacarbonylmanganese(I) complexes have been synthesized and characterized from their corresponding alkyl bromide compounds by the same method previously used by Closson *et al.*[1]. All these complexes and the synthetic pathway are shown in Scheme 1.

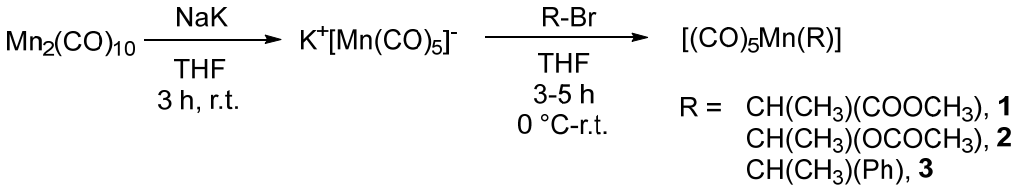

Scheme 1. General synthetic pathway of alkylpentacarbonylmanganese(I) complexes.

Alkyl bromides (in contrast to alkyl chlorides and alkyl iodides) have been extensively used as source of an alkyl chain in previous alkylpentacarbonylmanganese(I) synthetic investigations.[2,3] In fact, the synthesis of $[(Mn(CO)_5(CH(CH_3)(COOCH_2CH_3)]$, which is rather similar to compound **1** (ethyl instead of methyl in the ester group), was found most efficient when using the bromide substrate.[4] The different ester group substituent should not affect the alkyl halide reactivity. In this study, the different products obtained in the reaction of $Na[Mn(CO)_5]$ with several 2-halocarboxylate esters, $X\text{-}CR_1R_2COOCH_2CH_3$

(where R_1 = H or CH_3 and R_2 = H or CH_3) in THF were evidenced by ^{55}Mn NMR spectroscopy. In each case, the relative amount of $[Mn(CO)_5R]$, $[Mn(CO)_5X]$ and $[Mn_2(CO)_{10}]$ were quantified. In the case of a primary carbon (R_1 = R_2 = H, the better yield for the alkylpentacarbonylmanganese(I) complex was obtained when X = Cl, while for a secondary carbon (R_1 = H and R_2 = CH_3) the alkyl bromide led to a better yield. For the tertiary system (R_1 = R_2 = CH_3), no alkyl halide gave any of the desired alkyl manganese product. Moreover, because of the lower iodine electronegativity than the other halogens, the use of alkyl iodide increased the relative amount of $[Mn(CO)_5X]$ in all the systems tested.

Compound **1** has previously been identified by Casey *et al.*[5] as a by-product of the decarbonylation reaction of $[Mn(CO)_5(COCH_2CH_2COOCH_3)]$, which gives $[Mn(CO)_5(CH_2CH_2COOCH_3)]$ as expected as the main product, but compound **1** was not isolated and characterized. The proposed mechanism for this rearrangement was *via* a β-H elimination and reinsertion mechanism with a metal hydride intermediate. This appears related to the rearrangement of β-keto to α-keto iron compounds.[6] However, compound **2** is not reported in the literature to the best of our knowledge. Compound **3** was synthesized and detected with FTIR and optical rotatory dispersion (ORD) techniques in a pure enantiomeric form, (+)-$[Mn(CO)_5(CH(CH_3)(C_6H_5))]$, starting from the (-)-phenylethylbromide in a stereochemistry investigation of the formation and cleavage of alkyl-transition-metal derivatives.[7] However, it could not be isolated because of its spontaneous decomposition into $[Mn(CO)_5(COCH(CH_3)(C_6H_5))]$ among other by-products, according to the authors.

Compounds **1**, **2** and **3** were synthesized and characterized by the method described in Chapter 1. However, as shown in detail below, compounds **3** could not be properly isolated. As displayed in Scheme 1, all the syntheses started from the reduction of manganese carbonyl by NaK (sodium and potassium liquid alloy).

2.2. Results and discussion

2.2.1. Synthesis of potassium pentacarbonylmanganate

For all synthetic procedures, the potassium pentacarbonylmanganate salt was prepared from dimanganese decacarbonyl in THF. This salt is extremely air-sensitive, so all the operations were carried out in a Schlenk tube under argon and with dry solvents. Several reducing agents can be used to produce the $[Mn(CO)_5]^-$ reagent. The most common way in the older literature is by the employment of a Na amalgam, which affords the sodium salt. However, to avoid the use of mercury and the formation of $(CO)_5Mn\text{-}Hg\text{-}Mn(CO)_5$ complex as a by-product,[8] the NaK alloy was preferred, leading to the potassium pentacarbonyl manganate salt. The metallic sodium and potassium chunks were placed in a Schlenk tube under argon. Commonly, these metals are stored under mineral oil, so the freshly cut metal chunks must be cleaned with a *n*-pentane solution before use. Then, they were crushed together with a glass rod to obtain the liquid alloy.

A solution containing $[Mn_2(CO)_{10}]$ in dry THF was transferred from another Schlenk tube under argon in the Schlenk tube that contains the NaK and the resulting mixture was stirred at room temperature for 3 hours. The initially yellow or light orange (if it is concentrated) solution became rapidly orange, then red, then dark brown and finally dark green-brownish or green. The reaction can be monitored by FTIR spectroscopy to check whether the process is complete, as shown in Figure 1. The main carbonyl stretching bands of these compounds are reported in Table 1.

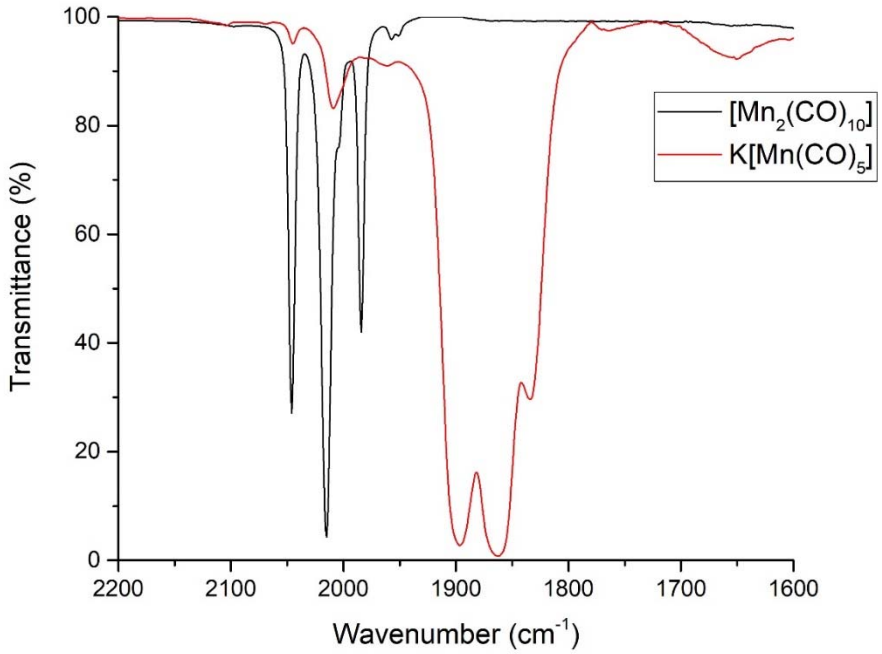

Figure 1. Carbonyl stretching bands of dimanganese decacarbonyl in pentane (black) and potassium pentacarbonylmanganate in THF (red).

Table 1. Main carbonyl stretching bands of dimanganese decacarbonyl and potassium pentacarbonylmanganate.

Compound	Solvent	$\tilde{\nu}_1$ (cm^{-1})	$\tilde{\nu}_2$ (cm^{-1})	$\tilde{\nu}_3$ (cm^{-1})
$[Mn_2(CO)_{10}]$	Pentane	2046	2015	1984
$K[Mn(CO)_5]$	THF	1897	1862	1834

The three main carbonyl stretching bands of dimanganese decacarbonyl undergo a batochromic shift (lower wavenumber) as expected due to the increase of the π-backbonding from the manganese atom to the carbonyl ligands.

Once the reduction reaction was complete, the solution was filtered under argon through a 2 cm Celite bed above the frit to avoid clogging. The mixture was transferred to a Schlenk tube by cannula to avoid the contact of the potassium pentacarbonylmanganate with oxygen or moisture (Figure 2). The resulting solution is usually brown or dark brown. However, depending on the concentration, it may display greenish tones. Because of its extreme sensitivity, this solution was not stored, but

rather obtained *in situ* and used directly in the next step for each of the acyl and alkyl pentacarbonylmanganese(I) syntheses.

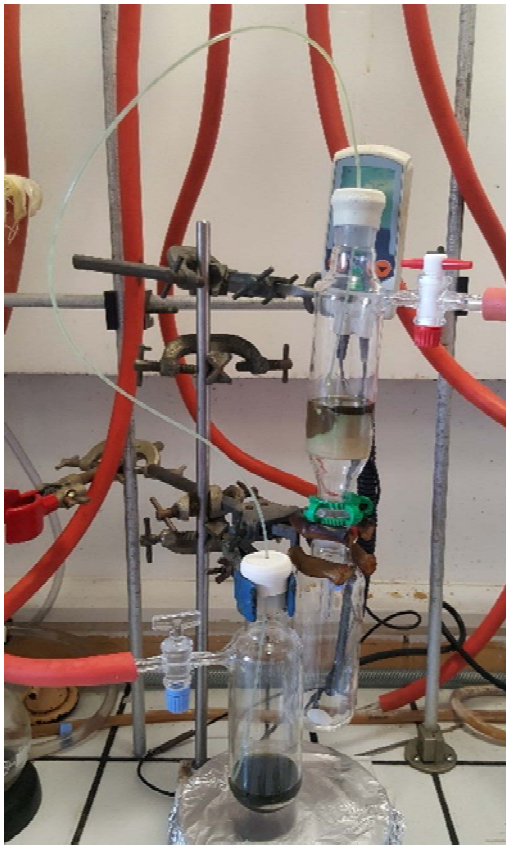

Figure 2. Picture of the filtration system used for the $K[Mn(CO)_5]$ solution to remove the residual NaK.

2.2.2. 1-Methyl-2-methoxy-2-oxoethylpentacarbonylmanganese(I), **1**

1-Methyl-2-methoxy-2-oxoethylpentacarbonylmanganese(I) complex was synthesized from the potassium pentacarbonyl manganate salt by a nucleophilic substitution with the corresponding alkyl bromide, the methyl 2-bromopropionate.

2.2.2.1. Synthesis of compound **1**

Methyl 2-bromoprionate was directly added dropwise to the filtered potassium pentacarbonyl manganate solution in THF. During the addition, the solution color changes to dark brown, then to light brown after 5 minutes and finally turns to yellow as shown in Figure 3.

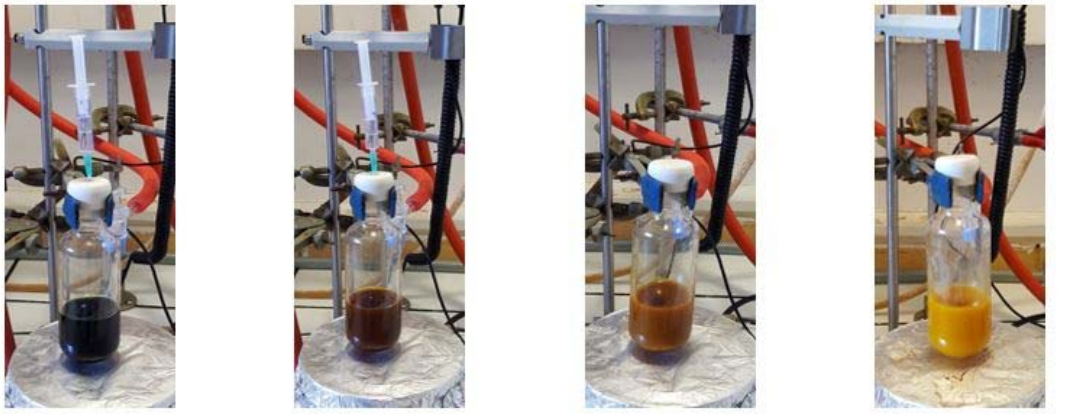

Figure 3. Pictures of the evolution during and after the addition of methyl 2-bromopropionate to the $K[Mn(CO)_5]$ solution.

The purification was carried out by column chromatography with standard silica gel as stationary phase and with *n*-pentane as mobile phase. Since compound **1** is not well-soluble in *n*-pentane, it is preferable to introduce it as a solid deposit in the column chromatography. For this, the solution from the synthesis was transferred to a flask together with a small amount of silica gel and then the solvent was removed. After evaporation, the silica gel containing the complex was laid on top of the column chromatography as a solid deposit. Then, using *n*-pentane as eluent, a first yellow fraction was obtained corresponding to the dimanganese decacarbonyl by-product formed during the reaction.[4] Then the polarity of eluent was increased using a 9:1 mixture of *n*-pentane and diethyl ether to recover the desired product as a light-yellow solution (yield 39%). Finally, the solvent was removed in the rotary evaporator to obtain the pure compound **1** a yellow oil (Figure 4).

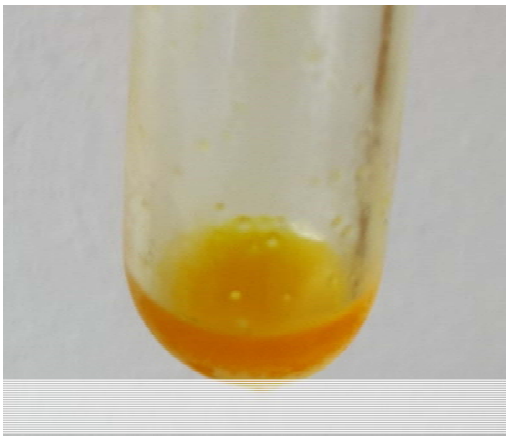

Figure 4. 1-Methyl-2-methoxy-2-oxoethyl(pentacarbonyl)manganese complex after purification by column chromatography.

It is to be noted that compound **1** is not very stable at room temperature in air, contrary to the analogous methyl and fluoroalkyl pentacarbonyl manganese(I) derivatives. Indeed, it decomposes slowly as shown by a darkening to brown. Thus, it is recommended not to store it for a long time and to keep it in a Schlenk tube under argon at low temperature and in the dark.

2.2.2.2. Characterization of compound **1**

The ^{1}H NMR spectrum of compound **1** (Figure 5) displays the three expected peaks for this complex. The first one is a singlet at δ 3.62 (3H) corresponding to the methyl group of the ester function. The second one is a quartet at δ 2.35 ppm (1H, $^{3}J_{HH}$ = 7 Hz) assigned to the CH bonded to manganese. Finally, the third one is a doublet centered at δ 1.55 (3H, $^{3}J_{HH}$ = 7 Hz) produced by the CH_3 next to the CH. All these NMR resonances are in good agreement with those reported by Casey *et al.* (δ 1.58, d, 3H, $^{3}J_{HH}$ = 7.5 Hz; 2.31, q, 1H, $^{3}J_{HH}$ = 7.5 Hz; 3.65, s, 3H).[5] No evidence of any β-H elimination that would produce methyl acrylate was noted, even though this compound possesses hydrogens at the β position, suggesting that compound **1** exhibits a certain stability contrary to other simpler alkylpentacarbonylmanganese(I) such as $[Mn(CO)_5(C_2H_5)]$ or $[Mn(CO)_5(n\text{-}C_3H_7)]$, which were reported to slowly decompose even at -10°C in the dark under an inert atmosphere.[9-11]

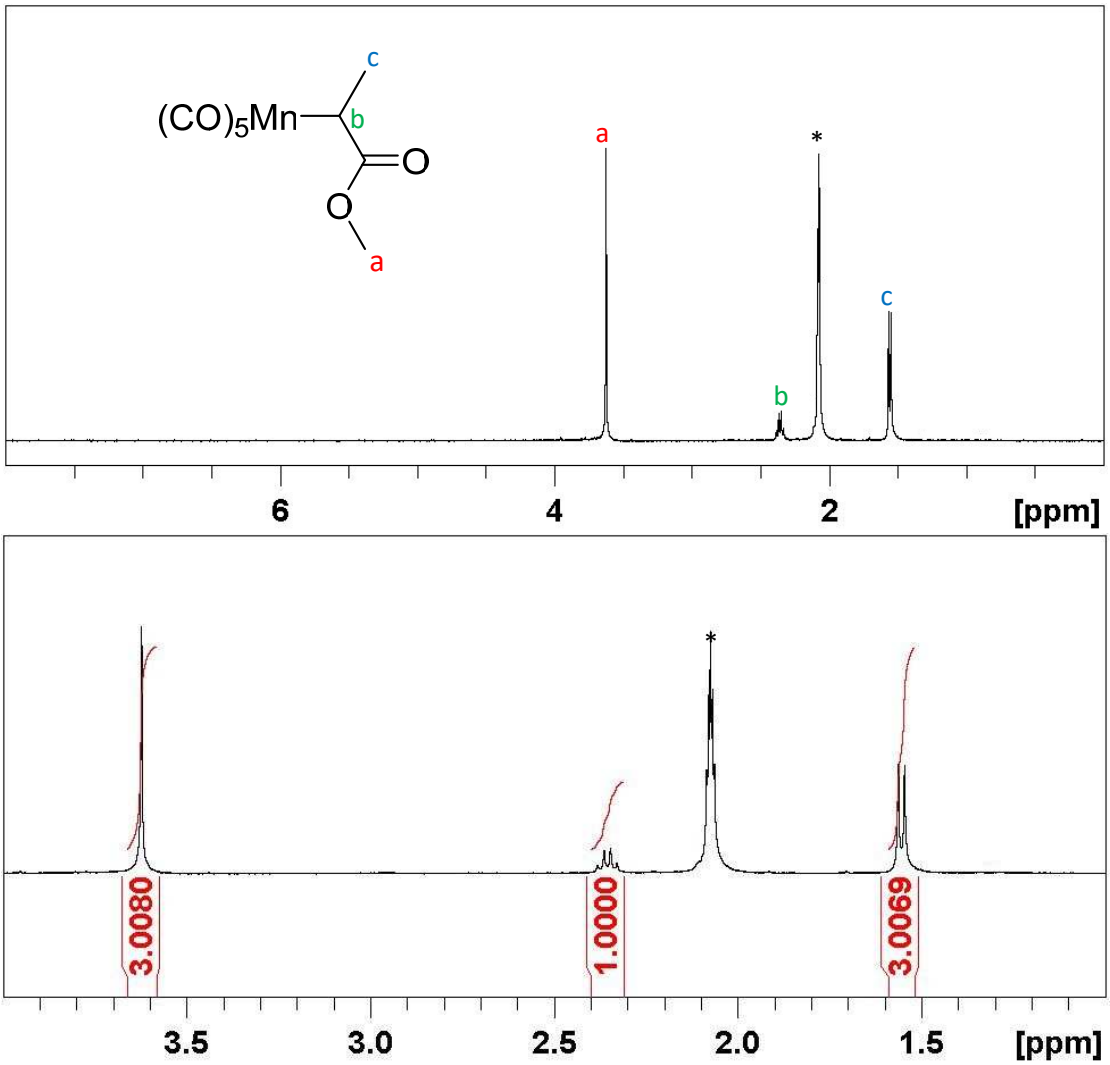

Figure 5. ^{1}H NMR spectra (400 MHz, acetone-d_6) of complex **9**: full spectrum above and expansion of the 1-4 ppm region with integral values below. The starred resonances are due to the solvent.

The FTIR spectrum of compound **1** in the carbonyl stretching region in *n*-pentane solution (Figure 6) exhibits five main signals, one at low frequency (1712 cm^{-1}) assigned to the ester carbonyl group, and four in the terminal metal carbonyl region (1900-2150 cm^{-1}). There is one more band than the expected pattern for a $Mn(CO)_5$ moiety in ideal C_{4v} symmetry ($2A_1+E$), which is related to symmetry lowering, resulting in the appearance of the "forbidden" and therefore not very strong B_1 band (Table 2). Is it to be noted that symmetry lowering should also, in principle, split the degenerate E band into two separate ones. This phenomenon was observed for other derivatives (see later in this manuscript) but not in this case.

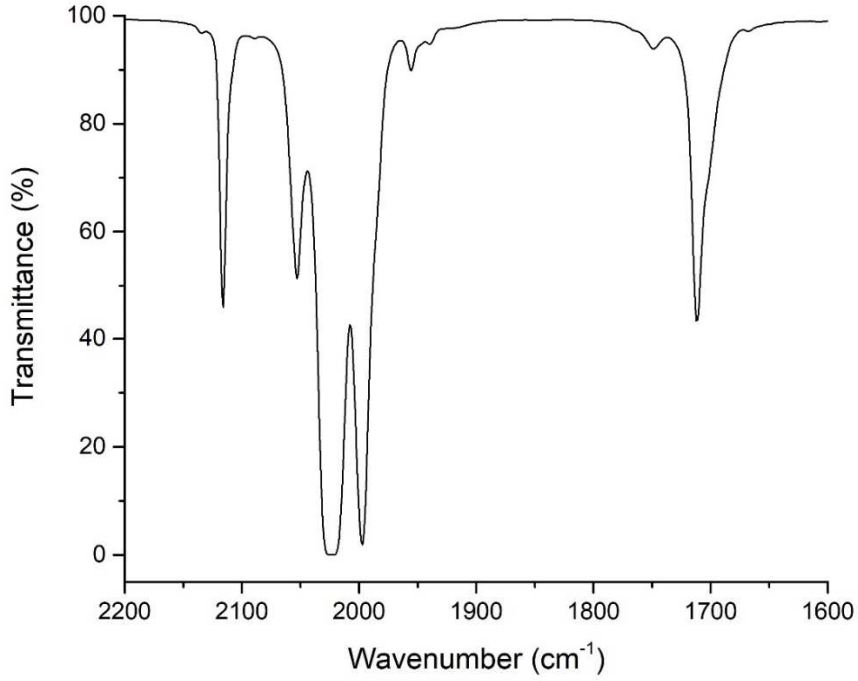

Figure 6. FTIR spectrum of compound **1** in the carbonyl stretching region in *n*-pentane solution.

Table 2. FTIR carbonyl stretching bands in n-pentane solution of compound **1**.

Vibration mode	A_1	B_1	E	A_1	Acyl group (ester)
Wavenumber (cm^{-1})	2116 m	2053 m	2024 vs	1997 s	1712 m

A few additional weak bands are also observed in the Mn-CO stretching region (2134, 1956, 1939 and 1749 cm^{-1}) which cannot be attributed to the symmetry lowering. A few of these may result from an acyl complex, probably $[Mn(CO)_5(COCH(CH_3)(COOCH_3))]$, formed by a migration of the alkyl group follow by an insertion of CO released by another complex. The release of CO can be stimulated by the coordination of a coordinating ligand such as a coordinating solvent.[12] In the present case, THF and diethyl ether were used for the synthesis and purification, respectively. However, these bands could also be attributed to the vibrations of ^{13}C isotopomers, namely $[Mn(^{12}CO)_4(eq\text{-}^{13}CO)(CH(CH_3)(COOCH_3))]$ and $[Mn(^{12}CO)_4(ax\text{-}^{13}CO)(CH(CH_3)(COOCH_3))]$.[13] This is suggested by the detailed frequency

analysis carried out for the fluoroalkyl derivatives, which will be described later in Chapter 3, Section 3.2.5.

2.2.3. 1-Acetyloxyethylpentacarbonylmanganese(I), **2**

The synthesis of $[Mn(CO)_5(CH(CH_3)(OCOCH_3))]$ (compound **2**) was attempted by nucleophilic substitution of the bromine atom in 1-bromoethyl acetate by the pentacarbonylmanganate anion (see Scheme 2).

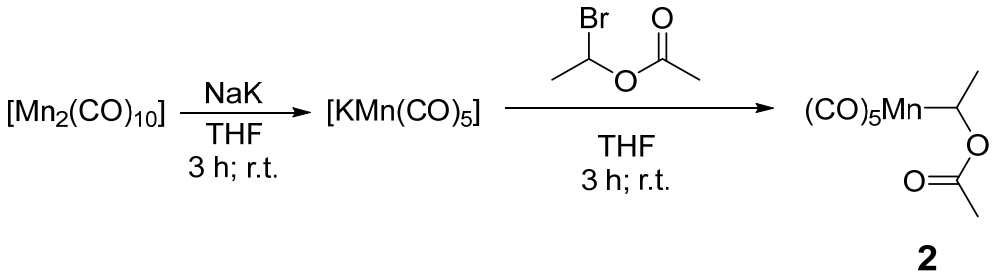

Scheme 2. Synthetic pathway of compound **2**.

Once the solution of potassium pentacarbonylmanganate was filtered, the stoichiometric amount of 1-bromoethyl acetate was added dropwise at room temperature (20 °C). The solution was stirred for 3 h at room temperature. The green-brownish solution of potassium pentacarbonylmangante changed to brown and then orange.

The crude product was purified by flash chromatography using a 12 g silica cartridge and *n*-pentane as eluent. The reaction crude was introduced as a solid deposit because of its low solubility in *n*-pentane. As for complex **1**, the column chromatography lead first to a yellow fraction corresponding to manganese carbonyl. Then, increasing the polarity of solvent gradually with diethyl ether up to a 1:1 mixture, one more fraction was obtained as a dark yellow oil after evaporation of the solvent. Storing this oil in the

fridge (3 °C) in a Schlenk tube under an atmosphere of argon for several days, small crystals were grown in the flask. These crystals were identified by single crystal X-Ray diffraction as the acyl derivative of the desired complex (Figure 7). Further details about the X-ray structure data can be found in the Appendix (Section A.2).

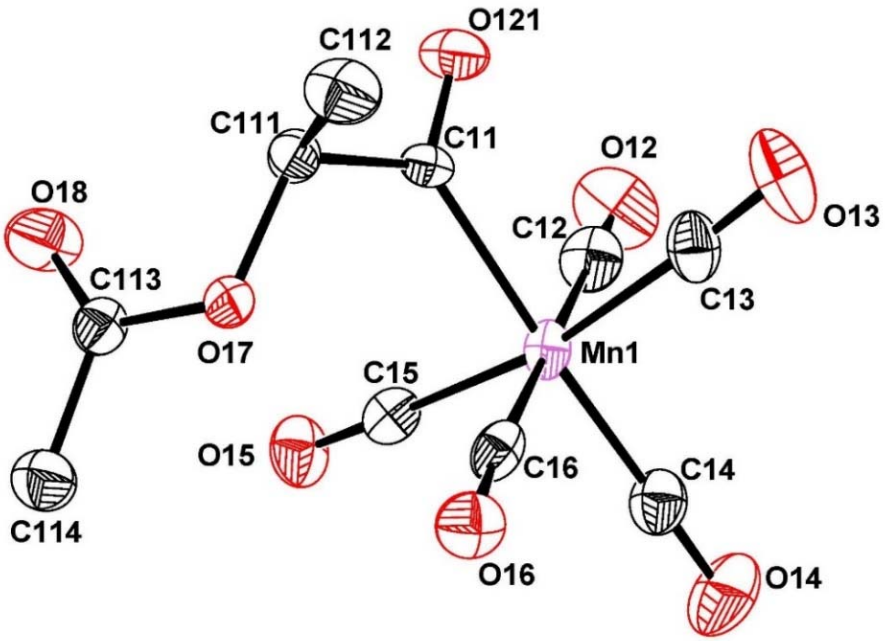

Figure 7. ORTEP view of one of the main products obtained during the synthesis of $[Mn(CO)_5(CH(CH_3)(OCOCH_3))]$, corresponding to the acyl derivate $[Mn(CO)_5(COCH(CH_3)(OCOCH_3))]$ (**2a**).

This carbonyl insertion reaction has been already observed for other alkylpentacarbonylmanganese(I) complexes such as the ethyl, *n*-propyl and 1-phenylethylpentacarbonylmanganese(I).[7,9-11] The proposed mechanism to yield this product is shown in Scheme 3 and probably involves the migratory insertion of the alkyl chain and the coordination of a coordinating ligand such as the solvents employed (THF and diethyl ether), producing intermediate **2b**. In order to afford **2a**, coordination of one additional CO ligand is necessary. This CO ligand may be generated from another molecule of **2**, with saturation of the vacant coordination site either by a solvent molecule (to yield **2c**) or by the alkyl carbonyl function, to yield **2d** with a 5-member ring.

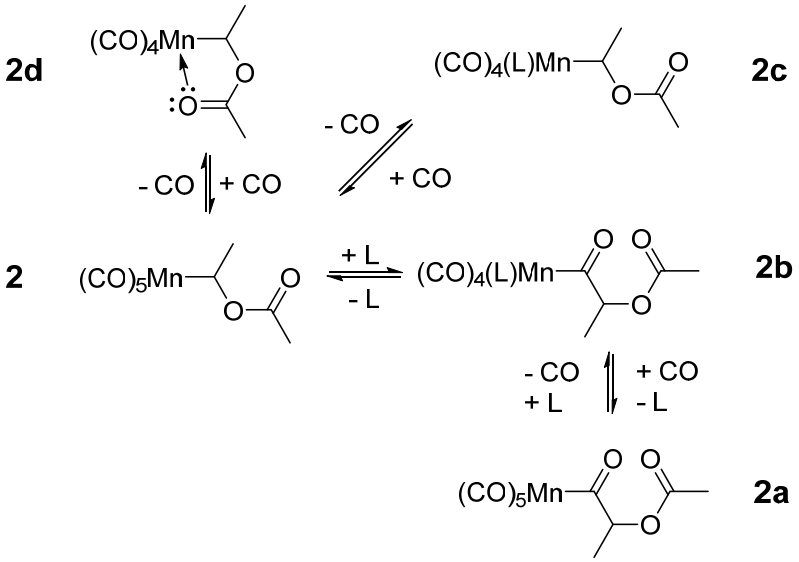

Scheme 3. Proposed mechanism of the formation of $[Mn(CO)_5(COCH(CH_3)(OCOCH_3)]$.

The ^1H NMR analysis of the isolated product fraction from the chromatographic separation (Figure 8) reveals that it contains four different products (43% of **2**, 30% of **2a**, 14% of **2c** and 13% of **2d**, determined by integration of ^1H NMR spectrum) with the expected signal pattern for the 1-acetyloxyethyl group (one quartet, one doublet and one singlet), all of them different from those of the starting reagent, the 1-bromoethyl acetate (δ 6.74, q; 2.08, s; 1.97, d). The ^1H-^1H COSY NMR spectrum allowed to correlate the CH quartets with the CH_3 doublets for all compounds (Figure 9).

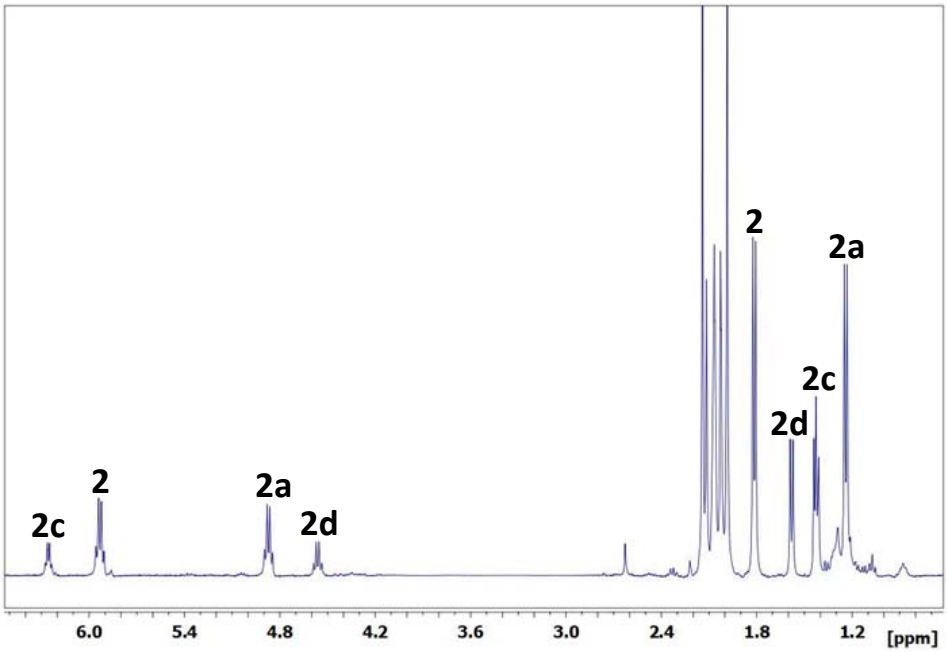

Figure 8. ^1H NMR spectrum (400 MHz, acetone-d_6) of the product mixture obtained after chromatographic purification of the crude reaction product. The assignment of the resonances of **2** and **2a** is proved by separate spectra recorded on the batches of crystals used for the X-ray diffraction studies, whereas the resonances assigned to compounds **2c** and **2d** are tentative.

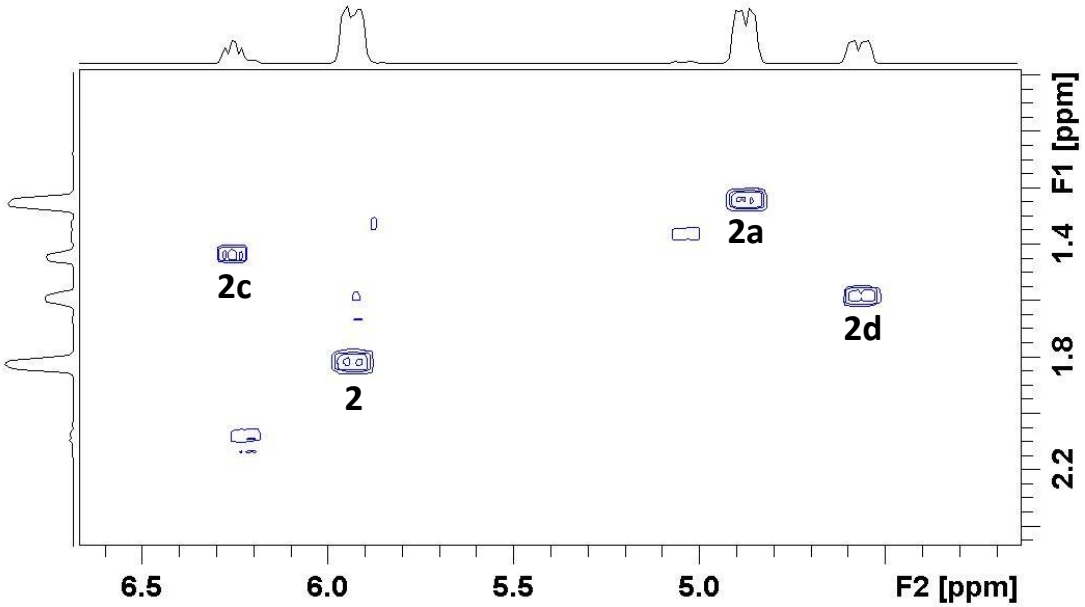

Figure 9. ^{1}H-^{1}H COSY NMR spectrum (400 MHz. acetone-d_6) of the purified product obtained during the synthesis of $[Mn(CO)_5(COCH(CH_3)(OCOCH_3)]$. The assignments of the **2c** and **2d** resonances are tentative.

The separation of the obtained crystals of **2a** permitted its ^{1}H NMR spectroscopic study as an individual species, yielding the resonances at δ 4.87 (q), 2.14 (s) and 1.24 (d) (see Figure 10), and thus allowing the assignment of these resonances in the NMR spectrum of the mixture shown in Figure 8.

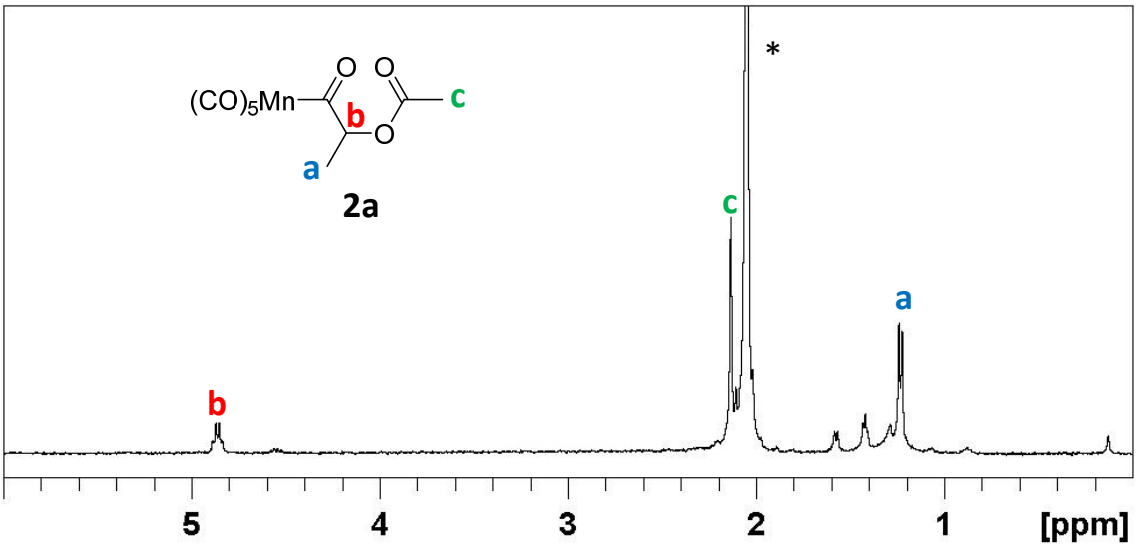

Figure 10. ^{1}H NMR spectrum (400 MHz, acetone-d_6) of compound **2a**.

Another attempt to synthesize compound **2** was performed adding the 1-bromoethyl acetate dropwise to the potassium pentacarbonylmanganate solution at

room temperature (30 °C). The solution was also stirred for 3 h. The solution color changed to brown and then to orange after 1 hour (Figure 11).

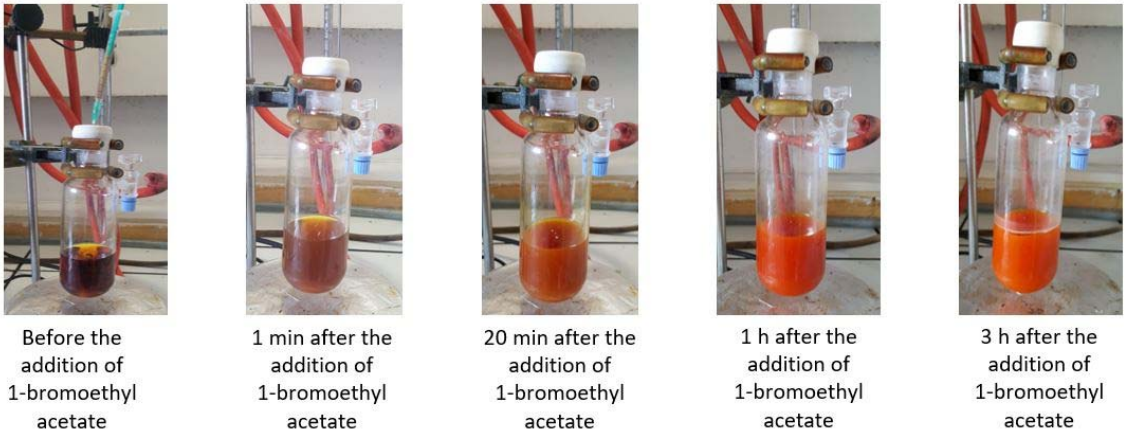

Figure 11. Pictures of the evolution after the addition of 1-bromoethyl acetate to the $K[Mn(CO)_5]$ solution.

The product was purified by column chromatography with silica gel and *n*-pentane as eluent to recover the first yellow fraction containing dimanganese decacarbonyl. Then the polarity of eluent was slightly increased using a mixture 95:5 of *n*-pentane and diethyl ether. Two more colored fractions were recovered: the first one led after evaporation to a yellow oil that was identified as the compound previously detected at δ 6.26 (q) and 1.44 (d), assigned to **2c** as explained below, as shown in the ^{1}H NMR spectrum (Figure 12). Unfortunately, this compound could not be crystallized and thus its structural assignment remains tentative. Finally, the second recovered fraction yielded a dark yellow-brownish oil, which corresponds to the expected alkyl compound **2** (^{1}H NMR resonances at δ 5.93 (q), 1.99 (s) and 1.81 (d)) as shown in Figure 13. This compound, upon storage in a hemolysis tube under argon in the fridge at 3 °C, yielded first a solid, and to the appearance of a few crystals several days later. The single-crystal X-ray diffraction analysis of one of them allowed its unambiguous identification as compound **2** (see Figure 14). Further details about the X-ray structure data can be found in the Appendix (Section A.1).

The similarity of the structure and electronic environment for the alkyl chain in compounds **2** and **2c** suggests that the resonances at δ 6.26 (q) and 1.44 (d) may be attributed to **2c**. Chelation of the carbonyl function in **2d**, on the other hand, should

more strongly perturb the resonances of the alkyl group. Thus, the NMR peaks at δ 4.56 (q) and 1.59 (d) are tentatively assigned to **2d** (see Figure 8).

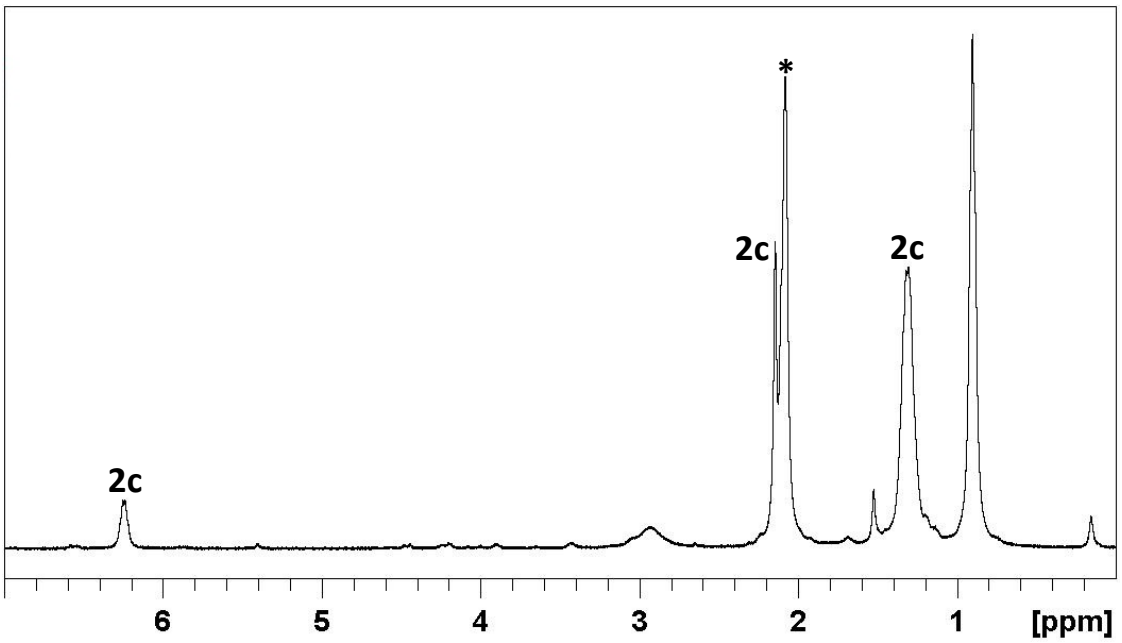

Figure 12. ^{1}H NMR (400 MHz, acetone-d_6) of fraction 2, probably corresponding to the compound **2c**. The starred resonance is due to the solvent.

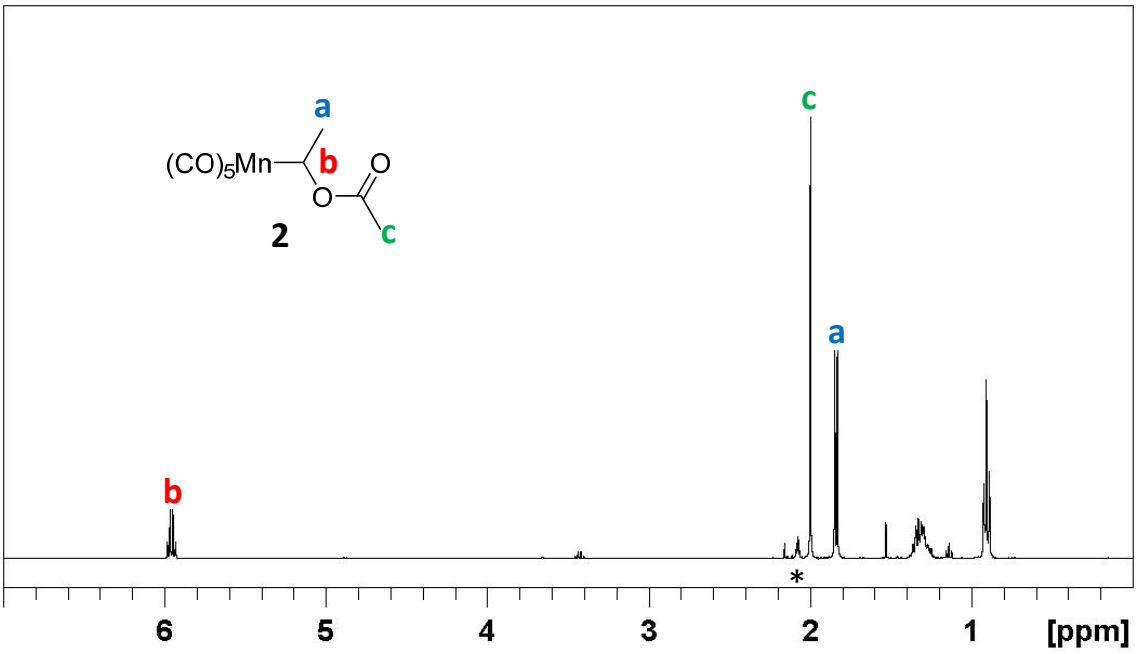

Figure 13. ^{1}H NMR spectrum (400 MHz, acetone-d_6) of fraction 3. The starred resonance is due to the solvent.

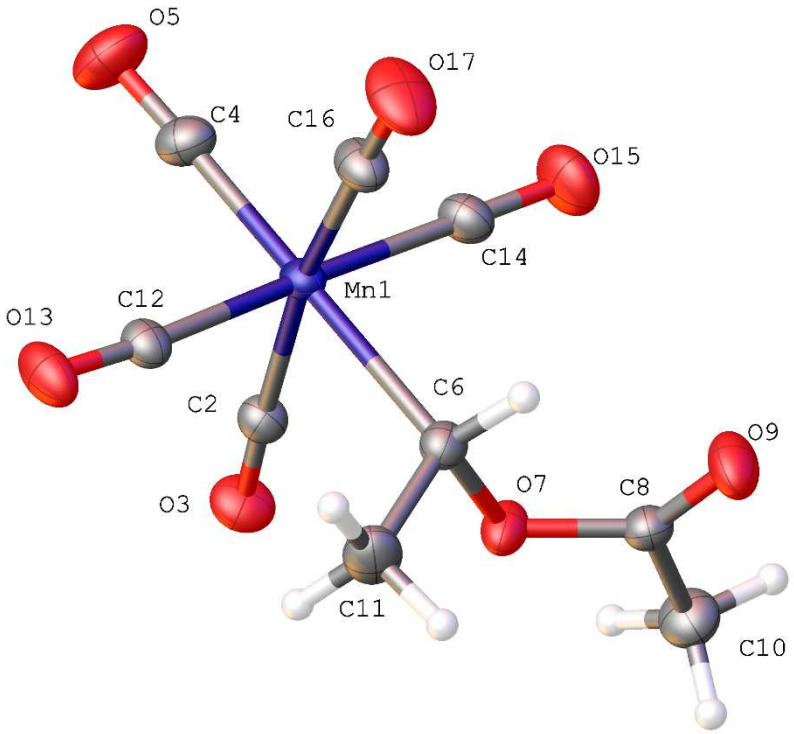

Figure 14. ORTEP view of compound **2**.

The FTIR spectrum of compound **2** in the carbonyl stretching region in *n*-pentane solution (Figure 15), like that of compound **1**, displays five main signals, one weak band at low wavenumber (1734 cm^{-1}) assigned to the ester carbonyl group, and four in the terminal metal carbonyl region (1900-2150 cm^{-1}), one more than the expected pattern for a $Mn(CO)_5$ moiety in ideal C_{4v} symmetry ($2A_1+E$), which is related to symmetry lowering, resulting in the appearance of the "forbidden" and therefore not very strong B_1 band (Table 3).

Table 3. FTIR carbonyl stretching bands of compound **2** in *n*-pentane solution.

Vibration mode	A_1	B_1	E	A_1	Acyl group
Wavenumber (cm^{-1})	2114 w	2052 m	2017 vs	1995 s	1734 w

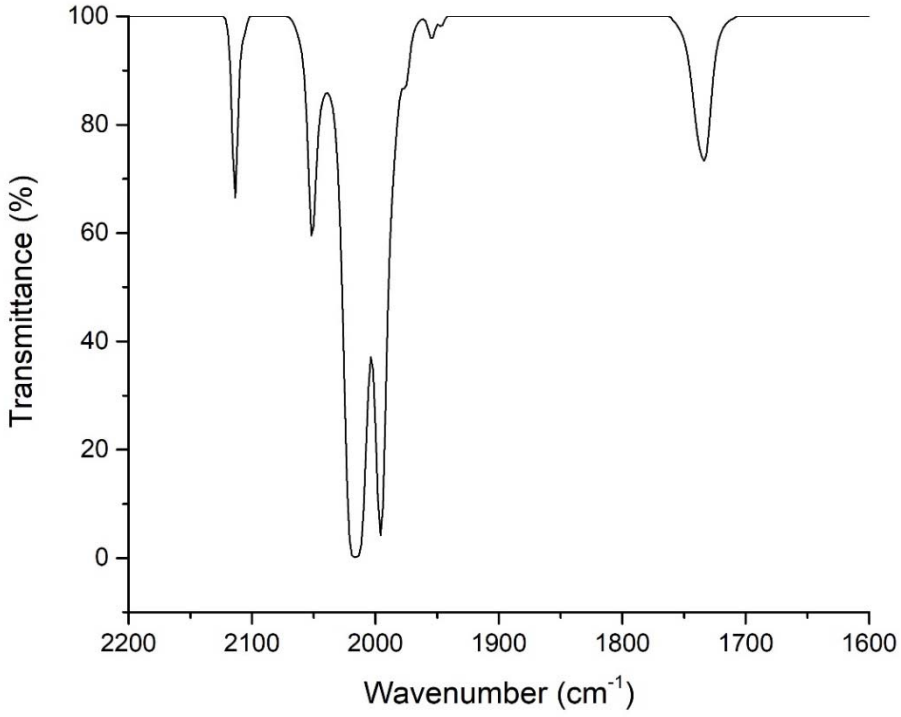

Figure 15. FTIR spectrum of compound **2** in the CO stretching region in *n*-pentane solution.

2.2.4. 1-Phenylethylpentacarbonylmanganese(I), **3**

The synthesis of $[Mn(CO)_5(CH(CH_3)(C_6H_5))]$ was attempted by the reaction of potassium pentacarbonylmanganate and 1-(bromoethyl)benzene *via* nucleophilic substitution (Scheme 4). However, this complex could not be isolated in a pure state.

1-(Bromoethyl)benzene was directly added dropwise to the filtered potassium pentacarbonyl manganate solution in THF at 0 °C under an argon atmosphere. The solution color changed to red. The mixture was stirred for 5 h, and then the solvent was evaporated under vacuum.

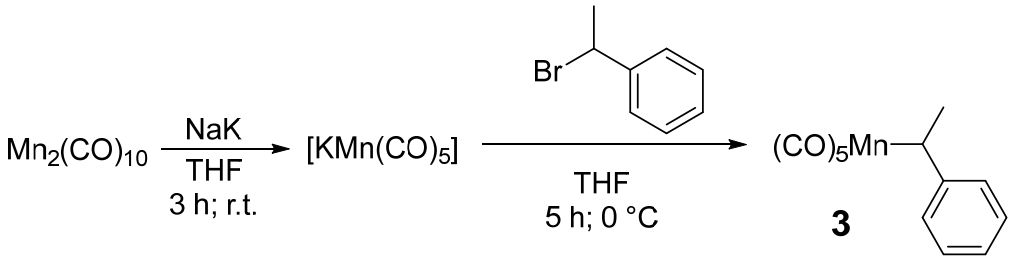

Scheme 4. Synthetic pathway employed to synthesized the compound **3**.

The first attempts to purify compound **3** were performed by a refrigerated column chromatography at -30 °C under an argon atmosphere using silica and neutral alumina as stationary phase and n-pentane as mobile phase. The crude reaction product was introduced as a solid deposit in the column chromatography because of its low solubility in *n*-pentane. As for compound **1** and **2**, the first yellow fraction corresponded to manganese carbonyl, then the polarity was slightly increased using a 95:5 mixture of *n*-pentane and diethyl ether. Thereafter, a second yellow fraction was recovered. The ^{1}H NMR spectrum shows the presence of at least two products in this fraction (Figure 16), both different from the 1-(bromoethyl)benzene (^{1}H NMR in acetone-d_6: δ 2.04, d; 5.40, q; 7.25-7.55, m). One of them may correspond to compound **3** or perhaps to the corresponding acyl complex **3a** as observed in a previous study.[7] The chemical shifts of this compound (δ 1.93, d; 3.35, q; 6.8-7.7, m), especially the quartet from the CH group, are rather similar to 3-phenyl-2-butanone (*cf.* ^{1}H NMR in CCl_4: δ 1.3, d; 3.6, q; 7.3, m),[14] indicating that this complex may indeed correspond to **3a** instead of **3**. However, the effect of manganese on the chemical shift is quite difficult to predict. Subsequent fractions contained a higher amount of the second major product of this mixture, allowing its identification by ^{1}H NMR (Figure 17) as 2-phenylpropanal (δ 9.67, d, 1H, J = 1.1 Hz; 7.44-7.16, m, 5H; 3.74, qd, 1H, J = 7 and 1.1 Hz; 1.39, d, 3H, J = 7 Hz; see Figure 16; *cf.* ^{1}H NMR in $CDCl_3$: δ 9.62, d, 1H, J = 1.5 Hz; 7.40-7.20 m, 5H; 3.55, qd, 1H, J = 7 and 1.5 Hz; 1.45, 3H, d, J = 7 Hz).[15] Probably this by-product was formed by migration of the alkyl chain to a CO ligand, followed by coordination of a ligand (probably the solvent, in this case the THF used during the synthesis or the diethyl ether used during the purification), leading to $[Mn(CO)_4(L)(COCH(CH_3)(C_6H_5))]$ (**3b**). This compound could subsequently react with a CO ligand, leading to $[Mn(CO)_5(COCH(CH_3)(C_6H_5))]$ (**3a**) as documented in a previous report and as proposed above for the formation of compound

2a.[7] Moreover, $[Mn(CO)_4(L)(COCH(CH_3)(C_6H_5))]$ could also react with the water present in the atmosphere or silica or alumina during the purification, yielding $[Mn(CO)_4(L)(OH)]$ and 2-phenylpropanal (Scheme 5). The addition of one equivalent of triphenylphosphine during the synthesis lead also to the formation of 2-phenylpropanal, in even higher yields.[7] In fact, the addition of a very coordinating ligand such as PPh_3 can promote the CO insertion.

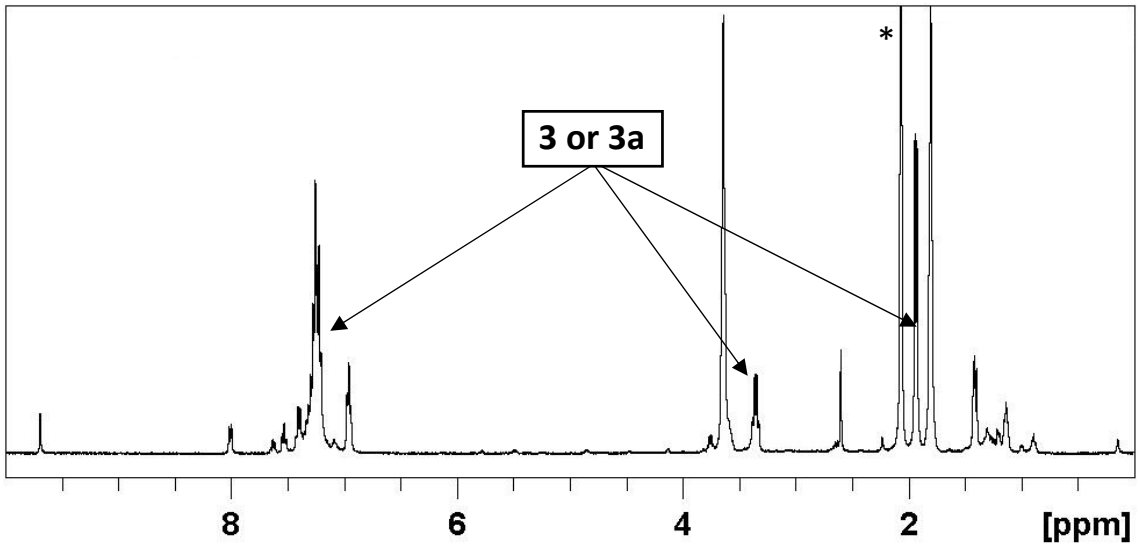

Figure 16. ^1H NMR spectrum (400 MHz, acetone-d_6) of compound **3 or 3a**, polluted by 2-phenylpropanal. The starred resonance is due to the solvent.

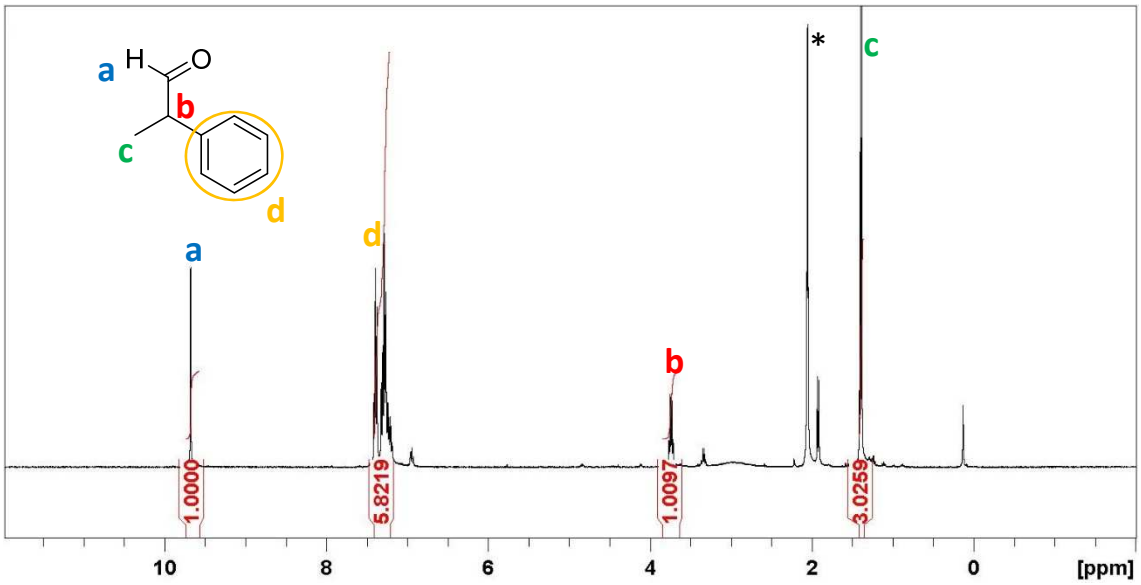

Figure 17. ^1H NMR spectrum (400 MHz, acetone-d_6) of 2-phenylpropanal isolated by the column chromatography. The starred resonance is due to the solvent.

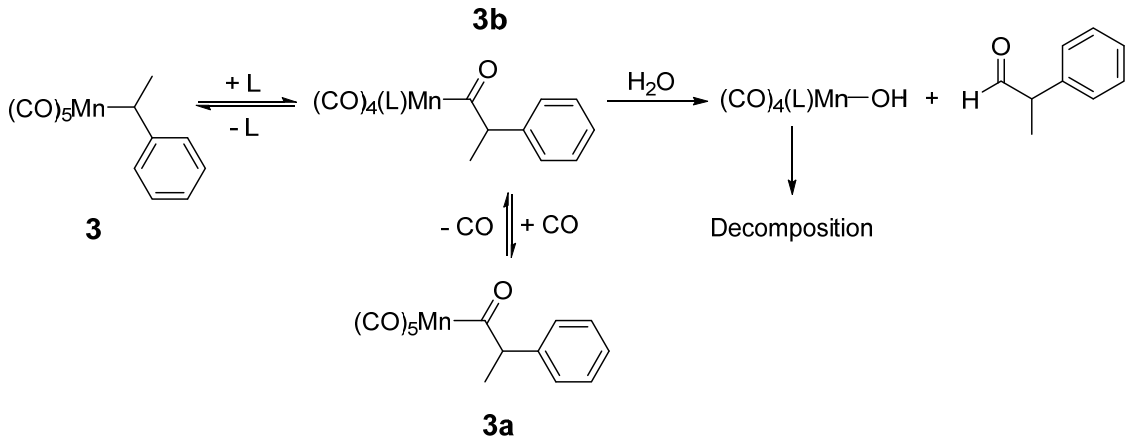

Scheme 5. Proposed mechanism for the formation of 2-phenylpropanoylpentacarbonylmanganese(I) and 2-phenylpropanal.

In view of the above result, which indicated the role of water in the compound decomposition, a subsequent purification attempt of compound **3** was performed by a column chromatography at -30 °C under argon using Florisil® (an activated magnesium silicate) as stationary phase and dried *n*-pentane as mobile phase. Florisil® is commonly used because, unlike the related adsorbents, such as alumina or silica gel, it contains less water and it appears to be without chemical effects on the adsorbed material, despite its slightly alkaline reaction in water,[16] therefore suggesting that the formation of 2-phenylpropanal may be avoided.

After the first yellow fraction of $[Mn_2(CO)_{10}]$, another brown-yellow fraction was collected, and evaporated under vacuum at -30 °C. The resulting residue was always maintained at this temperature under argon because of its high instability as previously reported.[7] The ^1H NMR analysis confirmed that the use of Florisil® prevented the formation of 2-phenylpropanal. However, the main product, supposedly 1-phenylethylpentacarbonylmanganes(I), could not be isolated in a pure state as revelated by FTIR and NMR spectroscopies.

The FTIR spectrum of compound **3** or **3a** (Figure 18 and Table 4) exhibits the characteristic bands of an alkylpentacarbonylmanganese(I) complex, showing the distinctive pattern for this complex family. The presence of an acyl band at 1600 cm^{-1} is characteristic of a carbonyl group in the alkyl chain. However, due to the low intensity of this signal and the pollution of the sample, it is not possible to be assured that it is the compound **3a**.

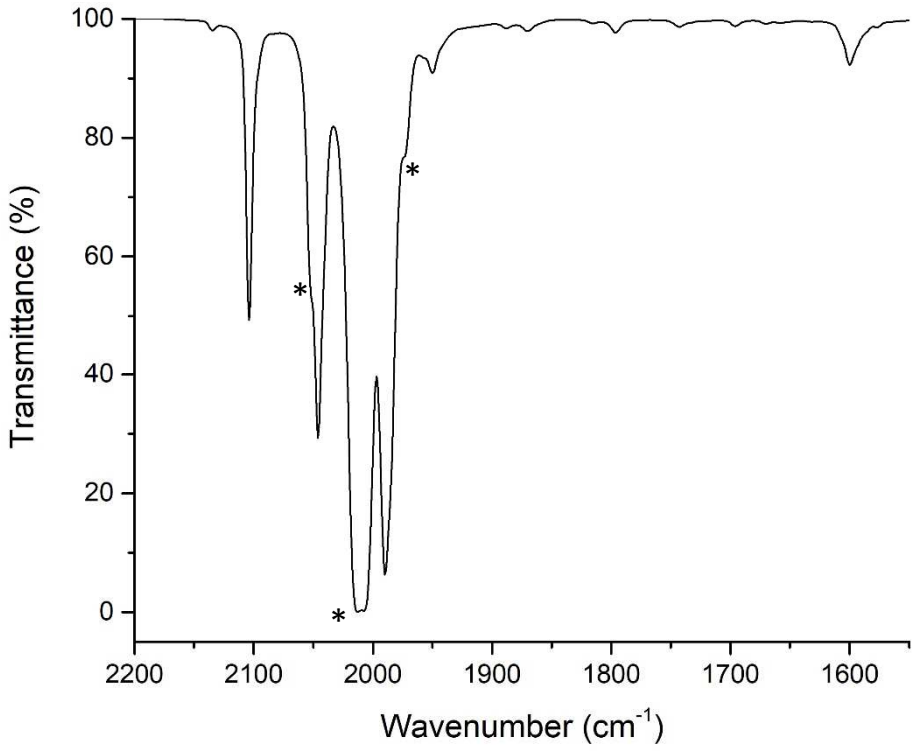

Figure 18. FTIR spectrum in the CO stretching region in *n*-pentane solution of the product resulting from the chromatographic separation on Florisil® at -30°C of the crude mixture from the attempted synthesis of **3.** The starred bands or shoulders are due to the $[Mn_2(CO)_{10}]$.

Table 4. FTIR carbonyl stretching bands in *n*-pentane solution of the product obtained in the synthesis of compound **3** or **3a**.

Vibration mode	**A_1**	**B_1**	**E**	**A_1**
Wavenumber (cm^{-1})	2104 m	2051 m	2008 vs	1990 s

Even though all the dimanganese decacarbonyl produced during the synthesis was removed in the first fraction of the chromatographic separation, this compound could still be observed in the FTIR spectrum of the second fraction (Figure 18, shoulder at 2046 and 1984 cm^{-1} and peak at 2015 cm^{-1}), probably due to the decomposition of compound **3** during purification in the chromatographic column. Moreover, several small signals were observed, some of them corresponding probably to the ^{13}C isotopomers, as the other complexes studied in this work. In addition, the presence of the corresponding acylpentacarbonylmanganese(I) complex (produced as suggested in Scheme 5) is

suggested by the presence of a weak carbonyl band at 1600 cm^{-1}. It is also possible to observe several small signals between 1700 and 1900 cm^{-1}, assigned to the overtones from the aromatic ring of the alkyl chain.

The ^{1}H NMR spectrum (Figure 19) displays signals of two different main products but no traces of 2-phenylpropanal was found when Florisil® was used for the chromatographic work-up. One of these compounds could correspond to the 1-phenylethylpentacarbonylmanganese(I) while the other one was attributed to 1-phenylethylbromide (^{1}H NMR 400 MHz in acetone-d_6: δ 2.04, d, $^{3}J_{HH}$ = 7 Hz, 3H; 5.40, q, $^{3}J_{HH}$ = 7Hz, 1H; 7.52-7.60, m, 5H).

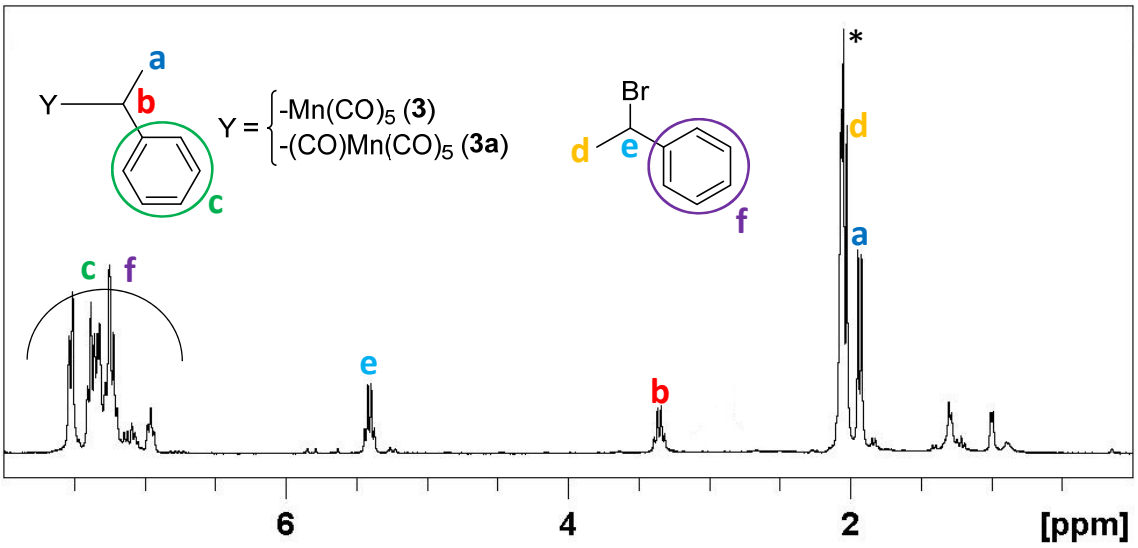

Figure 19. ^{1}H NMR spectrum (400 MHz, acetone-d_6) of compound **3** or **3a**, polluted by 1-(bromoethyl)benzene.

2.3. Conclusion

Three alkyl derivatives of pentacarbonylmanganese(I), $[Mn(CO)_5R]$ (R = $CH(CH_3)(COOCH_3)$, **1**; $CH(CH_3)(OCOCH_3)$, **2** and $CH(CH_3)(C_6H_5)$, **3**) have been prepared and investigated.

Compound **1** was previously reported in the literature by Casey *et al.*[5] as a by-product of the decarbonylation reaction of $[Mn(CO)_5(COCH_2CH_2COOCH_3)]$ but not

isolated and characterized. This contribution reports a synthetic pathway to obtain it in isolable quantities and in a pure state, and its complete characterization by FTIR and ^{1}H NMR spectroscopies.

Compound **2** has never been reported to the best of our knowledge. Its formation was accompanied by at least three other products. One of them, obtained in pure form and characterized by ^{1}H NMR and by single-crystal X-ray diffraction, was identified as the corresponding acyl complex (**2a**). A second attempt with different purification conditions led to the isolation of the pure compound **2**, which was characterized by ^{1}H NMR, FTIR and single-crystal X-ray diffraction.

Compound **3** was also previously reported (but not isolated in pure state) in a study of formation and cleavage of alkyl-transition-metal derivatives by Pearson's group.[7] The work reported here has also failed to produce this compound in a pure state, or at least to identify it, since the observed FTIR and ^{1}H NMR properties of the product mixture seem better consistent with the acyl derivative **3a**, although its formation seems confirmed since compound **3a** should be formed from compound **3**. It could not be isolated in a pure state, presumably because of their high aptitude to undergo the migratory insertion of the alkyl chain, followed by or in parallel to other decomposition processes (e.g. hydrolysis, homolytic bond cleavage). In addition, 2-phenylpropanal was detected as a decomposition product. A mechanism leading to the formation of this aldehyde has been proposed through the migration of the alkyl chain to a CO ligand, followed by ligand (probably solvent) coordination and final hydrolysis of the formed acyl compound by adventitious water. Indeed, the use of the less hydrated Florisil® stationary phase for the chromatographic separation of the product mixture avoided the formation of the aldehyde decomposition product.

2.4. Experimental section

General. All operations were carried out under an atmosphere of argon except for the purifications by column chromatography, which were carried out in air. For complex **3**, all operations including the column chromatography were carried out under an atmosphere of argon.

Materials. Compounds $[Mn_2(CO)_{10}]$ (98%, Strem Chemicals), methyl 2-bromopropionate (98%, Sigma-Aldrich), 1-bromoethyl acetate (95%, Fluorochem), tris(trimethylsilyl)silane (TTMSS, 97%, Sigma-Aldrich), 1,3,5-trioxane (99%, Fluorochem), benzene-d_6 (99.5%D, Euriso-top), acetone-d_6 (99.5%D, Euriso-top), silica gel (40-63 µm, VMR Chemicals), Florisil® (Sigma-Aldrich, 60-100 mesh) were used as received. Activated neutral alumina Brockmann I (Sigma-Aldrich) was dried under vacuum and at 200 °C before use. Laboratory Reagent grade (≥99.5%) diethyl ether, pentane and THF were purchased from Sigma-Aldrich. THF was purified by percolation through a dry activated alumina column. Potassium (98%, Aldrich) and sodium (≥99.8%, Aldrich) were washed in *n*-pentane to remove the mineral oil prior to use.

Single crystals of $[Mn(CO)_5(COCH(CH_3)(OCOCH_3))]$ and $[Mn(CO)_5(CH(CH_3)(OCOCH_3))]$ were obtained directly by storage of the product in a Schlenk tube or a hemolysis tube under an argon atmosphere in the fridge.

Instrumentation. The Nuclear Magnetic Resonance (NMR) spectra were recorded on a Bruker Avance™ III 400 MHz spectrometer. The instrumental parameters for recording ^1H NMR spectra were as follows: flip angle 30°, acquisition time 5.7 s, pulse delay 2 s, number of scans 64, and a pulse width of 3.05 µs. The Fourier transform infrared (FTIR) spectra on the *n*-pentane solutions were recorded in transmission mode with a PerkinElmer Spectrum One FT-IR Spectrophotometer using a CaF_2 window with a 4 mm thick and 0.05 mm path length.

Synthesis of 1-methyl-2-methoxy-2-oxoethylpentacarbonylmanganese(I), 1. In a Schlenk tube were introduced 400 mg (10.23 mmol) of metallic potassium and 250 mg (10.87 mmol) of metallic sodium under argon. They were crashed together to generate liquid "NaK" alloy. A solution of dimanganese decacarbonyl (2.00 g, 5.13 mmol) in 25 mL of dry THF was added and the resulting mixture was stirred for 3 h at room temperature. The mixture was filtered through Celite to yield a greenish-brown solution, rinsing the Celite with 10 mL of dry THF. Then, methyl 2-bromopropionate (1.71 g, 10.24 mmol) was added dropwise at room temperature, generating a brown solution, which subsequently turned to yellow. Solution was stirred at room temperature for 3 h, and then the solvent was evaporated under reduced pressure. The product was purified by column chromatography with a solid deposit through a silica gel column, using *n*-pentane as the mobile phase. After elimination of a first yellow fraction corresponding to $[Mn_2(CO)_{10}]$, the mobile phase polarity was increased using a 9:1 mixture of *n*-pentane and diethyl ether (9:1). Immediately a light-yellow fraction was collected, followed by evaporation to dryness under reduced pressure to afford the product as a yellow oil (1.13 g, 4.00 mmol, yield 39%).

Synthesis of 1-acetyloxyethylpentacarbonylmanganese(I), 2. In a Schlenk tube were introduced 300 mg (7.67 mmol) of metallic potassium and 250 mg (10.87 mmol) of metallic sodium under argon. They were crashed together to generate liquid "NaK" alloy. A solution of dimanganese decacarbonyl (1.50 g, 3.85 mmol) in 25 mL of dry THF was added and the resulting mixture was stirred for 3 h at room temperature. The mixture was filtered through Celite to yield a greenish-brown solution, rinsing the Celite with 5 mL of dry THF. Then, 1-bromoethyl acetate (1.27 mg, 7.60 mmol) was added dropwise at room temperature, generating an orange solution, which subsequently turned to bright red. The solution was stirred at room temperature for 3 h, and then the solvent was evaporated under reduced pressure. The product was purified by column chromatography with a solid deposit through a silica gel column, using *n*-pentane as the mobile phase. After elimination of a first yellow fraction corresponding to $[Mn_2(CO)_{10}]$, then the mobile phase polarity was slightly increased using a 95:5 mixture of *n*-pentane and diethyl ether. Two more fraction were then recovered, the first one yielding, after

evaporation to dryness, an unidentified product as a yellow oil and the second one yielding complex **2** as a yellow-brownish oil that became a solid upon cooling in the refrigerator at 3 °C (360 mg, 1.28 mmol, yield 17%).

Synthesis of 1-phenylethylpentacarbonylmanganese(I), 3. In a Schlenk tube were introduced 200 mg (5.12 mmol) of metallic potassium and 150 mg (6.52 mmol) of metallic sodium under argon. They were crashed together to generate liquid "NaK" alloy. A solution of dimanganese decacarbonyl (1.01 g, 2.59 mmol) in 20 mL of dry THF was added and the resulting mixture was stirred for 3 h at room temperature. The mixture was filtered through Celite to yield a greenish-brown solution, rinsing the Celite with 5 mL of dry THF. Then, 1-phenylethylbromide (922 mg, 4.98 mmol) was added dropwise at room temperature, generating a red solution. It was stirred at 0 °C for 5 h, and then the solvent was evaporated under reduced pressure. The product was purified by column chromatography under argon and refrigerated at -30 °C. The product was introduced by a cannula after evaporation of almost all the solvent under vacuum. Then *n*-pentane was used as mobile phase. After elimination of a first yellow fraction corresponding to $[Mn_2(CO)_{10}]$, the mobile phase polarity was increased using a 9:1 pentane and diethyl ether mixture. Fractions were collected under argon and kept at -30 °C. Since the product is not pure, a yield cannot be calculated for this reaction.

2.5. References

[1] R. D. Closson; J. Kozikowski; T. H. Coffield *J. Org. Chem.* **1957**, *22*, 598.
[2] R. B. King *Acc. Chem. Res.* **1970**, *3*, 417-427.
[3] J.-A. M. Andersen; J. R. Moss *Organometallics* **1994**, *13*, 5013-5020.
[4] A. P. Masters; T. S. Sorensen *Can. J. Chem.* **1990**, *68*, 492-501.
[5] C. P. Casey; W. R. Brunsvold; J. Koch *Inorg. Chem.* **1976**, *15*, 1991-1993.
[6] M. P. Cooke; R. M. Parlman *J. Am. Chem. Soc.* **1975**, *97*, 6863-6865.
[7] R. W. Johnson; R. G. Pearson *J. Chem. Soc., Chem. Commun.* **1970**, 986-987.
[8] R. B. King *J. Inorg. Nucl. Chem.* **1963**, *25*, 1296-1298.
[9] M. L. H. Green; P. L. I. Nagy *J. Organomet. Chem.* **1963**, *1*, 58-69.
[10] T. E. Gismondi; M. D. Rausch *J. Organomet. Chem.* **1985**, *284*, 59-71.
[11] T. L. Bent; J. D. Cotton *Organometallics* **1991**, *10*, 3156-3160.
[12] J.-A. M. Andersen; J. R. Moss *J. Organomet. Chem.* **1992**, *439*, C25-C27.
[13] K. Noack; U. Schaerer; Calderaz.F *J. Organomet. Chem.* **1967**, *8*, 517-526.
[14] J. C. Gilbert; D. H. Giamalva; U. Weerasooriya *J. Org. Chem.* **1983**, *48*, 5251-5256.
[15] M. W. C. Robinson; K. S. Pillinger; I. Mabbett; D. A. Timms; A. E. Graham *Tetrahedron* **2010**, *66*, 8377-8382.
[16] N. S. Radin In *Methods in Enzymology*; Academic Press: 1969; Vol. 14, p 268-272.

Chapter 3

Fluoroalkylpentacarbonyl-manganese(I) complexes

Outline:

3.Fluoroalkylpentacarbonylmanganese(I) complexes

3.1. Introduction

The aim of this chapter is the synthesis and characterization of four fluoroalkylpentacarbonylmanganese(I) complexes. Some of these complexes constitute a well-known family of organometallic compounds but new members, modeling the dormant chains of PVDF, have also been synthesized and fully characterized.

In addition, a deeper investigation on the synthesis and especially the characterization of the already known complexes has been achieved. For instance, an additional value of the present study is the symmetry analysis of the $[Mn(CO)_5R_F]$ carbonyl stretching vibrations, including those of the two major ^{13}C isotopomers, $[Mn(^{12}CO)_4(eq\text{-}^{13}CO)R_F]$ and $[Mn(^{12}CO)_4(ax\text{-}^{13}CO)R_F]$, by a combined experimental and DFT study with an unprecedented level of detail. All the complexes presented in this chapter were synthesized following the synthetic pathway shown in Scheme 1.

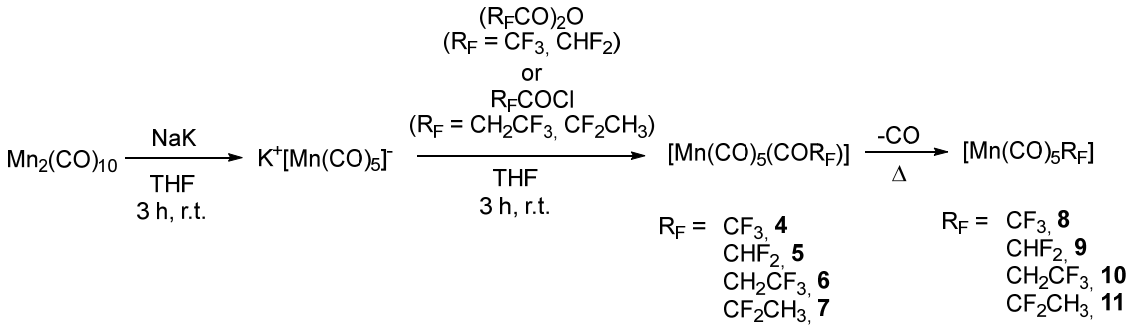

Scheme 1. General synthetic pathway of fluoroalkylpentacarbonylmanganese(I) complexes.

The acyl compounds **4** and **5** and the corresponding alkyl derivatives **8** and **9** were synthesized according to the literature procedure, with minor modifications.[1,2] For all other synthesized compounds, the purification steps were found more effective, faster and higher-yielding if carried out by column chromatography rather than by sublimation as in most of the previous reports. The new derivatives with R_F = CH_2CF_3 and CF_2CH_3 were obtained by a similar procedure, namely addition of *in-situ* generated $[Mn(CO)_5]^-$ to 3,3,3-trifluoropropanoyl chloride, CF_3CH_2COCl, and 2,2-difluoropropanoyl chloride, CH_3CF_2COCl, respectively, to yield the acyl derivatives **6** and **7**, which were then decarbonylated to the alkyl derivatives **10** and **11**. Both compounds with the CH_2CF_3 group (**6** and **10**) were isolated and fully characterized. The decarbonylation of **6** proceeded smoothly by heating at 70 °C and the alkyl product **10** was recovered in acceptable yields. It is to be noted that the more direct reaction between $[Mn(CO)_5]^-$ and CF_3CH_2I failed to produce **10**, giving instead a complex mixture, in which $[Mn(CO)_5I]$ was a major compound, identified by single crystal X-Ray diffraction. Quite clearly, the presence of three F atoms on the β-C atom is sufficient to invert the polarity of the C-I bond as when they are located on the α-C atom. The decarbonylation of **7**, on the other hand, was not successful under any of the employed conditions (different temperatures, times and solvents). The target product **11** was indeed formed, as indicated by the spectroscopic data (*vide infra*), but subsequently decomposed upon prolonged heating before completion of the acyl precursor decarbonylation. The reason for this behavior is presumably the weaker homolytic Mn-C bond strength in **11**, as suggested by DFT calculations (see Chapter 4),[3] resulting in a competition between the rate of thermal decarbonylation leading from **7** to **11** and the rate of product decomposition. Moreover, compound **11** is the only fluoroalkylpentacarbonylmanganese(I) complex synthesized in this study that contains hydrogen atoms in the β-position, promoting the β-H elimination after a carbonyl dissociation.

In all syntheses, the first step was the reduction of the dimanganese decacarbonyl precursor to the potassium pentacarbonylmanganate salt. This step was detailed in the previous chapter, Section 2.2.1. Then, the subsequent synthetic steps and the characterizations will be detailed for each complex, especially in the case of $[Mn(CO)_5(CF_3)]$ (complex **8**), which is more carefully detailed in Section 3.2.1.

3.2. Results and discussion

3.2.1. Trifluoromethylpentacarbonylmanganese(I), **8**

$[Mn(CO)_5(CF_3)]$ (compound **8**) was synthesized by decarbonylation of its acyl analogue, $[Mn(CO)_5(COCF_3)]$ (compound **4**). The acyl complex was synthesized from the potassium pentacarbonylmanganate salt solution in THF with trifluoroacetic anhydride (TFAA), as reported in the literature.[1,2] Several minor changes have been carried out to improve the reaction time, purity and yield.

3.2.1.1. Synthesis of trifluoroacetylpentacarbonylmanganese(I), **4**

Once the filtered solution of $K[Mn(CO)_5]$ was ready (see Chapter 2 Section 2.2.1), the stoichiometric amount of TFAA was added dropwise. In this case, the use of the anhydride instead of the acyl chloride is preferable since trifluoroacetyl chloride is a gas at room temperature while the anhydride is a liquid. During the addition, the color changed quickly to dark red, and the generation of a white smoke was visible inside the Schlenk tube. Then, 5 min after the addition, the color turned red and then orange. After 30 min, it became dark yellow and the final color was yellow (Figure 1).

The purification was carried out with a column chromatography with standard silica gel as stationary phase and with *n*-pentane as mobile phase to remove the $[Mn_2(CO)_{10}]$ by-product (Figure 2). Since the solubility of complex **4** in *n*-pentane is not high, it is preferable to introduce the crude product as a solid deposit dissolving the crude product in acetone, then adding a small amount of silica gel and finally removing the solvent. Then, using *n*-pentane (which is a good solvent for $[Mn_2(CO)_{10}]$) as eluent, a first yellow fraction was eluted quickly. Then the eluent polarity was increased using a 9:1 mixture of *n*-pentane and diethyl ether to promote the migration of complex **4**. Once the solvent was completely removed, **4** was recovered as a white or white-yellowish powder, with

a high tendency to crystallize in the flask as white needle-shape crystal (Figure 3). The best yield obtained in this reaction was 81%.

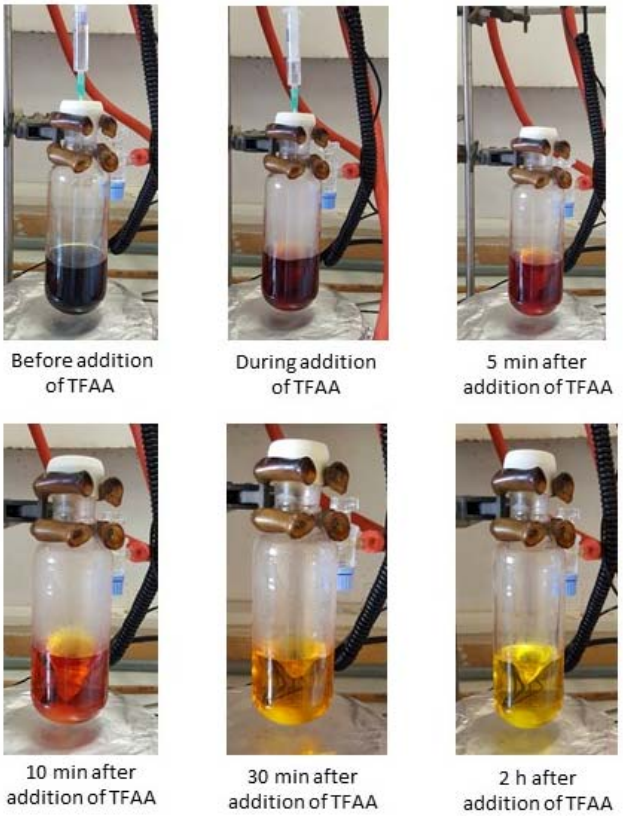

Figure 1. Pictures of the evolution after the addition of TFAA to the $K[Mn(CO)_5]$ solution.

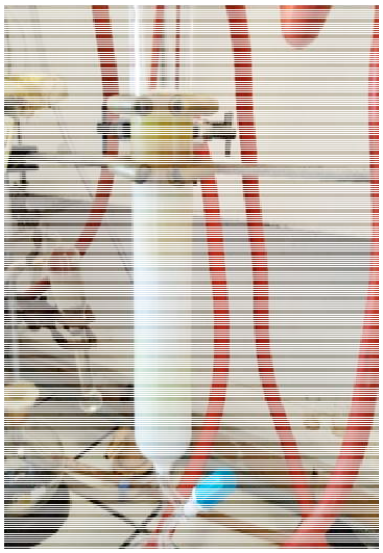

Figure 2. Picture of the column chromatography used to purify complex **4**.

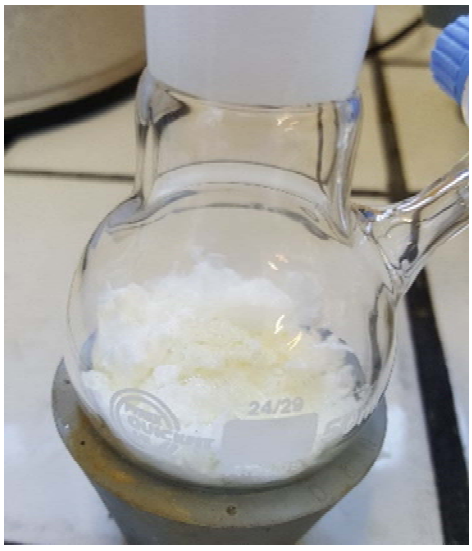

Figure 3. Picture of complex **4** obtained after purification by column chromatography. The volatile complex can crystallize directly after evaporation of the solvent, leading a crystalline powder with needle-shape crystals.

Compound **4** can be also purified by sublimation using a cold finger condenser. The bottom of the sublimator was heated to 55 °C under a static vacuum of 100 mbar. The product was recovered from the bottom of the cold finger condenser several times. This process was much slower than the column chromatography, requiring several days of sublimation. This method led to the formation of big needle-shape crystals on the cold finger condenser. A major drawback of this purification method is the difficulty to completely remove $[Mn_2(CO)_{10}]$ because this compound also has low volatility and co-sublimes with compound **4**.

3.2.1.2. Characterization of compound **4**

Although $[Mn(CO)_5(COCF_3)]$ has been known since 1959,[4,5] its ^{19}F and ^{13}C NMR properties had not been previously described. The ^{19}F NMR spectrum (Figure 4) shows a singlet at -81.9 ppm, which is an expected chemical shift for a CF_3 group next to a carbonyl group (e.g. CF_3COOH; δ -78.5 ppm).[6] No other peaks are present in the full spectrum. The ^{13}C NMR spectrum (Figure 5) displays a binomial (1:3:3:1) quartet, as expected, because of coupling to three equivalent F atoms at 115.0 ppm with a high coupling constant ($^1J_{CF}$ = 302 Hz). A broad peak is also observed at 207.3 ppm, attributed to the carbonyl ligands and probably also to the acyl carbonyl group.

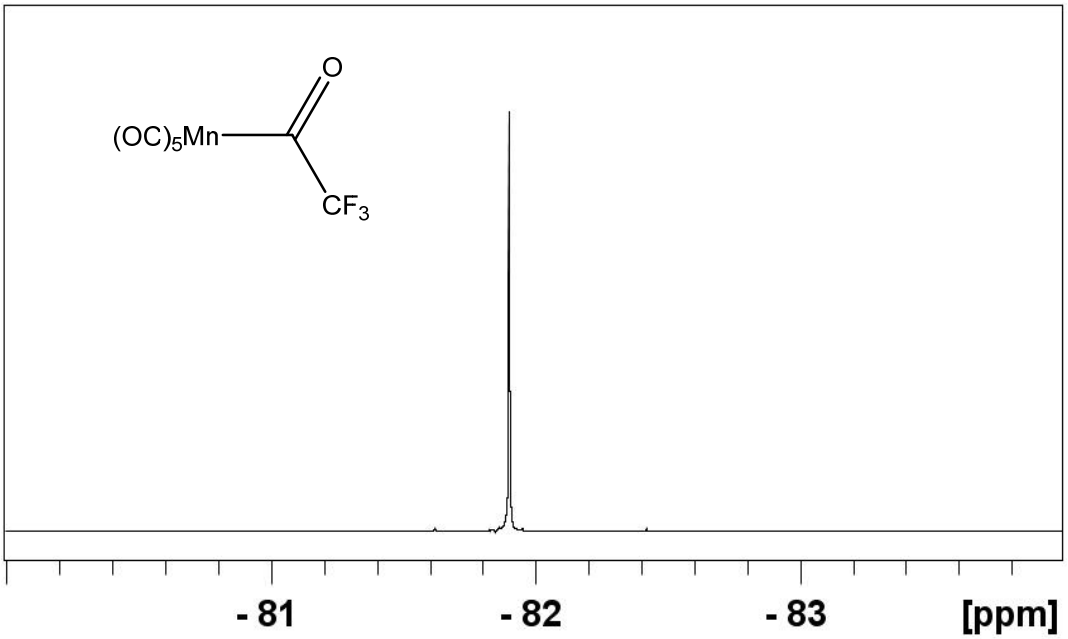

Figure 4. ^{19}F NMR spectrum (376.5 MHz, acetone-d_6) of compound **4**.

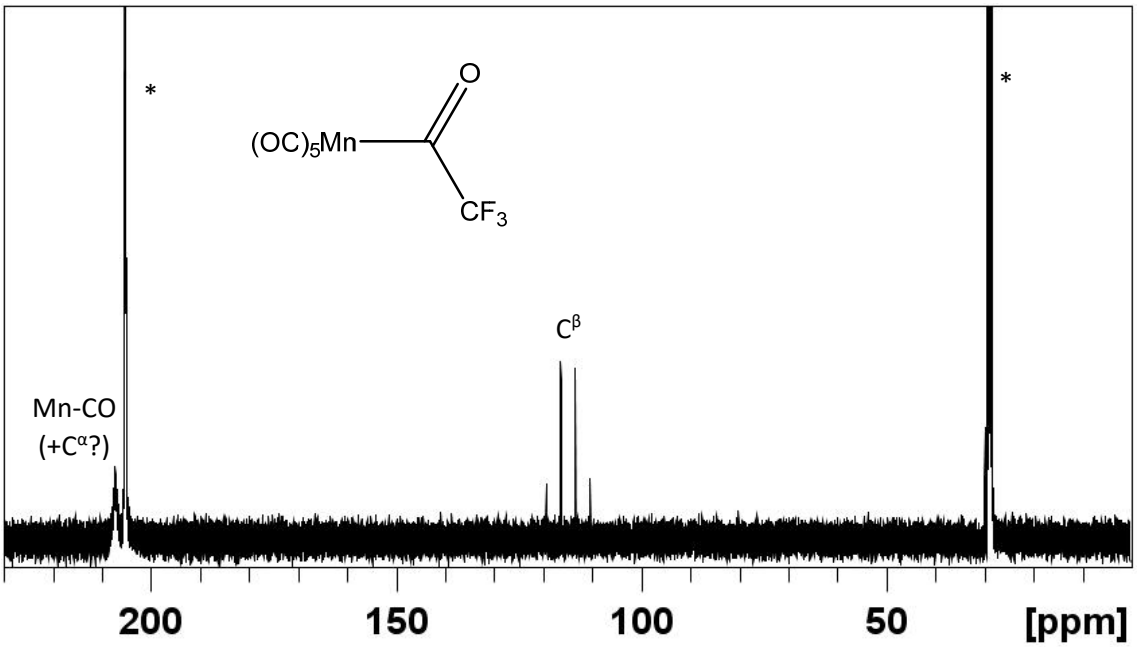

Figure 5. ^{13}C NMR spectrum (100.6 MHz, acetone-d_6) of compound **4**. The starred resonances are due to the solvent.

The FTIR spectrum of complex **4** in a *n*-pentane solution is shown in Figure 6. Previously, the IR properties of this compound had only been reported in the solid state (KBr pellet) with bands at 2139 (w-m), 2035 (vs) and 2002 (m, sh) cm^{-1}, assigned to the three bands expected for a $Mn(CO)_5$ vibrator in C_{4v} symmetry (A_1, E and A_1, respectively), plus a lower frequency band at 1643 cm^{-1} (m-s) for the acyl group.[7] These bands are also visible at similar frequencies (see values in Table 1) in the solution spectrum of Figure 6.

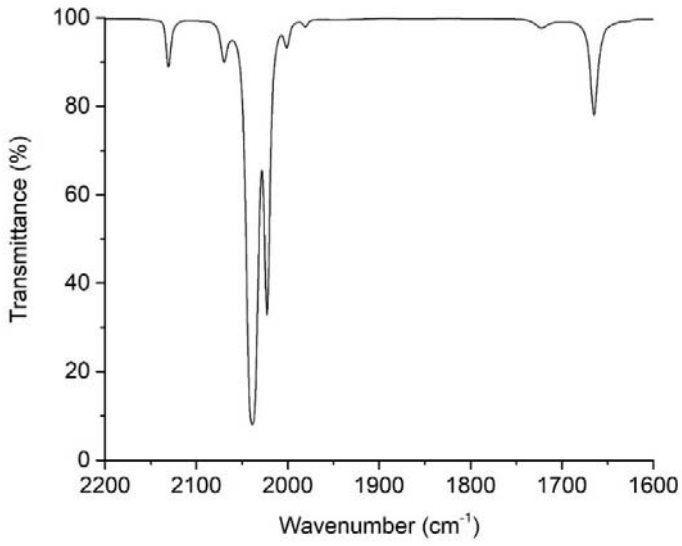

Figure 6. FTIR spectrum of complex **4** in the carbonyl stretching region in *n*-pentane solution.

Table 1. FTIR carbonyl stretching bands in *n*-pentane of complex **4**.

Vibration mode	A_1	B_1	E	A_1	Acyl group
Wavenumber (cm^{-1})	2131 w	2070 w	2039 vs	2023 s	1722 vw, 1665 w

However, the solution spectrum shows several additional bands. These cannot originate from by-products that contain the fluoroalkyl groups because the compound was spectroscopically pure (^{13}C, ^{19}F NMR). Certain bands probably derive from the presence of rotational isomers, as previously shown in the literature for other similar compounds,[8] for instance the second smaller band at low frequency (1722 cm^{-1}). Indeed, the timescale of the infrared technique is much faster than that of the NMR analysis. Therefore, different conformations that exchange very rapidly and give only averaged NMR spectra can produce distinct responses on the infrared timescale. Other bands may originate from symmetry lowering. In fact, if the rotation of the R_F group around the Mn-R_F axis is slow enough on the infrared timescale, the local symmetry of the $Mn(CO)_5$ group will be reduced to C_s or even C_1. Then, the forbidden (in C_{4v}) B_1 band can become observable as a weak band and the degenerate E band can split into two separate bands. In the spectrum of Figure 6, the strongest absorption of E type still appears as a single band, but the weak additional band at 2070 cm^{-1} is assigned to the "forbidden" B_1 band, by analogy with the previous assignment to similar compounds, e.g. $[Mn(CO)_5(CHF_2)]$ (see also below).[8] Finally, other weak bands may originate from isotopomers containing ^{13}C. This point will be analyzed more in detail for the fluoroalkyl derivatives in Section 3.2.5.

Complex **4** has not been previously structurally characterized. The crystal structure has been determined by X-ray diffraction during this thesis (Figure 7). A single crystal was obtained directly from the cold finger of the sublimator (55 °C, 100 mbar). Further details about the X-ray structure data can be found in Section 3.2.6 and in the Appendix (Section B.1).

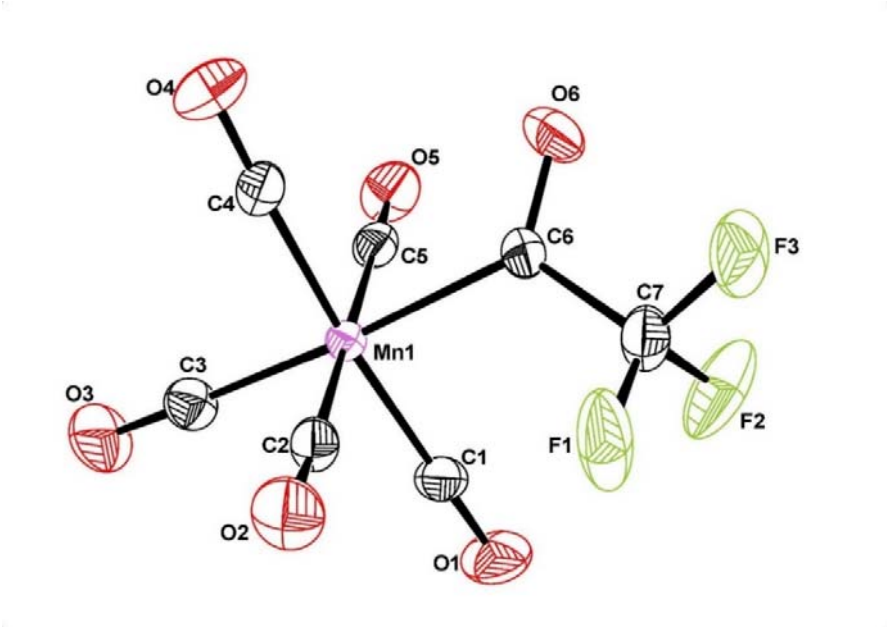

Figure 7. ORTEP view of compound **4**.

3.2.1.3. Synthesis of trifluoromethylpentacarbonylmanganese(I), **8**

Complex **8** was synthesized directly by decarbonylation of **4**. For this, a two-neck flask with a septum on one neck was connected to a condenser with a bubbler. The condenser was used to avoid loss of the complex by sublimation. The system was purged with argon for 15 minutes. Then, the two-neck flask was heated-up to 120 °C during 1.5 hours (or until the bubbling stopped). During this process, the complex melted and the color change progressively to yellow, probably due to the formation of a little amount of dimanganese decacarbonyl. Subsequently, the crude product was purified by column chromatography with silica gel as stationary phase and *n*-pentane as mobile phase. As for complex **4**, the solubility of compound **8** in *n*-pentane is not very high, so it is preferable to introduce it in the column as a solid deposit. A dimanganese decacarbonyl band was first eluted by *n*-pentane, then the eluent polarity was increased to a 9:1 mixture of *n*-pentane and diethyl ether to promote the migration of compound **8**. After solvent evaporation, a white volatile powder was obtained in 73% yield. The global yield for this synthesis (starting from $[Mn_2(CO)_{10}]$ and TFAA) was 59%.

Like compound **4**, compound **8** can also be purified by sublimation using the same conditions (sublimator equipped with a cold finger condenser at 100 mbar of static vacuum and heating the bottom of the sublimator at 55 °C).

3.2.1.4. Characterization of complex **8**

The ^{19}F NMR spectrum (376.5 MHz, acetone-d_6, Figure 8) shows only one peak at 5.65 ppm. This downfield shift, relative to the resonance of the acyl precursor **4** at -81.9 ppm, is a consequence of direct coordination of the alkyl group to the metal atom.

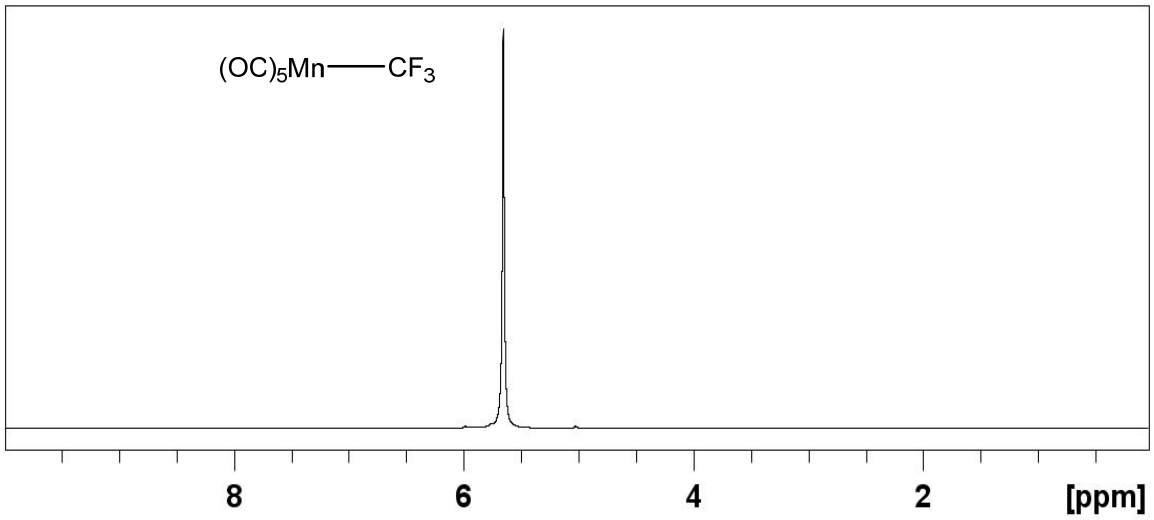

Figure 8. ^{19}F NMR spectrum (376.5 MHz, acetone-d_6) of compound **8**.

The ^{13}C NMR spectrum (Figure 9) presents a binomial quartet as expected at 153.3 ppm with a $^2J_{CF}$ = 355 Hz. Despite the high number of scans (10240) and the high concentration of the complex in the tube, the signal intensity of the carbon of the CF_3 group was very low for compound **8**.

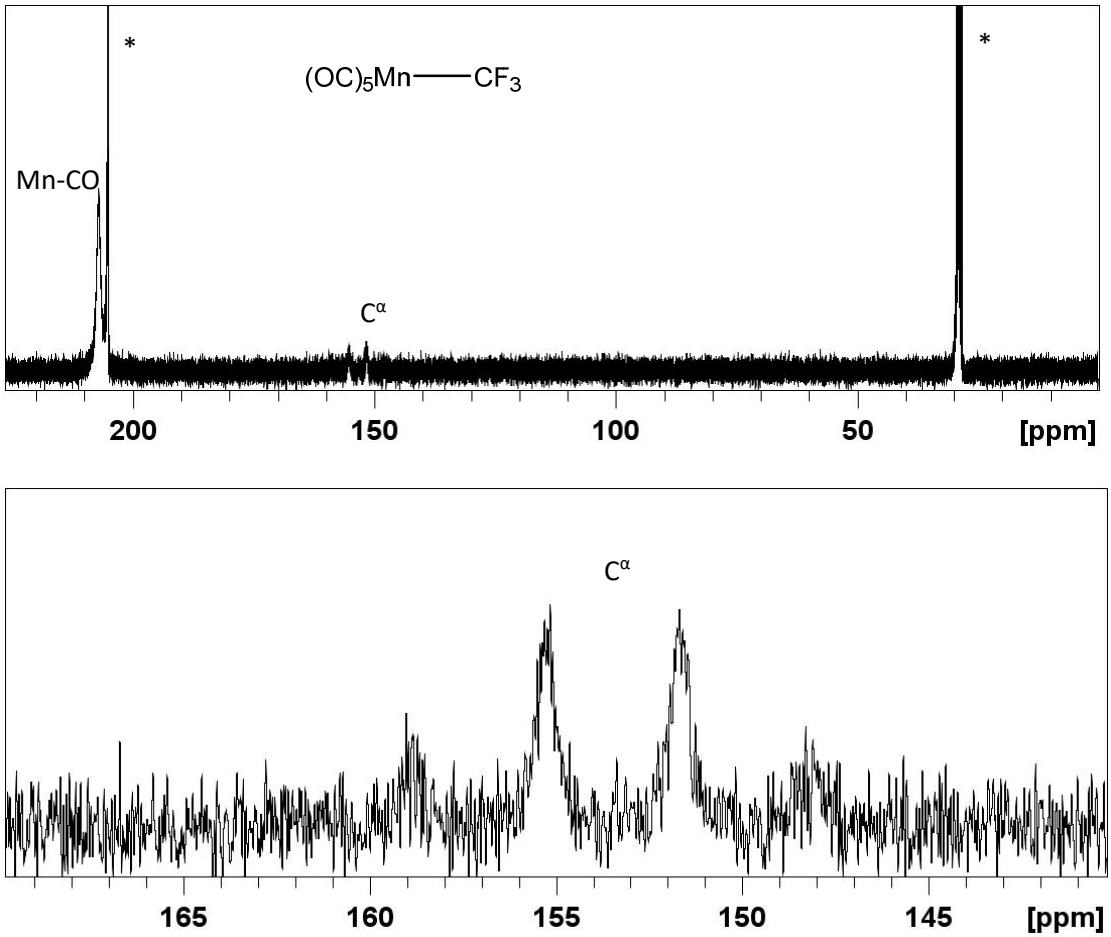

Figure 9. ^{13}C NMR spectra (100.6 MHz, acetone-d_6) of compound **8**: full spectrum above and expansion of the 140-170 ppm region below. The starred resonances are due to the solvent.

As for compound **4**, the FTIR spectrum of compound **8** (Figure 10) exhibits three main peaks in the carbonyl stretching region, associated to the three expected ones ($2A_1$+E) for the $Mn(CO)_5$ moiety in ideal C_{4v} symmetry, at the values reported in Table 2. These correspond closely to the values already reported in the literature for this compound in heptane[9] and in cyclohexane[10] solutions. In addition, the spectrum also shows several other small peaks or shoulders. One of these small peaks is a very weak band at 2075 cm^{-1}, corresponding to the "forbidden" B_1 band which becomes visible because of the lowering symmetry (Table 2). This was confirmed in a previous study by a Raman study, where this band becomes allowed.[10] A deeper discussion of the origin and assignment of the other weak bands is available later in Section 3.2.5. On the other hand, the carbonyl bands from the acyl group in **4** have completely disappeared, meaning that the decarbonylation was quantitative.

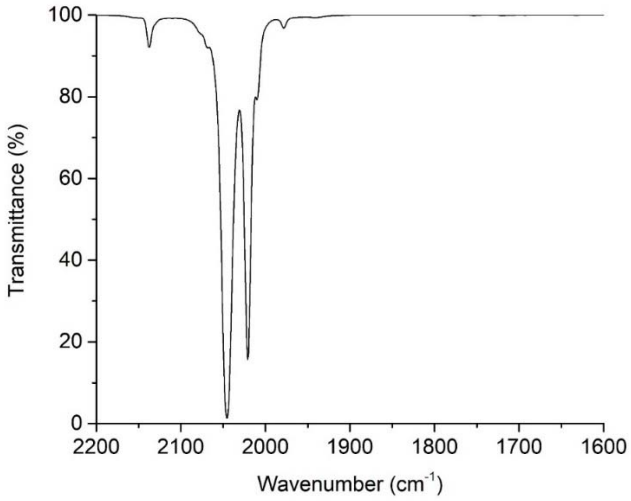

Figure 10. FTIR spectrum of compound **8** in the carbonyl stretching region in *n*-pentane solution.

Table 2. FTIR carbonyl stretching bands in *n*-pentane of complex **8**.

Vibration mode	A_1	B_1	E	A_1
Wavenumber (cm^{-1})	2137 w	2075 vw	2045 vs	2021 s

Like its precursor **4**, compound **8** has been known for quite some time but had not been structurally characterized. Its crystal structure has been determined in this work (Figure 11). Crystals were obtained directly from the cold finger of the sublimator (55 °C, 100 mbar). More details about the X-ray structure data can be found in Section 3.2.6 and in the Appendix (Section B.4).

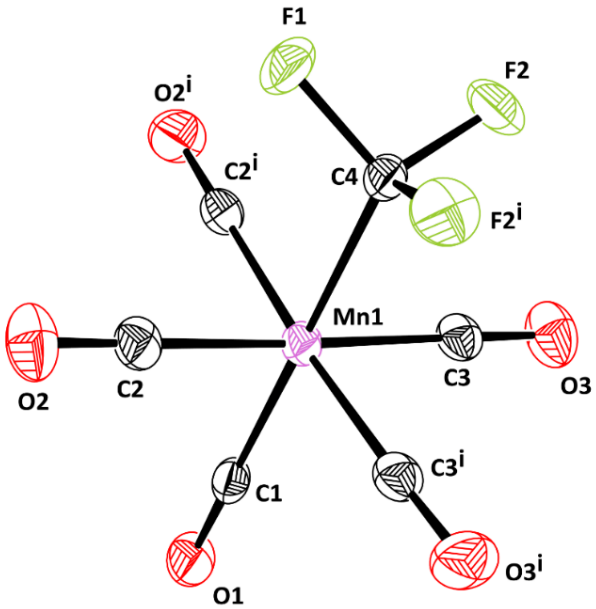

Figure 11. ORTEP view of compound **8**.

3.2.2. Difluoromethylpentacarbonylmanganese(I), **9**

$[Mn(CO)_5(CHF_2)]$ (compound **9**) was synthesized by decarbonylation of $[Mn(CO)_5(COCHF_2)]$ (compound **5**). The acyl complex was produced from the potassium pentacarbonylmanganate salt solution in THF with difluoroacetic anhydride (DFAA) as reported in the literature,[1,2] with some minor changes to improve the reaction time, purity and yield. These changes will be detailed below. DFFA was synthesized from difluoroacetic acid and phosphorous pentoxide as described in the literature.[11]

3.2.2.1. Synthesis of difluoroacetylpentacarbonylmanganese(I), **5**

Once the solution of $K[Mn(CO)_5]$ (obtained as described above in Chapter 2 Section 2.2.1) was filtered, the stoichiometric amount of DFAA was added dropwise (for more details about the synthesis of DFAA from the difluoroacetic acid and phosphorous pentoxide, refer to the experimental part). During the addition, the color quickly changed to red, then orange and it finally turned to light orange (Figure 12).

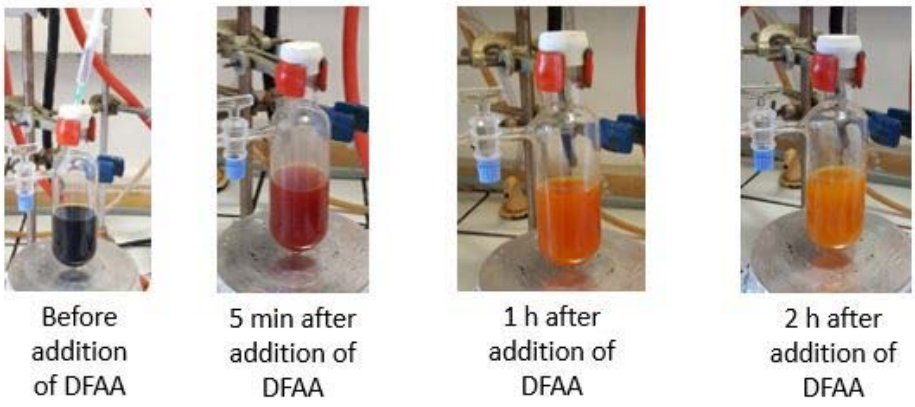

Figure 12. Pictures of the evolution of the solution by the addition of DFAA to the $K[Mn(CO)_5]$ solution.

Compound **5** was purified through column chromatography with silica gel as stationary phase and with *n*-pentane as mobile phase. The crude reaction was introduced in the column chromatography as a solid deposit because of the low solubility of the complex in *n*-pentane. A first yellow fraction was obtained

corresponding to $[Mn_2(CO)_{10}]$. A subsequent switch to a 9:1 mixture of *n*-pentane and diethyl ether mixture led to the elution of the desired product.

After solvent evaporation, the neat **5** is usually recovered as a yellow-brownish oil (Figure 13) that becomes a solid immediately by scratching the flash walls with a spatula. However, the product may also form directly as a light brown powder. After purification, the yield of this reaction was 75%. As for compounds **4** and **8**, compound **5** can be also purified by sublimation (100 mbar, 55 °C).

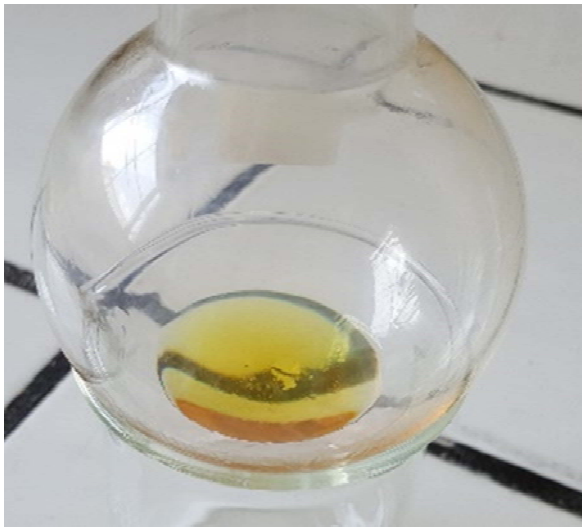

Figure 13. Picture of the purified $[Mn(CO)_5(COCF_2H)]$ as an oil.

3.2.2.2. Characterization of compound **5**

Although this is a well-known compound, the previously published NMR characterization was limited to a ^1H NMR spectrum in CCl_4.[8] The ^1H NMR spectrum in acetone-d_6 (Figure 14) shows a binomial triplet as expected at 5.24 ppm with a $^2J_{HF}$ = 57.8 Hz because of the presence of two fluorine atoms in the CHF_2 group. The chemical shift and coupling constant values are as expected for a CHF_2 group next to a carbonyl group (e.g. CHF_2COOH δ 6.13 ppm, $^2J_{HF}$ = 53.10 Hz in D_2O).[12] In the previously published spectrum in CCl_4, the resonance was reported at 4.85 ppm ($^2J_{HF}$ = 59 Hz).[8]

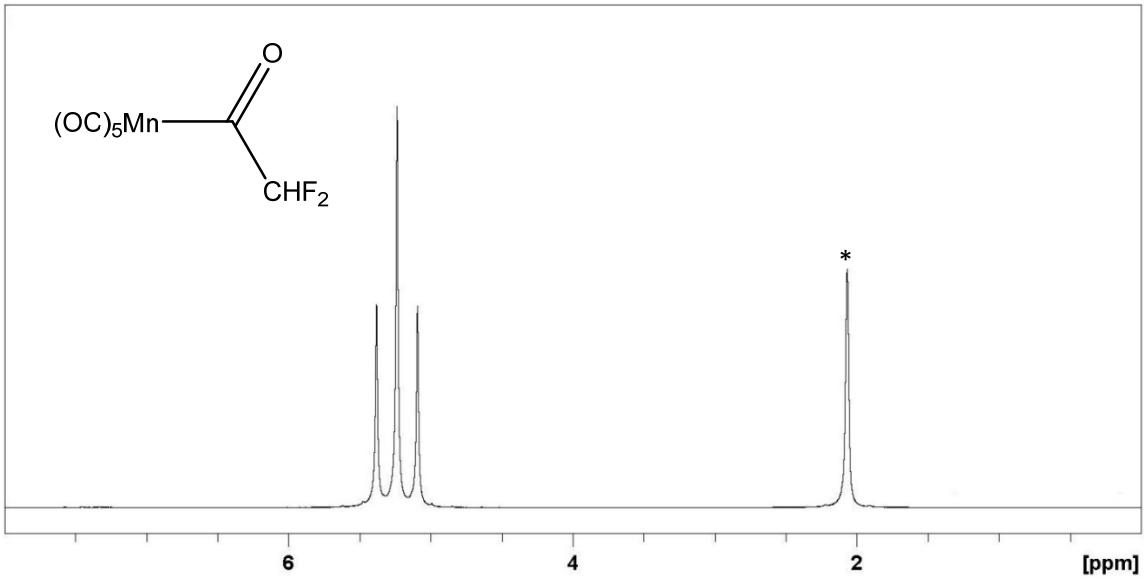

Figure 14. ^{1}H NMR spectrum (400 MHz, acetone-d_6) of compound **5**. The starred resonance is due to the solvent.

The ^{19}F NMR spectrum (Figure 15) displays a 1:1 doublet at -119.2 ppm with a $^{2}J_{FH}$ = 57.8 Hz because of the presence of a proton in the CHF_2 group. Again, these values are as expected (e.g. CHF_2COOH C^{β}: δ -126.98; $^{2}J_{HF}$ = 53.10 Hz in D_2O).[12]

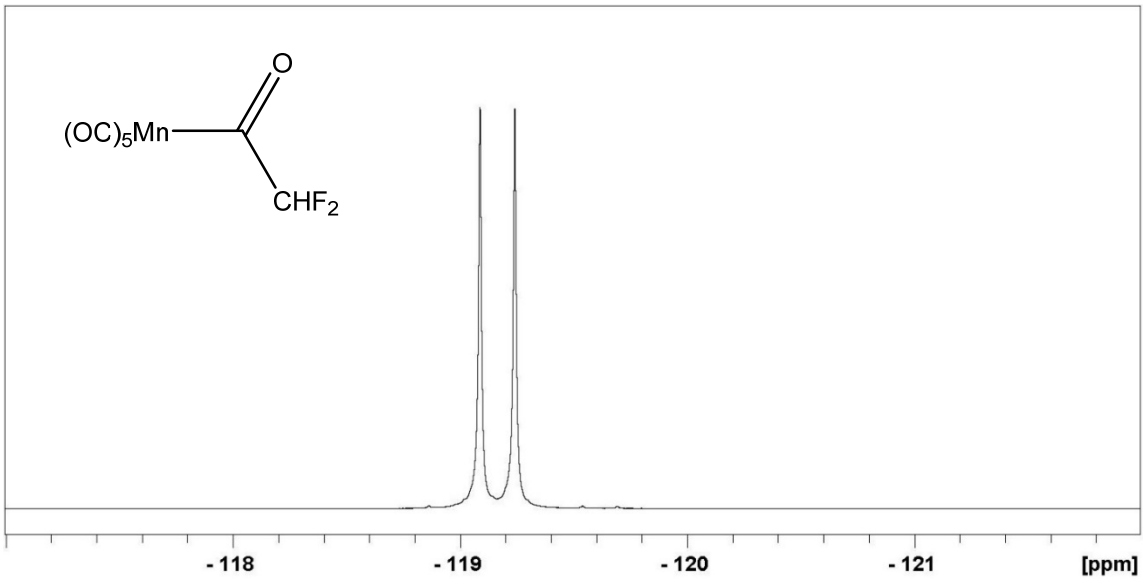

Figure 15. ^{19}F NMR spectrum (376.5 MHz, acetone-d_6) of compound **5**.

The ^{13}C NMR spectrum (Figure 16) exhibits at 111.5 ppm a doublet of triplets for C^{β} because of the presence of one proton and two fluorine atoms ($^{1}J_{CH}$ = 194 Hz, $^{1}J_{CF}$ = 256 Hz). All these values are similar to those measured for CF_2HCOOH (C^{β}: δ 107.25; $^{1}J_{CH}$ = 193.10 Hz; $^{1}J_{CF}$ = 245.9 Hz in D_2O).[12]

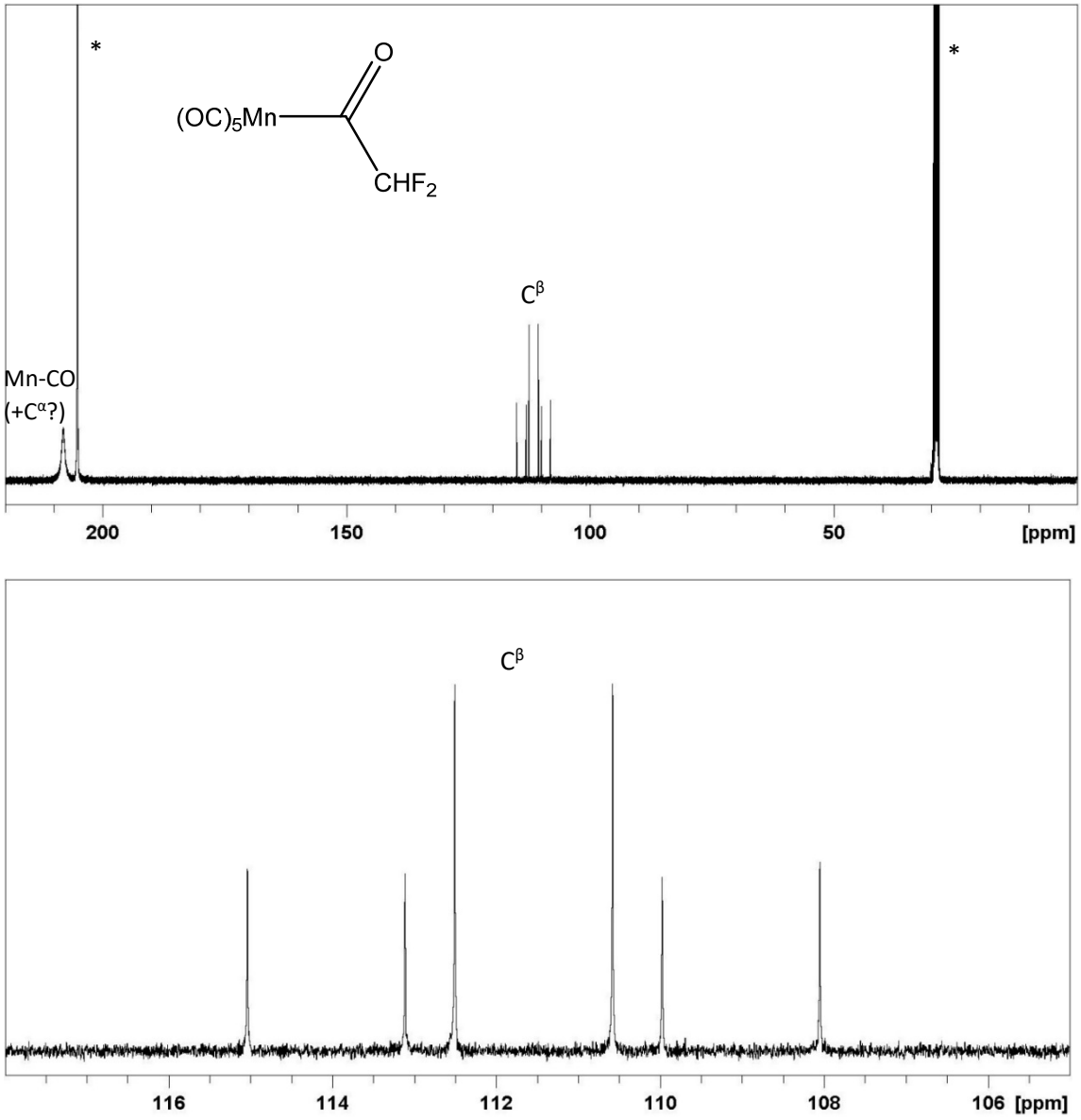

Figure 16. ^{13}C NMR spectra (100.6 MHz, acetone-d_6) of compound **5**: full spectrum above and expansion of the 105-118 ppm regions below. The starred resonances are due to the solvent.

FTIR spectroscopy yields the spectrum shown in Figure 17 (values reported in Table 3). Because of the symmetry lowering from the ideal C_{4v}, which is more pronounced for **5** than in **4**, the major E band is split and the "forbidden" B_1 band is more clearly visible. In addition, rotational isomerism results in the appearance of a second –COR vibration. These features correspond closely to those reported, also for a *n*-pentane solution, in a previous publication.[8] Additional weak bands are also observed in the Mn-CO stretching region and are believed to result from rotational isomers or ^{13}C isotopomers.

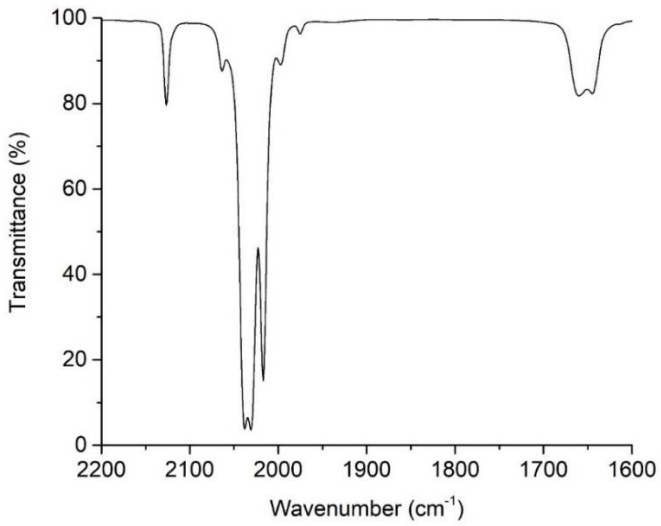

Figure 17. FTIR spectrum of compound **5** in the carbonyl stretching region in *n*-pentane solution.

Table 3. FTIR carbonyl stretching bands in *n*-pentane of complex **5**.

Vibration mode	A_1	B_1	E	A_1	Acyl group
Wavenumber (cm^{-1})	2127 w	2063 vw	2038 vs 2031 vs	2017 s	1660 w, 1645 w

The crystal structure of compound **5**, not previously reported, has been determined by single-crystal X-Ray diffraction (Figure 18). Crystals were obtained directly from the cold finger of the sublimator (55 °C, 100 mbar). More details about the X-ray structure data can be found in Section 3.2.6 and in the Appendix (Section B.2).

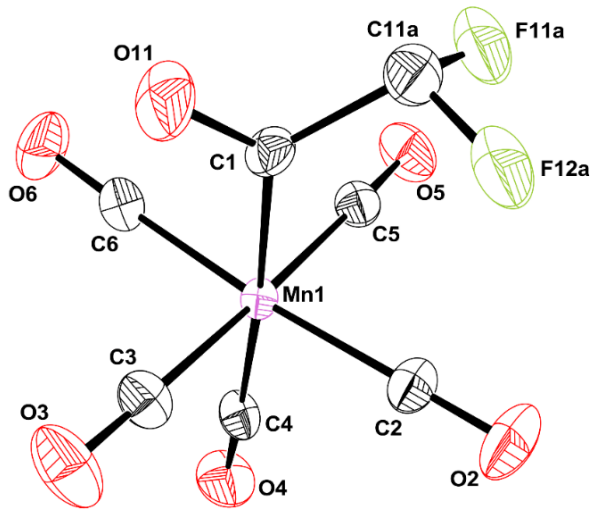

Figure 18. ORTEP view of compound **5**.

3.2.2.3. Synthesis of difluoromethylpentacarbonylmanganese(I), **9**

Compound **9** was synthesized directly by decarbonylation of **5** using the same procedure used for compound **8** in Section 3.2.1.3. and it was purified by column chromatography with the same conditions, also detailed in that section. Final product was obtained as a light brown volatile powder (yield 65%). The global yield of this reaction starting from the dimanganese decacarbonyl and the DFAA was 49%. As for the previous compounds, **6** can also be purified by sublimation (100 mbar, 55 °C).

3.2.2.4. Characterization of compound **9**

The NMR characterization of this well-known compound was previously limited to a ^{1}H spectrum in CCl_4.[9] The ^{1}H NMR spectrum of complex **9** in acetone-d_6 (Figure 19) presents a triplet at 7.46 ppm with a $^{2}J_{HF}$ of 48.6 Hz, which is downfield-shifted and with smaller H-F coupling relative to the resonance in **5** (5.24 ppm, $^{2}J_{HF}$ = 57.8 Hz) as the result of direct coordination to the metal center For the spectrum recorded in CCl_4, these values were reported as 7.23 ppm and 48.5 Hz, respectively.[9]

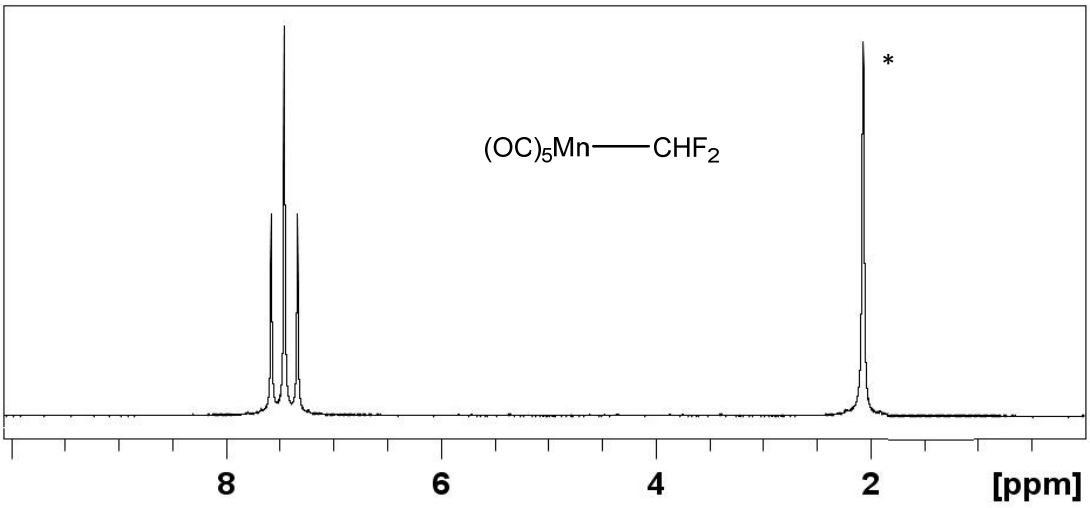

Figure 19. ^{1}H NMR spectrum (acetone-d_6, 400 MHz) of compound **9**. The starred resonance is due to the solvent.

The ^{19}F NMR spectrum (Figure 20) shows a doublet at -71.6 ppm with a $^{2}J_{FH}$ = 48.6 Hz. In this case, the direct coordination to the manganese(I) instead of the carbonyl

group provokes a downfield in the chemical shift of almost 20 ppm. The ^{13}C NMR spectrum (Figure 21) exhibits a doublet of triplets at 143.8 ppm with $^{1}J_{CF}$ = 287 Hz and $^{1}J_{CH}$ = 175 Hz.

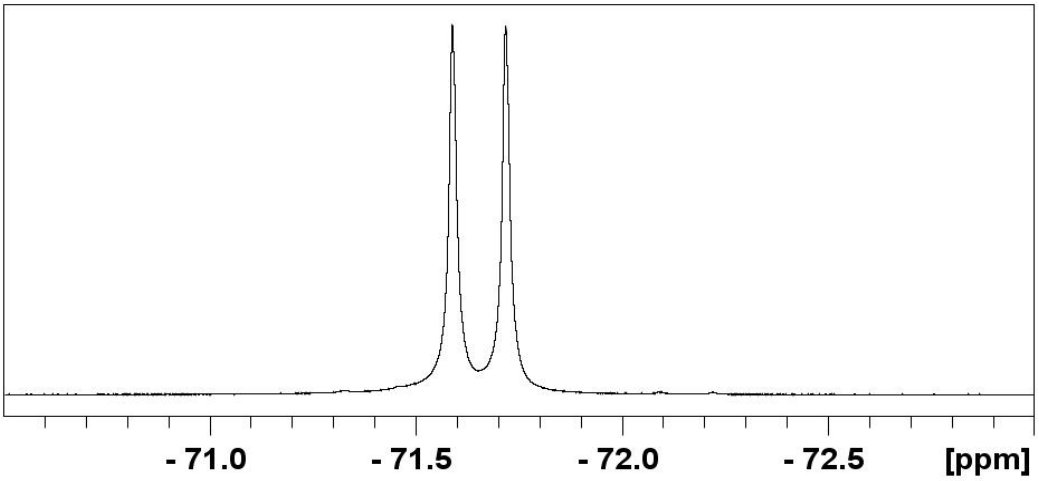

Figure 20. ^{19}F NMR spectrum (376.5 MHz, acetone-d_6) of compound **9**.

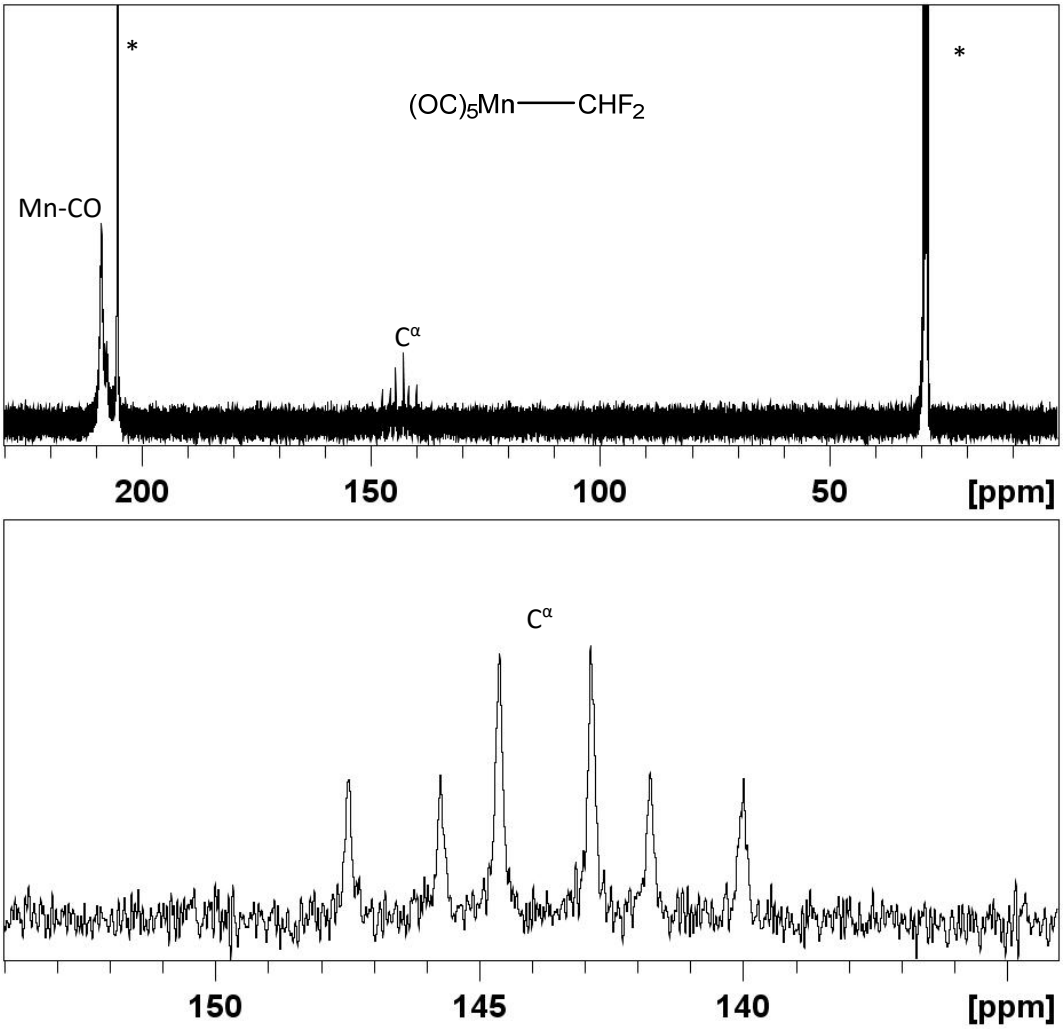

Figure 21. ^{13}C NMR spectra (100.6 MHz, acetone-d_6) of compound **9**: full spectrum above and expansion of the 154-134 ppm region below. The starred resonances are due to the solvent.

The FTIR spectrum (Figure 22, frequency values listed in Table 4) closely corresponds to that reported in the literature for a heptane solution.[9] The symmetry lowering of the $Mn(CO)_5$ moiety from ideal C_{4V} is in this case lesser than for the precursor **5** because the splitting of the E band is not evident, but the "forbidden" B_1 band is clearly visible. As for the spectrum of compound **8**, the absence of bands below 1700 cm^{-1} indicates that the decarbonylation was quantitative. The additional weak bands or shoulders that are observed in the Mn-CO stretching region will be further discussed and assigned in Section 3.3.7.

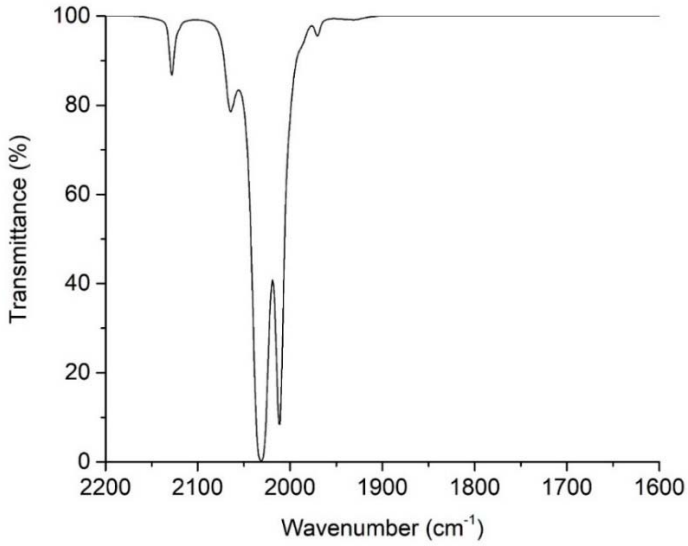

Figure 22. FTIR spectrum of compound **9** in the CO stretching region in *n*-pentane solution.

Table 4. FTIR carbonyl stretching bands in *n*-pentane of complex **9**.

Vibration mode	A_1	B_1	E	A_1
Wavenumber (cm^{-1})	2128 w	2064 vw	2031 vs	2011 s

It was also possible to obtain the previously unreported crystal structure of compound **6** by single-crystal X-Ray diffraction (Figure 23). The crystals grew directly from the cold finger of the sublimator. More details on the structure data can be found in Section 3.2.5 and in the Appendix (Section B.5).

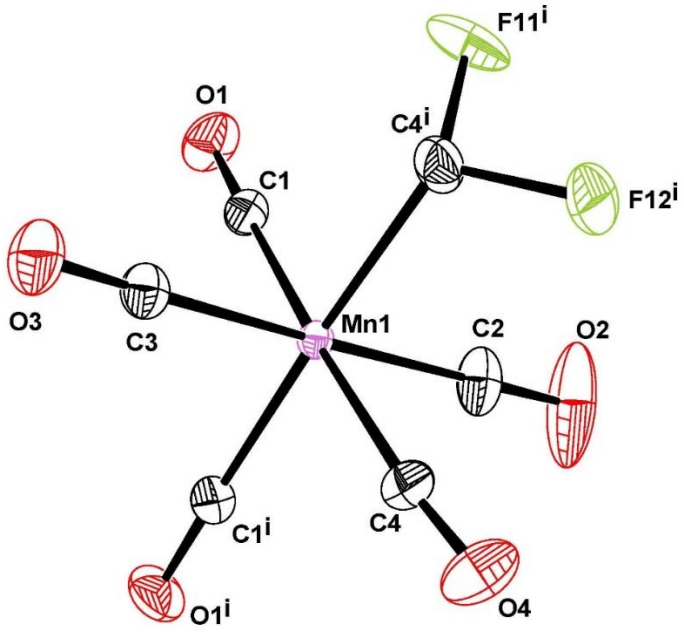

Figure 23. ORTEP view of compound **9**.

3.2.3. 2,2,2-Trifluoroethylpentacarbonylmanganese(I), **10**

$[Mn(CO)_5(CH_2CF_3)]$ (compound **10**) was synthesized by decarbonylation of $[Mn(CO)_5(COCH_2CF_3)]$ (compound **6**). The acyl complex was obtained from the $K[Mn(CO)_5]$ solution in THF with 3,3,3-trifluoropropanoyl chloride, which is commercially available. Neither compound **10**, nor its precursor **6**, were previously described in the literature.

3.2.3.1. Synthesis of 3,3,3-trifluoropropanoylpentacarbonylmanganese(I), **6**

The synthetic procedure was adapted from the synthetic pathways of compounds **4** and **5**. Once the filtered $K[Mn(CO)_5]$ solution was prepared, the stoichiometric amount of 3,3,3-trifluoropropanoyl chloride was added dropwise. During the addition, the mixture changed quickly to blood red. Then, 20 min after the addition, the color became red and finally orange (Figure 24).

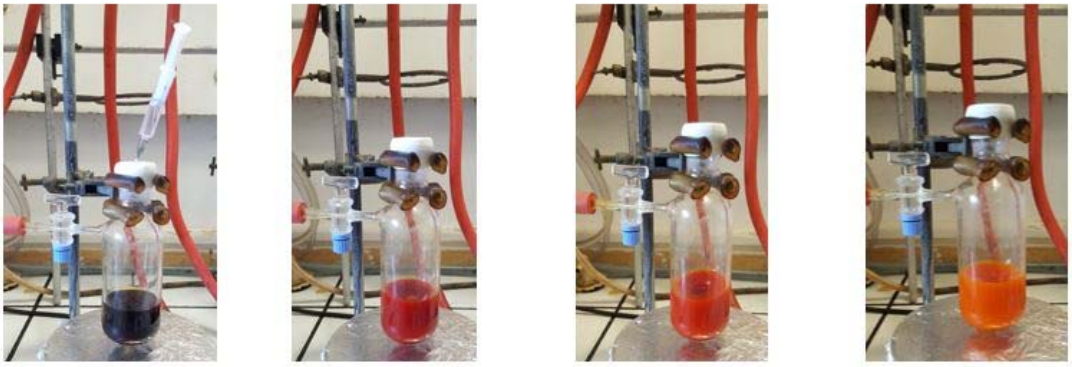

Figure 24. Pictures of the evolution after the addition of TFAA to the $K[Mn(CO)_5]$ solution.

The product was purified by column chromatography on silica gel after depositing the solid crude product embedded in silica gel as previously described for the other compounds. The $[Mn_2(CO)_{10}]$ by-produced was eluted first using *n*-pentane. Then, the desired product was recovered using a 9:1 mixture of *n*-pentane and diethyl ether.

After the solvent evaporation, **6** was obtained in 75% yield as a pale-yellow volatile and crystalline powder. In this case, sublimation (100 mbar, 55 °C) results in direct decarbonylation with formation of compound **10** in a pure form.

3.2.3.2. Characterization of compound **6**

The ^1H NMR spectrum of compound **6** (Figure 25) exhibits a binomial quartet as expected at 4.05 ppm with a $^3J_{HF}$ of 10.8 Hz. The peak is slightly deshielded compare to the analogous carboxylic acid CF_3CH_2COOH (δ 3.15, $^3J_{HF}$ = 9.75 Hz in CD_2Cl_2).[13]

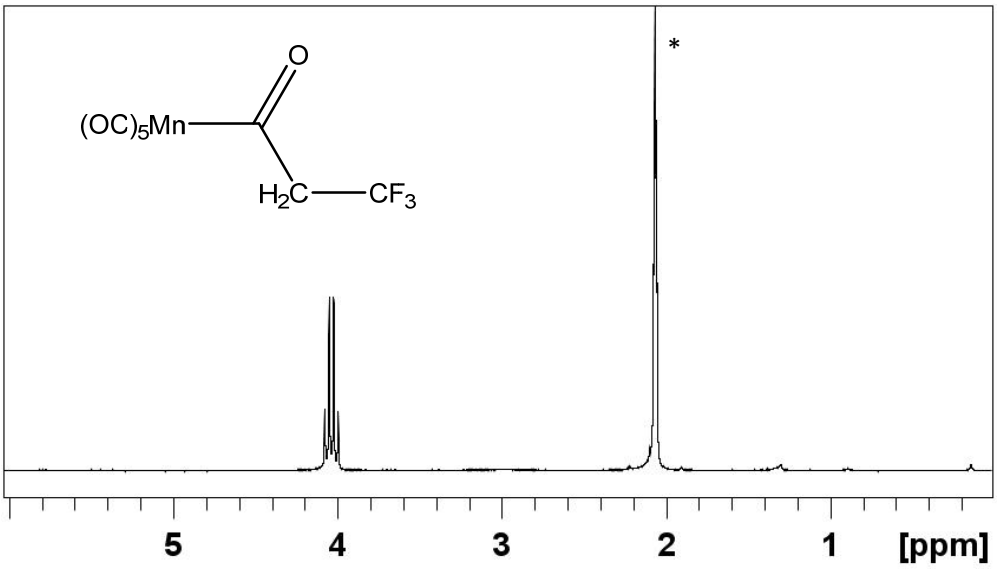

Figure 25. ^{1}H NMR spectrum (400 MHz, acetone-d_6) of compound **6**. The starred resonance is due to the solvent.

The ^{19}F NMR spectrum of compound **6** (Figure 26) shows a binomial triplet as expected at -63.4 ppm with a $^{3}J_{HF}$ of 10.8 Hz. In this case, the signal is approximatively at the same chemical shift as that of its analogous carboxylic acid CF_3CH_2COOH (δ -61, $^{3}J_{HF}$ = 9.75 Hz in CD_2Cl_2)[13] because the fluorine atoms are located on the C^{γ} atom, thus the electronic effect of the $Mn(CO)_5$ group *vs.* that of the COOH group is small.

The ^{13}C NMR spectrum of compound **6** (Figure 27) presents a triplet of quartets for the C^{β} and a quartet of triplets for the C^{γ}, as expected (C^{β}: δ 63.5; $^{2}J_{CF}$ = 22.6 Hz; $^{1}J_{CH}$ = 131 Hz; C^{γ}: 123.3; $^{1}J_{CF}$ = 279 Hz; $^{2}J_{CH}$ = 6.7 Hz). It is also possible to observe a broad peak corresponding to the carbonyl ligands at 207.3 ppm. Probably the signal of the acyl carbonyl group overlaps with this resonance.

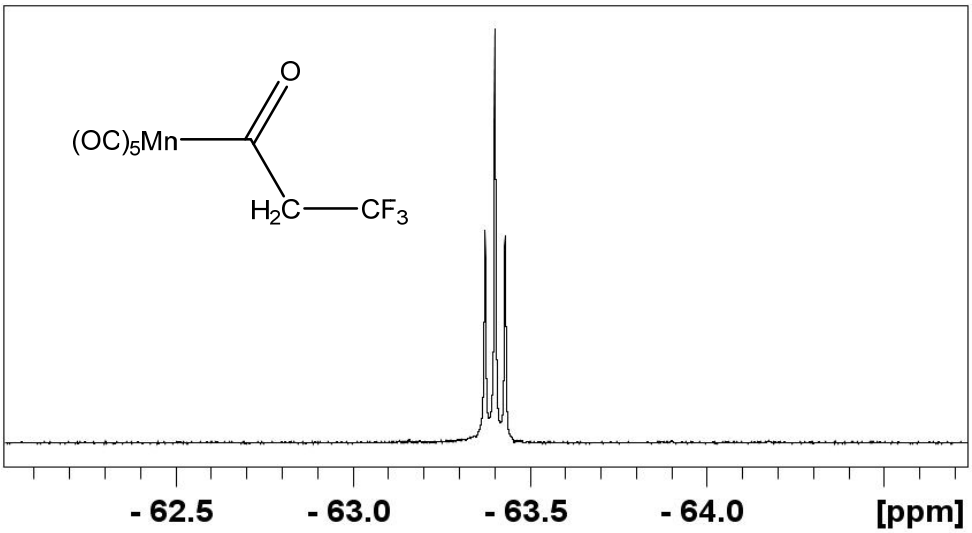

Figure 26. ^{19}F NMR spectrum (376.5 MHz, acetone-d_6) of compound **6**.

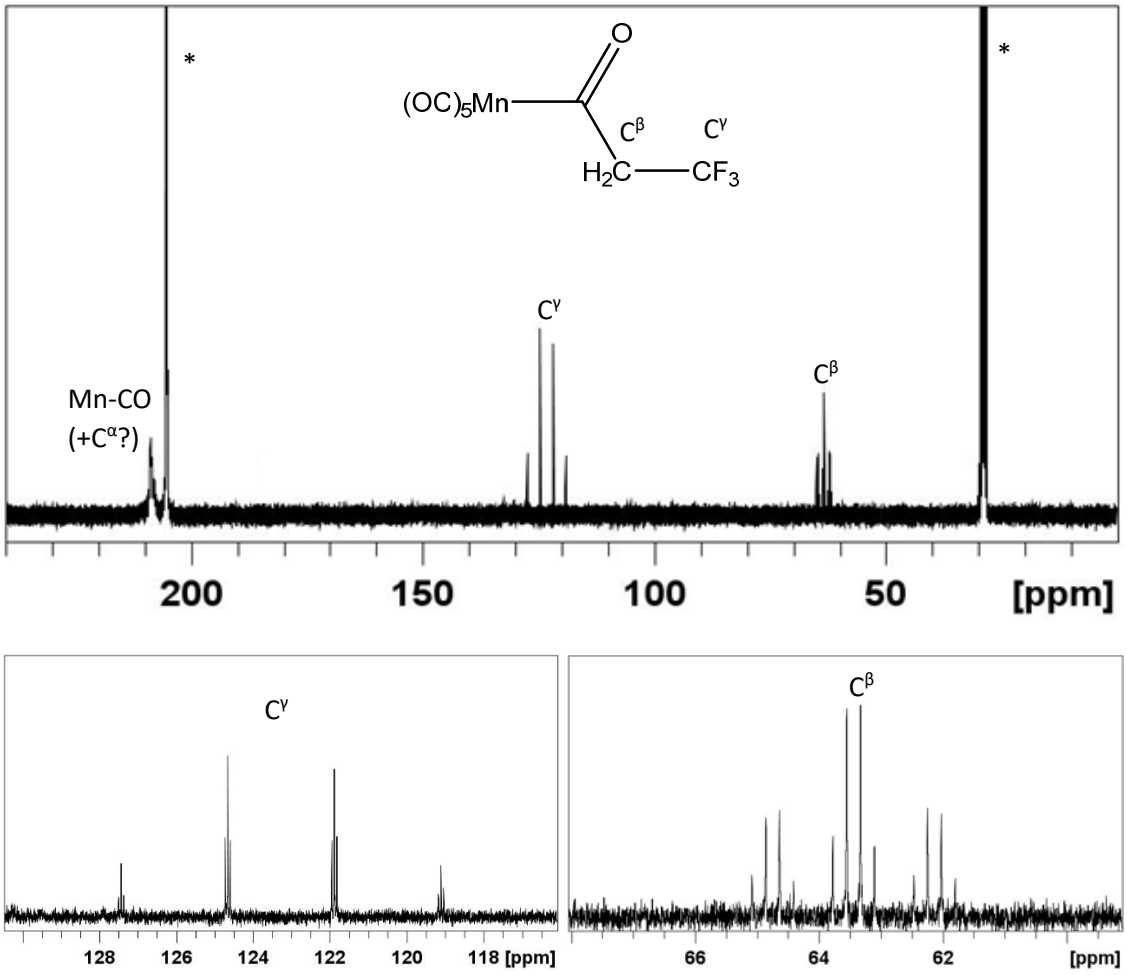

Figure 27. ^{13}C NMR spectra (100.6 MHz, acetone-d_6) of compound **6**: full spectrum above and expansions of the 129-117 and 68-60 ppm regions below. The starred resonances are due to the solvent.

The FTIR spectrum in *n*-pentane is shown in Figure 28. The assignment of the $Mn(CO)_5$ vibrations (Table 5) is straightforward on the basis of the spectra of the analogous compounds already discussed above. The lowering of symmetry causes in this case a visible splitting of the E band in addition to the observation of the "forbidden" B_1 band. In addition, rotational isomerism results in the appearance of a second –COR vibration. The additional weak bands probably result from the ^{13}C isotopomers.

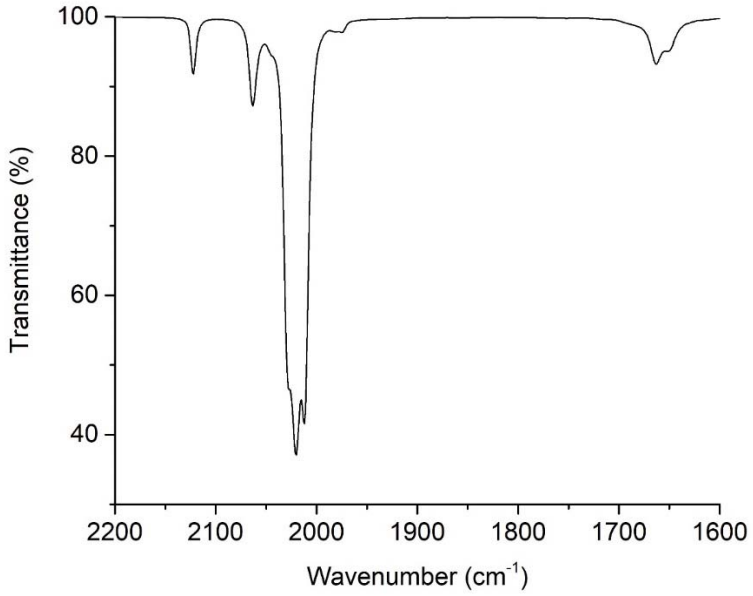

Figure 28. FTIR spectrum of compound **6** in the CO stretching region in *n*-pentane solution.

Table 5. FTIR carbonyl stretching bands in *n*-pentane of compound **6**.

Vibration mode	A_1	B_1	E	A_1	Acyl group
Wavenumber (cm^{-1})	2122 w	2063 w	2028 s 2020 vs	2012 s	1663 w 1652 w

No X-ray diffraction analysis could be carried out for compound **6** because of the difficulty to grow crystals. The compound could only be obtained as a microcrystalline powder.

3.2.3.3. Synthesis of 2,2,2-trifluoroethylpentacarbonylmanganese(I), **10**

Like the already known complexes (**8** and **9**),[1,2] $[Mn(CO)_5(CH_2CF_3)]$ (**10**) was synthesized directly by decarbonylation of its acyl analogue **6**. Decarbonylation was carried out at 70 °C without solvent under an argon atmosphere for 1.5 h (until the bubbling stopped). The use of higher temperatures results in the decomposition of complex **7** in several unidentified products without fluorine (no signal was observed in ^{19}F NMR spectra). During this process, the complex melts to become a brown liquid.

Compound **10** was purified by column chromotraphy with the same conditions previously used for compound **8** and **9**, yielding the product as a yellow solid (yield 80%). The overall yield of this reaction starting from the dimanganese decacarbonyl and 3,3,3-trifluoropropanoyl chloride was 60%.

3.2.3.4. Characterization of compound **10**

The ^{1}H NMR spectrum of complex **10** (Figure 29) shows a quartet at 1.40 ppm with a $^{3}J_{HF}$ = 15.9 Hz. The structural modification from **6** to **10** causes a significant upfield of the CH_2 signal since it is no longer affected by a carbonyl group in α-position.

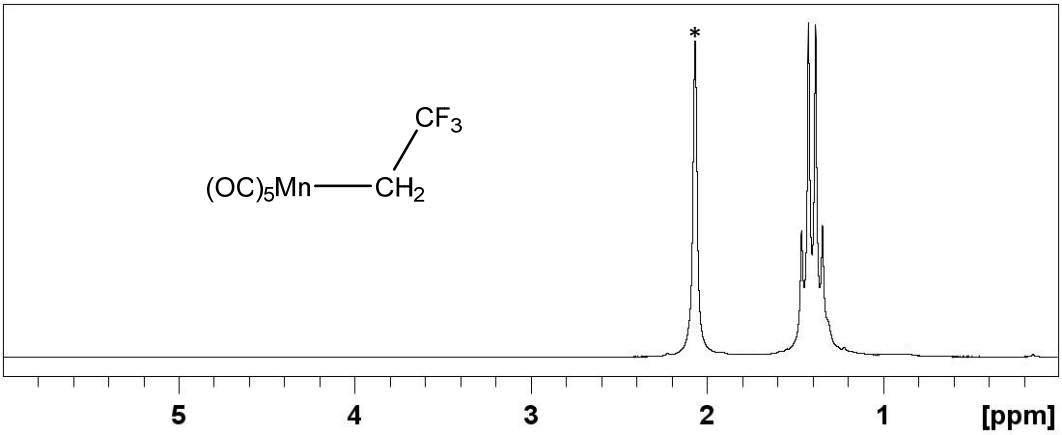

Figure 29. ^{1}H NMR spectrum (400 MHz, acetone-d_6) of compound **10**. The starred resonance is due to the solvent.

The ^{19}F NMR spectrum of compound **10** (Figure 30) exhibits a triplet at -52.3 ppm with a $^{3}J_{FH}$ = 16.9 Hz. In this case, there is a small downfield shift of 11.1 ppm for the CF_3 signal relative to the precursor **6**.

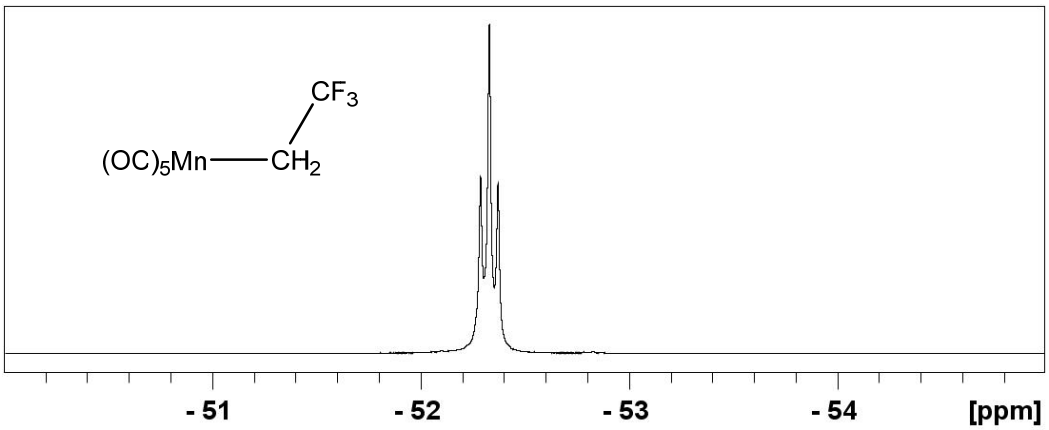

Figure 30. ^{19}F NMR spectrum (376.5 MHz, acetone-d_6) of compound **10**.

The ^{13}C NMR of compound **10** (Figure 31) reveals only a quartet of triplets for C^{β} at 133.7 ppm with a $^{1}J_{CF}$ = 273 Hz and a $^{2}J_{CH}$ = 6.0 Hz. The peak corresponding to C^{γ} could not be identified, perhaps because of overlap with the strong solvent resonance.

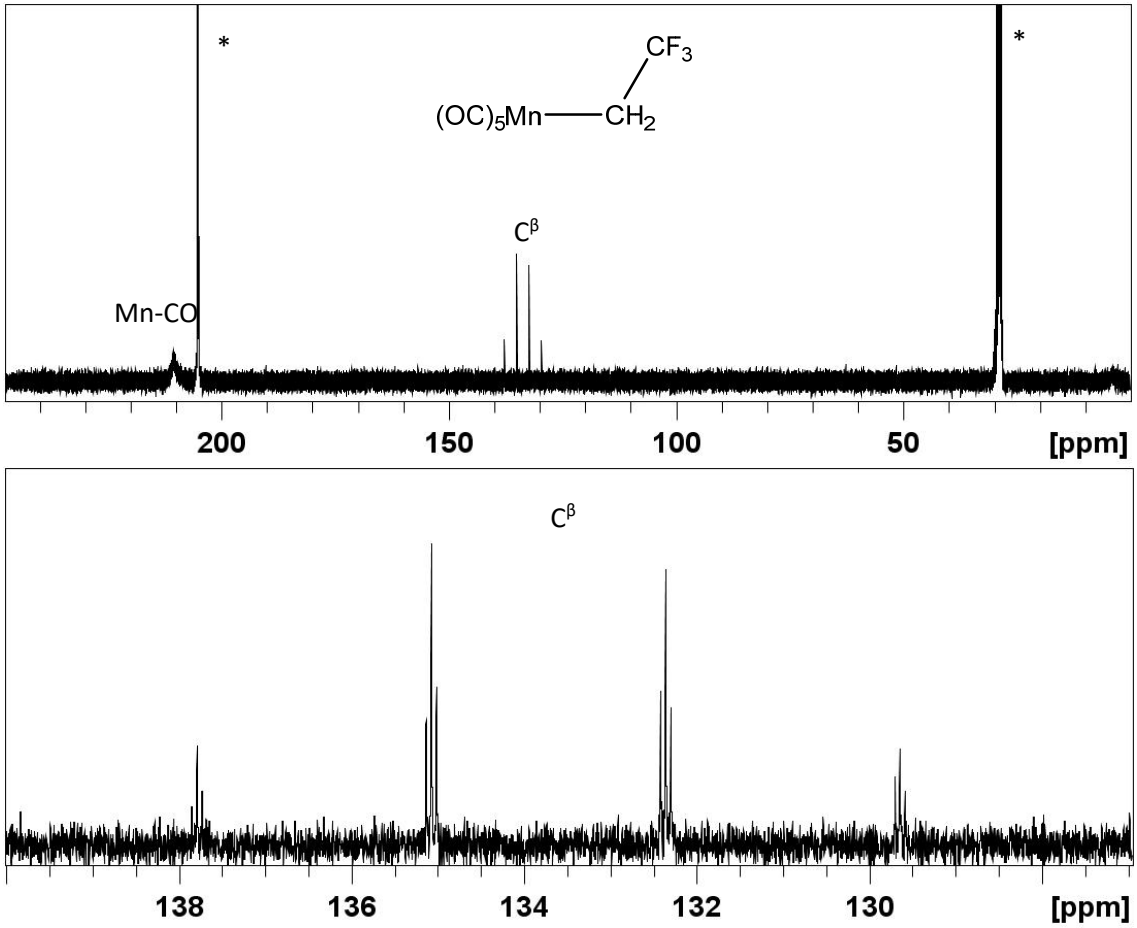

Figure 31. ^{13}C NMR spectra (100.6 MHz, acetone-d_6) of compound **10**: full spectrum above and expansion of the 127-140 ppm region below. The starred resonances are due to the solvent.

The FTIR spectrum of complex **10** in *n*-pentane is shown in Figure 32 and the peaks are reported in Table 6. The assignment of the expected $2A_1$+E (in C_{4v} symmetry) and of the "forbidden" B_1 bands, which is straightforward in comparison with the spectra of **8** and **9**, is shown in Table 10. In this case there is no observable splitting of the major E band. The additional weak bands or shoulders that are observed in the Mn-CO stretching region will be further discussed and assigned in Section 3.2.5. The absence of bands at < 1700 cm^{-1} confirms the quantitative decarbonylation of **6**.

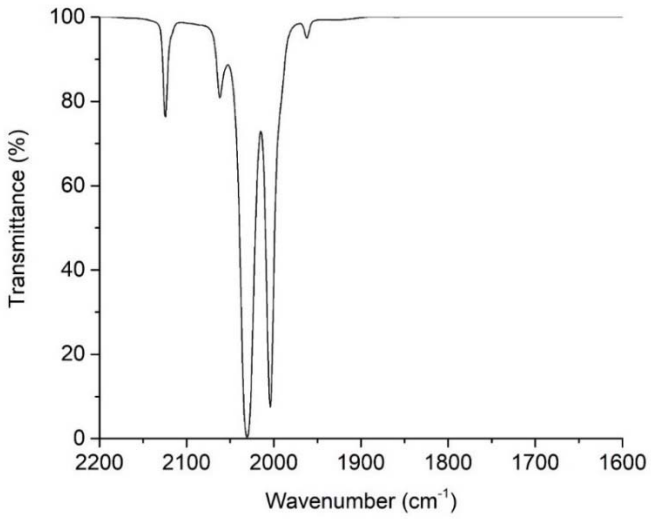

Figure 32. FTIR spectrum of compound **10** in the CO stretching region in *n*-pentane solution.

Table 6. FTIR carbonyl stretching bands in *n*-pentane of complex **10**.

Vibration mode	A_1	B_1	E	A_1
Wavenumber (cm^{-1})	2124 w	2062 w	2030 vs	2004 s

A single crystal X-ray diffraction investigation could be carried out for the new compound **10** (Figure 33). The crystals grew directly from the cold finger of the sublimator. More details on the X-ray structure data can be found in Section 3.2.6 and in the Appendix (Section B.6).

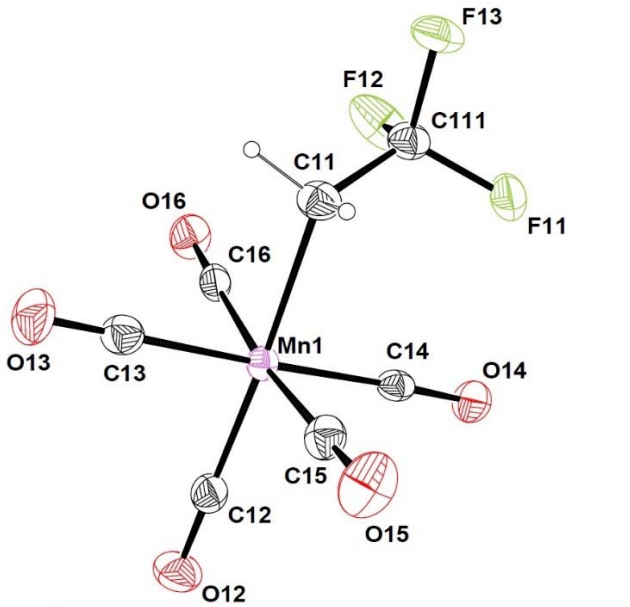

Figure 33. ORTEP view of compound **10**.

3.2.4. 1,1-Difluoroethylpentacarbonylmanganese(I), **11**

$[Mn(CO)_5(CF_2CH_3)]$ (compound **11**) was synthesized by decarbonylation of $[Mn(CO)_5(COCF_2CH_3)]$ (compound **7**). However, in this case decarbonylation does not work as well as for the other $[Mn(CO)_5R_F]$ complexes (R_F = CF_3, CHF_2, CH_2CF_3) synthesized in this work. Furthermore, the initial attempts to synthesize compound **7** using 2,2-difluoropropanoyl chloride synthesized from 2,2-difluoropropionic acid and thionyl chloride unexpectedly led to 2,2-difluoropropanoylthiopentacarbonylmanganese(I) complex (compound **12**), which will also be described in this section.

The attention was therefore later focused on oxalyl chloride for the synthesis of 2,2-difluoropropanoyl chloride,[14] avoiding the presence of sulfur. This synthesis provided the desired complex as described below.

3.2.4.1. Synthesis of 2,2-difluoropropanoylpentacarbonyl-manganese(I), **7**

a) Synthesis of **7** with 2,2-difluoropropanoyl chloride made from 2,2-difluoropropionic acid and thionyl chloride

As mentioned above, the synthesis of **7** using 2,2-difluoropropanoyl chloride which was previously prepared from 2,2-difluoropropionic acid and thionyl chloride led to an unexpected main product with a sulfur atom between the fluoroacyl chain and the manganese pentacarbonyl (Scheme 2). The unexpected product was identified as $[Mn(CO)_5(SCOCF_2CH_3)]$ by a single-crystal X-Ray diffraction analysis (Figure 34). For more extensive metric data refer to the Appendix (Section B.7). The formation of this compound is probably due to an incomplete purification of the acyl chloride and its contamination by thionyl chloride, or to the presence of other sulfur-containing impurities produced by an unexpected reaction between 2,2-difluoropropionic acid and thionyl chloride.

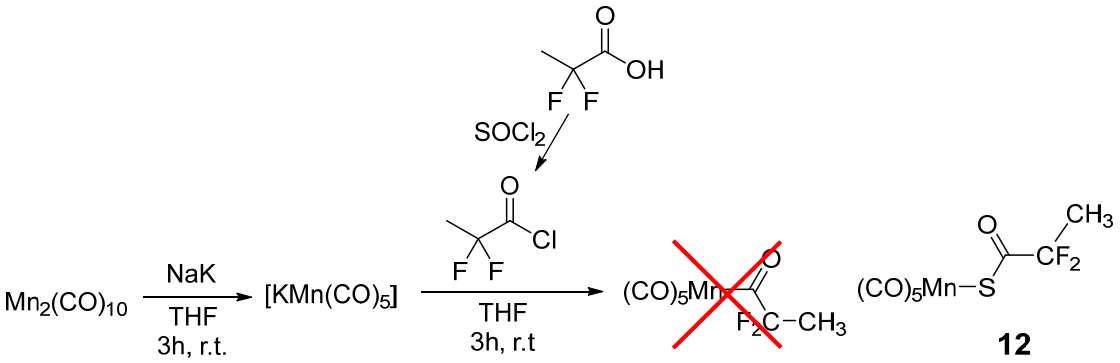

Scheme 2. Synthetic pathway of 2,2-difluoropropanoylpentacarbonylmanganese(I) complex using thionyl chloride for the synthesis of 2,2-difluoropropanoyl chloride leading to compound **12**.

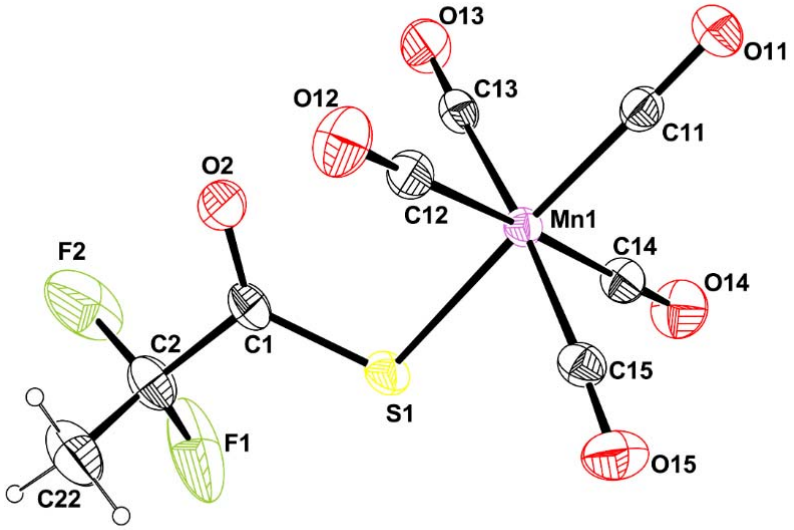

Figure 34. ORTEP view of compound **12**.

Before use, thionyl chloride was purified in the presence of sulfur at 80 °C for 1 h, followed by a distillation. Then, it was introduced in a flask under argon with 2,2-difluoropropionic acid and heated up to 80 °C for 1 hour. Finally, the 2,2-difluoropropanoyl chloride product was purified by distillation (b. p. 40 °C). Even though the boiling point of thionyl chloride is higher (b. p. 74.6 °C), it is possible that small amounts of this compound end up in the distilled product. It was not possible to check for the presence of thionyl chloride in the acyl chloride product because it has no easily measurable NMR active nucleus.

b) Synthesis of **7** with 2,2-difluoropropanoyl chloride made from 2,2-difluoropropionic acid and oxalyl chloride

The stoichiometric amount of 2,2-difluoropropanoyl chloride synthesized from 2,2-difluoropropionic acid and oxalyl chloride was added dropwise to the $K[Mn(CO)_5]$ solution (see Scheme 3). During the addition, the color changed quickly to orange. Then, 10 min after the addition, the color became dark yellow and finally yellow (Figure 35).

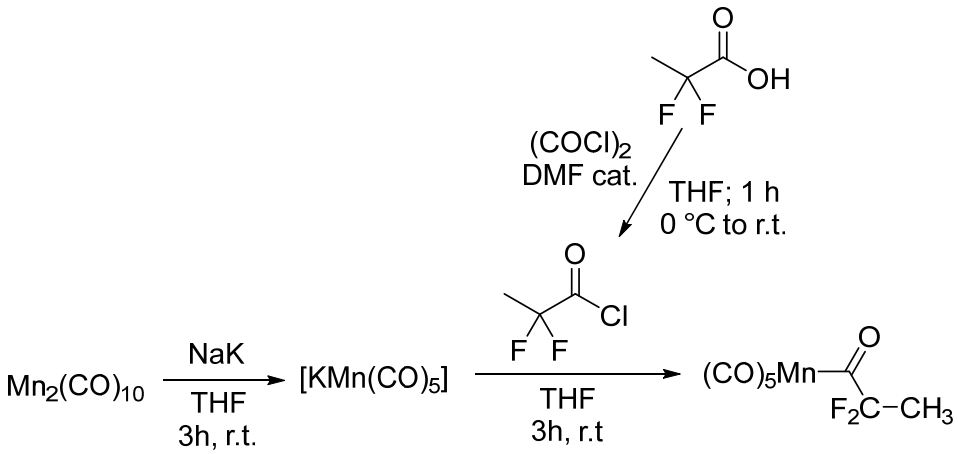

Scheme 3. Synthetic pathway of 2,2-difluoropropanoylpentacarbonylmanganese(I) complex using thionyl chloride for the synthesis of 2,2-difluoropropanoyl chloride.

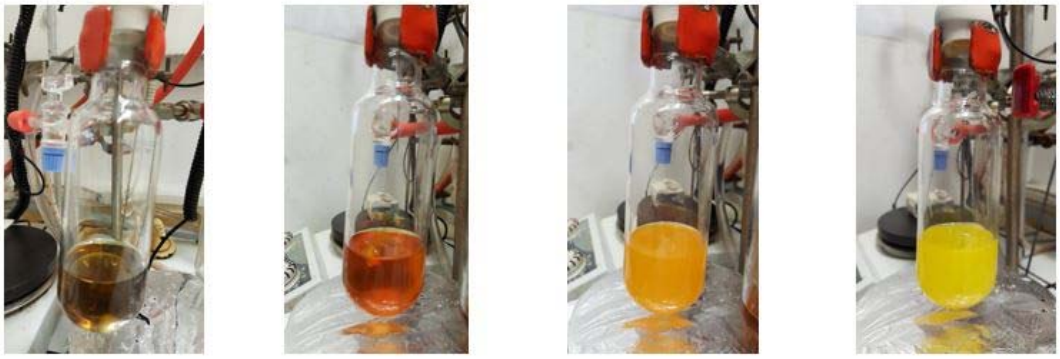

Before the addition of 2,2-difluoropropanoyl chloride

5 min after the addition of 2,2-difluoropropanoyl chloride

10 min after the addition of 2,2-difluoropropanoyl chloride

2 h after the addition of 2,2-trifluoropropanoyl chloride

Figure 35. Evolution after the addition of 2,2-difluoropropanoyl chloride to the $K[Mn(CO)_5]$ solution.

Thereafter, work-up as described previously for the other acyl complexes led to the isolation of complex **7** as a yellow-brownish crystalline powder (yield 33 %).

3.2.4.2. Characterization of compound **7**

The ^{1}H NMR spectrum of compound **7** (Figure 36) in acetone-d_6 exhibits a triplet at 1.49 ppm with a $^{3}J_{HF}$ of 19.3 Hz. There is a significant upfield shift and an increase of the coupling constant compared to the corresponding parameters of the carboxylic acid CH_3CF_2COOH (δ 2.58; $^{3}J_{HF}$ = 2.3 Hz).[15]

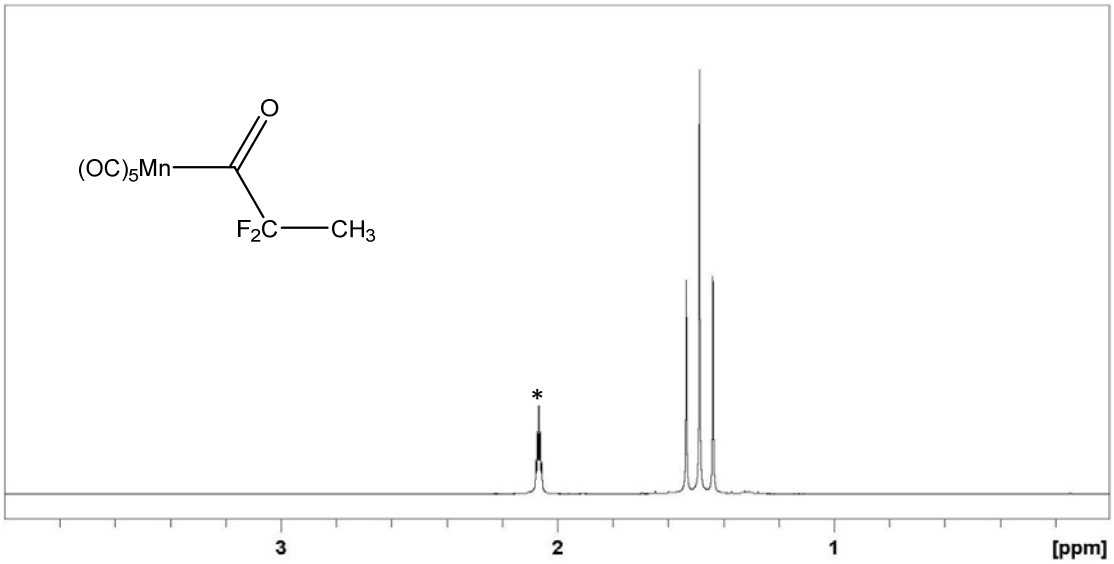

Figure 36. ^{1}H NMR spectrum (400 MHz, acetone-d_6) of compound **7**. The starred resonance is due to the solvent.

The ^{19}F NMR spectrum of compound **7** (Figure 37) displays a quartet at -91.5 ppm with a $^{3}J_{FH}$ of 19.4 Hz. Contrary to the ^{1}H NMR signal, the ^{19}F NMR signal is downfield-shifted compared to CH_3CF_2COOH (δ -105.5; $^{3}J_{HF}$ = 2.3 Hz).[15]

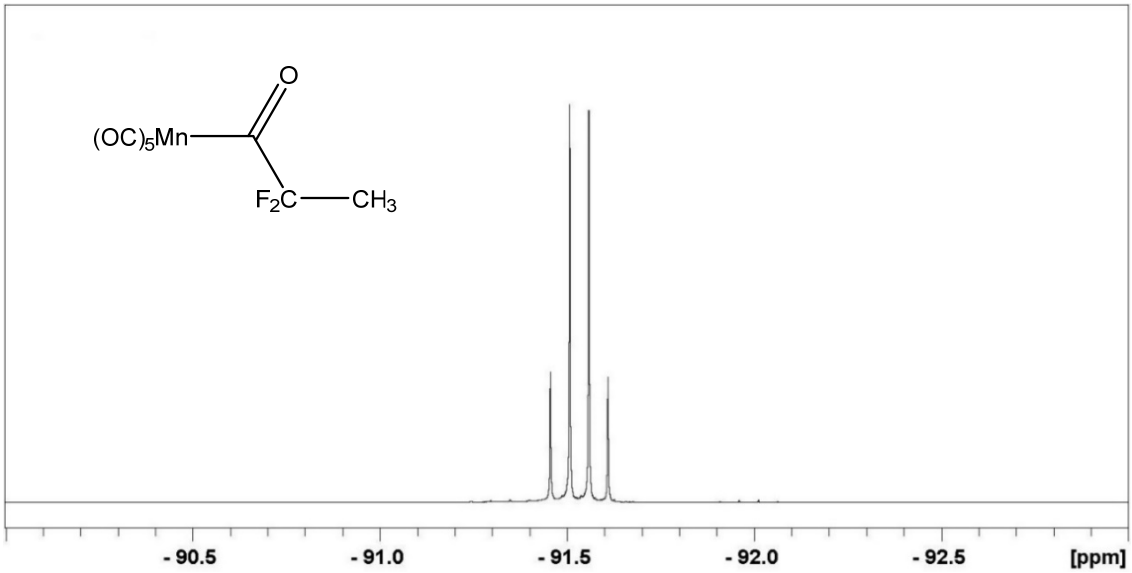

Figure 37. ^{19}F NMR spectrum (376.5 MHz, acetone-d_6) of compound **7**.

The ^{13}C NMR of compound **7** (Figure 38) exhibits a triplet of quartets for C^{β} at 117.9 ppm ($^{1}J_{CF}$ = 250 Hz; $^{2}J_{CH}$ = 5.1 Hz) and a quartet of triplets at 17.0 ppm ($^{2}J_{CF}$ = 26.1 Hz; $^{1}J_{CH}$ = 129.5 Hz) corresponding to C^{γ}.

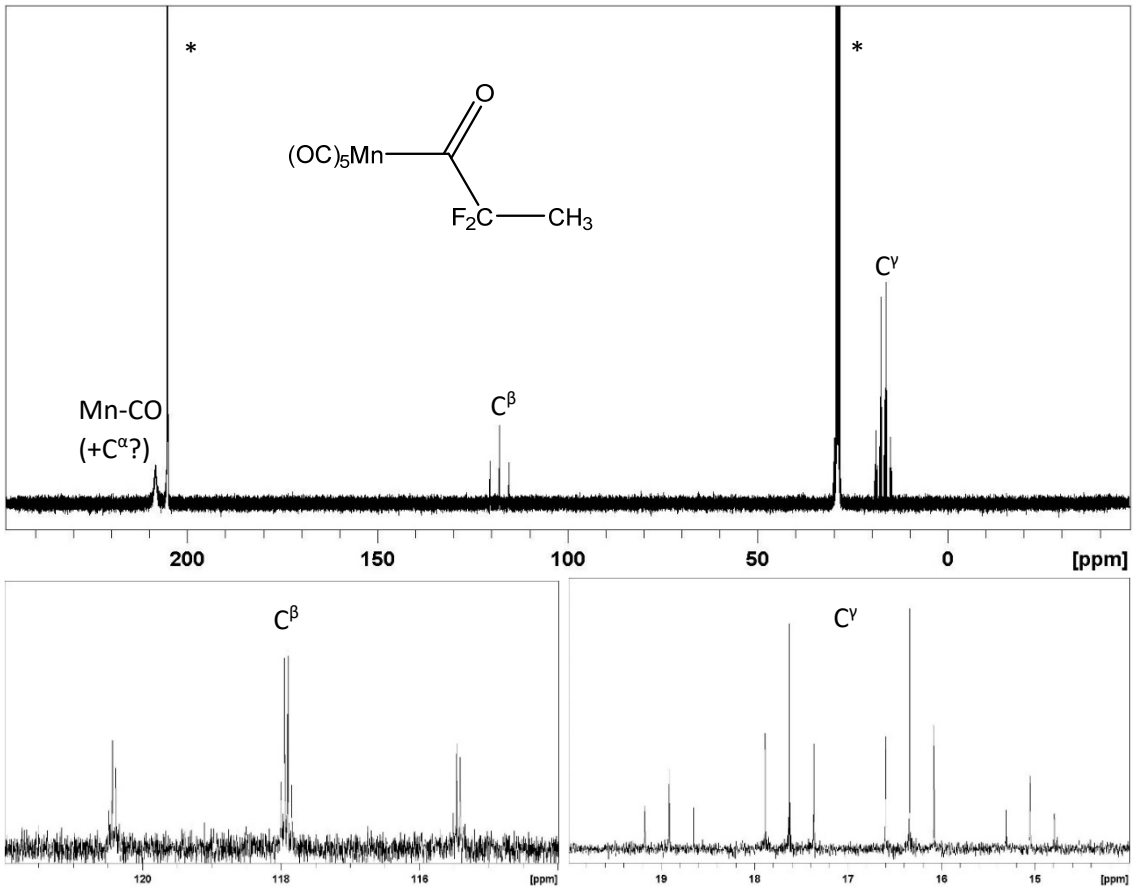

Figure 38. ^{13}C NMR spectra (100.6 MHz, acetone-d_6) of compound **7**: full spectrum above and expansions of the 128-114 and 20-14 ppm regions below. The starred resonances are due to the solvent.

The FTIR spectrum in *n*-pentane solution is shown in Figure 39 and the vibration band assignment is reported in Table 7. The spectrum shows all the expected features, with a clearly visible "forbidden" B_1 band and a split E band because of the symmetry lowering from the ideal C_{4v} for the $Mn(CO)_5$ group. In addition, as compounds **4**, **5** and **6**, rotational isomerism results in the appearance of a second –COR vibration. Additional weak bands are also observed in the Mn-CO stretching region, assigned like for the other analogous compounds to ^{13}C isotopomers.

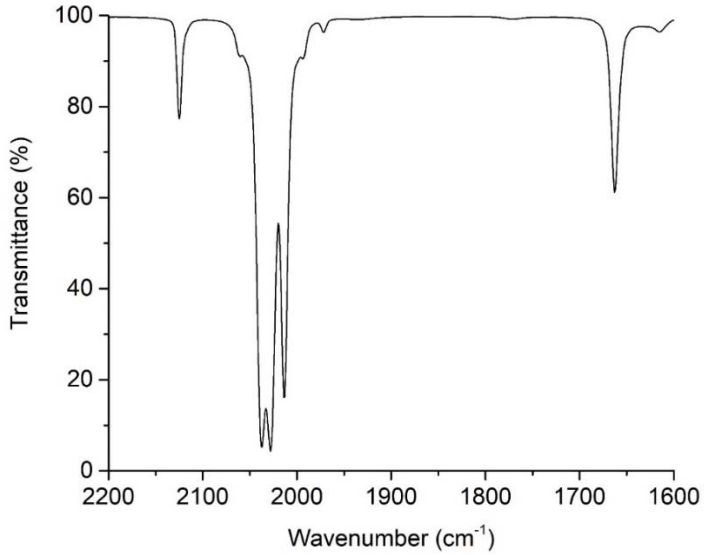

Figure 39. FTIR spectrum of compound **7** in the CO stretching region in *n*-pentane solution.

Table 7. FTIR carbonyl stretching bands in *n*-pentane of complex **7**.

Vibration mode	A_1	B_1	E	A_1	Acyl group
Wavenumber (cm^{-1})	2125 w	2061 w	2037 vs 2028 vs	2014 s	1663 m 1615 vw

Single crystal X-ray diffraction data could be obtained for the new compound **7** (Figure 40). Yellow-brownish crystals grew directly from the cold finger of the sublimator. More details about the X-ray structure data can be found in Section 3.2.6 and in the Appendix (Section B.3).

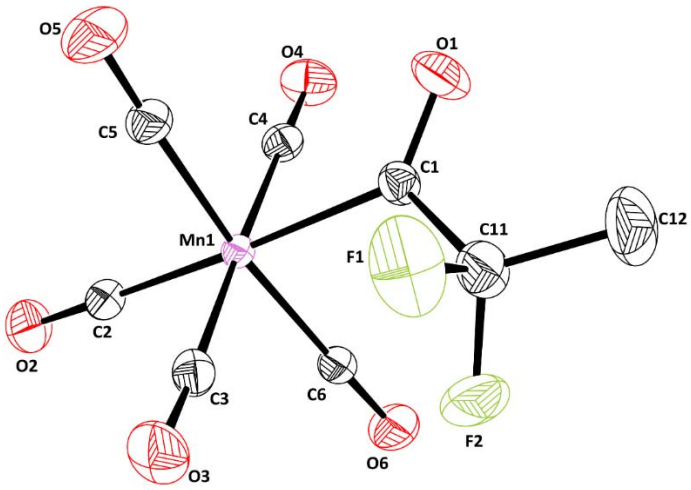

Figure 40. ORTEP view of compound **7**.

3.2.4.3. Attempted synthesis of 1,1-difluoroethylpentacarbonyl-manganese(I), **11**

Initial attempts to decarbonylate complex **7** under the same conditions used for complex **6** (no solvent, 1.5 h at 70 °C) did not produce the expected complex **11**. Several decarbonylation conditions were tested (different temperatures, times and solvents) as summarized in Table 8. All experiments were carried out under an argon atmosphere, and formation of the target product **11** was indicated by the spectroscopic data (*vide infra*). The relative yield is calculated by integration of both NMR signals (compound **7** and **11**) and normalizing to 1, hence decomposition is not considered. Evidence for the formation of **11** were obtained only in some cases (entries 5, 6, 7, 12 and 14).

Table 8. Conditions tested for decarbonylation of compound **7**.

Entry	Solvent	Temperature (°C)	Time (h)	Relative yield *
1	Without solvent	110	1.5	0
2	Without solvent	70	1.5	0
3	Without solvent	60	1	0 **
4	Without solvent	45	1	0 **
5	Cyclohexane, UV 256 nm	50	1	30
6	Cyclohexane, UV 256 nm	50	1.5	28
7	Cyclohexane, UV 300 nm	50	1	17
8	Acetone	56	1	0
9	EtOAc	80	1	0 **
10	MeCN	80	1	0
11	MEK	80	1	64
12	MEK	80	1.5	0
13	Cyclohexane	75	1	60
14	Without solvent	75	1.5	0
15	Without solvent	110	1.5	0

* Relative yield compared to remaining compound **7** (decomposition is not considered)
** A weak signal was observed at δ -99.3 (q)

Solvent-free decarbonylation does not give compound **11** at the tested times and temperatures (entries 1 to 4). However, a weak NMR resonance from an unidentified product was detected at -99.3 ppm (quartet) in entries 3 and 4. This signal was also observed for the decarbonylation in ethyl acetate at 80 °C for 1 h (entry 9). The best

conditions found for this reaction are those of entry 11 (80 °C, 1 hour, in methyl ethyl ketone) leading to a 64% spectroscopic yield for the decarbonylation. The use of cyclohexane as solvent at 75 °C led to a similar yield (60%, entry 13). In both cases, prolonged heating before completion of the acyl precursor decarbonylation led to its decomposition. Exposure of compound **11** in cyclohexane to UV radiation provokes the decarbonylation, especially with UV 256 nm (entries 5 and 6) but also with UV 300 nm in lower yield (entry 7). UV experiments were carried out in a quartz tube and the temperature raise to 50 °C because of the heat of the UV lamps. The product generated in this experiment could be obtained in a pure state for subsequent detailed spectroscopic and homolytic bond dissociation studies. All other attempts did not lead to complex **11** (either no reaction or decomposition). The reason for this behavior is presumably the weaker homolytic Mn-C bond strength in **11**, as suggested by DFT calculations (see Chapter 4),[3] resulting in a competition between the rate of thermal decarbonylation leading from **7** to **11** and the rate of product decomposition. In addition, compound **11** has three hydrogens in the β-position, giving possible a β-H-elimination reaction as its analogous alkyl complex, the ethylpenta-carbonylmanganese(I),[16-18] yielding vinylidene fluoride and hydridropentacarbonyl-manganese(I) (^{1}H NMR resonance expected at -7.9 ppm in C_6D_6).[19] However, no signal at this chemical shift was detected, indicating that the decomposition occurs *via* the Mn-C cleavage.

3.2.4.4. Characterization of compound **11**

Compound **11** was not obtained in sufficient amount to be characterized by all the techniques employed for the other complexes (^{13}C NMR, FTIR, single-crystal X-Ray diffraction and elemental analysis). However, the ^{1}H and ^{19}F NMR analyses of the crude reaction solution, which also contained the residual precursor complex **7**, were sufficient for its identification.

The ^{1}H NMR spectrum (Figure 41) in acetone-d_6 shows a binomial triplet at 2.01 ppm ($^3J_{HF}$ = 24.0 Hz), overlapping with the signal of the deuterated solvent. To confirm

the presence of the triplet, another ^{1}H NMR spectrum was taken in benzene-d_6. In this case, that peak shifted to 1.76 ppm.

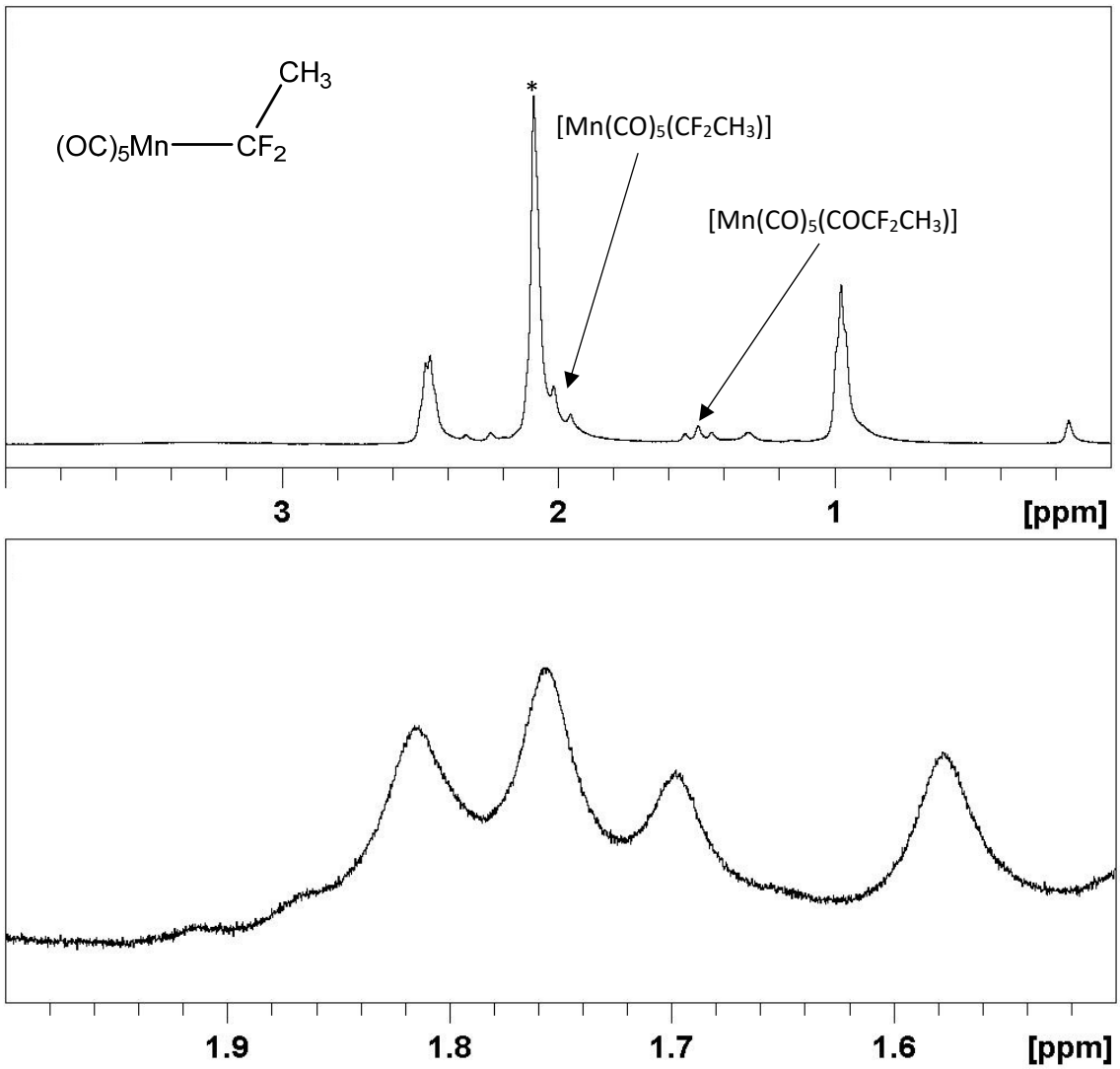

Figure 41. ^{1}H NMR spectra of the sample containing compound **11** (400 MHz): full spectrum above in acetone-d_6 and expansion of the 1.5-2 ppm region in benzene-d_6 below. The starred resonance is due to the solvent.

The ^{19}F NMR (Figure 42) exhibits a quartet at -28.9 ppm with a $^{3}J_{FH}$ = 23.9 Hz. There is a significant downfield shift compared to the corresponding acyl complex (compound **7**), which is still present as shown by the resonance at -91.5 ppm, because of the direct influence of the manganese(I) on the fluorine atoms.

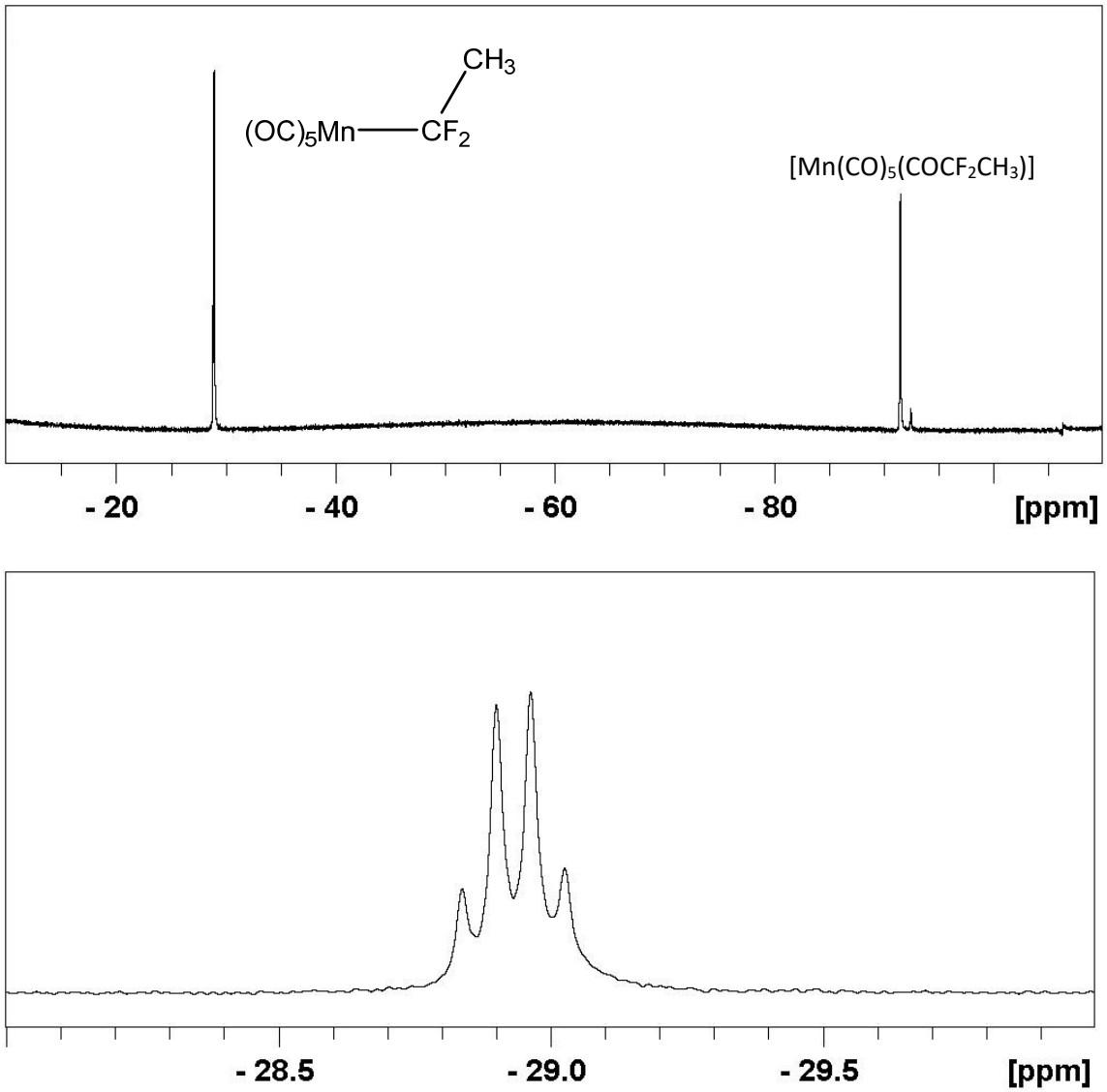

Figure 42. ^{19}F NMR spectrum (376.5 MHz, acetone-d_6) of the sample containing compound **11**: full spectrum above and expansion of the -26 to -30 ppm region below. The signal at -91.5 ppm is a quartet corresponding to the acyl derivative **7** (*cf.* Figure 37) for the incompletely decarbonylated sample.

3.2.5. Vibrational analysis of the fluoroalkylpentacarbonylmanganese(I) derivatives

As shown in the previous sections, the infrared analysis in the Mn-CO stretching region has revealed small absorption bands, in addition to those expected for the $Mn(CO)_5$ moiety, that were not properly assigned in the previous studies of the already investigated compounds. A few of these were also previously observed for the alkyl compounds **8** and **9** and attributed to ^{13}C-containing isotopomers,[20] but a detailed

symmetry analysis has not been previously carried out. These bands cannot originate from by-products that contain the fluoroalkyl groups because the compounds are spectroscopically pure (^{1}H, ^{13}C, ^{19}F NMR previously shown for each complex). Their assignment to by-products that do not contain the fluoroalkyl group is also unlikely because the frequencies of these small bands depend on the nature of the alkyl group. A full frequency analysis by DFT calculations was carried out by Prof. Rinaldo Poli for all fluoroalkyl complexes (**8**-**11**). A summary of the calculated frequencies is shown in Figure 43 while a comparison of the DFT-calculated and the experimental IR spectrum for the representative compound **8**, **9** and **10** is illustrated in Figures 44, 45 and 46, respectively. In these spectra, the calculated frequencies were used together with their corresponding calculated intensity to generate bands by applying a Lorentzian function with a 2 cm^{-1} width at half-height. The calculated spectra for all isotopomers were summed together, each weighed by its relative abundance. Given the natural abundance of ^{13}C (ca. 1%), there is a ca. 1% probability to have the [Mn(*ax*-^{13}CO)(^{12}CO)$_4$R$_F$] isotopomer and ca. 4% probability to have the [Mn(*eq*-^{13}CO)(^{12}CO)$_4$R$_F$], because there are four equivalent equatorial positions. This leaves a ca. 95% probability to have the isotopomer with ^{12}C on all five CO ligands. The probability that two or more than one CO ligand have a ^{13}C isotope is so low that these isotopomers were neglected in this computational study. The calculated spectra are shifted to higher wavenumbers relative to the experimental ones, which is a common phenomenon for DFT-calculated IR spectra, but the general shape of all spectra is reproduced quite well. The trend of the calculated frequencies is also the same as that observed experimentally, placing alkyl donor power in the order $CF_3 < CHF_2 < CH_2CF_3$. The computed frequencies also allow assessing the donor power of CF_2CH_3 substituent in **11**, for which a clean experimental spectrum could not be obtained, as being relatively similar to that of the CH_2CF_3 substituent in **10** (the frequency changes are small and of opposite sign for bands of different symmetry type). The calculations not only confirm the literature assignment of the main (all-^{12}C) isotopomer bands for compounds **8** and **9**, [8,10,20] but also allowed clear identification and assignment of a few weak bands related to the ^{13}C-containing isotopomers.

Three weak bands are visible on the low frequency side of the last band (A_1) of the main isotopomer. One results from the significant shift of one of the two E-type bands for the isomer with equatorial ^{13}C. A second one (not reported in the previously published spectra of **8** and **9**) is the lower-energy A_1 band for the isotopomer with axial ^{13}C. The assignment of the last one of these three bands, which is clearly visible at 2010 cm^{-1} for **8** (see Figure 44) but only as a shoulder of the stronger A_1 band for **9** and **10** (Figures 45 and 46, respectively), is less straightforward. On the basis of the DFT analysis (Figure 43), the only band that could appear in this region is the *eq*-^{13}C isotopomer lower-frequency A_1 vibration and this band is therefore tentatively assigned to this vibrational mode. However, the calculations predict a blue-shift upon isotopic substitution. This outcome may originate from an altered mixing of the Mn-CO vibrators in the two A_1 normal modes, whereas the mere isotopic substitution should lead to a red-shift. Possibly, the actual situation in *n*-pentane solution is different than in the gas phase and indeed results in the expected red-shift.

A shoulder on the low-frequency side of the high-frequency A_1 band, which is visible for all three compounds, seems attributable to the corresponding A_1 vibration of the *eq*-^{13}C isotopomer. The weak band at 2066 cm^{-1} for compound **8**, slightly blue-shifted from the strongest E band of the main isotopomer, is assigned to the *eq*-^{13}C isotopomer B_1 mode. This band gains in intensity relative to the corresponding one of the main isotopomer (243 relative to 0.2, see Figure 43) because the vibrator local C_{4v} symmetry is broken by the isotopic substitution. The weaker and further blue-shifted band in the experimental spectrum (shoulder at ca. 2080 cm^{-1}) is tentatively attributed to the B_1 vibration, possibly gaining intensity relative to the gas-phase calculated spectrum by dynamic symmetry breaking resulting from solvation. For the other two alkyl derivatives **9** and **10**, the lower symmetry of the alkyl group renders B_1 band more intense and clearly visible, as shown in both the experimental and calculated spectra, while that of the *eq*-^{13}C isotopomer is hidden underneath the stronger B_1 and E bands of the main isotopomer. All other calculated bands of the *eq*-^{13}C and *ax*-^{13}C isotopomers overlap with the stronger bands of the main all-^{12}C component.

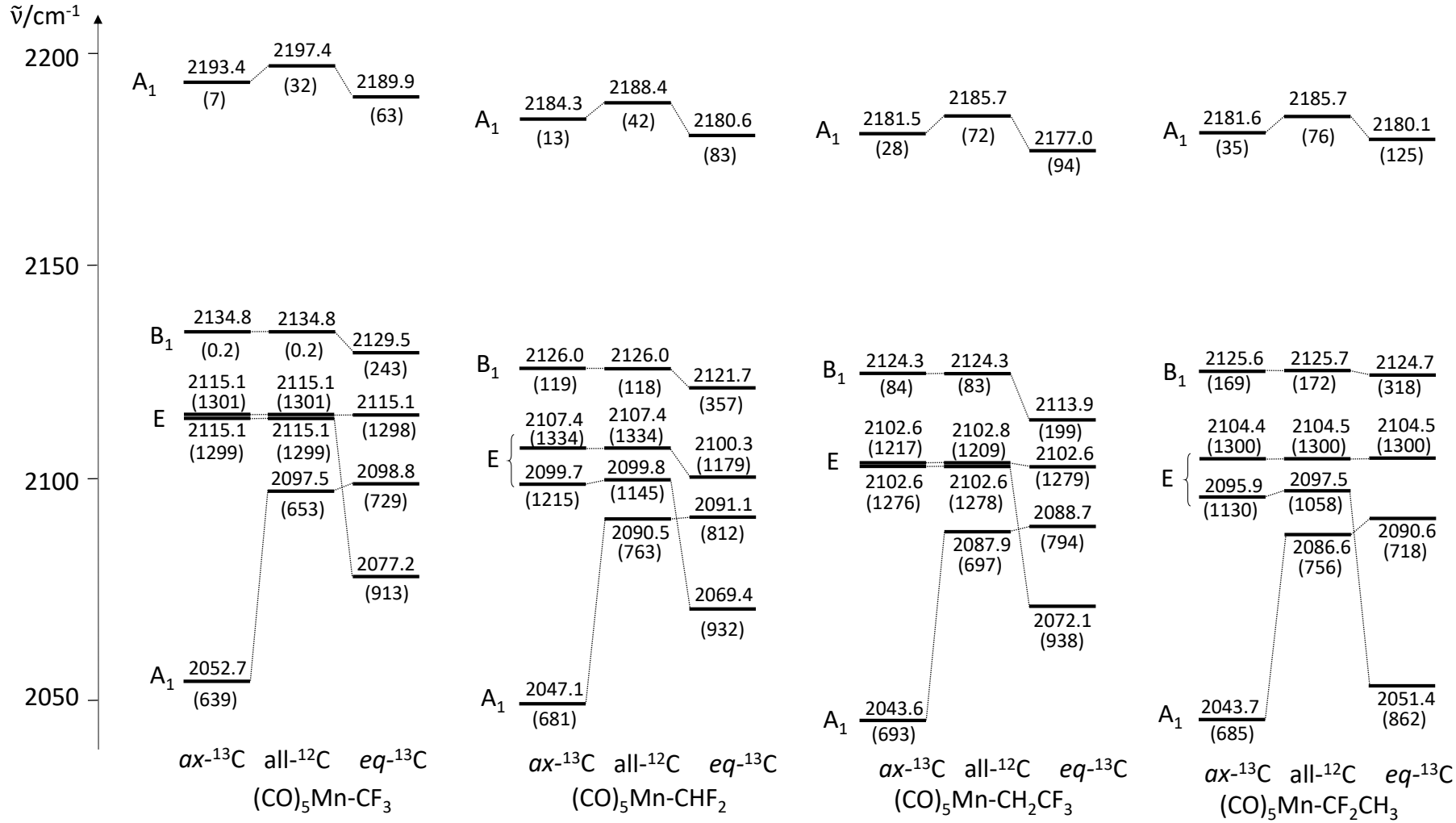

Figure 43: DFT-calculated terminal Mn-CO stretching frequencies (in cm^{-1}) and relative intensities (in parentheses) for complexes **8**, **9**, **10** and **11**.

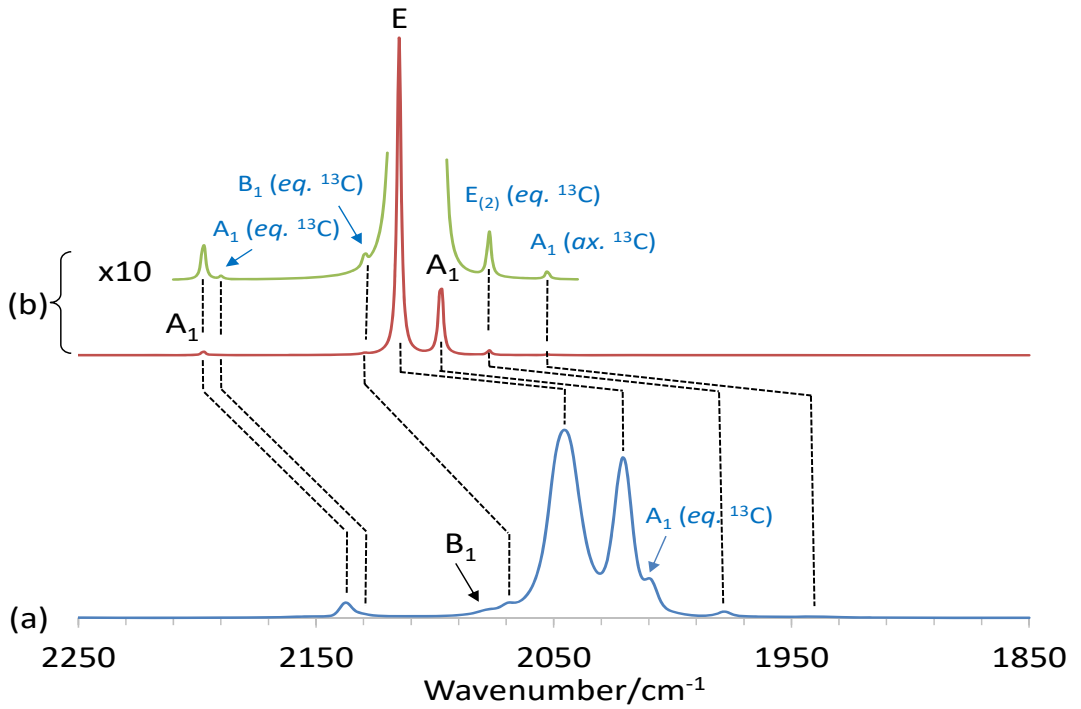

Figure 44. Experimental (a) and DFT-calculated (b) IR spectra of compound **8** in the terminal carbonyl stretching region.

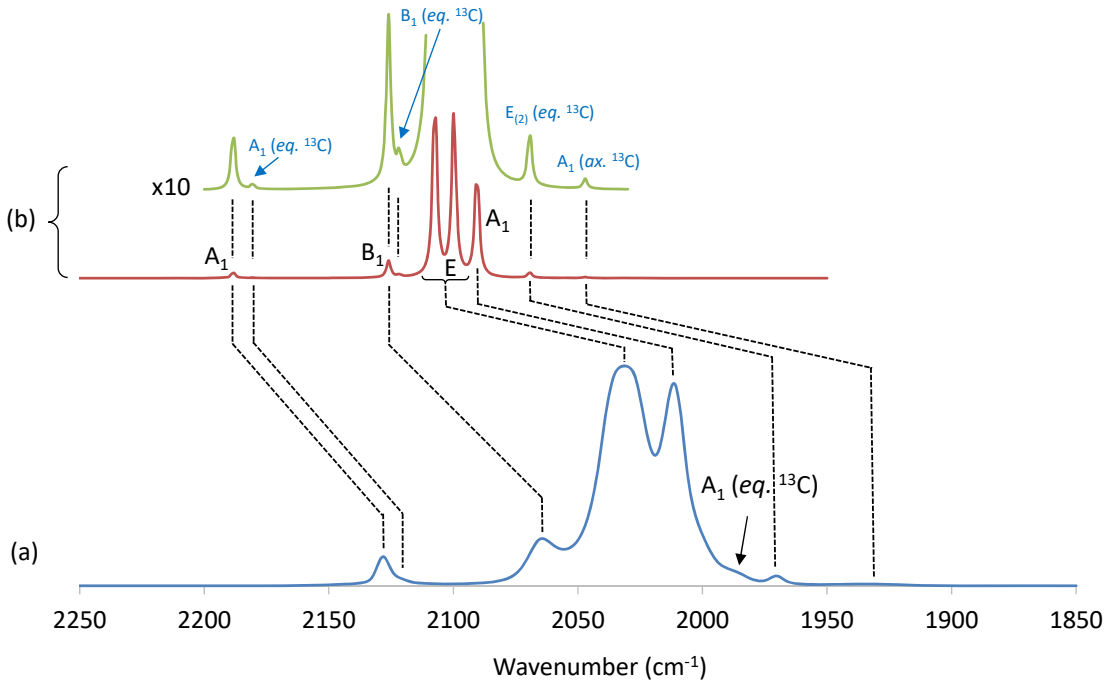

Figure 45. Experimental (a) and DFT-calculated (b) IR spectra of compound **9** in the terminal carbonyl stretching region.

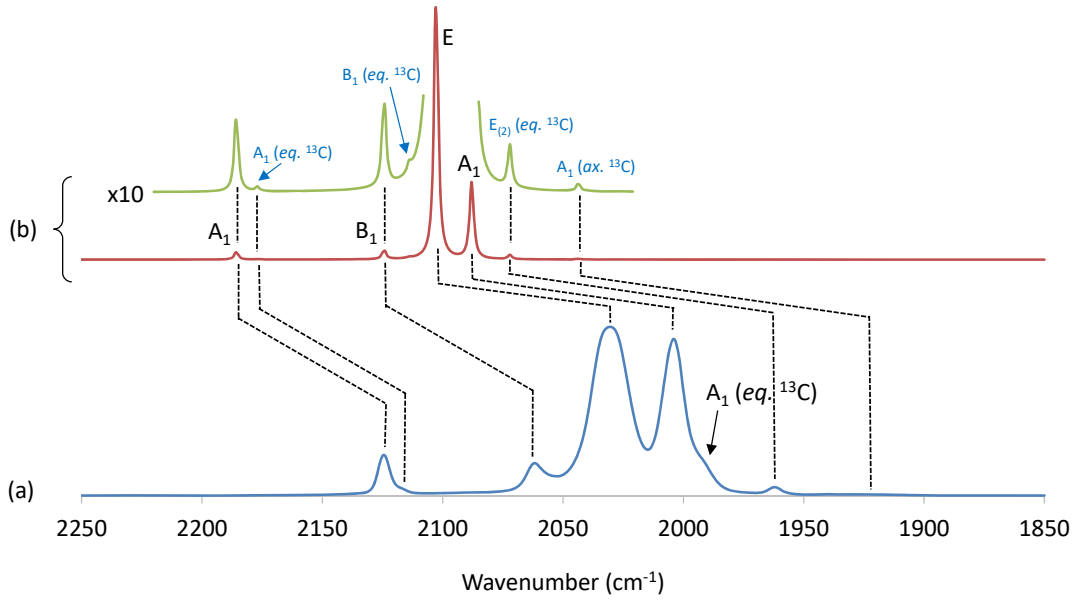

Figure 46. Experimental (a) and DFT-calculated (b) IR spectra of compound **10** in the terminal carbonyl stretching region.

3.2.6. Comparative analysis of the X-ray structures

As stated above, the CF_3 and CHF_2 acyl and alkyl systems have been known for quite some time[1,2] but have not been structurally characterized in the crystalline state. Indeed, X-ray diffraction studies of $[Mn(CO)_5(COR)]$ and $[Mn(CO)_5R]$ compounds are quite limited and do not include any example of fluorine-containing carbyl ligand bonded to Mn *via* an sp^3-hybridized C atom. On the other hand, there are a few $[Mn(CO)_5R]$ structures with F-containing groups bonded *via* an sp^2-hybridized C atom.[21-24] The relevant bond distances and angles of the fluoroalcyl and -alkyl structures determined during this thesis are collected in Table 16 and more extensive metric data are given in the Appendix (Section B).

Table 9. Selected bond distances (in Å) from the X-ray structures of $[Mn(CO)_5(COR_F)]$ and $[Mn(CO)_5R_F]$.

Parameter	Acyl compounds		
	4	**5**	**7**
Mn-C (COR_F)	2.051(3)	2.057(5)	2.0748(14)
Mn-CO_{trans}	1.869(3)	1.869(6)	1.8562(15)
Mn-CO_{cis}	1.872(3) 1.862(3) 1.863(3) 1.879(3)	1.875(6) 1.880(6) 1.862(5) 1.858(6)	1.8809(14) 1.8617(14) 1.8566(14) 1.8697(14)
Alkyl compounds			
	8	**9**	**10**[a]
Mn-C (R_F)	2.067(3)	1.971(2)[b]	2.167(2)/2.162(2)
Mn-CO_{trans}	1.858(3)	1.861(2)[b]	1.834(2)/1.842(2)
Mn-CO_{cis}	1.872(2) 1.873(2)	1.853(3) 1.859(3)	1.871(2)/1.870(2) 1.860(2)/1.865(2) 1.869(2)/1.868(2) 1.870(2)/1.869(2)

[a] Values for two independent molecules in the asymmetric unit. [b] Unreliable parameter because of symmetry-related disorder.

Of particular interest are the Mn-C distances to the R_F groups for the three alkyl complexes **8**, **9** and **10**, because the homolytic bond strengths to these alkyl groups have been predicted to be greater than in the non-F-substituted analogues.[3] For the structure of compound **9**, the molecule sits on a crystallographic mirror plane that imposes a symmetry disorder between the CHF_2 group and one of its *cis* CO ligands. A symmetry lowering did not provide a better crystallographic solution. Therefore, the parameters related to the two disordered groups are unreliable. In the better determined distance in **8**, with three α-F substituents, the Mn-CF_3 distance (2.067(3) Å) is ca. 0.1 Å shorter than the Mn-CH_2CF_3 distance in **10**, 2.162(2) Å. For comparison, other distances to sp^3-hybridized C atoms without any F substituents are 2.214(3) Å in $[Mn(CO)_5(CH_2CH{=}CHCOOPh)]$[25] and 2.195(6) and 2.196(8) Å in $[Mn(CO)_5(CH_2CH_2\text{-}o\text{-}C_6H_4\text{-}CH_2CH_2)Mn(CO)_5]$,[26] whereas positional disorder in the simpler reference compound $[Mn(CO)_5(CH_3)]$ prevented an accurate determination of the Mn-CH_3 distance.[27] The distance in $[Mn(CO)_5(CH_2Cl)]$, with one α-Cl substituent, is 2.125(10) Å.[28] These data suggest that electronegative substituents (particularly F, but even Cl), even when placed on the β-C atom as in **10**, strengthen the Mn-C bond, in agreement with the predictions of a recent DFT study.[3]

3.3. Conclusion

Four fluoroalkylpentacarbonylmanganese(I) complexes have been synthesized by decarbonylation of their corresponding acyl complexes, since the direct synthesis from the corresponding fluoroalkyl halides RX lead to $[Mn(CO)_5X]$ complex, even when fluorine is in β-position. Among the synthesized $[Mn(CO)_5R_F]$, two have been previously described in the literature ($R_F = CF_3$, **8**; CHF_2, **9**). However, the full characterization by ^1H, ^{19}F and ^{13}C NMR spectroscopy, FTIR spectroscopy and single-crystal X-ray diffraction is reported here for the first time. In addition, two new fluoroalkyl derivatives of pentacarbonylmanganese(I), $[Mn(CO)_5R_F]$ ($R_F = CH_2CF_3$, **10**; CF_2CH_3, **11**) have been prepared and investigated. Compound **11** could not be obtained in a pure state, presumably because the homolytic Mn-CF_2CH_3 bond dissociation occurs simultaneously with its generation under the harsh thermal or photochemical conditions of the acyl precursor decarbonylation. Moreover, the synthesis of the acyl precursor (**7**) using 2,2-difluoropropionic chloride synthesized from the 2,2-difluoropropanoic acid and thionyl chloride led to the formation of an unexpected complex, $[Mn(CO)_5(SCOCF_2CH_3)]$ (**12**), which has been characterized by single-crystal X-ray diffraction.

The spectroscopic characterization of compounds **4**-**11** by ^1H, ^{13}C and ^{19}F NMR spectroscopies provide useful and previously unavailable reference values for fluoroalkyl groups bonded to $Mn(CO)_5$. In addition, the FTIR properties of alkyl complexes **8**-**10** in *n*-pentane solution have been fully explored at an unprecedented level of detail with the assistance of DFT calculations, resulting in the full symmetry analysis of the major $[Mn(^{12}CO)_5R_F]$ and minor $[Mn(^{12}CO)_4(eq\text{-}^{13}CO)R_F]$ and $[Mn(^{12}CO)_4(ax\text{-}^{13}CO)R_F]$ isotopomers and in the unambiguous assignment of several observed weak bands.

3.4. Experimental section

General. All operations were carried out under an atmosphere of argon except for the purifications by column chromatography, which were carried out in air, and for the sublimations (under vacuum, products collected in air).

Materials. Compounds $[Mn_2(CO)_{10}]$ (98%, Strem Chemicals), trifluoroacetic anhydride (ReagentPlus® grade, ≥99%, Sigma-Aldrich), difluoroacetic acid (98%, Fluorochem), 3,3,3-trifluoropropionyl chloride (98%, Fluorochem), 1-Iodo-2,2,2-trifluoroethane (97%, Fluorochem), 2,2-difluoropropionic acid (98%, Fluorochem), P_2O_5 (≥98%, Fluka), (2,2,6,6-tetramethylpiperidin-yl)oxy (TEMPO, 98%, Acros Organics), tris(trimethylsilyl)silane (TTMSS, 97%, Sigma-Aldrich), hexafluorobenzene (99%, Aldrich), benzene-d_6 (99.5%D, Euriso-top), acetone-d_6 (99.5%D, Euriso-top), silica (40-63 µm, VMR Chemicals) were used as received. Laboratory Reagent grade (≥99.5%) diethyl ether, *n*-pentane and THF were purchased from Sigma-Aldrich. THF was purified by percolation through a dry activated alumina column. Thionyl chloride (ReagentPlus® grade, ≥99%, Sigma-Aldrich) was distilled in the presence of sulfur prior to use.

Difluoroacetic anhydride (from difluoroacetic acid and P_2O_5)[11] and 2,2-difluoropropionyl chloride (from 2,2-difluoropropionic acid and oxalyl chloride)[14] were synthesized as described in the literature. The preparations of compounds $[Mn(CO)_5(COCF_3)]$, $[Mn(CO)_5(CF_3)]$, $[Mn(CO)_5(COCHF_2)]$, and $[Mn(CO)_5(CHF_2)]$, were adapted from the literature procedures.[1,2] Purifications were carried out by column chromatography through a silica column, using *n*-pentane as the mobile phase to eliminate the $[Mn_2(CO)_{10}]$ impurity and then a 9:1 mixture of *n*-pentane and diethyl ether to elute the product. Single crystals of $[Mn(CO)_5(COCF_3)]$, $[Mn(CO)_5(CF_3)]$, $[Mn(CO)_5(COCHF_2)]$, $[Mn(CO)_5(CHF_2)]$ and $[Mn(CO)_5(CH_2CF_3)]$ for the X-ray diffraction analysis were grown by sublimation at 55 °C and 100 mbar. Single crystals of $[Mn(CO)_5(COCF_2CH_3)]$ were obtained directly in the flask after the evaporation of the solvent in a rotative evaporator.

Instrumentation. The Nuclear Magnetic Resonance (NMR) spectra were recorded on a Bruker Avance™ III 400 MHz spectrometer. The instrumental parameters for recording spectra were as follows: ^{1}H NMR: flip angle 30°, acquisition time 5.7 s, pulse delay 2 s, number of scans 64, and a pulse width of 3.05 µs; ^{19}F NMR: flip angle 30°, acquisition time 2 s, pulse delay 2 s, number of scans 64, and a pulse width of 3.76 µs; ^{13}C NMR: flip angle 30°, acquisition time 1.5 s, pulse delay 2 s, number of scans 10240, and a pulse width of 3.27 µs. The probe has a lower background ^{19}F signals compared to standard dual-channel probes. The Fourier transform infrared (FTIR) spectra on the *n*-pentane solutions were recorded in transmission mode with a PerkinElmer Spectrum One FT-IR Spectrophotometer using a CaF_2 window with a 4 mm thick and 0.05 mm path length. The elemental analyses were carried out by the analytical service of the LCC-Toulouse using a PerkinElmer 2400 CHNS/O Series II System (100V).

Synthesis of trifluoroacetylpentacarbonylmanganese(I), 4. In a Schlenk tube were introduced 390 mg (9.97 mmol) of metallic potassium and 250 mg (10.87 mmol) of metallic sodium under argon. They were crashed together to generate liquid “NaK” alloy. A solution of dimanganese decacarbonyl (2.00 g, 5.13 mmol) in 25 mL of dry THF was added and the resulting mixture was stirred for 3 h at room temperature, with IR monitoring to verify the completion of the reduction process. The mixture was filtered through Celite to yield a greenish-brown solution, rinsing the Celite with 10 mL of dry THF. Then, trifluoroacetic anhydride (2.16 g, 10.28 mmol) was added dropwise at room temperature, generating a dark red solution, which subsequently turned light red and finally yellow after 30 min. After additional stirring at room temperature (total 3 h), the solvent was evaporated under reduced pressure. The product was purified by column chromatography with a solid deposit through a silica gel column, using *n*-pentane as the mobile phase. After elimination of a first yellow fraction corresponding to $[Mn_2(CO)_{10}]$, the mobile phase polarity was increased using a 9:1 mixture of *n*-pentane and diethyl ether (9:1). Immediately a colorless fraction was collected, followed by evaporation to dryness under reduced pressure to afford the product as a white volatile solid generally as needle-shape crystals (2.42 g, 8.29 mmol, yield 81%). A single crystal for the X-ray diffraction analysis was obtained by sublimation at 55 °C and 100 mbar.

Synthesis of trifluoromethylpentacarbonylmanganese(I), 8. Compound $[Mn(CO)_5(COCF_3)]$ (1.89 g, 6.47 mmol) was introduced in a in a 50 mL two-neck flask connected to a reflux condenser to avoid any sublimation losses. The flask was then heated under normal pressure to 120°C for for 1.5 h. During this time, the solid accumulating at the bottom of the condenser was periodically removed and dropped back to the warm flask bottom. The resulting yellow solid was purified by column chromatography through a silica column, using *n*-pentane as the mobile phase. After elimination of a first yellow fraction corresponding to $[Mn_2(CO)_{10}]$, the mobile phase polarity was increased using a 9:1 mixture of *n*-pentane and diethyl ether. Then a colorless fraction was immediately collected and evaporated to dryness under reduced pressure, yielding the product as a white crystalline powder (1.25 g, 4.74 mmol, yield 73%). A single crystal for the X-ray diffraction analysis was obtained by sublimation at 55 °C and 100 mbar.

Synthesis of difluoroacetylpentacarbonylmanganese(I), 5. In a Schlenk tube were introduced 500 mg (12.79 mmol) of metallic potassium and 280 mg (13.05 mmol) of metallic sodium under argon. They were crashed together to generate liquid “NaK” alloy. A solution of dimanganese decacarbonyl (4.00 g, 10.26 mmol) in 40 mL of dry THF was added and the resulting mixture was stirred for 3 h at room temperature, with IR monitoring to verify the completion of the reduction process. The mixture was filtered through Celite to yield a greenish-brown solution, rinsing the Celite with 10 mL of dry THF. Then, difluoroacetic anhydride (3.60 g, 20.68 mmol) synthesized from difluoroacetic acid and phosphorous pentoxide was added dropwise at room temperature, generating a red solution, which subsequently turned to orange after 1h. After additional stirring at room temperature (total 3 h), the solvent was evaporated under reduced pressure. The product was purified by column chromatography with a solid deposit through a silica gel column, using *n*-pentane as the mobile phase. After elimination of a first yellow fraction corresponding to $[Mn_2(CO)_{10}]$, the mobile phase polarity was increased with a mixture of *n*-pentane and diethyl ether (9:1). Immediately a light-yellow band was collected, followed by evaporation to dryness under reduced

pressure to afford the product as a light orange-brownish oil (4.20 g, 15.33 mmol, yield 75%) that becomes a solid by scratching walls of the flash. A single crystal for the X-ray diffraction analysis was obtained by sublimation at 55 °C and 100 mbar.

Synthesis of difluoromethylpentacarbonylmanganese(I), 9. Compound $[Mn(CO)_5(COCHF_2)]$ (4.20 g, 15.33 mmol) was introduced in a in a 50 mL two-neck flask connected to a reflux condenser to avoid any sublimation losses. The flask was then heated under normal pressure to 120°C for for 1.5 h. During this time, the solid that accumulates at the bottom of the condenser was periodically removed and dropped back to the warm flask bottom. The resulting yellow solid was purified by column chromatography through a silica column, using *n*-pentane as the mobile phase. After elimination of a first yellow fraction corresponding to $[Mn_2(CO)_{10}]$, the mobile phase polarity was increased using a mixture of *n*-pentane and diethyl ether (9:1). Then a light-yellow band was immediately collected and evaporated to dryness under reduced pressure, yielding the product as a light brown crystalline powder (2.47 g, 10.04 mmol, yield 65%). A single crystal for the X-ray diffraction analysis was obtained by sublimation at 55 °C and 100 mbar.

Synthesis of 3,3,3-trifluoropropanoylpentacarbonylmanganese(I), 6. In a Schlenk tube were introduced 395 mg (10.10 mmol) of metallic potassium and 260 mg (11.31 mmol) of metallic sodium under argon. They were crashed together to generate liquid “NaK” alloy. A solution of dimanganese decacarbonyl (3.00 g, 7.69 mmol) in 30 mL of dry THF was added and the resulting mixture was stirred for 3 h at room temperature, with IR monitoring to verify the completion of the reduction process. The mixture was filtered through Celite to yield a greenish-brown solution, rinsing the Celite with 10 mL of dry THF. Then, 3,3,3-trifluoropropanoyl chloride (2.25 g, 15.36 mmol) was added dropwise at room temperature, generating a light red solution, which subsequently turned bright red and finally orange after 1 h. After additional stirring at room temperature (total 3 h), the solvent was evaporated under reduced pressure. The product was purified by column chromatography through a silica gel column, using *n*-pentane as the mobile phase. After elimination of a first yellow fraction corresponding to $[Mn_2(CO)_{10}]$, the

mobile phase polarity was increased using a mixture of *n*-pentane and diethyl ether (9:1). A light-yellow band was collected, followed by evaporation to dryness under reduced pressure to afford the product as a pale-yellow solid (3.56 g, 11.5 mmol, yield 75%).

Synthesis of 2,2,2-trifluoroethylpentacarbonylmanganese(I), 10. Compound $[Mn(CO)_5(COCH_2CF_3)]$ (2.25 g, 7.35 mmol) was introduced in a two-neck flask connected to a reflux condenser to avoid any sublimation losses. The flask was then heated under normal pressure to 80°C for 1.5 h. During this time, the solid that accumulates at the bottom of the condenser was periodically removed and dropped back to the warm flask bottom. The resulting light-brown powder was purified by column chromatography through a silica column, using *n*-pentane as the mobile phase. After elimination of a first yellow fraction corresponding to $[Mn_2(CO)_{10}]$, the mobile phase polarity was increased using a mixture of *n*-pentane and diethyl ether (9:1). Then a light-yellow band was collected and evaporated to dryness under reduced pressure, yielding the product as a yellow solid (1.63 g, 5.86 mmol, yield 80%). A single crystal for the X-ray diffraction analysis was obtained by sublimation at 55 °C and 100 mbar. Decarbonylation of $[Mn(CO)_5(COCH_2CF_3)]$ could also be accomplished by heating the solid in a sublimation apparatus under vacuum at 55 °C under 100 mbar for 5 days. Starting the reaction from 1.978 g of dimanganese decacarbonyl (5.07 mmol) and 1.473 g of 3,3,3-trifluoropropanoyl chloride (10.06 mmol) and following the same synthetic procedure, the pure product (1.122 g, 4.04 mmol, yield 40 %) was directly collected as a light-yellow microcrystalline powder from the cold finger.

Synthesis of 2,2-Difluoropropanoylpentacarbonylmanganese(I), 7. In a Schlenk tube were introduced 400 mg (10.23 mmol) of metallic potassium and 300 mg (13.05 mmol) of metallic sodium under argon. They were crashed together to generate liquid “NaK” alloy. A solution of dimanganese decacarbonyl (3.00 g, 7.69 mmol) in 30 mL of dry THF was added and the resulting mixture was stirred for 3 h at room temperature, with IR monitoring to verify the completion of the reduction process. The mixture was filtered through Celite to yield a greenish-brown solution, rinsing the Celite with 10 mL of dry

THF. 2,2-trifluoropropanoyl chloride (1.98 g, 15.45 mmol) was added dropwise at room temperature. The latter was produced *in situ* as follows. 2,2-Difluoropropionic acid (1.70 g, 15.45 mmol) was introduced in 50 mL two-neck flask connected to a bubbler and dissolved in 5 mL of dry THF. Then oxalyl chloride (2.11 g, 16.62 mmol) was added dropwise and finally 150 µL of dry DMF was added. The mixture was stirred for 1 h (until bubbling stopped). After the addition of 2,2-difluoroporpanoyl chloride, the solution turns to light red solution, which subsequently turned bright red and finally orange after 1 h. After additional stirring at room temperature (total 3 h), the solvent was evaporated under reduced pressure. The product was purified by column chromatography through a silica gel column, using *n*-pentane as the mobile phase. After elimination of a first yellow fraction corresponding to $[Mn_2(CO)_{10}]$, the mobile phase polarity was increased using a mixture of *n*-pentane and diethyl ether (9:1). Then a light-yellow (nearly colorless) band was collected, followed by evaporation to dryness under reduced pressure to afford the product as volatile brownish-white needle-shape microcrystals (1.49 g, 5.17 mmol, yield 33%). A third fraction of an orange unidentified oil was recovered immediately after that of the product.

Synthesis of 1,1-Difluoroethylpentacarbonylmanganese(I), 11. Compound $[Mn(CO)_5(COCF_2CH_3)]$ (20 mg, 0.069 mmol) was introduced in a 50 mL two-neck flask and dissolved in 5 mL of 2-butanone. The system was connected to a refrigerant and to a bubbler and purge during for 15 min with an argon flow. Then it was heated up to 80°C for 1 h. The solvent was finally removed by evaporation under reduced pressure leading to a yellow powder which contain the complex **8** (yield 64%, determined by relative integration of $[Mn(CO)_5(COCF_2CH_3)]$ and $[Mn(CO)_5(CF_2CH_3)]$ signals). The small amount obtained after decarbonylation reaction did not allow its purification by column chromatography. Additional experiments carried out with a greater amount of complex and heating for a longer period let to decomposition of the desired product and lower spectroscopic yields.

3.5. References

[1] R. B. King In *Organometallic Syntheses*; Academic Press: NY, 1965; Vol. 1, p 145-147.
[2] R. B. King *Acc. Chem. Res.* **1970**, *3*, 417-427.
[3] R. Poli; S. M. W. Rahaman; V. Ladmiral; B. Ameduri *J. Organomet. Chem.* **2018**, *864*, 12-18.
[4] T. H. Coffield; J. Kozikowski; R. D. Closson *Abstracts of the International Conference on Coordination Chemistry, London* **April 1959**, 126.
[5] H. D. Kaesz; R. B. King; F. G. A. Stone *Z. Naturforsch. B* **1960**, *15*, 763-764.
[6] A. Battais; B. Boutevin; Y. Pietrasanta; P. Sierra *J. Fluorine Chem.* **1981**, *19*, 35-42.
[7] W. Beck; W. Hieber; H. Tengler *Chem. Ber.* **1961**, *94*, 862-872.
[8] F. Calderazzo; K. Noack; U. Schaerer *J. Organomet. Chem.* **1966**, *6*, 265-271.
[9] K. Noack; U. Schaerer; F. Calderazzo *J. Organometal. Chem.* **1967**, *8*, 517-526.
[10] F. A. Cotton; A. Musco; G. Yagupsky *Inorg. Chem.* **1967**, *6*, 1357-1364.
[11] E. Sawicki *J. Org. Chem.* **1956**, *21*, 376-376.
[12] A. Foris *Magn. Reson. Chem.* **2004**, *42*, 534-555.
[13] C. Wakselman; M. Tordeux *J. Fluorine Chem.* **1982**, *21*, 99-106.
[14] B. K. Albrecht; J. E. Audia; L. A. Dakin; M. Duplessis; V. S. Gehling; J. C. Harmange; C. G. Nasveschuk; R. G. Vaswani (Constellation Pharmaceuticals Inc.). Indole derivatives as modulators of methyl modifying enzymes, compositions and uses thereof. WO 2015/023915 A1, 2015.
[15] D. Velayutham; K. Jayaraman; K. Kulangiappar; N. Ilayaraja; Y. R. Babu; P. S. Rao; S. N. Reddy; K. V. Babu; M. Noel *J. Fluorine Chem.* **2006**, *127*, 1111-1118.
[16] B. Wozniak; J. D. Ruddick; G. Wilkinson *J. Chem. Soc. A* **1971**, 3116-3120.
[17] P. M. Treichel In *Comprehensive Organometallic Chemistry*; Stone, F. G. A., Abel, E. W., Eds.; Pergamon Press: Oxford, 1982; Vol. 4, p 92.
[18] F. A. Cotton *Advanced Inorganic Chemistry*; 4th ed.; John Wiley: New York, 1980.
[19] J. W. Kee; C. C. Chong; C. K. Toh; Y. Y. Chong; W. Y. Fan *J. Organomet. Chem.* **2013**, *724*, 1-6.
[20] K. Noack; U. Schaerer; F. Calderazzo *J. Organometal. Chem.* **1967**, *8*, 517-526.
[21] F. W. Einstein; H. Luth; J. Trotter *J. Chem. Soc. A* **1967**, 89-93.
[22] R. P. Hughes; S. J. Doig; R. C. Hemond; W. L. Smith; R. E. Davis; S. M. Gadol; K. D. Holland *Organometallics* **1990**, *9*, 2745-2753.
[23] D. Lentz; S. Willemsen *Angew. Chem. Int. Ed.* **2001**, *40*, 2087-2091.
[24] M. F. Kuehnel; D. Lentz *Dalton Trans.* **2009**, 4747-4755.
[25] A. P. Masters; J. F. Richardson; T. S. Sorensen *Canad. J. Chem.* **1990**, *68*, 2221-2227.
[26] E. Lindner; W. Wassing; R. Fawzi; M. Steimann *Z. Natuforsch. B* **1993**, *48*, 1651-1660.
[27] M. A. Andrews; J. Eckert; J. A. Goldstone; L. Passell; B. Swanson *J. Am. Chem. Soc.* **1983**, *105*, 2262-2269.
[28] B. K. Nicholson; J. S. McIndoe; D. A. Clemente; W. T. Robinson *Struct. Chem.* **2008**, *19*, 489-492.

Chapter 4

Manganese-carbon bond dissociation enthalpy studies of [Mn(CO)$_5$R] complexes

Outline:

4. Manganese-carbon bond dissociation enthalpy studies of [Mn(CO)$_5$R] complexes

4.1. Introduction

A recently published computational study[1] of the Mn^{I}-R_F bond dissociation enthalpies (BDEs) in all possible fluorinated ethyl derivatives, [Mn(CO)$_5$($CH_{2-n}F_nCH_{3-m}F_m$)] (n = 0-2; m = 0-3), has shown that these bonds are much stronger than the corresponding Co^{III}-R_F ones in the related [(acac)$_2$Co($CH_{2-n}F_nCH_{3-m}F_m$)] compounds (acac = acetylacetonate). The BDE range is 42-53.5 kcal·mol^{-1} for the former family *vs.* 22-30.5 kcal·mol^{-1} for the latter one, the value within each range depending on the C^{α} and C^{β} F substitution. The reversible dissociative activation of the [(acac)$_2$$Co^{III}$-$PVDF_H$] and [(acac)$_2$$Co^{III}$-$PVDF_T$] bonds to generate free radicals and [Co(acac)$_2$] was experimentally demonstrated by the successful OMRP of VDF.[2] Thus, thermal activation of these bonds to produce radicals under the same conditions appears less likely. In order to learn more about the possible radical generation by Mn^{I}-R homolytic cleavage in [Mn(CO)$_5$R], an experimental determination of the Mn-C BDE in these compounds have been undertaken. An additional reason to do this study was to verify the validity of the DFT predictions, especially because the BDEs obtained by the DFT study are significantly greater than the previous experimental estimates for compounds [Mn(CO)$_5$(CF_3)] and [Mn(CO)$_5$(CHF_2)] based on Calvet calorimetry[3] and photoionization mass spectrometry.[4] It is also to be noted that another previous computational investigation[5] predicted stronger bonds for these two compounds, relative to the experimental estimates available at that time (Table 1). However, those experimental estimates were indirect determination that made use of several assumptions. In the present study, a more direct method based on kinetics measurements has been used.

Table 1. Activation parameters reported in the literature for the homolytic Mn-R_F bond cleavage in compounds **8**, **9**, **10** and **11**.

Compound	$\Delta H^{\ddagger}$ (kcal·mol^{-1})			$\Delta S^{\ddagger}$ (cal·mol^{-1}·K^{-1})
	Exp	DFT [c]	DFT [d]	DFT [c]
[Mn(CO)$_5$(CF$_3$)] (**8**)	43.5±2.6 [a] 48.5±1.4 [b]	55.1	53.6	45.8
[Mn(CO)$_5$CHF$_2$] (**9**)	34.4±2.6 [a]	48.0	48.5	43.2
[Mn(CO)$_5$(CH$_2$CF$_3$)] (**10**)	-	50.5	-	48.8
[Mn(CO)$_5$(CF$_2$CH$_3$)] (**11**)	-	46.0	-	48.5

[a] Determined by photoionization mass spectrometry from ref. [6]. [b] Determined by Calvet microcalorimetry from ref. [4]. [c] Values from ref. [1]. [d] Values from ref. [5].

For this purpose, a few manganese pentacarbonyl derivatives with R_F = CF_3 and CHF_2 previously described in the literature have been used, but also new compounds with R_F = CH_2CF_3 and CF_2CH_3. The synthesis and characterization of which is reported here for the very first time. Both compounds have been especially selected because they represent models of the putative head and tail dormant species resulting from the hypothetical chain trapping of VDF by [(CO)$_5$Mn$^{\bullet}$]. Polymerization tests of VDF using these complexes will be described in Chapter 5.

The BDEs were only determined for compounds **1**, **8**, **9** and **10**, because compound **2**, **3** and **11** could not be obtained in sufficient quantities or in a satisfactory pure state. Under thermal activation at constant temperature, the residual [Mn(CO)$_5$R] concentration was monitored by ^{1}H NMR spectroscopy for alkylpentacarbonylmanganese(I) complexes and by ^{19}F NMR spectroscopy for fluoroalkylpentacarbonylmanganese(I) in the presence of 1,3,5-trioxane or hexafluorobenzene respectively as internal standard plus a high amount of a radical trapping agent (T, see Scheme 1), sufficient to ensure saturation kinetics (reaction rate limited by the bond cleavage step and a first-order decay, d[Mn(CO)$_5$R]/dt = - k_a[Mn(CO)$_5$R]).

$$[(CO)_5Mn\text{-}R] \underset{k_{da}}{\overset{k_a}{\rightleftharpoons}} [(CO)_5Mn]^\bullet + R^\bullet \qquad (1)$$

$$R^\bullet + T \xrightarrow{k_{trap,R}} \text{trapped product} \qquad (2)$$

$$\begin{cases} [(CO)_5Mn]^\bullet + T \xrightarrow{k_{trap,Mn}} \text{trapped product} & (3a) \\ 2\,[(CO)_5Mn]^\bullet \xrightarrow{k_{dim}} [Mn_2(CO)_{10}] & (3b) \end{cases}$$

Scheme 1. Thermal decomposition of alkylpentacarbonylmanganese(I) compounds in the presence of a radical trap.

The same protocol was previously employed in the literature for the measurement of activation barriers for other radical-generating reactions such as for homolytic splitting of metal-metal bonds,[7] the Co^{III}-R cleavage in vitamin B_{12}[8,9] and related model compounds,[10-12] or the alkyl halide activation by metal catalysts in atom transfer radical polymerization systems.[13-16] For the metal-metal and metal-carbon breaking processes, where the reverse reaction is assumed to have a minimal activation barrier, the kinetic activation enthalpy was considered as a good upper-limit approximation of the thermodynamic bond dissociation enthalpy (BDE). An important difference between the present system and the above-cited precedents is that the co-product of the organic radical (Scheme 1, equation 1), namely $[(CO)_5Mn^\bullet]$, is itself a reactive radical. In addition to efficiently trapping the $R_F^\bullet$ radical in equation 2 ($k_{trap,R}[T] >> k_{da}[(CO)_5Mn^\bullet]$), the trapping agent T may also possess the ability to efficiently trap the $[(CO)_5Mn^\bullet]$ radical (Scheme 1, equation 3a) ($k_{trap,Mn}[T] >> k_{da}[R^\bullet]$). It is also known from flash photolysis studies that the bimolecular coupling of the $[(CO)_5Mn^\bullet]$ radicals (Scheme 1, equation 3b) is an extremely fast process ($k_{dim} = 1.9 \cdot 10^9\ M^{-1}s^{-1}$).[17]

Once the conditions allowing saturation behavior are established (notably the minimum amount of trapping species needed to ensure a zero-order dependence on [T]), several rate constants are determined under these conditions at different temperatures. Then Eyring's equation (Equation 4, see below) is used to plot ln(k/T) *vs.* 1/T to calculate the enthalpy and entropy of activation by a linear fit. The enthalpy of activation is a close approximation in excess of the BDE.

Eyring's equation (linear form): $ln\frac{k}{T} = \frac{\Delta H^{\ddagger}}{R} \cdot \frac{1}{T} + ln\frac{k_B}{h} + \frac{\Delta S^{\ddagger}}{R}$ (Equation 4)

where:

- k is the reaction rate constant
- T = absolute temperature
- $\Delta H^{\ddagger}$ = enthalpy of activation
- R = gas constant
- k_B = Boltzmann constant
- h = Planck's constant
- $\Delta S^{\ddagger}$ = entropy of activation

4.2. Results and discussion

The selection of an appropriate trapping agent is of key importance. A successful trapping agent must not only react rapidly and irreversibly with R (and possibly also with [(CO)$_5$Mn$^{\bullet}$]). It must also be inert relative to the starting compound, [Mn(CO)$_5$R], under the thermal degradation conditions.

Initially (2,2,6,6-tetramethylpiperidin-1-yl)oxyl (TEMPO) was considered as a radical trap agent, since this compound was used in several of the above-mentioned radical trapping studies. However, preliminary experiments carried out on compound **10** (^{19}F NMR δ -51.9 in C_6D_6) at 70 °C for 3 h with 25 equivalents of TEMPO in toluene and using 1,3,5-tris(trifluoromethyl)benzene as internal standard (^{19}F NMR δ -62.0 in C_6D_6) did not lead to the formation of the expected TEMPO-CH_2CF_3 product (^{19}F NMR signal reported at δ -71.58 in $CDCl_3$)[18] (Figure 1). Only one unidentified product was observed at δ -81.0 ppm. Furthermore, this experiment did not reveal the expected simple kinetic behavior with high concentrations of TEMPO (Figure 2), while the experiments carried out with 5 and 15 equivalents show the expected trend, suggesting close to saturation behavior, further increase of the TEMPO/Mn ratio resulted in the same slope but also a non-zero intercept, indicating a faster initial decay.

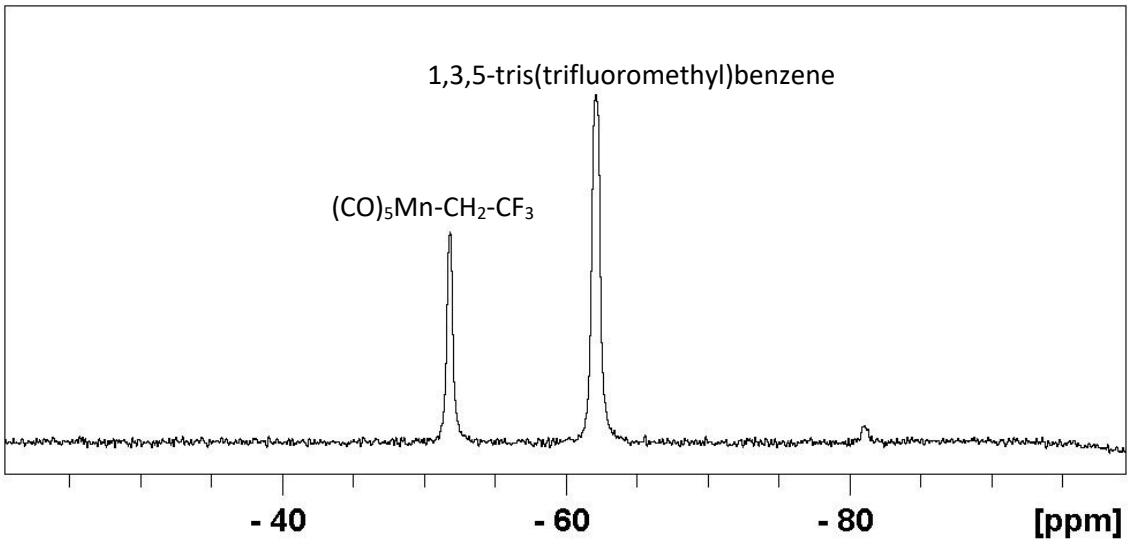

Figure 1. ^{19}F NMR spectrum (376.5 MHz, benzene-d_6) of compound **10** in presence of 25 equivalents of TEMPO at 70 °C after 3 h.

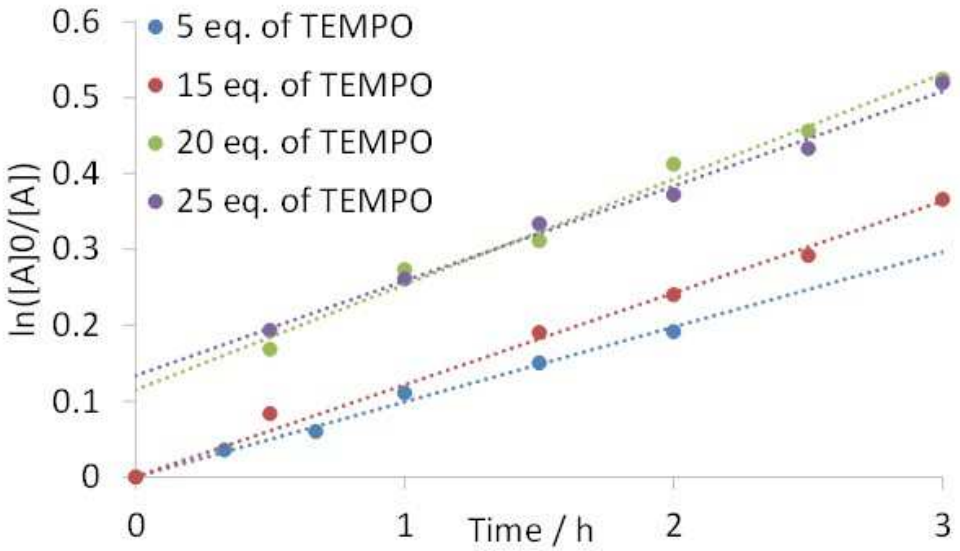

Figure 2. Results of the [Mn(CO)$_5$(CH$_2$CF$_3$)] decomposition at 70 °C in C_6D_6 at different TEMPO/[Mn(CO)$_5$(CH$_2$CF$_3$)] ratios.

A potential problem is the action of TEMPO as a ligand.[19-21] Coordination to Mn^I may occur at a site left vacant by CO dissociation or by migratory insertion, followed by degradation by a pathway that does not involve Mn-C bond cleavage as the initial step (Scheme 2). This reaction depends on the TEMPO concentration: with high concentrations TEMPO may be able to coordinate to a site left vacant. The determined activation parameters would not provide an indication of the Mn-C bond strength.

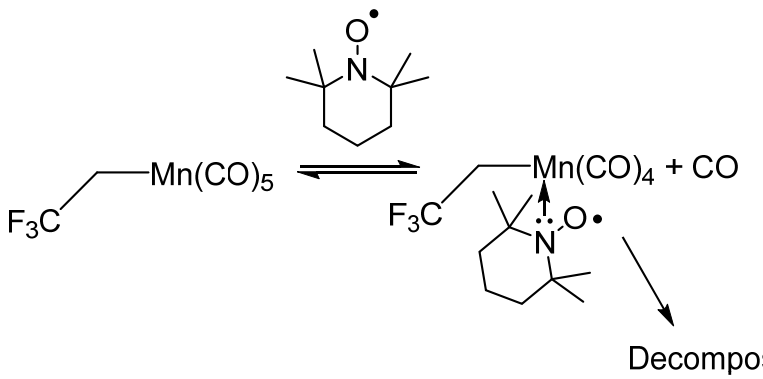

Scheme 2. Proposed mechanism of the $[Mn(CO)_5(CH_2CF_3)]$ decomposition in the presence of TEMPO at high concentrations.

The attention was therefore turned toward tris(trimethylsilyl)silane (TTMSS), since this molecule can be reasonably expected to display poorer coordinating properties than TEMPO (Scheme 3). It has been extensively used as a radical-based reducing agent[22,23] and as an efficient H atom donor to a variety of carbon-centered radicals $R^{\bullet}$.[24-26] It has also been shown that the $(Me_3Si)_3Si^{\bullet}$ radical generated by H atom transfer dimerizes to $Si_2(SiMe_3)_6$ (equation 4).[27] Furthermore, $Si_2(SiMe_3)_6$ is known to react with $[Mn_2(CO)_{10}]$ to produce $[(CO)_5Mn(Si(SiMe_3)_3)]$ with liberation of H_2 (Scheme 3, equation 5).[28,29] The use of Me_3SiH to trap $H_3C^{\bullet}$ radicals thermally generated from $[Mn(CO)_5(CH_3)]$ has previously been described, although the investigation did not assess the barrier to the homolytic bond cleavage.[30] The experimental BDE measurements are detailed below for each complex, whereas a summary and a discussion of these values and a comparison with the computed ones and the ones reported in the literature is in a separate section (section 4.3).

$$[(CO)_5Mn\text{-}R] \underset{k_{da}}{\overset{k_a}{\rightleftharpoons}} [(CO)_5Mn]^{\bullet} + R^{\bullet} \quad (1)$$

$$R^{\bullet} + H\text{-}Si(SiMe_3)_3 \xrightarrow{k_{trap}} R\text{-}H + {}^{\bullet}Si(SiMe_3)_3 \quad (2)$$

$$2\,[(CO)_5Mn]^{\bullet} \xrightarrow{k_{dim,Mn}} [Mn_2(CO)_{10}] \quad (3)$$

$$2\,{}^{\bullet}Si(SiMe_3)_3 \xrightarrow{k_{dim,Si}} Si_2(SiMe_3)_6 \quad (4)$$

$$[Mn_2(CO)_{10}] + H\text{-}Si(SiMe_3)_3 \xrightarrow{k_{trap,Mn}} [(CO)_5Mn\text{-}Si(SiMe_3)_3] + H_2 \quad (5)$$

Scheme 3. Thermal decomposition of $[Mn(CO)_5(R)]$ (R = alkyl or fluoroalkyl chain) in the presence of TTMSS as a radical trap.

4.2.1. Experimental determination of the Mn-CF_3 BDE in **8**

All the reactions were carried out in NMR tubes under argon directly inside the NMR spectrometer probe at the indicated temperatures, using benzene-d_6 as solvent and hexafluorobenzene as internal standard to determine the relative amount of the remaining complex **8** at each time.

First, the observed pseudo-first-order rate constants (k_{obs}) were determined for different TTMSS/Mn molar ratios at the same temperature to ensure that the saturation behavior was reached. For this, k_{obs} must be equal at different equivalents of TTMSS. Measurements were carried out at 100 °C with 5, 7 and 10 equivalents of TTMSS relative to the amount of compound **8** (Scheme 4). Decomposition of this complex was monitored by ^{19}F NMR each 730 s (Figure 3).

$$[Mn(CO)_5(CF_3)] \xrightarrow[C_6D_6;\ C_6F_6,\ 100\ °C]{(TMS)_3SiH,\ (5,\ 7\ and\ 10\ equiv.)} CF_3H + Si_2(TMS)_6 + [Mn(CO)_5(Si(TMS)_3)] + ...$$

Scheme 4. Expected products of the thermal decomposition of [Mn(CO)$_5$(CF$_3$)] in C_6D_6 at 100 °C in the presence of different equivalents of TTMSS.

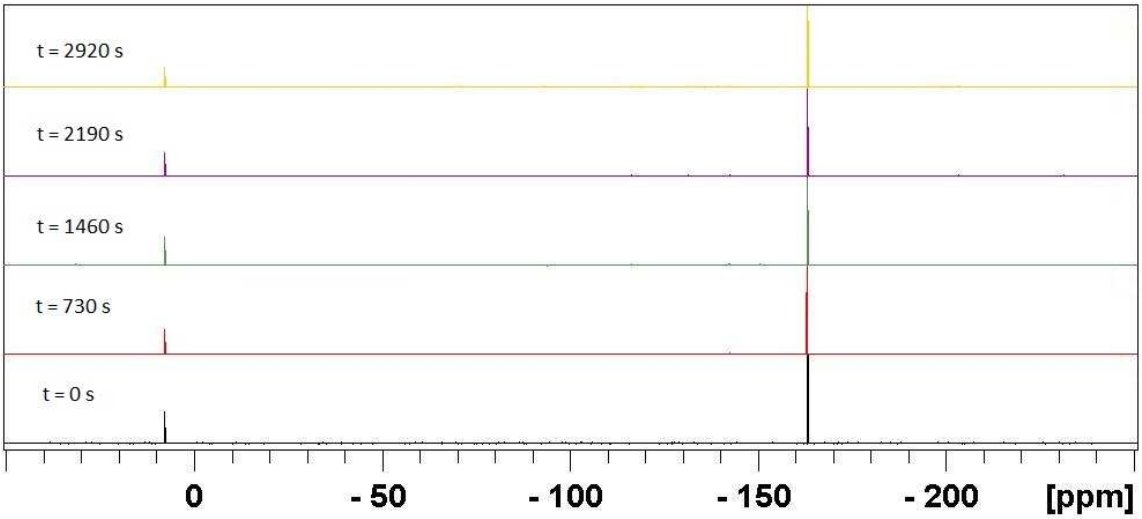

Figure 3. ^{19}F NMR monitoring (376.5 MHz, C_6D_6) of [Mn(CO)$_5$(CF$_3$)] with 10 equivalents of TTMSS at 100 °C at various reaction times. The resonance observed at -163.1 ppm belongs to the hexafluorobenzene internal standard.

The expected trapping of the primary $CF_3^{\bullet}$ radical by TTMSS should lead to CF_3H, the identification of which by ^{19}F NMR is complicated by its volatility (b.p. = -82.1 °C) and by its low solubility in the C_6D_6 solvent, leading to its escape to the head space of the

NMR tube at the high temperatures used in the experiments. The expected signal for this product was not clearly evident from the ^{19}F NMR spectrum. However, evidence for its presence was obtained by ^{1}H-^{19}F HETEROCOSY NMR spectroscopy at 10 °C, where a quartet at δ 5.59 (^{1}H) coupled with a doublet at δ -78.03 (^{19}F) with a coupling constant $^{2}J_{FH}$ of 78 Hz was observed (see Figure 4), which is in good agreement with the ^{1}H and ^{19}F NMR resonance reported in the literature at 6.25 ($^{2}J_{HF}$ = 79.2 Hz) in cyclohexane[31] and -78.6 ($^{2}J_{FH}$ = 79 Hz),[32] respectively. The ^{1}H NMR resonance is slightly shielded compared to the value reported in the literature probably because of the deuterated solvent used (benzene-d_6).

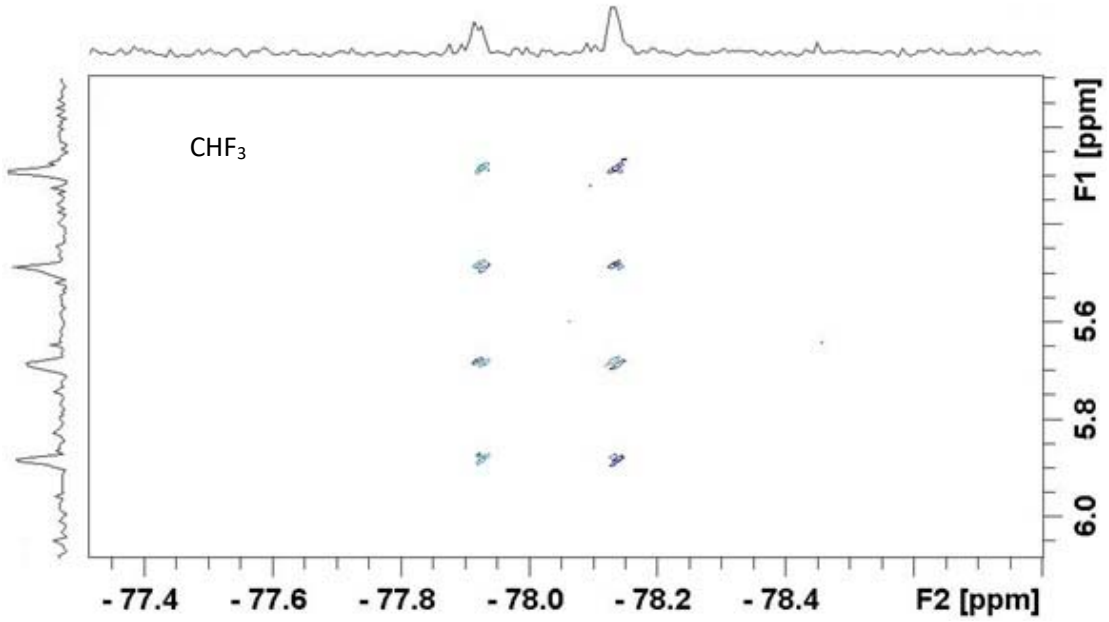

Figure 4. ^{1}H-^{19}F HETEROCOSY NMR spectrum at 10 °C proving the generation of CHF_3 during the decomposition of compound **8** by heating 1 hour in the presence of 10 equivalents of TTMSS at 100 °C.

The relative remaining amount of **8** was determined in the ^{19}F NMR spectra by relative integration of the signals of the complex (7.9 ppm) and the internal standard, the hexafluorobenzene (-163.1 ppm). The signal of hexafluorobenzene was integrated from -162.8 ppm to -163.2 ppm, and its value was set to 1 in all the spectra. Then, the complex signal was integrated from 7.7 ppm to 8.1 ppm. Knowing the initial concentration of complex in each tube (C_0), the concentration of complex at time t (C_t) was determined as $C_t = C_0 I_t / I_0$, where I_0 and I_t stand for the integral value of the NMR

signal of the complex at t = 0 and at t, respectively. The $\ln[C_0/C_t]$ *vs.* time plots led to straight lines, the slopes of which represents k_{obs} (Figure 5 and Table 2).

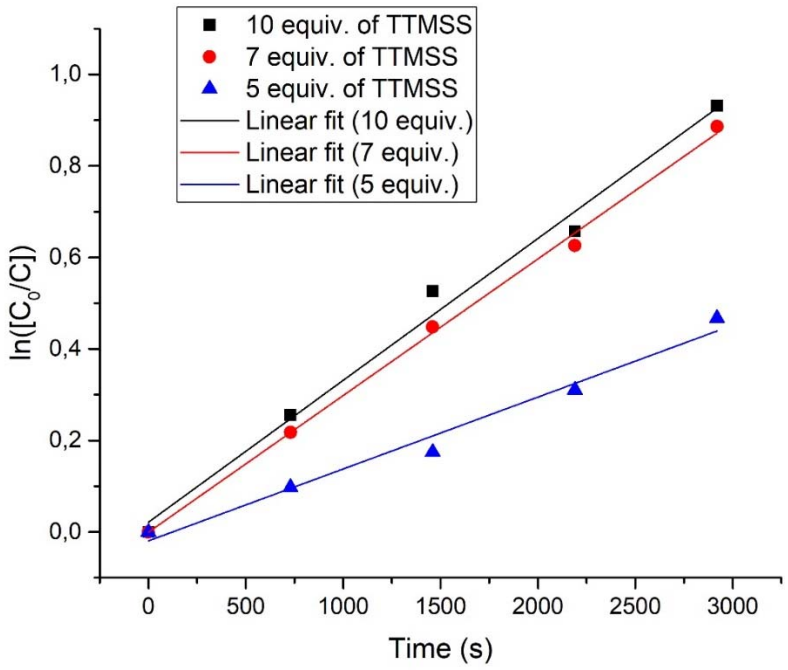

Figure 5. First order decay of [Mn(CO)$_5$(CF$_3$)] at 100°C in C_6D_6 at different TTMSS/Mn ratios.

Table 2. Reaction rate constants obtained from the first order decay of [Mn(CO)$_5$(CF$_3$)] at 100°C in C_6D_6 for different TTMSS/Mn ratios.

Entry	TTMSS/Mn ratio	k_{obs}/s^{-1}
1	5	$(1.48\pm0.08)\cdot10^{-4}$
2	7	$(2.98\pm0.05)\cdot10^{-4}$
3	10	$(3.10\pm0.18)\cdot10^{-4}$

The k_{obs} values in Table 2 are similar for entries 2 and 3 (7 and 10 equivalents of TTMSS respectively), meaning that the saturation plateau is reached for a TTMSS/Mn molar ratio of 10. This means that the k_{obs} obtained under these conditions is equal to the true first-order rate constant for the Mn-CF$_3$ bond cleavage.

Then, two additional experiments using 10 equivalents of TTMSS were carried out at 95 and 90 °C. Using the same method as above, the first-order rate constants were obtained from the linear fit for each temperature (Figure 6).

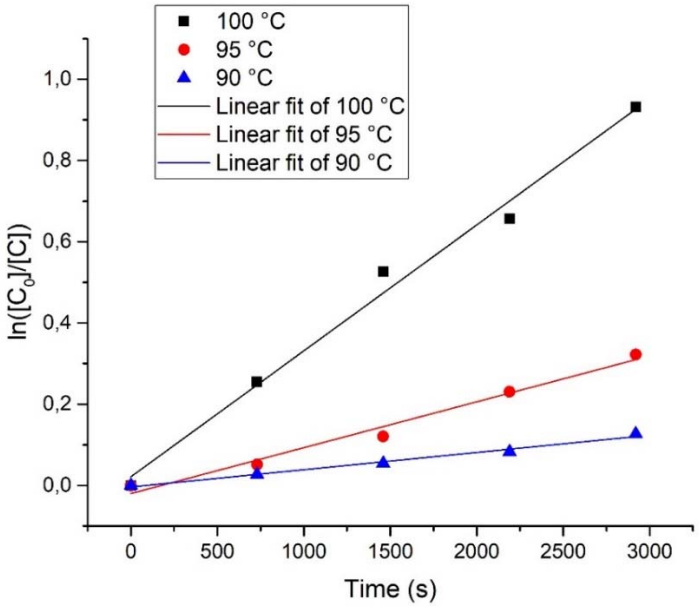

Figure 6. First order decay of [Mn(CO)$_5$(CF$_3$)] in C_6D_6 at 100, 95 and 90 °C.

The rate constants obtained at 100, 95 and 90 °C were used to construct the Eyring plot, ln(k/T) *vs.* 1/T, shown in Figure 7. The Eyring analysis of the decay rate constants provided the activation parameters $\Delta H^{\ddagger}$ and $\Delta S^{\ddagger}$, reported in Table 3. As mentioned above, a deeper discussion about these values and a comparison with the values reported in the literature and those obtained by DFT calculation is placed on section 4.3. In addition, several by-products were observed by ^{19}F NMR during the decomposition of compound **8**. These will be described in a separate section (section 4.4).

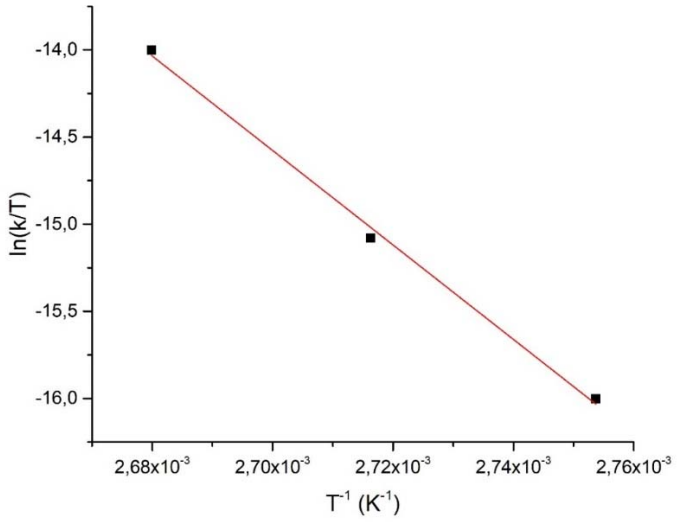

Figure 7. Eyring plot of k_{obs} as a function of the temperature for the decomposition of compound **8**.

Table 3. Kinetics and activation parameters for the decay of [Mn(CO)$_5$(CHF$_2$)] in C_6D_6.

T (°C)	k_{obs}/ s^{-1}	$\Delta H^{\ddagger}$ / kcal mol^{-1}	$\Delta S^{\ddagger}$ / cal mol^{-1} K^{-1}
100	$(3.10\pm0.18)\cdot10^{-4}$	(53.8 ± 3.5)	(66.0 ± 9.5)
95	$(1.04\pm0.06)\cdot10^{-4}$		
90	$(4.08\pm0.29)\cdot10^{-5}$		

4.2.2. Experimental determination of the Mn-CHF_2 BDE in **9**

The procedure is to the same as for the above-described Mn-CF_3 BDE determination for complex **8** (Section 4.2.1.1), so it will only be summarized in this case. Three experiments using a TTMSS/Mn molar ratio of 10 were carried out at 75, 80 and 85 °C. The ^{19}F NMR monitoring gave rise to data very similar to those shown in Figure 5 for compound **8**. It also gave evidence in favor of the formation of the expected product CH_2F_2 (see Figure 8) with a triplet at δ -142.4 ($^2J_{FH}$ = 49.8 Hz) in good agreement with values reported in the literature (*cf.* δ -143.6, $^2J_{FH}$ = 50.1 Hz),[32] even though it could not provide quantitative information because of the low b.p. (-51.7 °C) and low solubility of this compound in C_6D_6, resulting in its extensive escape toward the NMR tube head space. The rate constants were obtained from the linear fit of the first-order plots for each temperature (Figure 9).

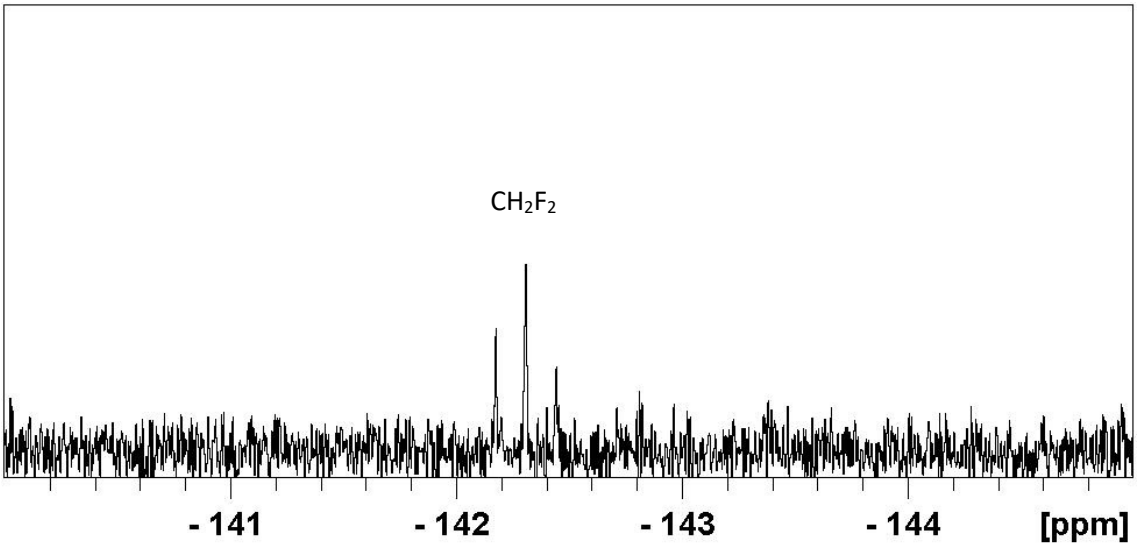

Figure 8. ^{19}F NMR spectrum (376.5 MHz, benzene-d6) proving the generation of CH_2F_2 during the decomposition of compound **9** by heating 1 hour with 10 equivalents of TTMSS at 85 °C.

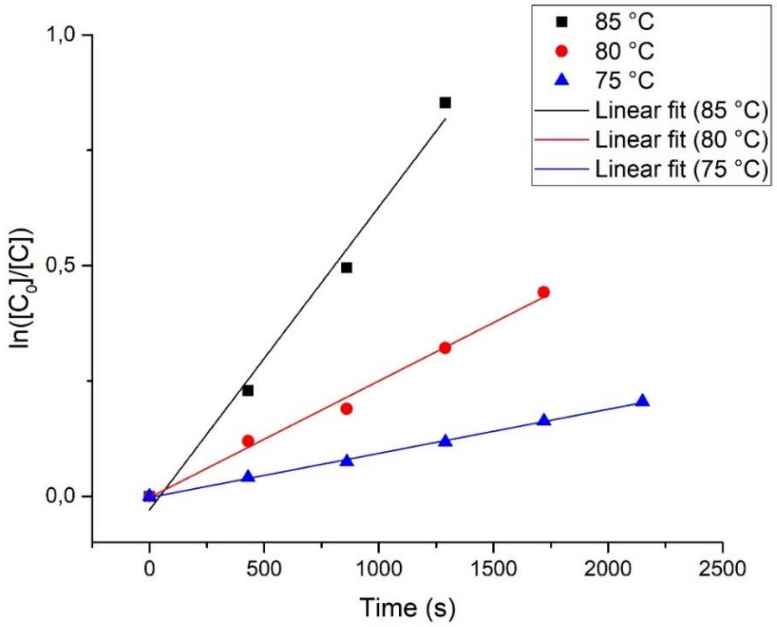

Figure 9. First order decay of $[Mn(CO)_5(CHF_2)]$ in C_6D_6 at 85, 80 and 75 °C.

With the kinetic constant values and through the linear form of the Eyring's equation (Figure 10), it was then possible to determine the activation parameters values $\Delta H^{\ddagger}$ and $\Delta S^{\ddagger}$, shown in Table 4. In addition, as for the compound **8,** several by-products were observed in the ^{19}F NMR spectra (see section 4.4 for more details).

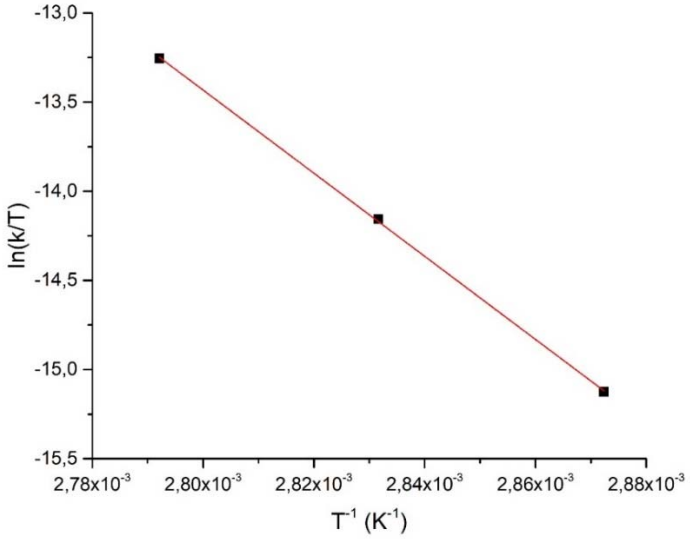

Figure 10. Eyring plot of k_{obs} as a function of the temperature for the decomposition of compound **9**.

Table 4. Kinetics and activation parameters for the decay of [Mn(CO)$_5$(CHF$_2$)] in C_6D_6.

T (°C)	k_a / s^{-1}	$\Delta H^{\ddagger}$ / kcal mol^{-1}	$\Delta S^{\ddagger}$ / cal mol^{-1} K^{-1}
85	$(6.27\pm0.33)\cdot10^{-4}$	(46.3 ±1.6)	(55.8±4.7)
80	$(2.51\pm0.08)\cdot10^{-4}$		
75	$(9.40\pm0.13)\cdot10^{-5}$		

4.2.3. Experimental determination of the Mn-CH_2CF_3 BDE in **10**

The procedure was once again the same as those described above for complexes **8** (Section 4.2.1) and **9** (Section 4.2.2). The ^{19}F monitoring gave results very similar to those reported for the decomposition of **8** and provided evidence for the formation of the expected CF_3-CH_3 product (Figure 11), exhibiting a quartet at δ -60.7 ($^3J_{FH}$ = 12.6 Hz), in good agreement with the already reported values (*cf.* δ -61.7, $^3J_{FH}$ = 12.8 Hz).[33] Once again, since this compound is a gas (b.p. = -47.6 °C) and has low solubility in C_6D_6, it predominantly escaped into the tube head space and the NMR measurement could not be used to extract quantitative information.

The experiments were carried out with a TTMSS/Mn molar ratio of 10 at 90, 80 and 70 °C. The rate constants were obtained from the linear fit of the first-order plots for each temperature (Figure 12) and the $\Delta H^{\ddagger}$ and $\Delta S^{\ddagger}$ values (Table 5) were derived from the fit of the linear form of the Eyring equation. In this case, the formation of by-products was much less extensive, as discussed in section 4.4.

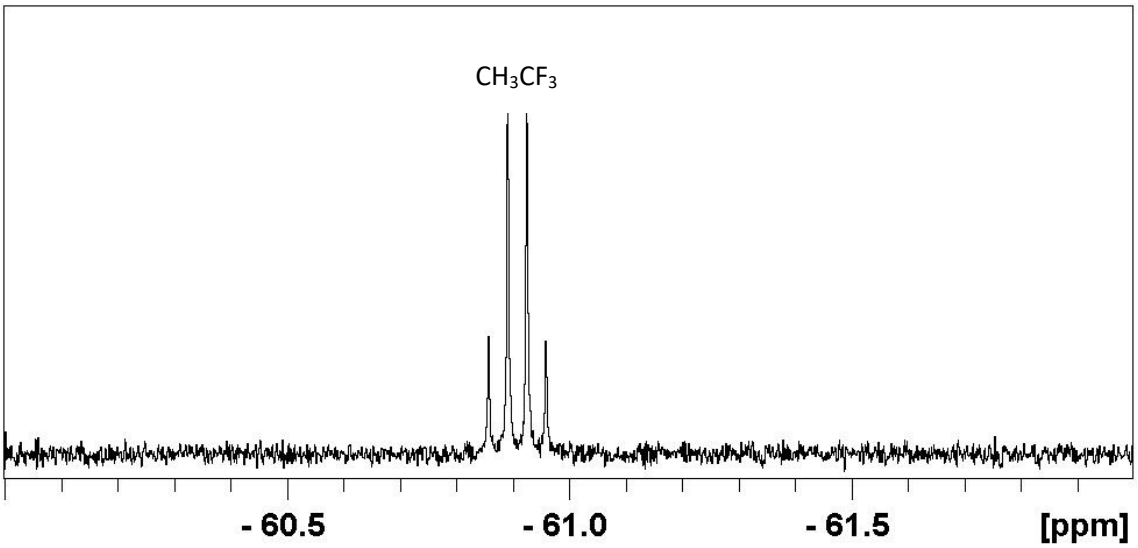

Figure 11. ^{19}F NMR spectrum (376.5 MHz, benzene-d6) proving the generation of CH_3CF_3 during the decomposition of compound **7** by heating 80 minutes with 10 equivalents of TTMSS at 90 °C.

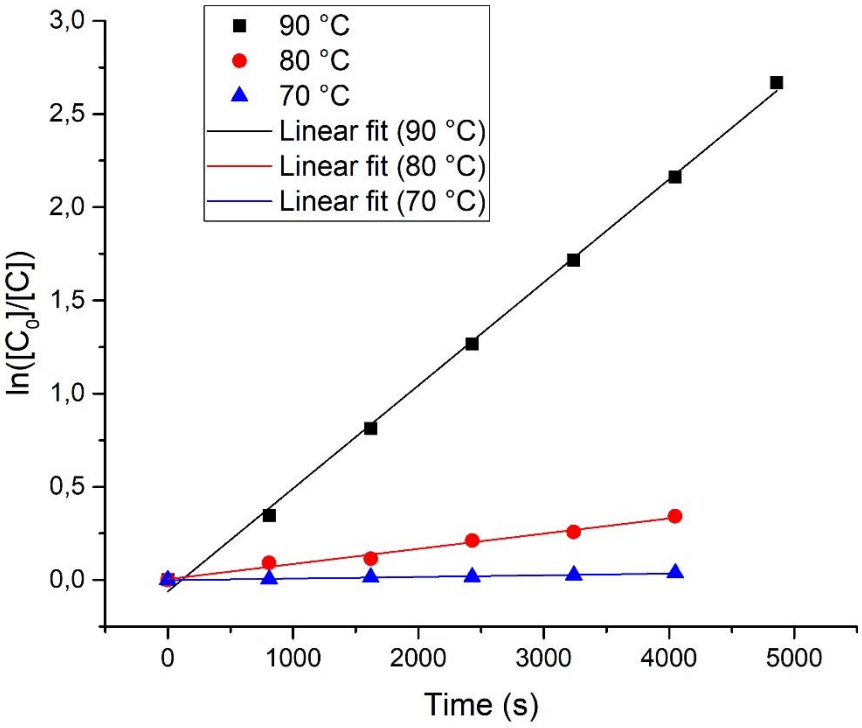

Figure 12. First order decay of [Mn(CO)$_5$(CH$_2$CF$_3$)] in C_6D_6 at 90, 80 and 70 °C.

Table 5. Kinetics and activation parameters for the decay of [Mn(CO)$_5$(CH$_2$CF$_3$)] in C_6D_6.

T (°C)	k_a / s^{-1}	$\Delta H^{\ddagger}$ / kcal mol^{-1}	$\Delta S^{\ddagger}$ / cal mol^{-1} K^{-1}
90	$(5.35\pm0.07)\cdot10^{-4}$	(50.6 ±0.8)	(65.4±2.2)
80	$(7.84\pm0.47)\cdot10^{-5}$		
70	$(8.52\pm0.41)\cdot10^{-6}$		

4.2.4. Experimental determination of the Mn-CH(CH$_3$)(COOCH$_3$) BDE in **1**

The same procedure described above for the Mn-C BDE determination for compounds **8**, **9** and **10** was again applied here, except that the increased thermal fragility of the Mn-C bond in compound **1** required the use of lower temperatures. All the reactions were carried out in NMR tubes under argon into the NMR spectrometer at the indicated temperatures, using 10 equivalents of TTMSS as radical trap, benzene-d_6

as solvent and 1,3,5-trioxane as internal standard to determine the relative amount of the remaining 1 at each time.

Initial experiments at 90 °C lead to an extremely fast decomposition of compound **1** due to the weakness of the Mn-C bond in this compound relative to the above-described fluoroalkylpentacarbonylmanganese(I) complexes. The kinetics experiments were therefore carried out at 70, 65 and 60 °C. The expected main product is the propanoic acid methyl ester, the ^{1}H NMR resonances of which (500 MHz, $CDCl_3$) are reported at δ = 1.17 (t, $^3J_{HH}$ = 7.5 Hz, 3H, CH_3), 2.36 (q, $^3J_{HH}$ = 7.5 Hz, 2H, CH_2) and 3.70 (s, 3H, OCH_3).[34] However, several by-products were also formed and the CH_2 and OCH_3 resonances of all these compounds and of the residual compound 1 partially overlap, making it difficult to clearly assign these signals and to extract kinetics data from them. The formation of the expected propanoic acid methyl ester was suggested by a triplet at δ 0.96 with J = 6 Hz. The relative amount of compound **1** at different times was calculated by the relative integration of the signals of 1,3,5-trioxane (4.45 to 4.55 ppm in benzene-d_6) and the doublet of the CH_3 protons next to the CH group (1.40 to 1.55 ppm in benzene-d_6), which was located in a clean region with no overlap with the resonances of other species, see Figure 13.

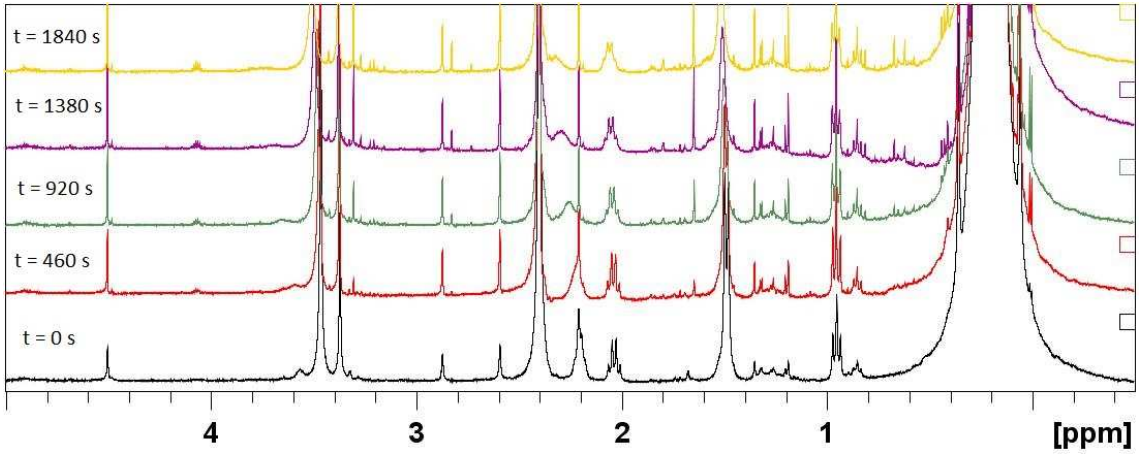

Figure 13. ^{19}F NMR monitoring (400 MHz, C_6D_6) of [$(CO)_5Mn(CH(CH_3)(COOCH_3))$] with 10 equivalents of TTMSS at 70 °C at various reaction times.

The kinetic constant values obtained from the first order decay of complex **1** at 70, 65 and 60 °C (Figure 14) were used to obtain the activation parameters through the Eyring plot (Figure 15), shown in Table 6.

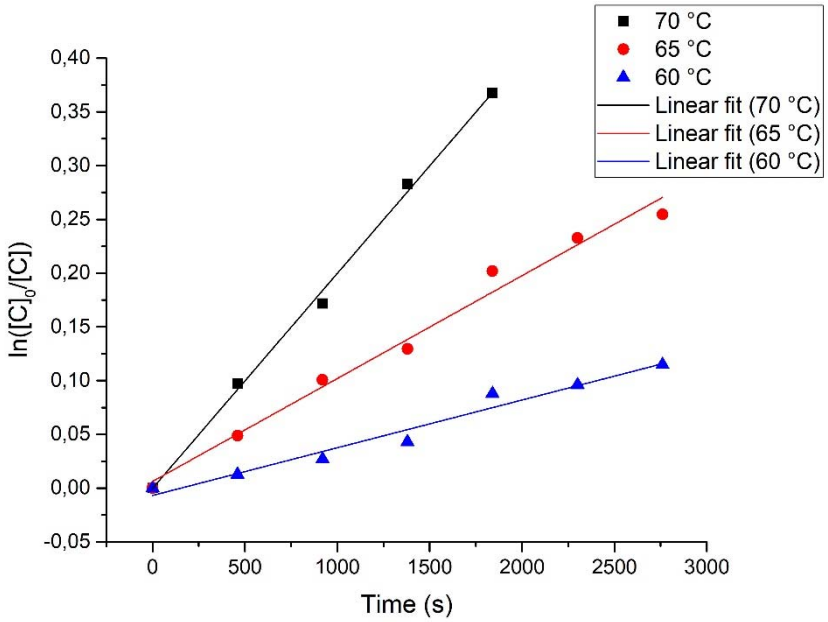

Figure 14. First order decay of [(CO)$_5$Mn(CH(CH$_3$)(COOCH$_3$))] in C_6D_6 at 70, 65 and 60 °C.

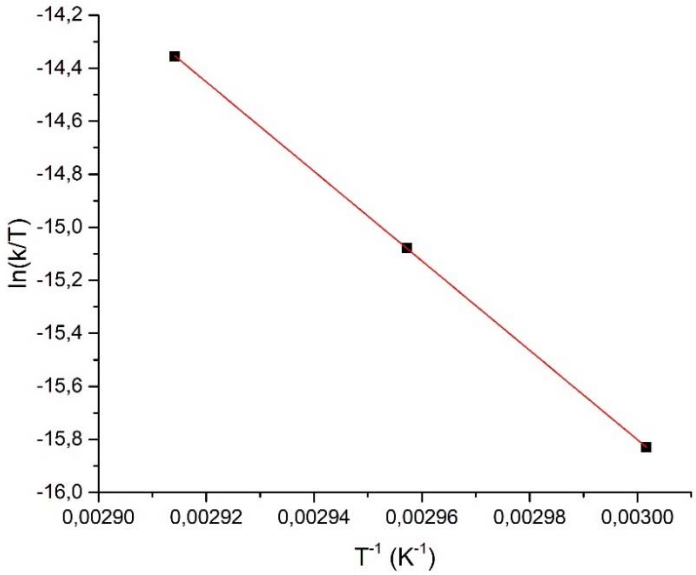

Figure 15. Eyring plot of k_{obs} as function of temperature for the decomposition of compound **9**.

Table 6. Kinetics and activation parameters for the decay of compound **9** in C_6D_6.

T/°C	k_a / s^{-1}	$\Delta H^{\ddagger}$ / kcal mol^{-1}	$\Delta S^{\ddagger}$ / cal mol^{-1} K^{-1}
70	(2.00±0.03)·10^{-4}	(35.3±2.8)	(27.2±8.1)
65	(9.6±0.5)·10^{-5}		
60	(4.1±0.4)·10^{-5}		

4.2.5. Discussion of the Mn-C homolytic bond strength in the alkyl and fluoroalkylpentacarbonylmanganese(I) derivatives

The activation parameters determined for the homolytic bond breaking in compounds **1**, **8**, **9** and **10** are summarized in Table 6. The activation enthalpies obtained from the present study for compounds **8** and **9** are more significant than the thermodynamic bond dissociation enthalpies (BDEs) reported in previous studies, determined either by Calvet calorimetry or by photoionization mass spectrometry.[3,4] This discrepancy might result from an overestimation of the BDEs by the kinetic approach but the reverse bond formation process should proceed via a very low activation barrier, thus $\Delta H^{\ddagger} \approx$ BDE. The BDEs estimated by DFT calculations in a recently published contribution[1] are in much closer agreement with the $\Delta H^{\ddagger}$ values determined by the present study. It is also worth underlining that the activation entropies obtained from the Eyring analyses of the rate data are high and positive, also in relatively good agreement with the values obtained by DFT calculation for the full bond breaking process. Note that other calculations of the Mn-C bond strength for compounds **8** and **9**, carried out at a slightly different level of theory by Folga and Ziegler,[35] also gave high values in close agreement with those of the more recent DFT study and these authors concluded that the experimental estimates of the Mn-C BDEs available at that time were too low. We point out that the calculated BDE for compound **11** (46.0 kcal mol^{-1}),[1] is slightly lower than those of the other three compounds, possibly rationalizing the failure to obtain this product by clean decarbonylation of **7**. Finally, the results of both experimental and computational study show that compound **1** has a lower BDE than the fluoroalkylpentacarbonylmanganese(I) complexes and thus can generate radicals by a homolytic cleavage of the Mn-R easier. Indeed, the strong electron-withdrawing inductive effect of fluorine in the alkyl chain strengthens the Mn-R bond attracting the electronic density of manganese. This provokes a decrease of the π-backbonding from manganese to the carbonyl ligands so a weakening of the manganese-carbonyl ligand bond and a strengthening of the C≡O bond, resulting in a slight increase of the frequencies of the carbonyl stretching bands. In fact, all the respective carbonyl

stretching bands of fluoroalkyl compounds (**8** to **11**) are in higher frequencies than the corresponding vibration in compound **1**.

Table 7. Summary of the kinetics and activation parameters for the decay of compounds 1, **8**, **9** and **10** in C_6D_6.

Complex	T / °C	k_a / s^{-1}	$\Delta H^{\ddagger}$ / kcal·mol^{-1}		$\Delta S^{\ddagger}$ / cal·mol^{-1}·K^{-1}	
			Exp.	DFT[a]	Exp.	DFT[a]
1	70	$1.99\cdot10^{-4}$	(35.3±2.8)	36.9	(27.2±8.1)	45.3
	65	$9.60\cdot10^{-5}$				
	60	$5.36\cdot10^{-5}$				
8	100	$(3.10\pm0.18)\cdot10^{-4}$	(53.8±3.5) [b]	55.1	(66.0±9.5)	45.8
	95	$(1.04\pm0.06)\cdot10^{-4}$				
	90	$(4.08\pm0.29)\cdot10^{-5}$				
9	85	$(6.27\pm0.33)\cdot10^{-4}$	(46.3±1.6) [c]	48.0	(55.8±4.7)	43.2
	80	$(2.51\pm0.08)\cdot10^{-4}$				
	75	$(9.40\pm0.13)\cdot10^{-5}$				
10	90	$(5.35\pm0.07)\cdot10^{-4}$	(50.6±0.8)	50.5	(65.4±2.2)	48.8
	80	$(7.84\pm0.47)\cdot10^{-5}$				
	70	$(8.52\pm0.41)\cdot10^{-6}$				

[a] Values from ref. [1]. [b] Reported as 48.5±1.4 kcal/mol by Calvet calorimetry[3] after re-evaluation,[4] and as 43.5±2.6 kcal/mol by photoionization mass spectrometry.[4] [c] Reported as 34.4±2.6 kcal/mol by photoionization mass spectrometry.[4]

4.2.6. Analysis of side-reactions in the decomposition of [Mn(CO)$_5$R$_F$] complexes

Given the forcing conditions used for the BDE determination for compounds **8-10**, it is reasonable to question the existence of competing processes, and indeed the ^{19}F NMR monitoring indicated the presence of additional products as already mentioned above in sections 4.2.1, 4.2.2 and 4.2.3, hinting to the presence of alternative decomposition pathways. Indeed, alkylpentacarbonylmanganese(I) derivatives are known to be prone to thermally activated migratory insertion and decarbonylation processes. These would generate vacant coordination sites opening access to other reaction pathways such as α- and β-elimination processes of atoms (H, F) from the alkyl chain. The interactions of silane with the reaction intermediates generated by migratory insertion and by decarbonylation have been investigated *in silico* (the DFT calculations

were carried out by Prof. Rinaldo Poli), confirming that the homolytic cleavage pathway is the preferred one. However, a more careful inspection of the NMR spectra revealed the formation of other products, indicating that the reactions depicted in Scheme 3 and 4 represent only part of the compound decomposition pathway.

For the decomposition of **8**, the full ^{19}F NMR spectrum revealed several products (Figure 16). The resonance of the starting compound **8** at δ 7.8 (*cf.* 5.6 in acetone-d_6) was still present after 1 h at 100°C (70% conversion). The main resonance at δ -163.0 belongs to hexafluorobenzene, which was used as internal standard for the quantitative kinetics study. A key ^{19}F resonance is a strong singlet at δ -256.2, characterized by ^{29}Si satellites (doublet, $^1J_{SiF}$ = 327 Hz), see Figure 17, which is assigned to compound $(Me_3Si)_3SiF$. The coupling constant is typical for a direct F-Si bond and the spectral parameters are in close agreement with those reported in the literature for this compound (δ -261, $^1J_{SiF}$ = 335 Hz[36] or 327.8 Hz from the ^{29}Si NMR study).[37] The ^{1}H-^{19}F HETEROCOSY NMR spectrum shows that this resonance is coupled to a ^{1}H NMR resonance at δ 0.21 (see Figure 18), which is also in agreement with the literature value (δ = -0.21 in C_6H_6)[36]. As the only source of F in the experiment is the alkyl group of compound **8**, this observation constitutes clear evidence for C-F bond breaking. Integration of this resonance against the C_6F_6 internal standard (used for the kinetics investigation) shows that 67% of compound **8** has undergone the side reaction leading to $(Me_3Si)_3SiF$.

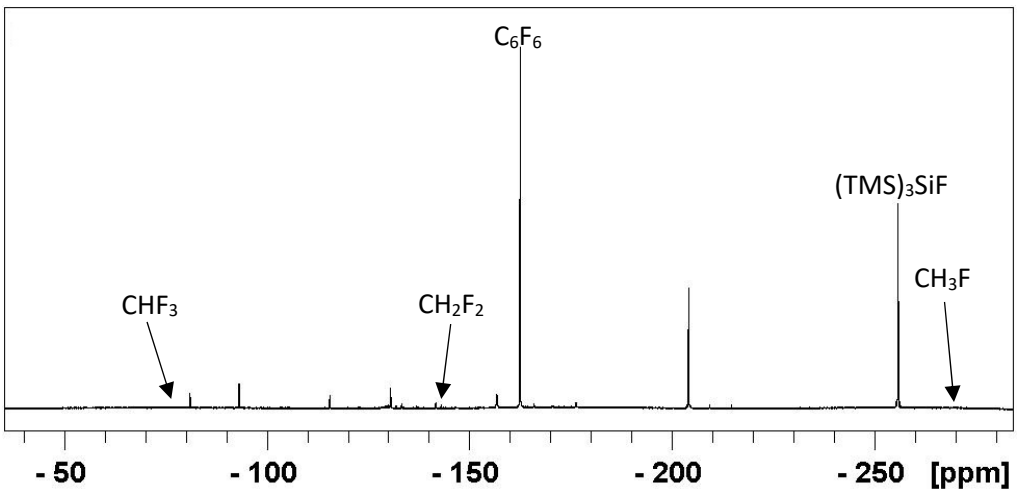

Figure 16. ^{19}F NMR spectrum (376.5 MHz, benzene-d_6) at 10 °C during the decomposition of compound **5** by heating 1 hour in presence of with 10 equivalents of TTMSS at 100 °C.

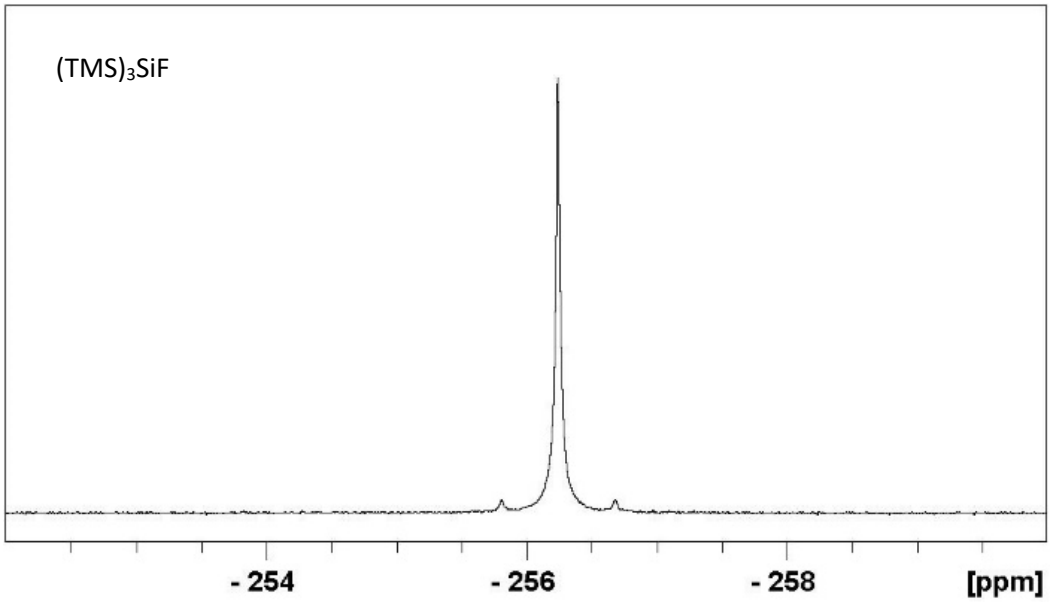

Figure 17. Expansion of the -252 to -260 ppm region of the ^{19}F NMR spectrum (376.5 MHz, benzene-d_6, Figure 13) recorded at 10 °C after the decomposition of compound **1** at 100°C for 1 hour in the presence of 10 equivalents of TTMSS, proving the presence of $(Me_3Si)_3SiF$.

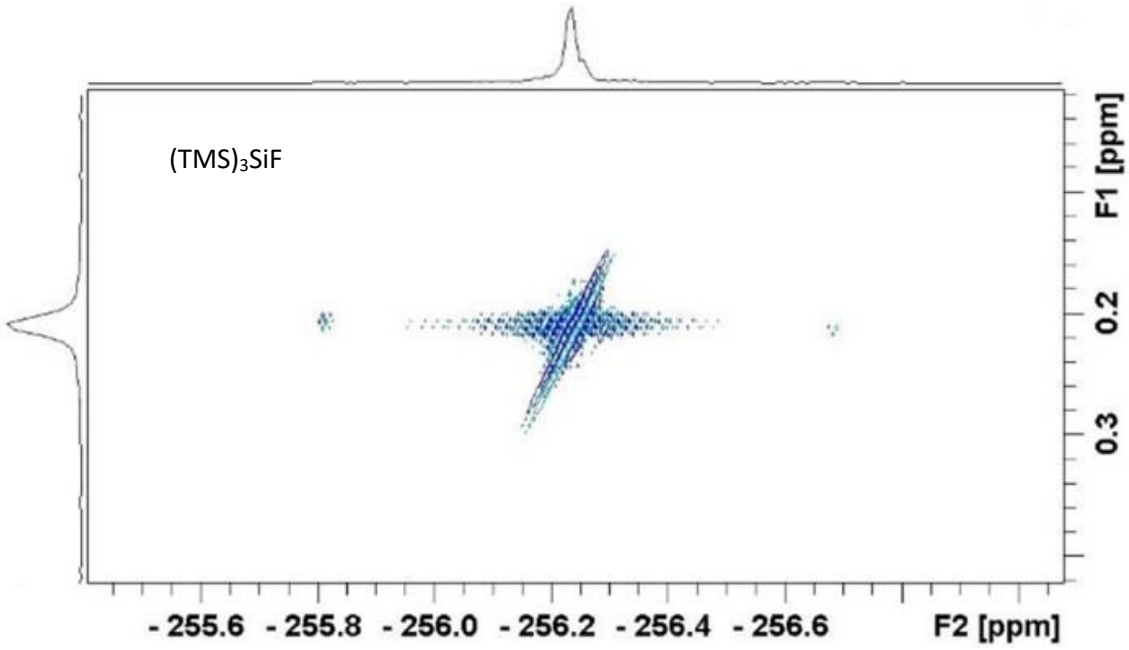

Figure 18. ^{1}H-^{19}F HETEROCOSY NMR spectrum at 10 °C proving the generation of $(Me_3Si)_3SiF$ during the decomposition of compound 5 by heating 1 hour in the presence of 10 equivalents of TTMSS at 100 °C.

Confirmation of this occurrence comes from the identification of a little triplet resonance at the expected position for CH_2F_2 (δ -142.15, $^2J_{FH}$ = 50 Hz, see Figure 19; *cf.* δ -142.0, $^2J_{HF}$ = 50.3 Hz reported in the literature).[38] This signal correlates with a ^{1}H resonance at δ 4.95 in the ^{1}H-^{19}F NMR HETEROCOSY spectrum (*cf.* δ 5.45, $^2J_{HF}$ = 50.22 Hz in cyclohexane[31]) as shown in Figure 20. The fact that this resonance is much smaller

than that of $(Me_3Si)_3SiF$ results from the volatility and small solubility of gaseous CH_2F_2. The spectrum shows evidence for even deeper defluorination of the alkyl group, since an even smaller resonance is detected at the position expected for CH_3F (δ -270.34). The quartet feature is not well resolved, but the relationship with a ^1H doublet resonance ($^2J_{HF}$ ca. 46 Hz) at δ -4.22 is clearly indicated by the ^1H-^{19}F HETEROCOSY NMR spectrum (see Figure 21). These values match rather well those available in the literature (δ_F -270.6, δ_H 4.18, $^2J_{FH}$ = 46 Hz).[39]

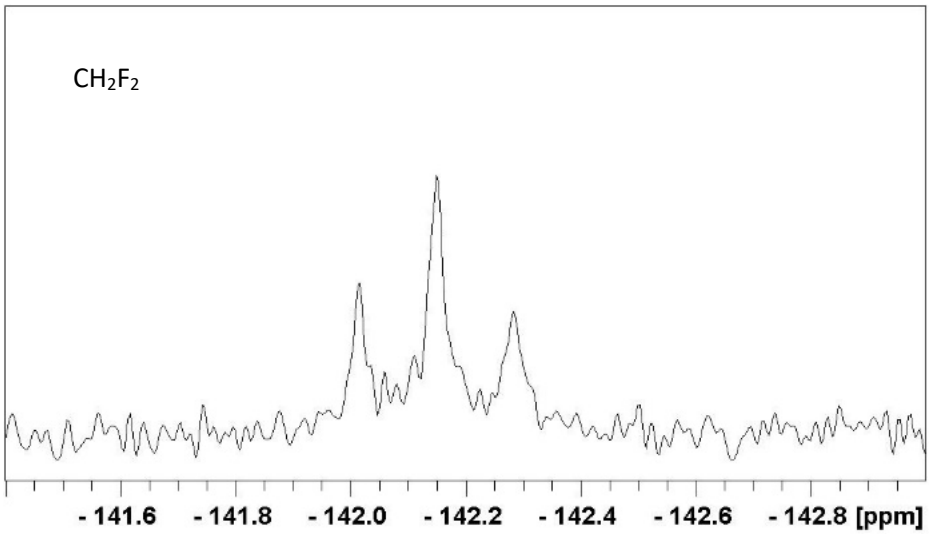

Figure 19. Expansion of the -141.4 to -143 ppm region of the ^{19}F NMR spectrum (376.5 MHz, benzene-d_6, Figure 13) recorded at 10 °C after the decomposition of compound **8** at 100°C for 1 hour in the presence of 10 equivalents of TTMSS, proving the presence of CH_2CF_2.

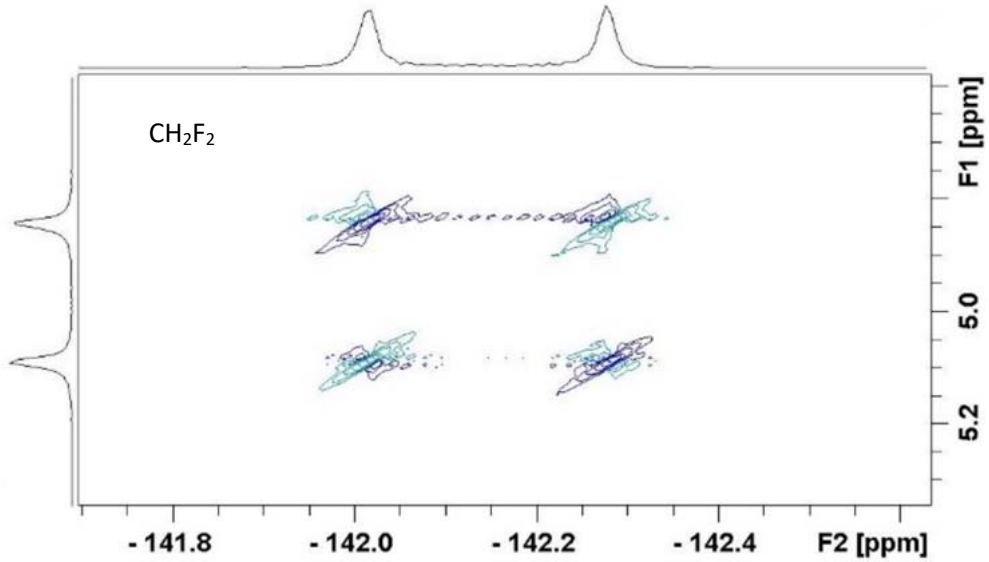

Figure 20. ^1H-^{19}F HETEROCOSY NMR spectrum at 10 °C proving the generation of CH_2F_2 during the decomposition of compound **8** by heating 1 hour in the presence of 10 equivalents of TTMSS at 100 °C.

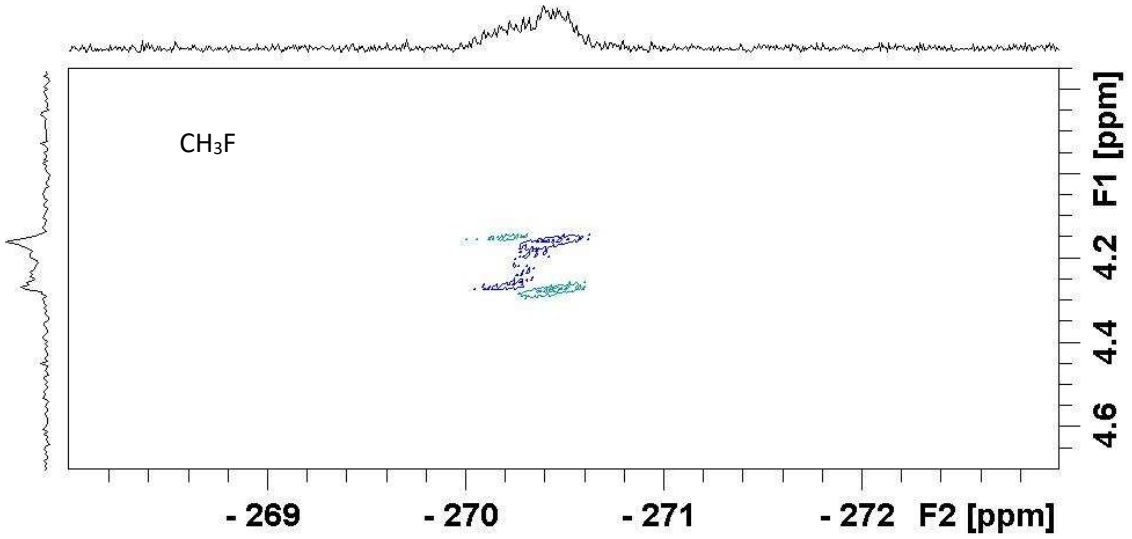

Figure 21. ^{1}H-^{19}F HETEROCOSY NMR spectrum at 10 °C proving the generation of CH_3F during the decomposition of compound **8** by heating 1 hour in the presence of 10 equivalents of TTMSS at 100 °C.

Other signals present in the full spectrum of the decomposition of compound **8** in the presence of TTMSS (Figure 16) could not be assigned, for instance the rather intense resonance at δ -204.6, see Figure 22. It is a binomial triplet with J = 11 Hz, suggesting $^{3}J_{FH}$, also showing silicon satellites with a coupling constant of 325 Hz, which is characteristic of $^{1}J_{FSi}$. These satellites remained visible also in the ^{19}F{^{1}H} and ^{19}F{^{13}C} spectra, whereas the triplet collapsed to a singlet in the ^{19}F{^{1}H} spectrum. These features suggest a F-Si-CH_2-X moiety, indicating the occurrence of Si-Si bond breaking and Si-C bond formation, in addition to Si-F bond formation. The other smaller resonances at δ -215.16, -209.76, -176.81, -157.26, -143.49, -131.00, -115.99, -93.63 (q, J = 8 Hz) and -81.55, could not be assigned either. We imagine that the putative F-Si$(TMS)_2$-CH_2-X product may be generated from the primary F-Si$(TMS)_3$ product by a secondary process of C-H activation, presumably favored by an unsaturated (16-electron) Mn^{I} intermediate, followed by rearrangement. The additional reaction pathways that occur during the decomposition of [$(CO)_5$Mn-R_F] were not the subject of further investigations. Only the primary process, that leads to the H/F exchange on R_F in competition with the homolytic Mn-C bond breaking was the object of the computational investigation (see below).

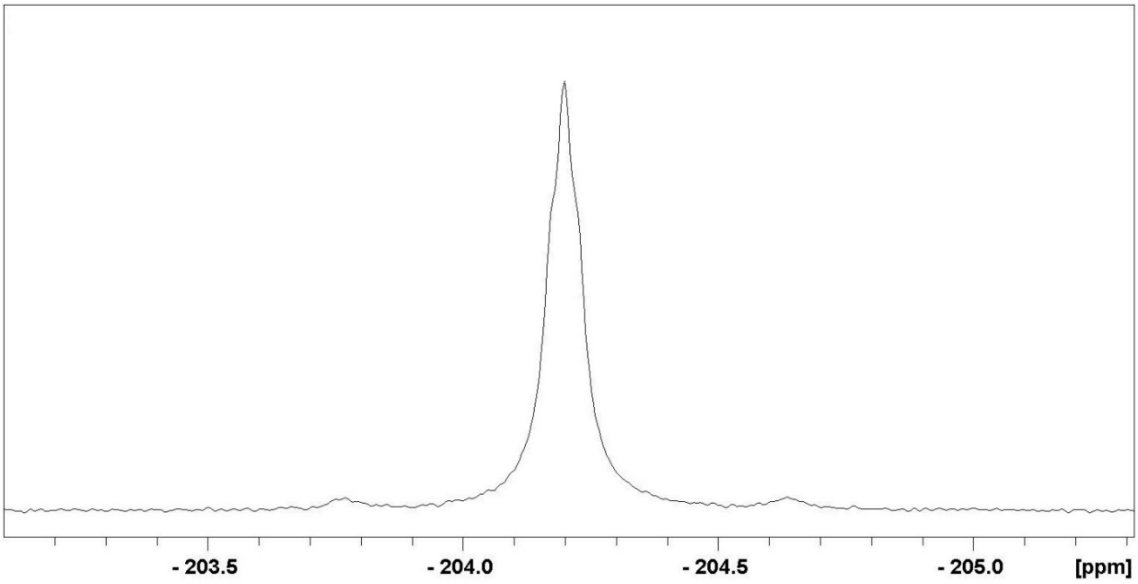

Figure 22. Expansion of the -203.1 to -205.3 ppm region of the ^{19}F spectrum (376.5 MHz, benzene-d_6) shown in Figure 16.

For the decomposition of compound **9** in the presence of TTMSS, in addition to the resonance of the CH_2F_2 product of Mn-R_F homolytic cleavage and trapping by TTMSS, the resonance of $(Me_3Si)_3SiF$ at δ -255.12 was again observed (see Figure 23), indicating the occurrence of C-F activation for the CHF_2 group. However, the signal of the other expected product, CH_3F, could not be detected. Integration of the $(Me_3Si)_3SiF$ resonance against the C_6F_6 internal standard gave only 10% of side reaction for compound **9**.

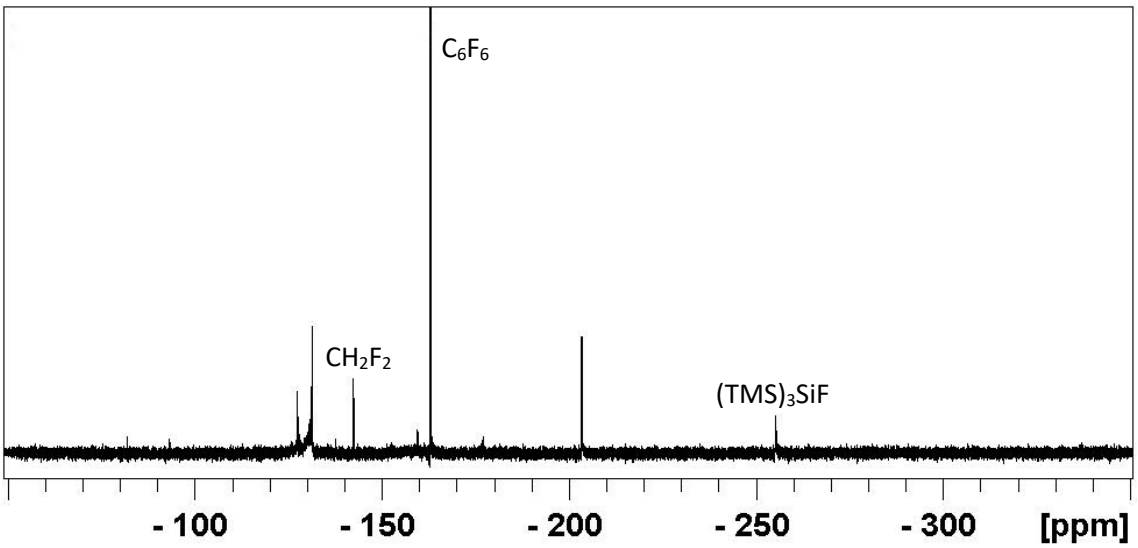

Figure 23. ^{19}F NMR spectrum (376.5 MHz, benzene-d6) during the decomposition of compound **9** by heating 1 hour with 10 equivalents of TTMSS at 85 °C.

In this spectrum, the expected CH_2F_2 product of homolytic cleavage and TTMSS trapping was clearly observed (triplet at δ -142.3, $^2J_{FH}$ = 52 Hz, see expansion in Figure 8). There was no residual compound **9** (doublet resonance initially observed at δ -69.19, *cf.* -71.6 in acetone-d_6). The same unassigned resonance at δ -203.4 as in the experiment of compound **8** is also observed here, indicating that this product does not contain R_F. Note that the resonance at δ -203.4 is more intense than that of $(TMS)_3Si$-F at δ -255.2 in the present spectrum, whereas it was less intense in the spectrum shown in Figure 16. Other resonances at δ -131.34, -131.00, -127.31, -93.26 and -81.87 belong to other unidentified products. The resonances at -131.00, -93.26 and -81.87 appear identical to those observed in the spectrum shown in Figure 16, suggesting that they belong to compounds that do not contain R_F. Their small intensity does not allow to establish whether they feature ^{29}Si satellites.

On the other hand, the degradation of **10**, although showing a few unidentified resonances in the ^{19}F NMR spectrum in addition to that of the expected CH_3CF_3 product at δ -60.86 (see the full spectrum in Figure 21), was not accompanied by the observation of either $(Me_3Si)_3SiF$ or the putative products of H/F exchange, namely CH_3CHF_2 or CH_3CH_2F, for which the resonances are expected at δ -25.9 and +77.0, respectively.[40] This result suggests that the reaction pathway leading to the formation of $(Me_3Si)_3SiF$ by H/F exchange with the R_F group is specific for groups that contain the F atom on the α-C atom and does not occur when the F substitution is on the β-C atom.

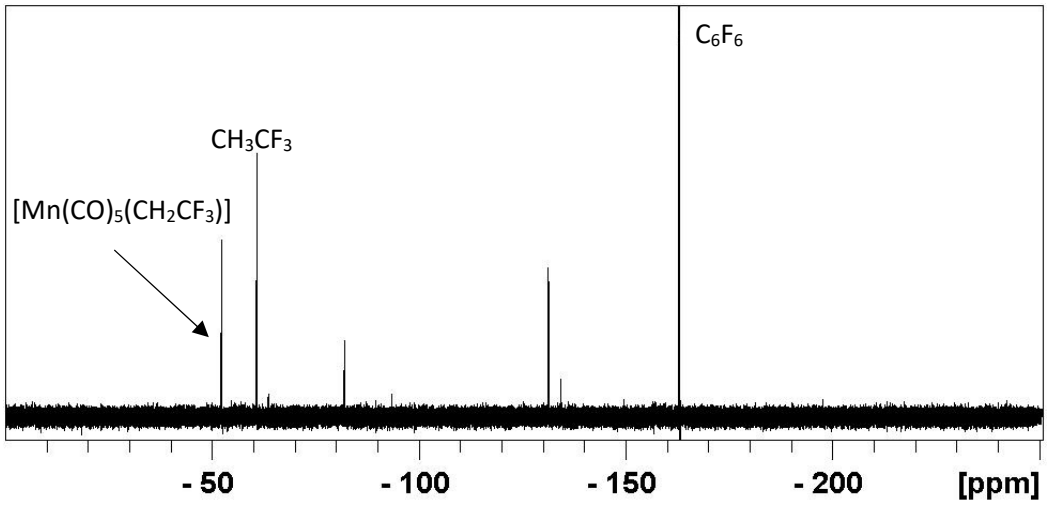

Figure 24. ^{19}F NMR spectrum (376.5 MHz, benzene-d6) during the decomposition of compound **10** by heating 80 minutes with 10 equivalents of TTMSS at 90 °C.

4.2.7. DFT investigation of the homolytic cleavage and the side reaction pathway

The calculations were carried by Prof. Rinaldo Poli at the same level of theory as in the study of the Mn-R_F bond strengths in compounds **8-10**.[1] The main target of these investigations was the rationalization of the observed H/F exchange process for compounds **8** and **9** but not for compound **10** and to elucidate its mechanism. In addition, we also wished to assess the relative importance of the homolytic bond cleavage *vs.* the alternative pathway(s), in order to assess the quality of the previously determined activation parameters (Table 1) as legitimate approximations of the thermodynamic bond dissociation parameters.

The two key experimental observations are that the H/F exchange occurs solely when the compound bears F atoms on the alkyl α-C atom and that the impact of this secondary reaction decreases in the order **8** > **9**. The likely source of the H atom is the silane reagent, since the exchange leads to the formation of the $(Me_3Si)_3SiF$ co-product containing a very stable Si-F bond. The full mechanistic exploration was carried out only for compound **8**. TTMSS was modeled by SiH_4 for the purpose of computational efficiency.

Since recent literature reports have shown the possibility of β-F elimination processes as key steps in catalyzed hydrodefluorination and C-B, C-C and C-Si bond formation processes involving fluorinated olefins,[41-46] a first mechanistic hypothesis consisted of an R_F migratory insertion, which would transfer the F atom from the α to the β position (Scheme 5). Alkylpentacarbonylmanganese(I) compounds are well-known to undergo this process rather easily.[47,48] From the starting compound **A** (complex **8**), migratory insertion of the CF_3 group leads to a 16-electron $[Mn(CO)_4(COR_F)]$ intermediate **B**, which may be able to undergo a β-F elimination (Scheme 5, upper path) yielding the difluoroketene complex **C**. The action of the silane may then lead to a difluoroacyl complex **D** where one coordination site is taken by the fluorosilane co-product. Final decoordination of the fluorosilane and disinsertion from the 16-electron acyl derivative **E** would generate **F** (complex **9**), from which the observed CH_2F_2 side product would

eventually be generated by the homolytic cleavage and silane-trapping sequence of Scheme 3.

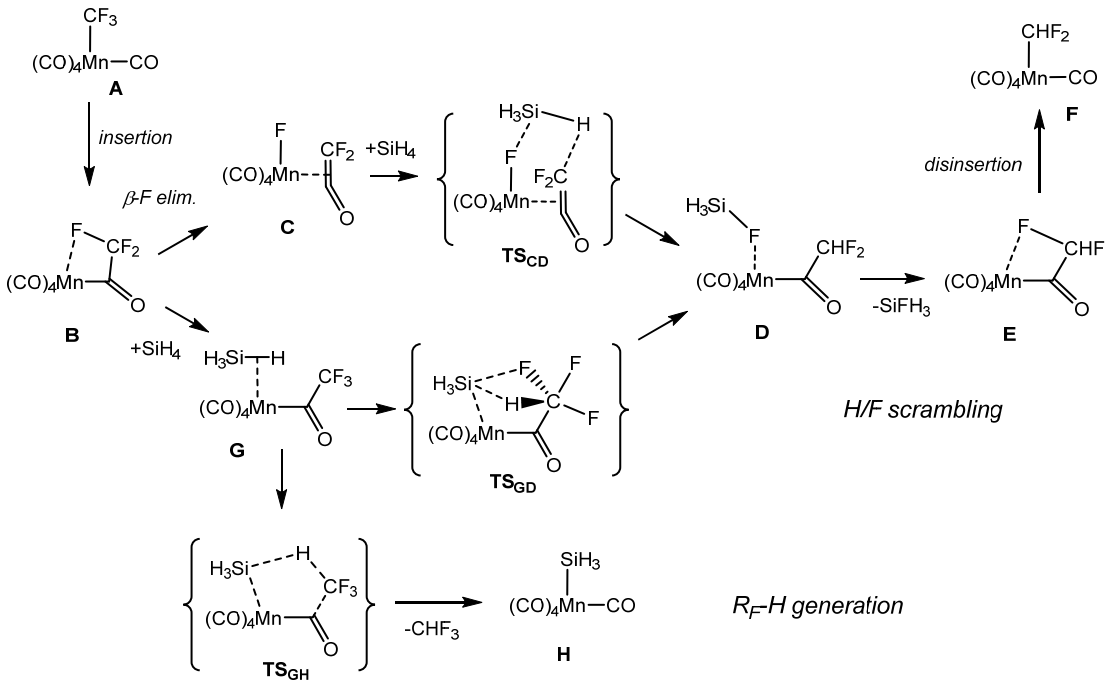

Scheme 5. Possible H/F exchange and CHF_3 generation from an acyl intermediate in compound **8**.

The DFT calculations indicate that the migratory insertion intermediate **B** is indeed accessible, via transition state $\mathbf{TS_{AB}}$, since the latter has a lower Gibbs energy than the homolytic bond cleavage process, see Figure 25. Not unexpectedly, the open coordination site in this unsaturated compound is stabilized by donation from a lone pair of one of the fluorine atoms of the trifluoroacetyl group. However, the proposed intermediate **C** is shown by the calculations to lie at very high energy, 56.2 kcal/mol above **A**. The transition state $\mathbf{TS_{BC}}$ would obviously be at even higher energy. Therefore, this pathway is not kinetically competent for the observed H/F exchange. An alternative way to transform **B** into **D** would consist of the silane addition to **B** to generate adduct **G**, which would then accomplish the H/F exchange associatively via hypervalent C and Si atoms (Scheme 5, lower path). The optimization of the silane adduct **G** has indeed provided a stable local minimum, shown in Figure 25. This is an electronically saturated σ-complex, where the silane Si-H bond provides two electrons to the metal center. The interaction is very weak, since the Gibbs energy is slightly higher than the sum of the

two isolated species, but does not exclude this compound as a competent reaction intermediate. However, all attempts to locate system **TS$_{GD}$** or a related stationary point along the path from **G** to **D** failed, leading instead to the rearrangement to an oxacyclopropyl compound **J** via an intermediate **I**. Details of these attempts and on the resulting products are available in the Appendix, Section C. In addition, intermediate **G** may also be envisaged to yield the observed CHF_3 product directly, with concomitant formation of the manganese silyl derivative **H** (Scheme 5). While this possibility would not account for the H/F exchange process, it would constitute a possible lower energy pathway, relative to the homolytic Mn-C bond cleavage, for the production of the main R_F-H decomposition product. However, attempts to locate **TS$_{GH}$** also failed and a relaxed scan along the C···H distance indicated that this transition state must be located at > 60 kcal/mol higher than (**A** + SiH_4), see details in the appendix, Figure C.2. In conclusion, no viable pathway could be found for either the H/F scrambling process or for the CHF_3 product formation via the acyl product of migratory insertion.

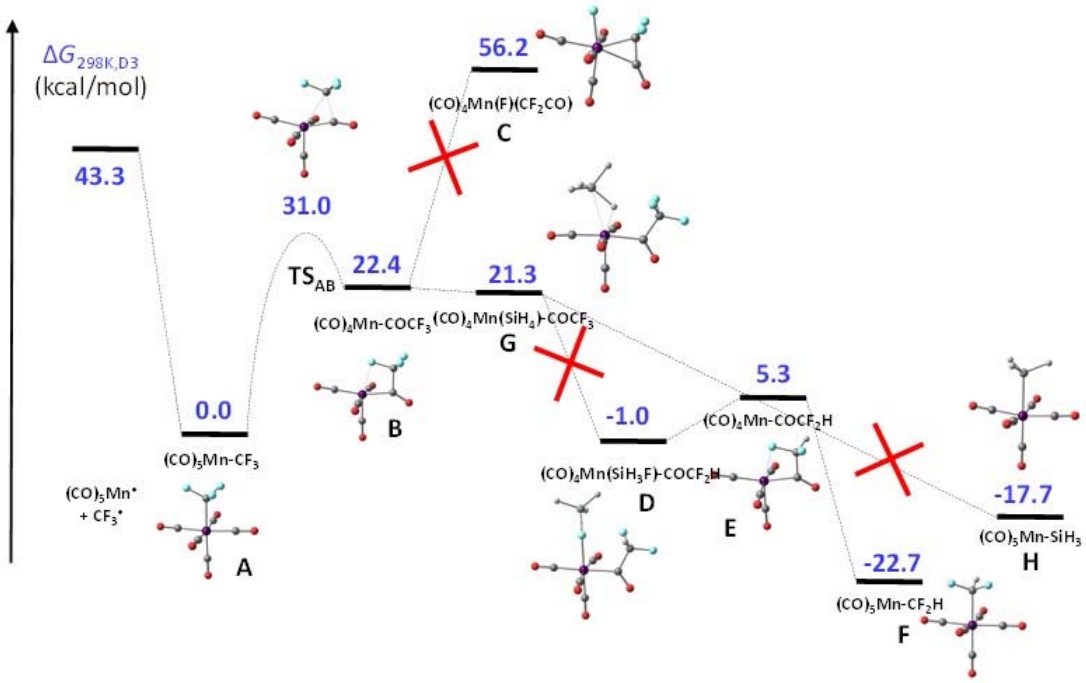

Figure 25. Energy profiles (relative D3-corrected G_{298} values in kcal/mol) and views of the optimized geometries for the pathways illustrated in Scheme 5.

An alternative process, known to occur for pentacarbonylmanganese(I) derivatives under thermal solicitation, is carbon monoxide dissociation, transforming **A** to the

tetracarbonyl derivative **K** (Scheme 6). From this intermediate, a conceivable pathway leading to the H/F scrambling would involve α-F elimination to yield a fluoro(difluoroalkylidene) derivative **L**, which would react with the silane to yield the difluoromethyl derivative **M** with a coordinated $SiFH_3$. The latter would finally be replaced by carbon monoxide and yield **F**, source of the observed CH_2F_2 by-product by the homolytic bond cleavage pathway. Like β-F elimination, α-F elimination was shown to be implicated in a variety of stoichiometric and catalytic reactions,[46,49-55] although to the best of our knowledge this phenomenon is unprecedented in manganese chemistry.

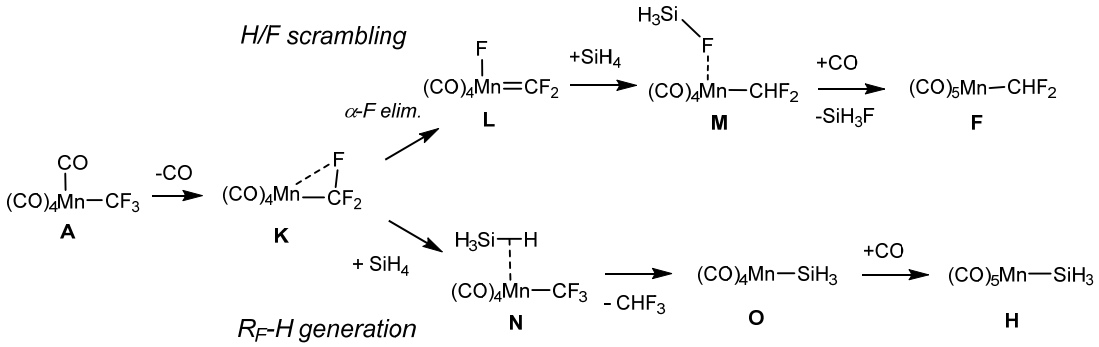

Scheme 6. Possible H/F exchange and CHF_3 generation following the decarbonylation of compound **8** (**A**).

The energy profile for this pathway is displayed in Figure 26, again in comparison with the homolytic bond cleavage process, which is shown on the left-hand side. The decarbonylation is predicted by the calculations to be thermodynamically accessible. The coordinatively unsaturated tetracarbonyl derivative **K** is stabilized by the lone pair of one of the α-F atoms, resulting in a significant distortion of the C atom geometry (Mn-C-F angle of 78.2° and C-F bond lengthened to 1.460 Å, *vs.* distances of 1.339 Å for the other two C-F bonds). The α-F elimination process is also thermally accessible, the transition state (**TS_{KL}**) being located at a slightly lower energy than that of the homolytic bond cleavage products. The interaction with SiH_4 leading to H/F scrambling is also accessible, with an energy cost very close to that of the bond cleavage, with a transition state (**TS_{LM}**) located only 0.4 kcal/mol higher than the bond cleavage products. Relaxation of this TS leads to a van der Waals adduct of **L** with SiH_4 on the reactant side and to **M** on the product side. The relative energy of **TS_{LM}** seems consistent with the fact that this is an observed competitive reaction in addition to the homolytic bond cleavage.

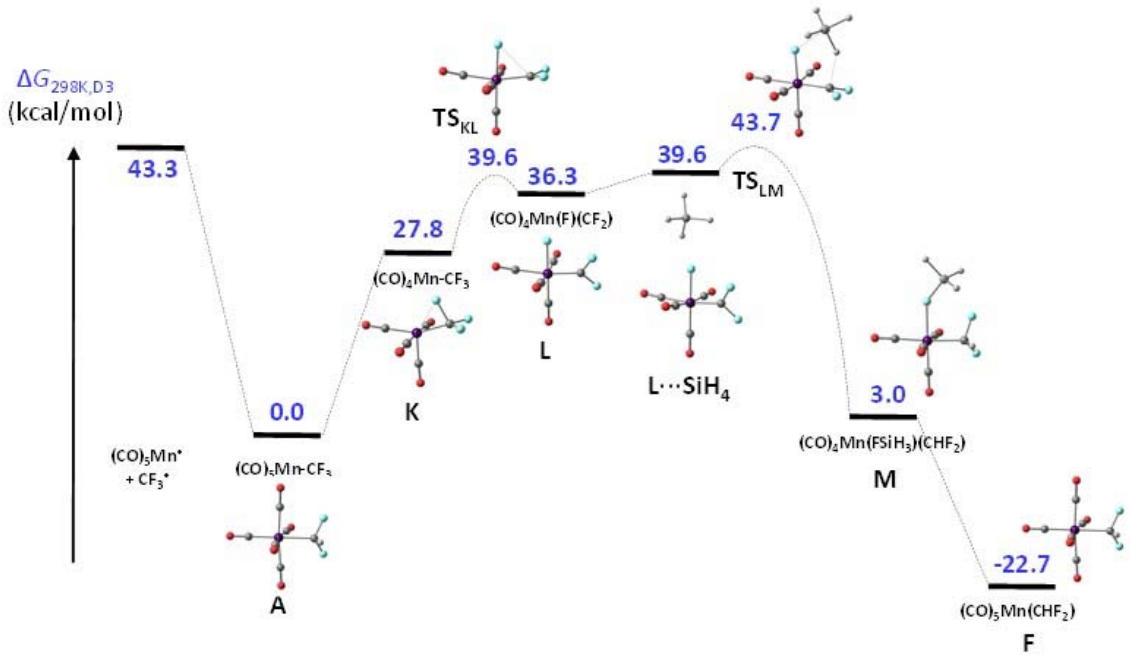

Figure 26. Energy profile (relative D3-corrected G_{298} values in kcal/mol) and views of the optimized geometries for the H/F scrambling pathway triggered by decarbonylation in compound **8** (Scheme 6).

The intermediate **K** also opens access to another possible pathway for release of the observed CHF_3 product, as shown in Scheme 6. Coordination of the silane yields the σ-complex **N**, where transfer of the silane H atom to the C atom produces the coordinatively unsaturated silyl complex **O**, which is then saturated by CO coordination to generate **H**. The DFT-calculated energy profile shows the feasibility of this process, see Figure 27. Coordination of the silane to **K** to yield **N** is favorable, even more than coordination to **B** to yield **G** (Figure 25), perhaps because the stabilization of the manganese unsaturation by the α-F atom in **K** is weaker than that by the β-F atom in **B**. The rate-determining transition state (**TS_{NO}**) of the H transfer from the silane ligand to the CF_3 group is lower than the energy of the bond cleavage products.

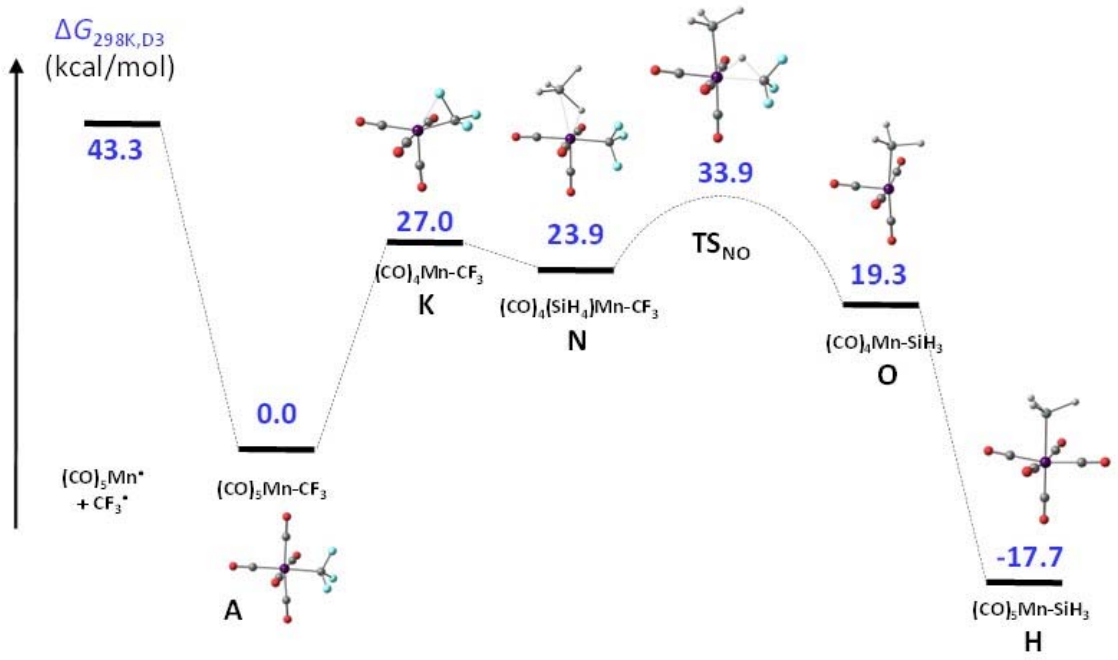

Figure 27. Energy profile (relative D3-corrected G_{298} values in kcal/mol) and views of the optimized geometries for the CHF_3 product release triggered by decarbonylation in compound **8** (Scheme 6).

The relatively facile formation of the R_F-H by the silane-assisted pathway of Scheme 6 and illustrated in Figure 27, as suggested by the DFT calculations, led us to question whether this may be the operating pathway, rather than the homolytic bond cleavage, for the decomposition of the $[Mn(CO)_5R_F]$ compounds **8**, **9** and **10** in the presence of TTMSS. In order to learn more about this, the activation parameters ($\Delta H^{\ddagger}$ and $\Delta S^{\ddagger}$) for the pathway of Figure 27 were derived under the conditions used for the decomposition experiments. The experiments were carried out in the temperature range 85-100°C, but since the individual values of $\Delta H^{\ddagger}$ and $\Delta S^{\ddagger}$ are supposed to vary very little in this range, the calculations were carried out only at 100°C. The major effect on the variation of $\Delta G^{\ddagger}$ is related to the change of T in the ($\Delta H^{\ddagger}$ - $T\Delta S^{\ddagger}$) expression. These values are shown in Table 8 (raw data are in the appendix, Table C.1), where they are compared with the corresponding values calculated for the homolytic bond cleavage at the same temperature. These can also be compared with the experimentally determined activation parameters shown in Table 7. These calculations were also extended to the critical structures related to both pathways for the decomposition of **9** and **10**, still using 100 °C as representative temperature.

Table 8. DFT-calculated parameters (Δ*G* and Δ*H* values in kcal mol^{-1}; Δ*S* values in cal mol^{-1} K^{-1}) for the generation of R_F-H at different temperatures.[a]

Parameter	$R_F = CF_3$ (8)	$R_F = CHF_2$ (9)	$R_F = CH_2CF_3$ (10)
Homolytic cleavage			
ΔG_{298} / ΔH_{298} / ΔS_{298}	43.3/55.1/39.6	37.0/48.0/37.1	37.9/50.5/42.5
ΔG_{373} / ΔH_{373} / ΔS_{373}	39.9/54.8/40.1	33.8/47.8/37.8	34.2/50.5/43.6
Silane-assisted pathway (Figure 27)			
$\Delta G^{\ddagger}_{298}$ / $\Delta H^{\ddagger}_{298}$ / $\Delta S^{\ddagger}_{298}$	33.8/32.9/-3.4	31.9/29.5/-6.1	27.4/26.2/-3.9
$\Delta G^{\ddagger}_{373}$ / $\Delta H^{\ddagger}_{373}$ / $\Delta S^{\ddagger}_{373}$	34.1/32.9/-3.3	31.8/29.5/-6.1	27.7/26.2/-3.8

[a] Difference between $\mathbf{TS_{NO}}$+CO and **A**+SiH_4.

Two relevant points emerge from this comparison. The first one is that, although the calculated Δ*G* value of the homolytic cleavage pathway remains higher than the $\Delta G^{\ddagger}$ of the silane-assisted pathway ($\mathbf{TS_{NO}}$) for all three systems and at both temperatures, the gap between the two Δ*G* values is significantly reduced upon raising the temperature, because of the large positive Δ*S* of the homolytic bond cleavage process *vs.* the much smaller value of the silane-assisted process. The near-zero activation entropy of the silane-assisted pathway results from the balance of the positive CO dissociation entropy and the negative silane coordination entropy. The second point is that the calculated $\Delta S^{\ddagger}$ of the silane-assisted pathway is in much greater disagreement than that of the homolytic bond breaking process with the $\Delta S^{\ddagger}$ value determined experimentally which is a large positive value (see Table 7). This observation allows us to conclude that the major, or exclusive, pathway leading to the R_F-H evolution must be the homolytic bond cleavage completed by radical trapping, as initially anticipated (Scheme 3). The reason why the calculations wrongly predict a preference for the silane-assisted pathway is probably related to the use of SiH_4 as a simplified model for the much bulkier TTMSS. While the barrier of the homolytic cleavage does not depend on the silane nature, the energy of the rate-determining TS of the silane-assisted pathway is most certainly raised by the steric hindrance of the TTMSS molecule, relative to the starting materials, in a significant way. Therefore, the computational study validates the proposition, that the thermal decomposition of **8**-**10** occurs by Mn-R_F homolytic cleavage according to

Scheme 3. Indeed, this proposition was further suggested by the experimental observation that compound **8** is able to initiate the radical polymerization of vinylidene fluoride as will show in Chapter 5.

Full investigation of the decomposition of **8** described above showed that the H/D scrambling pathway proceeds via CO-dissociation and α-F elimination. It is of interest to probe the importance of this pathway for both compounds **8** and **9**, relative to the Mn-C homolytic cleavage, because the experimental study shows a very different impact of this secondary reaction in the order **8** > **9**. Therefore, the H/F exchange pathway according to Scheme 6 for compound **8** has also been calculated for compound **9** (Scheme 7) and the resulting energy profile is shown in Figure 28, once again in comparison with the homolytic Mn-CHF$_2$ bond cleavage on the left-hand side. For clarity, the labels are the same as in Scheme 6 with an additional prime symbol.

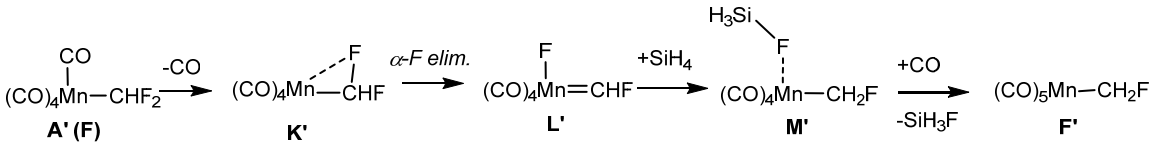

Scheme 7. H/F exchange pathway for compound **9**.

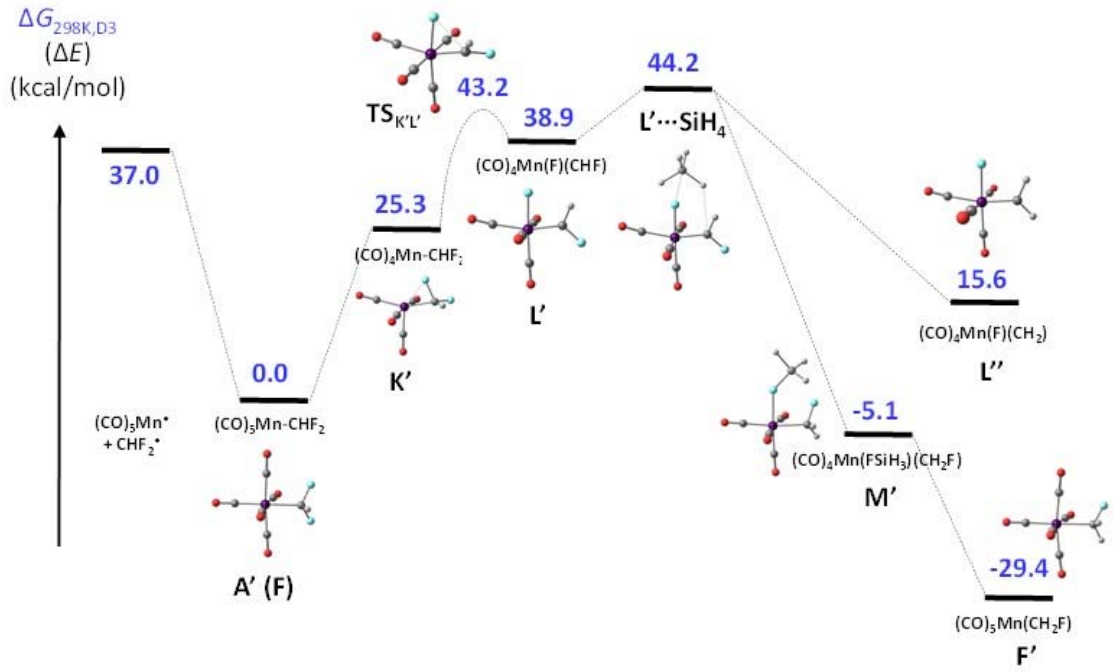

Figure 28. Energy profile (relative D3-corrected G_{298} values in kcal/mol) and views of the optimized geometries for the H/F scrambling pathway triggered by decarbonylation in compound **9** (Scheme 7).

The energy profile for the H/F exchange pathway of compound **9** is very similar to that of compound **8** (Figure 26). The decarbonylation process to generate **K'** is a bit less energy demanding than the generation of the corresponding **K** from compound **8**, possibly because of a better stabilization of unsaturation by the F atom in the less electron withdrawing CHF_2 group. On the other hand, the subsequent α-F elimination process has a higher barrier and leads to a less stable alkylidene derivative. Whereas the transition state leading to this intermediate for compound **8** (**TS_{KL}**) is lower than the homolytic bond cleavage products, the reverse is true for the pathway in compound **9** (**$TS_{K'L'}$**). The better stabilization of the system, relative to the starting [$(CO)_5MnR_F$] by difluorocarbene in **L** than by fluorocarbene in **L'** may be related to the greater stabilizing effect by π back-donation than by σ donation. The van der Waals adduct with SiH_4, **L···SiH_4**, could also be located for system **9**, but the transition state **$TS_{L'M'}$** could not, in spite of several attempts guided by relaxed scans. Probably, the collapse to the H/F scrambled product [$Mn(CO)_4(FSiH_4)(CH_2F)$] (**M'**) has a very low barrier with a shallow (low imaginary frequency) transition state, making the optimization of this stationary point particularly problematic. There is in fact a greater thermodynamic drive for **L'→M'** than for **L→M**. On the basis of Hammond's principle, this step is therefore expected to be associated with a lower barrier for **9**. During one of the several relaxed scans aimed at locating **$TS_{L'M'}$**, it was also found that SiH_4 can easily exchange its H atom directly with the F atom on the alkylidene group. This leads to the alkylidene complex **L"**, which is also shown in Figure 28, and represents another mechanism leading to the same result of H/F exchange. We were also unable to locate the transition state for this process. A view of a representative point along the relaxed scan of this new pathway is noted in the Appendix (Figure C.5).

It is now appropriate to compare the relative activation barriers for the homolytic bond breaking process and for the H/F exchange process under the conditions used for the decomposition experiments. For compound **9**, the van der Waals adduct **L'···SiH_4** was used as a low estimate of the rate-limiting transition state for the H/F exchange process, since the latter could not be optimized. Once again, since the *H* and *S* values do not change dramatically with temperature in the 70-100 °C range and the change in *ΔG* is mostly related to the effect of *T* in the (*ΔH-TΔS*) expression, the calculations were only carried out at the representative temperature of 100 °C. The results are shown in Table

9, with the raw energy data in the Appendix (Table C.2). The barrier height on the *G* scale does not change very much with temperature, because the Δ*S* value is relatively small, resulting from the compensation between the CO dissociation and SiH_4 association.

Table 9. DFT-calculated activation parameters (Δ*G* and Δ*H* values in kcal mol^{-1}; Δ*S* values in cal mol^{-1} K^{-1}) for the H/F scrambling at different temperatures for compounds **8** and **9**.[a]

Parameter	$R_F = CF_3$ (8)	$R_F = CHF_2$ (9)
$\Delta G^{\ddagger}_{298}$ / $\Delta H^{\ddagger}_{298}$ / $\Delta S^{\ddagger}_{298}$	43.7/43.6/-0.3	44.2/45.5/4.6
$\Delta G^{\ddagger}_{373}$ / $\Delta H^{\ddagger}_{373}$ / $\Delta S^{\ddagger}_{373}$	43.7/43.8/0.0	43.8/45.9/5.6

[a] Difference between $\mathbf{TS_{LM}}$+CO and **A**+SiH_4 for compound **8**; estimated from the difference between **L'···SiH$_4$**+CO and **A'**+SiH_4 for compound **9**.

A comparison of the barriers of the two competitive processes, namely homolytic bond cleavage (Table 8) and H/F exchange (Table 9), the balance is much more in favor of homolytic bond cleavage for compound **9** (33.8 kcal/mol *vs.* 43.8 for the competitive H/F exchange pathway) than for compound **8** (39.9 kcal/mol *vs.* 43.7 for the alternative pathway). This difference essentially derives from the weaker Mn-CHF_2 bond in **9** relative to the Mn-CF_3 bond in **8** (Table 8), whereas the barriers to the H/F exchange process for the two compounds are essentially unchanged (or slightly in favor of **8**, considering that the value calculated for **9** is a low estimate, Table 9). This trend is qualitatively in agreement with the experimentally observed greater impact of the H/F exchange process for compound **8** than for compound **9**.

Finally, the impact of the H/F exchange reaction on the kinetic estimation of the Mn-R_F bond strength by the thermal decomposition study was considered, particularly in the case of compound **8** for which this secondary reaction occurs to a greater extent. An important indicator is the activation entropy, which was experimentally determined as large and positive for all three compounds (Table 7). The computed Δ*S* values for the homolytic bond cleavage are also positive, although lower (Table 8), whereas the H/F exchange reaction for compounds **8** and **9** is associated to much lower, nearly zero, activation entropies. The experimentally determined values are influenced by large uncertainties and the computed values are certainly affected by many approximations, such as the neglect of solvation effects. However, this comparison suggests that the experimentally determined $\Delta S^{\ddagger}$ values are mostly determined by the homolytic bond

cleavage process. A safe conclusion is that the experimentally determined $\Delta H^{\ddagger}$ values are low estimates of the activation enthalpy leading to the Mn-R_F bond cleavage. The expected error is obviously higher in the presence of a higher fraction of H/F exchange: **10** (no exchange) << **9** (10% exchange) < **8** (67% exchange). Upon consideration of the excellent match between the experimental (50.6±0.8 kcal/mol) and computed (50.5 kcal/mol) values for compound **10**, and comparison of the experimental and computed values for compounds **8** and **9** (Table 7), we conclude that the effect of the H/F exchange pathway on the estimation of the Mn-R_F BDE must be quite small, less than 2 kcal/mol, which is within the experimental error on the determined $\Delta H^{\ddagger}$ value.

As a final note, we advance the hypothesis that at least a few of the unidentified minor by-products (in addition to R_FH generated by bond cleavage for **8**, **9** and **10** and to the identified H/F exchange products for **8** and **9**) result from additional reactivity pathways of the intermediate carbene complexes (**L**, **L'** and **L''** in Figure 26 and Figure 28). It has been widely appreciated that the decomposition of free perfluoroalkyl anions, used during organic synthesis investigations, leads to products derived from difluorocarbene,[56-68] e. g. tetrafluoroethylene and its polymer from difluorocarbene. For instance, after decoordination of CF_2 from **L** or CHF from **L'** or CH_2 from **L''**, a silicon reagent (either $(Me_3Si)_3SiH$ or $(Me_3Si)_3SiF$ or both) could undergo C-H oxidative addition to the vacant coordination site in $[Mn(CO)_4F]$, eventually leading to different F-containing silicon products and molecules derived from R_F. Other products may derive from oxidative additions across the Si-Si bond of TTMSS. The β-F elimination from compound **10** (after decarbonylation) does not take place because TMS_3SiF could not be detected, even in trace amounts, in that experiment. However, we cannot exclude the possible contribution of α-H elimination. Full elucidation of these pathways would require additional experimental and computational work.

4.3. Conclusion

A new and accurate method associated to homolytically strong metal-fluoroalkyl bonds has been used. Indeed, this method can potentially be applied to a wide range of compounds that contain homolytically strong bonds.

The experimental determination of the homolytic Mn-R bond cleavage activation parameters for **1** and **10** as well as for the well-known analogues with R = CF_3 (**8**) and CHF_2 (**9**), carried out by saturation kinetics with trapping by TTMSS, gave values in close agreement with recent DFT estimations[1] but significantly higher than previous determinations by other experimental methods.[4,6] Obtained results in BDE values shows that CF_3 (**8**) > CH_2CF_3 (**10**) > CHF_2 (**9**) > $CH(CH_3)(COOCH_3)$ (**1**). Indeed, the presence of three fluorine atoms instead of two in the alkyl chain, even in β-position, make stronger the Mn-R bond. The lowest BDE was found in the compound **1** as expected, rather lower than the fluoroalkyl complex with the least BDE.

In addition, another phenomenon that accompanies the homolytic bond breaking of process for compounds **8** and **9** has been highlighted, namely the α-F elimination leading to H/F exchange in the presence of the H atom donor TTMSS. This process was revealed in the ^{19}F NMR spectrum by the formation of $(Me_3Si)_3SiF$ and occurs only for compounds **8** and **9**, which contain F atoms in the α position, but not for compound **10** where the F atoms are located only on the β-C atom. For other previously investigated systems, it was shown that α-F elimination is preferred over β-F elimination when both α and β C-F bonds are present.[49,50,52,53,55] but this phenomenon is shown here for the first time in organomanganese chemistry. The DFT study suggests that this process is only possible after creating a vacant coordination site on the Mn center by CO dissociation, whereas the alternative migratory insertion followed by β-F elimination is not viable. Furthermore, the impact of this H/F exchange pathway decreases in the order **8** > **9** because the Mn-C bond weakens in the same direction, whereas the barrier to the H/F exchange remains approximately unchanged. The analysis of the barriers of these two competing processes at 100°C has validated the proposition that the determined $\Delta H^{\ddagger}$ values for the

thermal decomposition are good estimates of the Mn-R_F BDE. The generation of other minor by-products, as revealed by the ^{19}F NMR spectra, indicates the presence of yet additional reaction pathways undertaken by one or more of the thermally generated intermediates from the starting [$Mn(CO)_5R_F$] complexes. These pathways are, however, much less important than the H/F exchange pathway analyzed in the present contribution.

4.4. Experimental section

Investigation of the Homolytic Mn-R Bond Cleavage. All experiments were carried out using the same procedure. As a representative example, [$Mn(CO)_5(CF_3)$] (159.3 mg, 0.60 mmol) was dissolved in 5.0 mL of C_6D_6 together with 8 drops of C_6F_6 as internal standard. Aliquots of this solution (0.5 mL) were transferred into NMR tubes, then the desired amount of $(TMS)_3SiH$ was added and the thermal decomposition was monitored at the desired temperatures by ^{19}F NMR. The signal of hexafluorobenzene (internal standard) is integrated from -162.8 ppm to -163.2 ppm, and the value of the internal standard was set to 1 in all the spectra. Then, the complex signal was integrated from 7.7 ppm to 8.1 ppm. Knowing the initial concentration of complex in each tube (C_0), the concentration of complex at time t (C_t) was determined by the as $C_t = C_0 I_t / I_0$, where I_0 and I_t stand for the integral value of the NMR signal of the complex at t = 0 and at t, respectively. The $\ln[C_0/C_t]$ *vs.* time plots led to straight lines, the slopes of which represents k.

Computational Details. The computational work was carried out by Prof. Rinaldo Poli using the Gaussian09 suite of programs.[69] Gas-phase geometry optimizations were performed without any symmetry constraint using the BPW91* functional[70] and the 6-31G(d,p) basis functions for all light atoms (H, C, F, O, S), whereas the Mn, atom was treated with the SDD basis set augmented by an f polarization function (α = 2.195).[71] The unrestricted formulation was used for open-shell molecules, yielding only minor spin contamination ($<S^2>$ at convergence was very close to the expected value of 0.75 for doublet states, the maximum deviation being 0.757 for [$(CO)_5Mn^{\bullet}$]). All final

geometries were characterized as local minima by verifying that all second derivatives of the energy were positive. Thermochemical corrections were obtained at 298.15 K and at 373 K on the basis of frequency calculations, using the standard approximations (ideal gas, rigid rotor and harmonic oscillator). Corrections for dispersion were carried out at the fixed BPW91* optimized geometries using Grimme's D3 empirical method (BPW91*-D3), using SR6 and S8 parameters identical to those optimized for B3PW91.[72] A further correction of 1.95 Kcal/mol was applied to bring the G values from the gas phase (1 atm) to the solution (1 mol/L) standard state.[73] Since the reactions take place in the apolar C_6D_6 solvent, no solvation correction was carried out.

4.5. References

[1] R. Poli; S. M. W. Rahaman; V. Ladmiral; B. Ameduri *J. Organomet. Chem.* **2018**, *864*, 12-18.
[2] S. Banerjee; V. Ladmiral; A. Debuigne; C. Detrembleur; R. Poli; B. Améduri *Angew. Chem. Int. Ed.* **2018**, *57*, 2934–2937.
[3] J. A. Connor; M. T. Zafaranimoattar; J. Bickerton; N. I. Elsaied; S. Suradi; R. Carson; G. Altakhin; H. A. Skinner *Organometallics* **1982**, *1*, 1166-1174.
[4] J. A. Martinho Simões; J. L. Beauchamp *Chem. Rev.* **1990**, *90*, 629-688.
[5] E. Folga; T. Ziegler *J. Am. Chem. Soc.* **1993**, *115*, 5169-5176.
[6] J. A. Connor; M. T. Zafarani-Moattar; J. Bickerton; N. I. El Saied; S. Suradi; R. Carson; G. Al Takhin; H. A. Skinner *Organometallics* **1982**, *1*, 1166-1174.
[7] S. C. Tenhaeff; K. J. Covert; M. P. Castellani; J. Grunkemeier; C. Kunz; J. R. Weakley; T. Koenig; D. R. Tyler *Organometallics* **1993**, *12*, 5000-5004.
[8] R. G. Finke; B. P. Hay *Inorg. Chem.* **1984**, *23*, 3041-3043.
[9] J. Halpern; S. H. Kim; T. W. Leung *J. Am. Chem. Soc.* **1984**, *106*, 8317-8319.
[10] G. N. Schrauzer; J. H. Grate *J. Am. Chem. Soc.* **1981**, *103*, 541-546.
[11] R. J. Blau; J. H. Espenson *J. Am. Chem. Soc.* **1985**, *107*, 3530-3533.
[12] S. H. Kim; H. L. Chen; N. Feilchenfeld; J. Halpern *J. Am. Chem. Soc.* **1988**, *110*, 3120-3126.
[13] A. Goto; T. Fukuda *Macromol. Rapid Commun.* **1999**, *20*, 633-636.
[14] K. Matyjaszewski; H.-j. Paik; P. Zhou; S. J. Diamanti *Macromolecules* **2001**, *34*, 5125-5131.
[15] A. K. Nanda; K. Matyjaszewski *Macromolecules* **2003**, *36*, 8222-8224.
[16] T. Pintauer; W. Braunecker; E. Collange; R. Poli; K. Matyjaszewski *Macromolecules* **2004**, *37*, 2679-2682.
[17] T. J. Meyer; J. V. Caspar *Chem. Rev.* **1985**, *85*, 187-218.
[18] Y. Zhu; J. Gong; Y. Wan *J. Org. Chem.* **2017**, *82*, 7428-7436.
[19] P. Jaitner; W. Huber; G. Huttner; O. Scheidsteger *J. Organomet. Chem.* **1983**, *259*, C1-C5.
[20] D. Rehder; P. Jaitner *J. Organomet. Chem.* **1987**, *329*, 337-342.
[21] J. P. Lomont; S. C. Nguyen; C. B. Harris *J. Am. Chem. Soc.* **2013**, *135*, 11266-11273.

[22] C. Chatgilialoglu; D. Griller; M. Lesage *J. Org. Chem.* **1988**, *53*, 3641-3642.
[23] M. Ballestri; C. Chatgilialoglu; K. B. Clark; D. Griller; B. Giese; B. Kopping *J. Org. Chem.* **1991**, *56*, 678-683.
[24] C. Chatgilialoglu; D. Griller; M. Lesage *J. Org. Chem.* **1989**, *54*, 2492-2494.
[25] C. Chatgilialoglu; J. Dickhaut; B. Giese *J. Org. Chem.* **1991**, *56*, 6399-6403.
[26] C. Chatgilialoglu *Helv. Chim. Acta* **2006**, *89*, 2387-2398.
[27] M. Ishikawa; A. Nakamura; M. Kumada *J. Organometal. Chem.* **1973**, *59*, C11-C12.
[28] B. K. Nicholson; J. Simpson *J. Organometal. Chem.* **1971**, *32*, C29-C30.
[29] B. K. Nicholson; J. Simpson; W. T. Robinson *J. Organometal. Chem.* **1973**, *47*, 403-412.
[30] D. K. Russell; I. M. T. Davidson; A. M. Ellis; G. P. Mills; M. Pennington; I. M. Povey; J. B. Raynor; S. Saydam *Chem. Vap. Deposition* **1998**, *4*, 103-107.
[31] S. G. Frankiss *J. Phys. Chem.* **1963**, *67*, 752-755.
[32] P. Sartori; W. Habel *J. Fluorine Chem.* **1980**, *16*, 265-276.
[33] P. Sartori; W. Habel *J. Fluorine Chem.* **1981**, *18*, 131-141.
[34] T. Zweifel; J.-V. Naubron; T. Büttner; T. Ott; H. Grützmacher *Angew. Chem., Int. Ed.* **2008**, *47*, 3245-3249.
[35] E. Folga; T. Ziegler *J. Am. Chem. Soc.* **1993**, *115*, 5169-5176.
[36] H. Buerger; W. Kilian; K. Burczyk *J. Organometal. Chem.* **1970**, *21*, 291-301.
[37] H. C. Marsmann; W. Raml; E. Hengge *Z. Naturforsch., B Anorg. Chem., Org. Chem.* **1980**, *35B*, 1541-1547.
[38] M. Ahrens; G. Scholz; T. Braun; E. Kemnitz *Angew. Chem. Int. Ed.* **2013**, *52*, 5328-5332.
[39] M. J. Pellerite *J. Fluorine Chem.* **1990**, *49*, 43-66.
[40] D. D. Elleman; L. C. Brown; D. Williams *J. Mol. Spectrosc.* **1961**, *7*, 307-321.
[41] J. Hu; X. Han; Y. Yuan; Z. Shi *Angew. Chem. Int. Ed.* **2017**, *56*, 13342-13346.
[42] R. Kojima; K. Kubota; H. Ito *Chem. Commun.* **2017**, *53*, 10688-10691.
[43] J. Zhang; W. Dai; Q. Liu; S. Cao *Org. Lett.* **2017**, *19*, 3283-3286.
[44] K. Kikushima; H. Sakaguchi; H. Saijo; M. Ohashi; S. Ogoshi *Chem. Lett.* **2015**, *44*, 1019-1021.
[45] H. Sakaguchi; M. Ohashi; S. Ogoshi *Angew. Chem. Int. Ed.* **2018**, *57*, 328-332.
[46] T. Fujita; K. Fuchibe; J. Ichikawa *Angew. Chem. Int. Ed.* **2018**.
[47] F. Calderazzo; F. A. Cotton *Inorg. Chem.* **1962**, *1*, 30-36.
[48] F. Calderazzo; F. A. Cotton *Chim. e Indus.* **1964**, *46*, 1165-1169.
[49] R. R. Burch; J. C. Calabrese; S. D. Ittel *Organometallics* **1988**, *7*, 1642-1648.
[50] C. J. Bourgeois; R. P. Hughes; J. Yuan; A. G. DiPasquale; A. L. Rheingold *Organometallics* **2006**, *25*, 2908-2910.
[51] M. Takachi; Y. Kita; M. Tobisu; Y. Fukumoto; N. Chatani *Angew. Chem. Int. Ed.* **2010**, *49*, 8717-8720.
[52] K. A. Giffin; D. J. Harrison; I. Korobkov; R. T. Baker *Organometallics* **2013**, *32*, 7424-7430.
[53] N. O. Andrella; A. J. Sicard; S. I. Gorelsky; I. Korobkov; R. T. Baker *Chem. Sci.* **2015**, *6*, 6392-6397.
[54] T. Fujita; Y. Watabe; T. Ichitsuka; J. Ichikawa *Chem. Eur. J.* **2015**, *21*, 13225-13228.
[55] M. Ohashi; Y. Ueda; S. Ogoshi *Angew. Chem. Int. Ed.* **2017**, *56*, 2435-2439.
[56] R. N. Haszeldine *J. Chem. Soc.* **1954**, 1273-1279.
[57] O. R. Pierce; E. T. McBee; G. F. Judd *J. Am. Chem. Soc.* **1954**, *76*, 474-478.
[58] T. Shono; M. Ishifune; T. Okada; S. Kashimura *J. Org. Chem.* **1991**, *56*, 2-4.
[59] J. Russell; N. Roques *Tetrahedron* **1998**, *54*, 13771-13782.
[60] B. Folleas; I. Marek; J. F. Normant; L. Saint-Jalmes *Tetrahedron Lett.* **1998**, *39*, 2973-2976.
[61] B. Folleas; I. Marek; J. F. Normant; L. Saint-Jalmes *Tetrahedron* **2000**, *56*, 275-283.
[62] S. Large; N. Roques; B. R. Langlois *J. Org. Chem.* **2000**, *65*, 8848-8856.
[63] B. R. Langlois; T. Billard *Synthesis-Stuttgart* **2003**, 185-194.

[64] A. Zanardi; M. A. Novikov; E. Martin; J. Benet-Buchholz; V. V. Grushin *J. Am. Chem. Soc.* **2011**, *133*, 20901-20913.
[65] H. Kawai; Z. Yuan; E. Tokunaga; N. Shibata *Org. Biomol. Chem.* **2013**, *11*, 1446-1450.
[66] Y. Zhang; M. Fujiu; H. Serizawa; K. Mikami *J. Fluorine Chem.* **2013**, *156*, 367-371.
[67] G. K. S. Prakash; F. Wang; Z. Zhang; R. Haiges; M. Rahm; K. O. Christe; T. Mathew; G. A. Olah *Angew. Chem. Int. Ed.* **2014**, *53*, 11575-11578.
[68] C. F. Ni; J. B. Hu *Chem. Soc. Rev.* **2016**, *45*, 5441-5454.
[69] M. J. Frisch; G. W. Trucks; H. B. Schlegel; G. E. Scuseria; M. A. Robb; J. R. Cheeseman; G. Scalmani; V. Barone; B. Mennucci; G. A. Petersson; H. Nakatsuji; M. Caricato; X. Li; H. P. Hratchian; A. F. Izmaylov; J. Bloino; G. Zheng; J. L. Sonnenberg; M. Hada; M. Ehara; K. Toyota; R. Fukuda; J. Hasegawa; M. Ishida; T. Nakajima; Y. Honda; O. Kitao; H. Nakai; T. Vreven; J. Montgomery, J. A.; J. E. Peralta; F. Ogliaro; M. Bearpark; J. J. Heyd; E. Brothers; K. N. Kudin; V. N. Staroverov; R. Kobayashi; J. Normand; K. Raghavachari; A. Rendell; J. C. Burant; S. S. Iyengar; J. Tomasi; M. Cossi; N. Rega; N. J. Millam; M. Klene; J. E. Knox; J. B. Cross; V. Bakken; C. Adamo; J. Jaramillo; R. Gomperts; R. E. Stratmann; O. Yazyev; A. J. Austin; R. Cammi; C. Pomelli; J. W. Ochterski; R. L. Martin; K. Morokuma; V. G. Zakrzewski; G. A. Voth; P. Salvador; J. J. Dannenberg; S. Dapprich; A. D. Daniels; Ö. Farkas; J. B. Foresman; J. V. Ortiz; J. Cioslowski; D. J. Fox *Gaussian 09, Revision D.01*; Gaussian, Inc.: Wallingford CT, 2009.
[70] M. Reiher *Inorg. Chem.* **2002**, *41*, 6928-6935.
[71] A. W. Ehlers; M. Böhme; S. Dapprich; A. Gobbi; A. Hoellwarth; V. Jonas; K. F. Koehler; R. Stegmann; A. Veldkamp; G. Frenking *Chem. Phys. Lett.* **1993**, *208*, 111-114.
[72] S. Grimme; J. Antony; S. Ehrlich; H. Krieg *J. Chem. Phys.* **2010**, *132*.
[73] V. S. Bryantsev; M. S. Diallo; W. A. Goddard, III *J. Phys. Chem. B* **2008**, *112*, 9709-9719.

Chapter 5

Polymerization of various monomers in the presence of [Mn(CO)$_5$R] complexes

Outline:

5. Polymerization of various monomers in the presence of [Mn(CO)$_5$R] complexes

5.1. Introduction

The aim of this chapter is to study the alkyl and fluoroalkylpentacarbonyl-manganese(I) complexes synthesized is the previous chapters as initiators and possibly controlling agents in the polymerization of a few fluorinated and non-fluorinated monomers. These complexes do not appear to have found direct use in catalysis, whereas many other organomanganese complexes are now intensively investigated as precatalysts for various transformations such as hydrosilylation,[1-3] dehydrogenative coupling,[3-6] C-H[7] and C-F[8] activation, etc. However, the possible implication of alkyl and fluoroalkylpentacarbonylmanganese(I) systems in reversible-deactivation radical polymerization (RDRP) has recently been mentioned in contributions by Asandei *et al.*,[9,10] who described a beneficial role of [$Mn_2(CO)_{10}$] on the polymerization of vinylidene fluoride (VDF, $H_2C=CF_2$) by the iodine transfer polymerization (ITP) controlling method. As mentioned in Chapter 1, in this polymerization technique most of the chains at any given time reside in an iodine-capped dormant form, PVDF-I, and are reversibly reactivated by a rapid degenerative exchange with the active radical chains, PVDF$^\bullet$, which insures a controlled growth by the degenerative transfer protocol.[11-13]

The radical polymerization of VDF produces two different types of chain ends as shown in Scheme 1, head (H, way 1) and tail (T, way 2), following the regular head-to-tail (dominant) monomer addition (PVDF-$CH_2CF_2^\bullet$ or $PVDF_H^\bullet$) and the inverted head-to-head monomer addition (PVDF-$CF_2CH_2^\bullet$ or $PVDF_T^\bullet$), respectively. The proportion of inverted monomer additions is only 3.5-6% under typical polymerization conditions,[14-17] but this defect is sufficient to limit the efficiency of ITP and RAFT because the $PVDF_T$ dormant chains are less easily reactivated, accumulate during the polymerization and the control is eventually lost.[18]

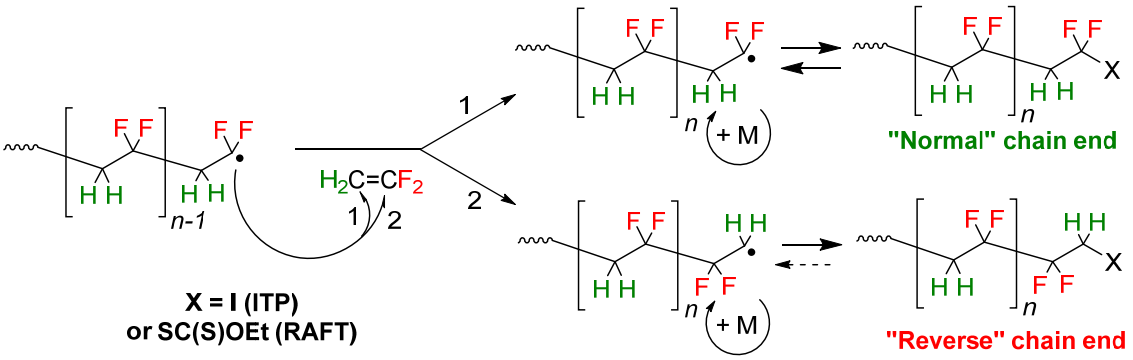

Scheme 1. Formation of $PVDF_H$ and $PVDF_T$ dormant species in ITP or RAFT polymerization.

Carrying out the polymerization in the presence of $[Mn_2(CO)_{10}]$ and under visible light irradiation leads to the reactivation of both dormant species. This was attributed to the ability of $[(CO)_5Mn^{\bullet}]$ radical, produced by photolytic Mn-Mn bond cleavage, to abstract an iodine atom from the dormant chain ends, including from the more recalcitrant PVDFT-I, to form $[Mn(CO)_5I]$ and regenerate the reactive radical chain.[9,10] In those contributions, the possible direct interaction between $[(CO)_5Mn^{\bullet}]$ radical and the growing radical chains, leading to the organometallic dormant species $[Mn(CO)_5(PVDF_H)]$ and $[Mn(CO)_5(PVDF_T)]$, was also mentioned. However, no evidence for the formation of these species was obtained and it was stated that, if formed, such species may be readily reactivated under the thermal (40 °C) and photochemical (visible light) operating conditions of the polymerization. Given our interest in organometallic-mediated radical polymerization (OMRP)[19-21] and in the application of this method to the controlled polymerization of fluorinated monomers,[22-25] we were interested in probing the possible dissociative activation of the Mn-C bond in $[Mn(CO)_5R_F]$ under both thermal and photochemical conditions.

Experimental BDE studies carried out in Chapter 4, in good agreement with the computational studies,[26] suggest that the alkyl and fluoroalkylpentacarbonyl-manganese(I) complexes (**1**, **8**, **9** and **10**) synthesized in this work are able to initiate the radical polymerization by the generation of the corresponding alkyl or fluoroalkyl radical. The question remains whether $[(CO)_5Mn^{\bullet}]$ radical can control the growth of polymers through an OMRP process. However, the possibility that there is some control

is low because the pentacarbonyl manganese radical tends to dimerize in solution to generate the manganese carbonyl, but it may be reactivated. Moreover, the Mn-C bond in the fluoroalkylpentacarbonylmanganese(I) complexes are relatively strong. In order to check whether there is any control, kinetic studies of the polymerization reactions were performed.

The monomers used for these investigations are vinylidene difluoride (VDF), *tert*-butyl-2-trifluoromethacrylate (MAF-TBE), vinyl acetate (VAc), methyl acrylate (MA) and styrene (S). The obtained polymers have been characterized by a few or all of the following techniques: ^{1}H and ^{19}F NMR, FTIR, size exclusion chromatography (SEC) with a refractive index detector, thermogravimetric analysis (TGA) and differential scanning calorimetry (DSC).

The reactivity of the radical generated by the manganese complex is a key factor on the initiation of the polymerization. It should be considered that fluorinated radicals are more reactive radicals than the alkyl ones. This is noted in the addition of the radicals to alkenes. For instance, the addition kinetic constant of $CF_3^{\bullet}$ radical to styrene is 53 mol·L^{-1}·s^{-1} *vs.* 0.12 mol·L^{-1}·s^{-1} for a $RCH_2^{\bullet}$ radical.[27] Fluorinated substituents have a high impact on the stability of alkyl radicals because of the inductive and resonance effects. Inductive effect destabilizes the radical whereas the resonances effects stabilize it because of the delocalization of the odd electron.[27] From a DFT study of several fluorinated methanes and ethanes, it could be concluded that one or two fluorine atoms in the α-position stabilize the radical, whereas three fluorine atoms result in a destabilization. A similar effect is observed when the fluorine atoms are in the β-position.[28,29] It is important to note that the stability of hydrocarbon radicals increase with the substitution (e.g.: $H_3C^{\bullet}$ radical is less stable than $CH_3CH_2^{\bullet}$).[28]

The stability of the radicals correlates with their reactivity onto alkenes. However, the alkene substituents also have an important effect, establishing the regiochemistry of the addition reaction. Defining the position attacked by the radical as α, substituents at this carbon atom produce both polar and steric effects, while the β substituents exert chiefly polar effects on the rates of addition. Furthermore, the radical substituents produce both polar and steric effects on the rate of addition to alkenes.[30,31]

Sokolov *et al.*[32] studied the reactivity of $F_3C^\bullet$ and other perfluorinated radicals with several fluorinated olefins and ethylene, concluding that the reactivity of $F_3C^\bullet$ decreases with the number of fluorine atoms on the monomer (e.g.: addition of $F_3C^\bullet$ on ethylene is almost 15 times faster than on VDF).

5.2. Results and discussion

5.2.1. Polymerizations of VDF with $[Mn(CO)_5R_F]$

Several polymerizations of VDF using fluoroalkyl(pentacarbonyl)manganese complexes as initiators were carried out under thermal and photochemical conditions (Scheme 2). In the case of thermal activation, the temperature was chosen as a function of the BDE value of each complex, determined in Chapter 4. The photochemical initiation was performed by visible light using LED bulbs or by UV radiation using an UV chamber with 16 UV monochromatic lamps with a wavelength of 300 nm.

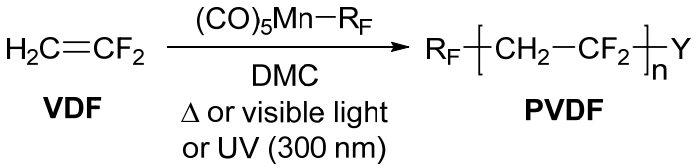

Scheme 2. General synthetic pathway employed to synthesize PVDF using fluoroalkylpentacarbonylmanganese(I) complexes as initiators under thermal or photochemical conditions. Y stands for $Mn(CO)_5$ or H or R_F.

As mentioned above, VDF is a gas at room temperature (b. p. -84 °C). Thus, all reactions were performed in sealed Carius tubes with 5 mL of dimethyl carbonate (DMC) as solvent. DMC has been reported as the best solvent for VDF polymerization by Asandei and co-workers.[9] In addition, this solvent enables this monomer to have a high reaction rate, moreover, VDF[33] and PVDF are relatively soluble in DMC and has a relatively hydrogen transfer side-reaction rate, although transfer to solvent cannot be fully suppressed.

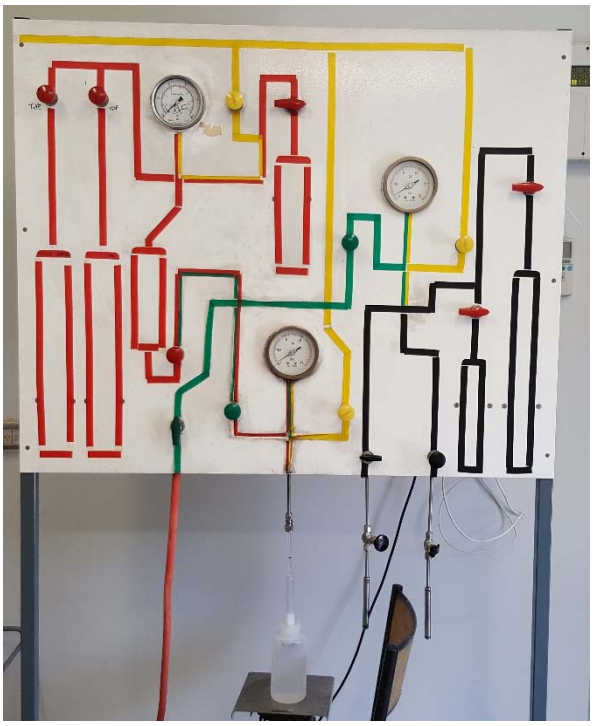

Figure 1. Custom-made manifold used to remove air and then to introduce the VDF in the Carius tubes.

Control experiments carried out with [$Mn_2(CO)_{10}$] did not yield any PVDF. Since [$Mn_2(CO)_{10}$] is known to generate [$(CO)_5Mn^{\bullet}$] radical under both thermal and photochemical conditions, it can be concluded that the free [$(CO)_5Mn^{\bullet}$] radicals are not capable to add onto VDF to initiate the polymerization. These results confirm previous studies by Bamford *et al.*[34] and by Asandei *et al.*,[9] where [$(CO)_5Mn^{\bullet}$] radical photoproduced from [$Mn_2(CO)_{10}$] was unable to initiate the radical polymerization of VDF (although it does initiate those of C_2F_4 and C_2F_3Cl).

5.2.2. VDF/[Mn(CO)$_5$(CF$_3$)]

Among all the fluoroalkylpentacarbonylmanganese(I) synthesized in this work, compound **8** possesses the stronger Mn-C BDE according to the theoretical and experimental BDE determination. Therefore, it is necessary to apply a relatively high temperature to cleave the Mn-CF_3 bond. The addition of the produced $F_3C^{\bullet}$ radical to a monomer should be effective and fast because of the low stability and high reactivity of

this radical. Polymerizations were carried out using three different activation methods to cleave the Mn-CF_3 bond homolytically: thermal activation at 100 °C, activation with visible light and UV monochromatic irradiation (300 nm).

5.2.2.1. Thermal activation

Several polymerizations were carried out with compound **8** activated thermally and the reactions were stopped at different times. The reaction conditions and analytical data of the resulting polymers are summarized in Table 1. All reactions were performed targeting a degree of polymerization of 50, expecting a molar mass *ca.* 3500 g·mol^{-1} under the assumption that the $F_3C^{\bullet}$ radical initiates the polymerization and that the pentacarbonylmanganese radical controls the polymerization by reversibly binding to the PVDF chains (OMRP mechanism).

Table 1. Experimental conditions and results for the polymerization of VDF in the presence of [Mn(CO)$_5$(CF_3)] initiated by thermal activation (100 °C).

Entry	Target DP	Temperature (°C)	Reaction time (h)	Yield [a] (%)	M_n [b] (g·mol^{-1})	Đ	H-H [c] (%)
1	50	50	24	0	-	-	-
2	50	100	2	6	16000	1.42	3.6
3	50	100	4	15	23000	1.48	3.4
4	50	100	6	38	20100	1.50	3.7
5	50	100	24	68	16900	1.53	3.9

[a] Determined from the weight of the isolated polymer. [b] Calculated by SEC in DMF with refractive index detection (calibrated with PMMA standards). [c] Determined by relative integration of the ^{19}F NMR resonances.

A first VDF polymerization test was performed at 50 °C for 24 h (entry 1). These conditions do not lead to the formation of any PVDF, meaning that this temperature is not sufficient to homolytically cleave the Mn-CF_3 bond in compound **8**. However, PVDF was produced in high yields at higher temperature (100 °C, entries 2 to 6). As shown in the previous chapter, 100 °C is sufficient to generate $F_3C^{\bullet}$ radicals from compound **8** in C_6D_6 ($t_{½}$ ≈ 37 min, and $t_{99\%}$ ≈ 4 h). Hence, new polymer chains should be generated until *ca.* 4 h after the beginning of the polymerization assuming that $t_{1/2}$ in DCM/VDF is similar

to that determined in C_6D_6. The generation of new radicals up to 4 hours of reaction may explain the slight increase of dispersity between entries 2 and 3 (1.42 to 1.48), whereas the number average molar masses increase during this period. Then, the dispersity continuous to increase slowly, whereas the molar masses decrease (entries 3 to 5). The percentage of H-H additions (3.4-3.9%) corresponds to the regular rate of a PVDF formed by radical polymerization.[35] It was calculated by relative integration of the ^{19}F NMR spectrum using the following equation:

$$H-H(\%) = \frac{I_c}{I_{a+b}+I_c+I_d} \times 100 \qquad \text{(Equation 1)}$$

In equation 1, I_{a+b} is the integral value of the resonances from the regular addition (head-to-tail) (a and b in Figure 3), I_c is the integral value of the resonance of a reverse addition (c in Figure 3) and I_d is the integral value of the resonance next to a reverse addition (d in Figure 3).

The $F_3C^{\bullet}$ radicals generated by compound **8** should attack preferentially the tail of VDF (CH_2); the attack to the head end has been reported to occur at less than 3% frequency at 150 °C.[36] Thus, the use of this radical should not significantly affect the percentage of inverted monomer additions.

The ^1H NMR spectrum of the polymer recovered from entry 5 exhibits the characteristics resonances of PVDF, which were assigned according to the literature as shown in Figure 2.[37] The clearly visible triplet ($^2J_{HF}$ = 55 Hz) of triplets ($^3J_{HH}$ = 7 Hz, not clearly seen in this spectrum) at δ 6.44 results from the -CH_2-CF_2*H* chain-ends formed by hydrogen transfer from the solvent onto a macroradical terminated by -CH_2-$CF_2^{\bullet}$. Similarly, this hydrogen transfer onto -CF_2-$CH_2^{\bullet}$ produces a triplet ($^3J_{HF}$ = 18 Hz) centered at δ 1.85 assigned to the methylene group of -CF_2-C*H*$_3$.[9,37,38] The transfer side-reaction leads to a decrease of the number average molar mass and to an increase of dispersity as observed in entries 3 to 5. Two relatively intense resonances at δ 4.38 and 3.79 may be assigned to the *H*$_3$C-OCO-C*H*$_2$-CH_2-CF_2- chain ends of the polymer chains initiated by the DMC radicals after the hydrogen transfer, because their relative intensities are close to those expected relative to that of the CH_2CF_2*H* signal (1:2:3 for the δ 6.44, 4.38 and 3.79 resonances, respectively).[38,39]

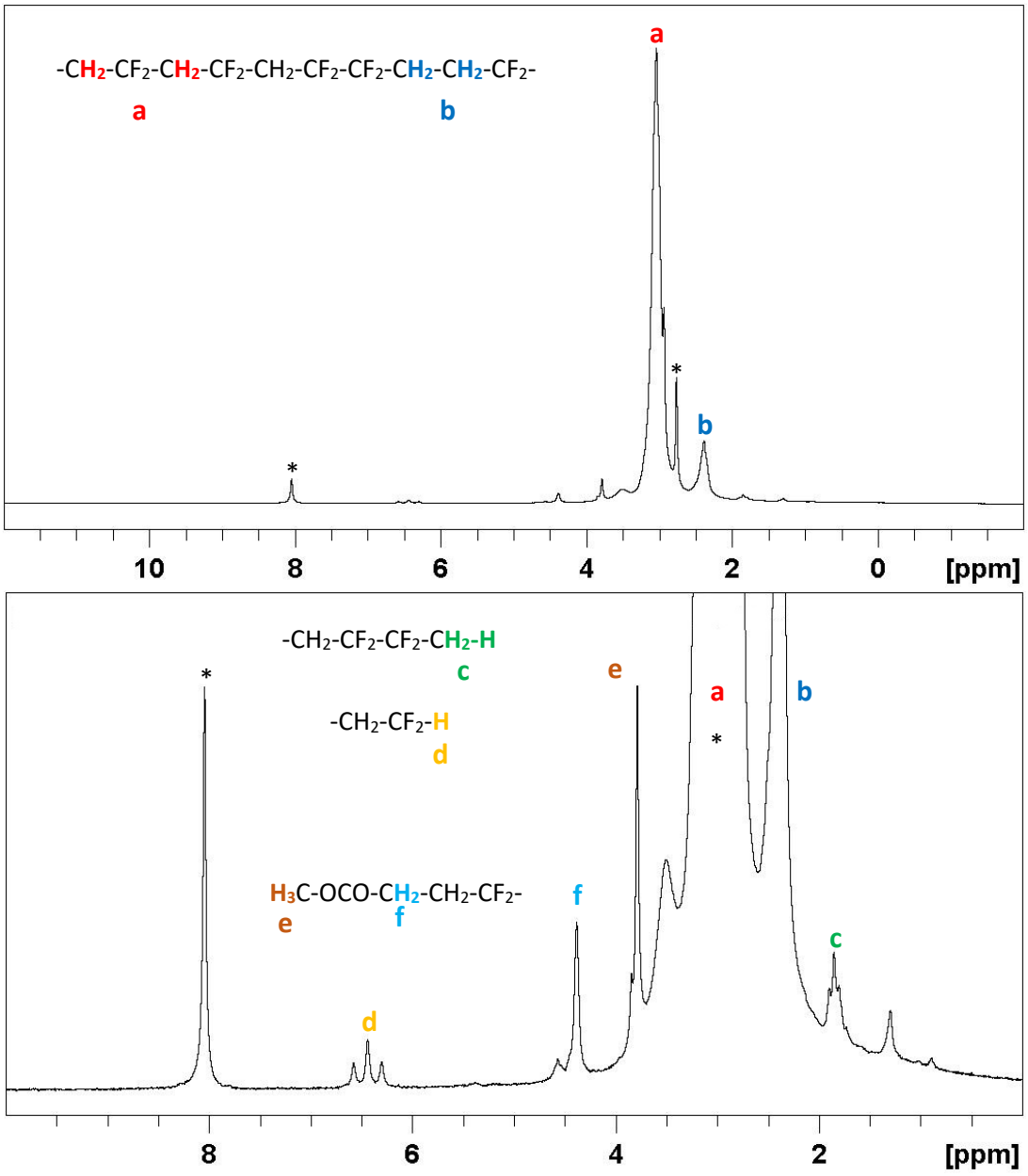

Figure 2. ^{1}H NMR spectrum (400 MHz, DMF-d_7) of the PVDF isolated from entry 5 of Table 1. Full spectrum above and expansion of the 0 to 8 ppm region below. The starred resonances are due to the solvent.

The ^{19}F NMR spectrum of the same polymer also shows all the expected resonances of PVDF,[37] detailed on the spectrum (Figure 3). In addition, several unidentified tiny signals are present at δ -150.66, -99.67, -98.98 and -85.68. However, the CF_3 chain-end produced by the initiation of the $F_3C^{\bullet}$ radical expected around δ -60.8[40,41] could not be observed, probably because of the high molar mass of the polymer (16900 g·mol^{-1})

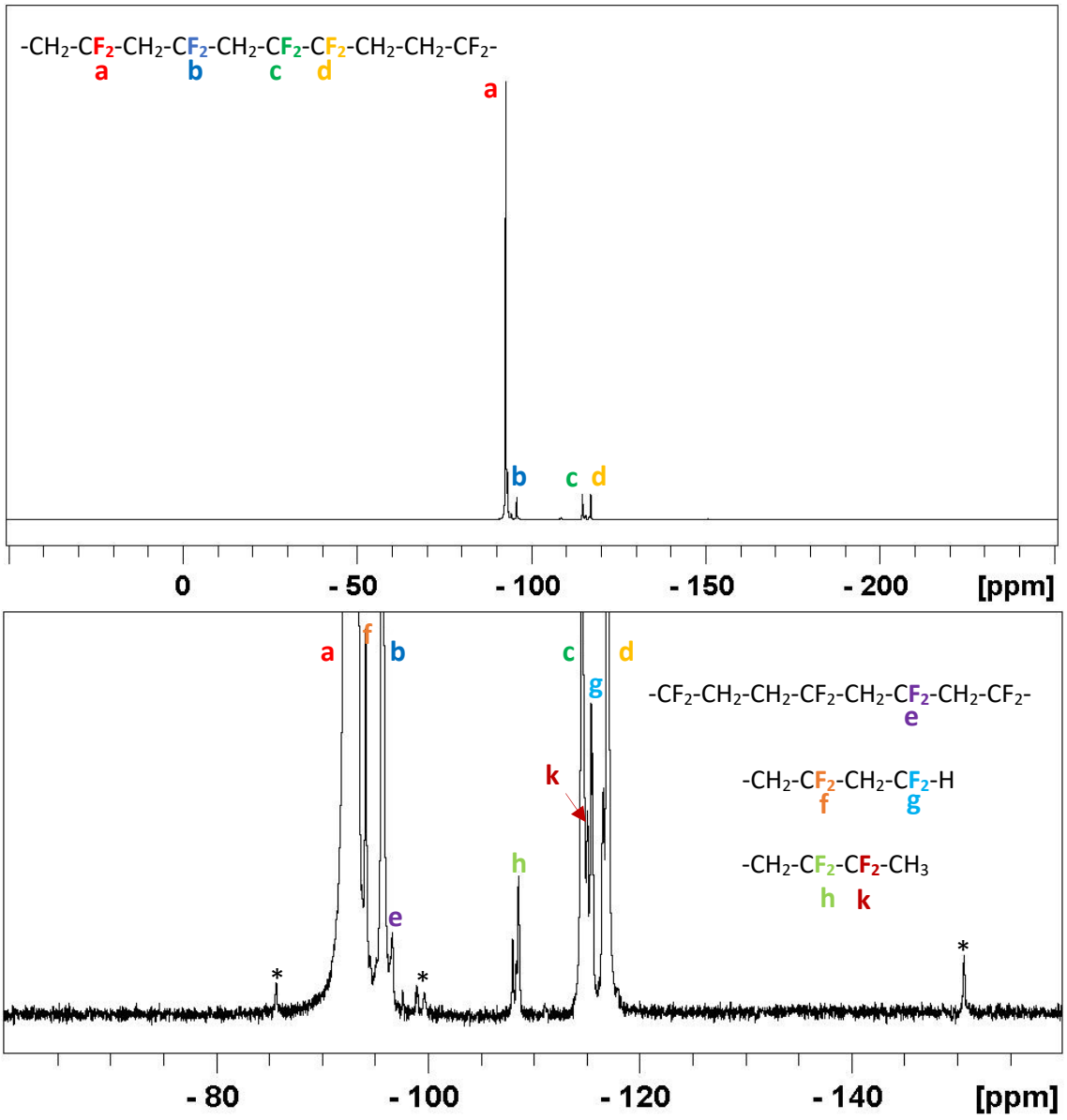

Figure 3. ^{19}F NMR spectrum (376.5 MHz, DMF-d_7) of the PVDF isolated from entry 5. Full spectrum above and expansion of the -160 to -60 ppm region below. The starred resonances could not be attributed to any expect signal of possible products.

The polymerization kinetics is close to that expected for a first-order behavior, as shown in Figure 3. The monomer concentration [M] was calculated from the PVDF yields as shown in Equation 2, since an accurate direct measurement of the VDF conversion is very difficult because the monomer is a gas.

$$Conversion\ (\%) = (\ 1 - \frac{m_{PVDF}}{m_{VDF} + m_{complex}}) \times 100 \qquad \text{(Equation 2)}$$

Only entry 4 (t = 6h) deviates slightly from the linear behavior, probably because of experimental error in the polymer yield measurement (each point come from a different Carius tube, namely from a different experiment).

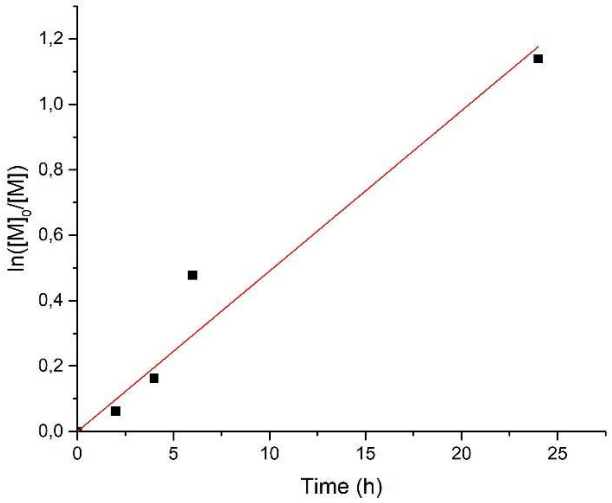

Figure 4. First-order kinetic plot for the polymerization of VDF in presence of [Mn(CO)$_5$(CF$_3$)] initiated thermally (100 °C) .

The size exclusion chromatograms of entries 2 to 5 (Figure 5) show two different populations: the main one shows a significant molar mass increase at the beginning (entries 2 to 3), and then a decrease (entries 3 to 5), proving the lack of control during the reaction. The signal of the second population at low molar mass can be attributed to short oligomers that have abstracted a hydrogen and are thus dead, since the analysis was done to the crude and no to a precipitated polymer. The negative signal in the size exclusion chromatograms results from the lower refractive index of PVDF relative to the DMF eluent.[42-44]

The general behavior of this polymerization does not correspond to a controlled radical polymerization. In fact, the rise of the dispersity accompanied by a decrease of the molar masses (Figure 6), as frequently observed in conventional radical polymerization, may indicate a hydrogen transfer, due to the presence of DMC. This stops the growing of macroradicals leading to dead species and generating new radicals that can create new small active chains initiated by the $H_3COCOOCH_2^{\bullet}$ radical. However,

despite the lack of control, a high conversion (68%) was reached after 24 h, suggesting that complex **8** is an efficient initiator of VDF polymerization.

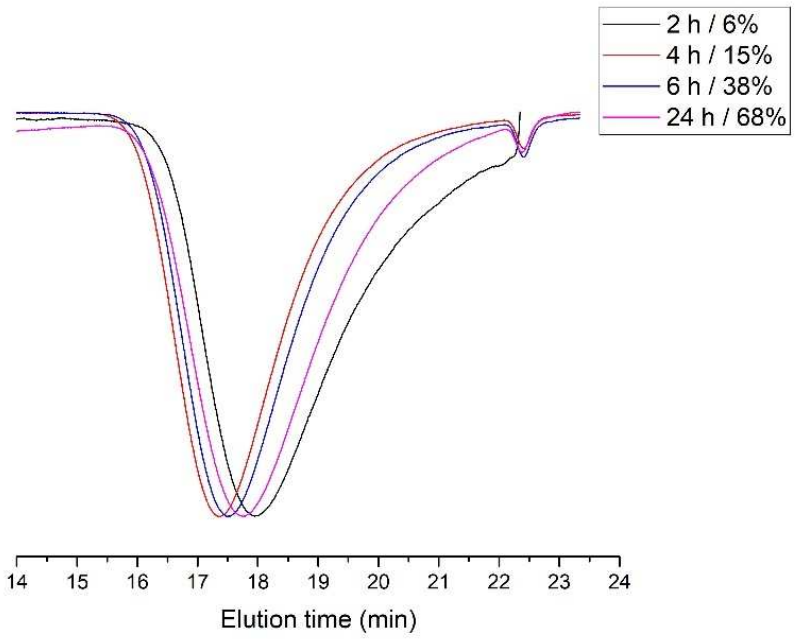

Figure 5. SEC traces of PVDF (entries 2, 3, 4 and 5 of Table 1) in DMF.

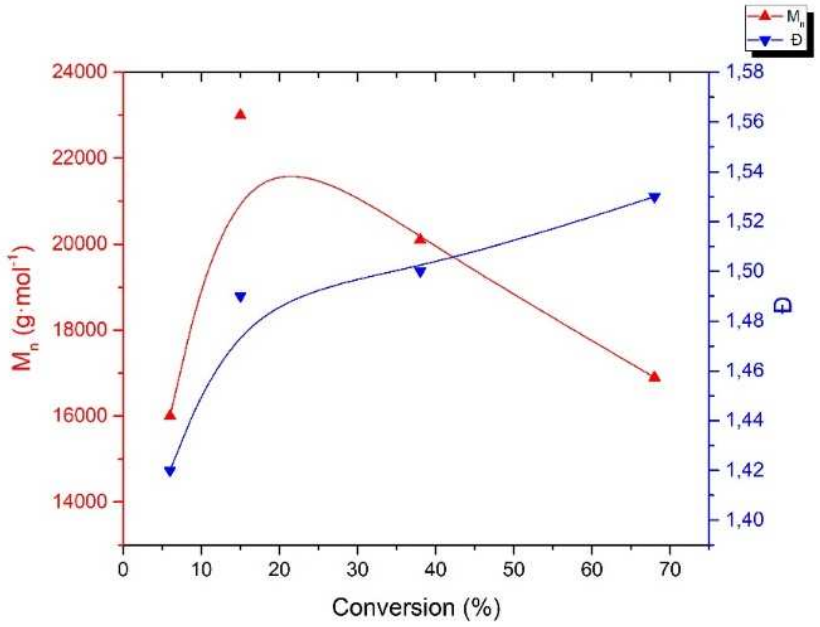

Figure 6. Number average molecular mass and dispersity vs conversion of polymerization of VDF with complex **8** initiated thermally (100 °C).

5.2.2.2. Visible light activation

Visible light irradiation may be able to cleave the Mn-R_F bond of [$Mn(CO)_5R_F$] as well as it cleaves the Mn-Mn bond in dimanganese decacarbonyl.[9,34] In order to test this possibility for compound **8** to generate $F_3C^\bullet$ radicals and initiate the radical polymerization, four photopolymerizations were carried out with different reactions time. The experimental conditions and results are presented in Table 2.

PVDF was obtained in high yields (60% for entry 9 after 24 h of reaction). It is important to note that the temperature was 40 °C during the experiment because of the heat released by the light bulbs. However, the entry 1 of Table 1 proves that this temperature is not sufficient to generate radicals. Thus, it is confirmed that the radicals are produced by the visible light irradiation.

Table 2. Experemintal conditions and results of the polymerization of VDF in the presence of [$Mn(CO)_5(CF_3)$] with visible light irradiation.

Entry	Target DP	Reaction time (h)	Yield [a] (%)	M_n [b] (g·mol^{-1})	Đ	H-H [c] (%)
6	50	2	6	-	-	3.6
7	50	4	14	53000	1.65	3.7
8	50	6	19	48300	1.61	3.5
9	50	24	60	40300	1.47	3.5

[a] Determined from the weight of the isolated polymer. [b] Calculated by SEC in DMF with refractive index detection (calibrated with PMMA standards). [c] Determined by relative integration of the ^{19}F NMR resonances.

The ^{1}H NMR spectrum of the polymer recovered from entry 9 reveals all the expected resonance of PVDF according to the literature as shown in Figure 7, including all minor peaks that characterize the chain-end groups resulting from the chain transfer processes.[37]

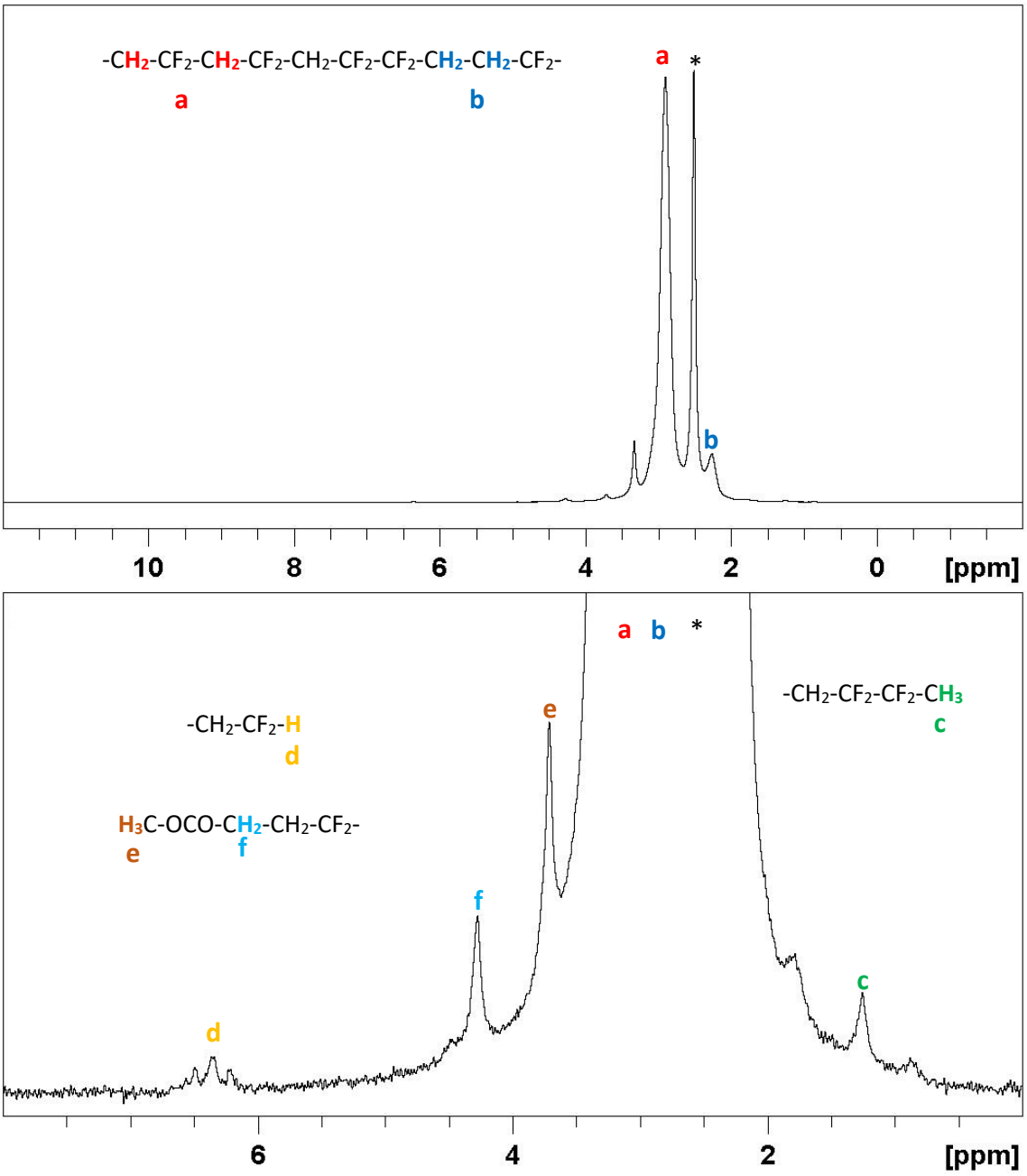

Figure 7. ^{1}H NMR spectrum (400 MHz, DMSO-d_6) of the PVDF isolated from entry 9 of Table 2. Full spectrum above and expansion of the 0 to 8 ppm region below. The starred resonances are due to the solvent.

The ^{19}F NMR spectrum of the same polymer (Figure 8) also exhibits all the characteristic resonances of PVDF, including those expected for the chain ends generated by the transfer process (*cf.* with Figure 3).[37] In this case, contrary to the PVDF obtained by thermal activation, the four unassigned signals at δ -150.66, -99.67, -98.98 and -85.68 are not visible, suggesting that a few side-reactions were produced in the VDF polymerization initiated thermally but not with visible light initiation. As in the

thermal activation, it is not possible to identified the expected CF_3 chain-end at δ -61.[40,41]

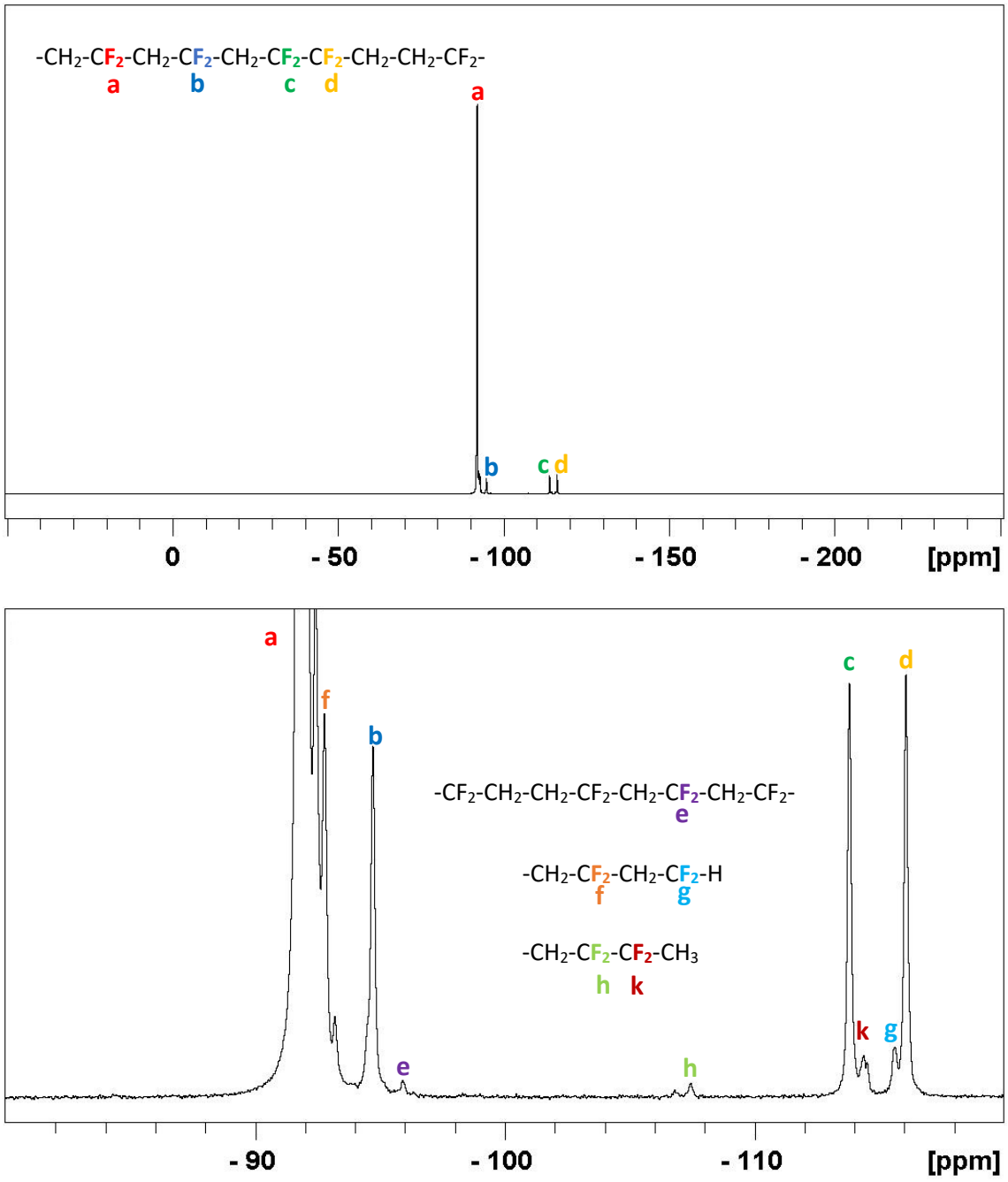

Figure 8. ^{19}F NMR spectrum of the PVDF isolated from entry 6 (376.5 MHz, DMSO-d_6). Full spectrum above and expansion of the -120 to -80 ppm region below.

Representation of the first-order kinetic plot confirms that the polymerization proceeds with an approximately constant radical concentration, since the data points are well-aligned (see Figure 9). The conversions were calculated following Equation 2 (see Section 5.2.2.1).

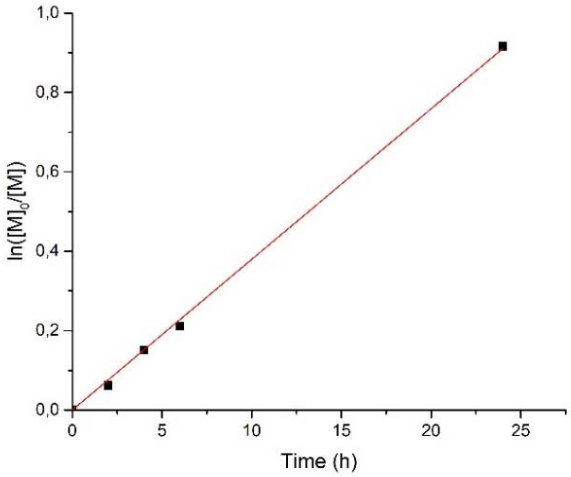

Figure 9. First-order kinetic plot for the polymerization of VDF initiated by visible light in presence of [Mn(CO)$_5$(CF$_3$)].

The size exclusion chromatograms represented in Figure 10 show the polymer mass evolution during the polymerization. The average molar mass decreases since the elution time of the polymer after 4 h (entry 7) is lower than that after 24 h (entry 9).

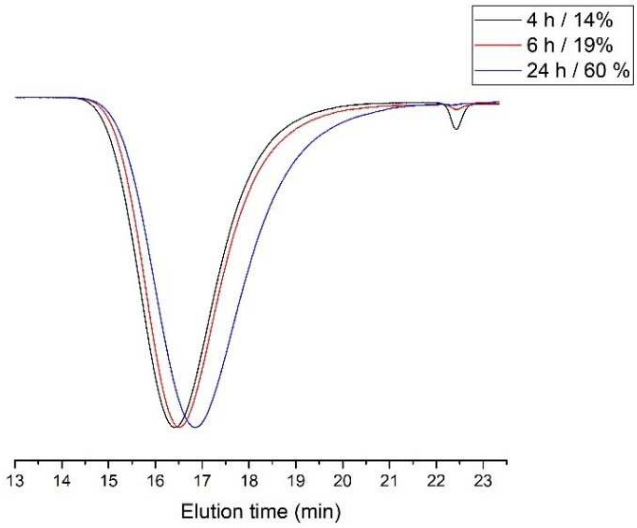

Figure 10. SEC traces of PVDF (entries 7, 8 and 9 of Table 2) in DMF.

The molar masses and dispersities of entries 7, 8 and 9 of Table 2 are represented in Figure 11. Molar masses decrease with conversion like a conventional radical polymerization. Nonetheless, the dispersity decreases. These results are probably due to experimental errors.

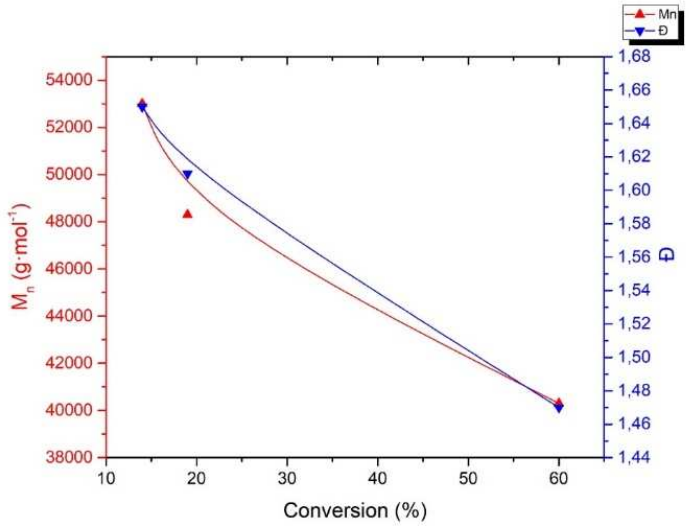

Figure 11. Plot of number average molar mass and dispersity vs conversion of VDF polymerization initiated by visible light in presence of $[Mn(CO)_5(CF_3)]$.

5.2.2.3. UV activation

The previous section has shown that visible light irradiation can activate compound **8** generating $F_3C^{\bullet}$. Therefore, UV irradiation should also produce the same effect since the UV irradiation is more energetic. However, differences may be expected on yield, molar mass and dispersity. Several polymerizations were carried out under a monochromatic UV radiation (300 nm). The temperature reached inside the UV chamber was 50 °C because of the heat released by the UV lamps. However, this temperature is insufficient to trigger the polymerization (entry 1 of Table 1) in the presence of compound **8**, while the reaction under UV irradiation led to PVDF in very high yields (74% after 24 h) as shown in Table 3. Like for the polymerizations activated by a thermal or a visible light photochemical stimulus, the percentage of head-to-head addition was as expected for a PVDF (3.4-3.9%).[35]

Table 3. Experemintal conditions and results of the polymerization of VDF in presence of $[Mn(CO)_5(CF_3)]$ initiated by UV irradiation (300 nm).

Entry	Target DP	Reaction time (h)	Yield [a] (%)	M_n [b] ($g \cdot mol^{-1}$)	Đ	H-H [c] (%)
10	50	2	9	11000	1.84	3.4
11	50	6	18	19200	1.76	3.7
12	50	24	74	26000	1.63	3.9

[a] Determined from the weight of the isolated polymer. [b] Calculated by SEC in DMF with refractive index detection (calibrated with PMMA standards). [c] Determined by relative integration of the ^{19}F NMR resonances.

The ^{1}H NMR spectrum exhibits the expected resonances of PVDF[37] as show in Figure 12. The assignment of these signals is shown on the spectrum. In this case, hydrogen transfer rate seems lower relative to the thermal and visible light activation (*cf.* with Figures 1 and 6). However, it is not possible to compare rigorously because no internal standard was used in the polymerizations.

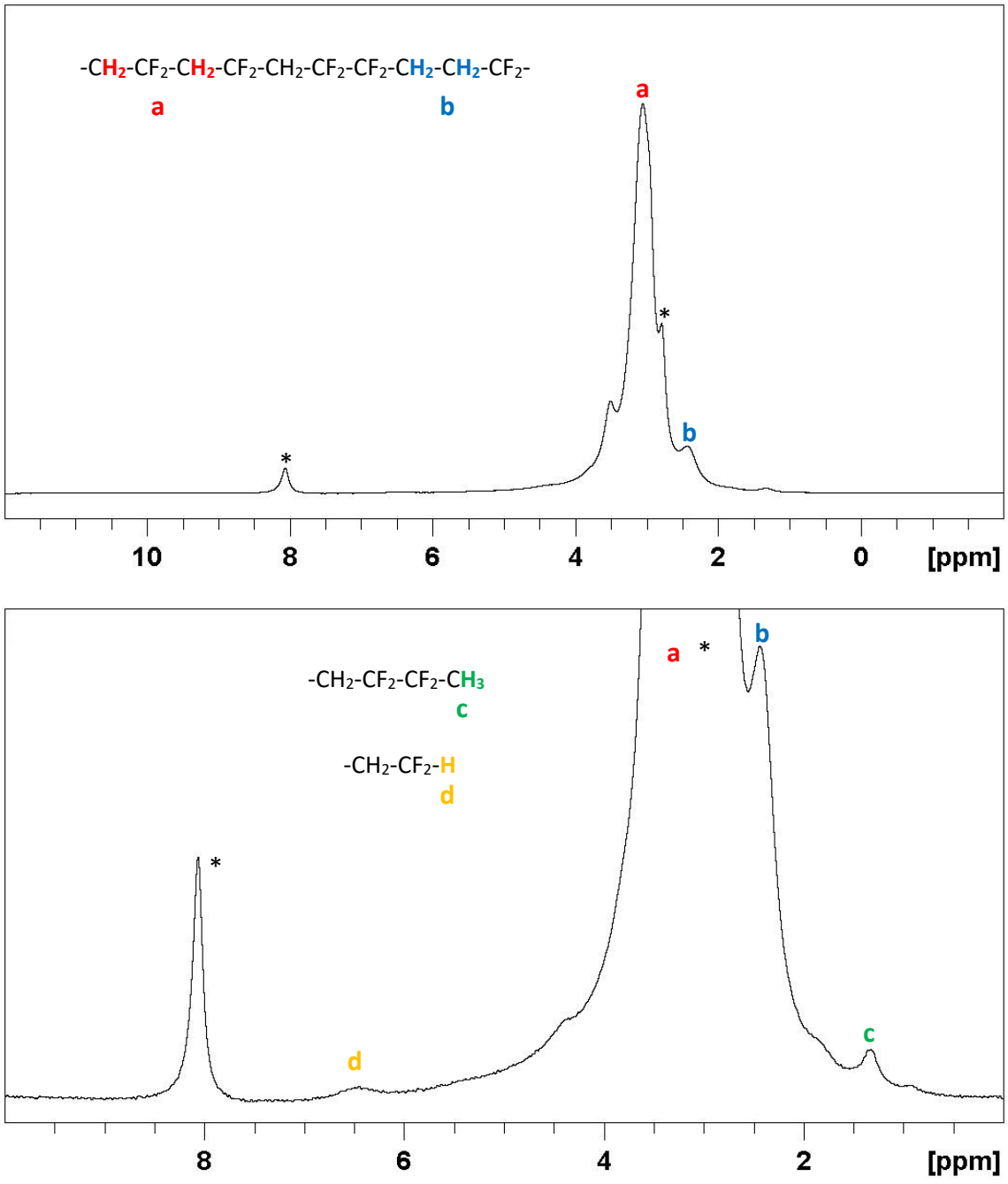

Figure 12. ^{1}H NMR spectrum (400 MHz, DMF-d_7) of the PVDF isolated from entry 12 of Table 3. Full spectrum above and expansion of the 0 to 10 ppm region below. The starred resonances are due to the solvent.

The ^{19}F NMR spectrum of entry 12 also displays the main resonances of PVDF.[37] The spectrum and the peaks attribution are presented in Figure 13. Despite the high molar mass, the presence of a small signal at δ -61.4 could be identified as the CF_3 of the chain-end as reported in the literature,[40,41] generated by the initiation of the $F_3C^{\bullet}$ radical. In addition, the unidentified resonance at δ -85.7 already observed in VDF polymerization with compound **8** initiated by thermal activation was also detected.

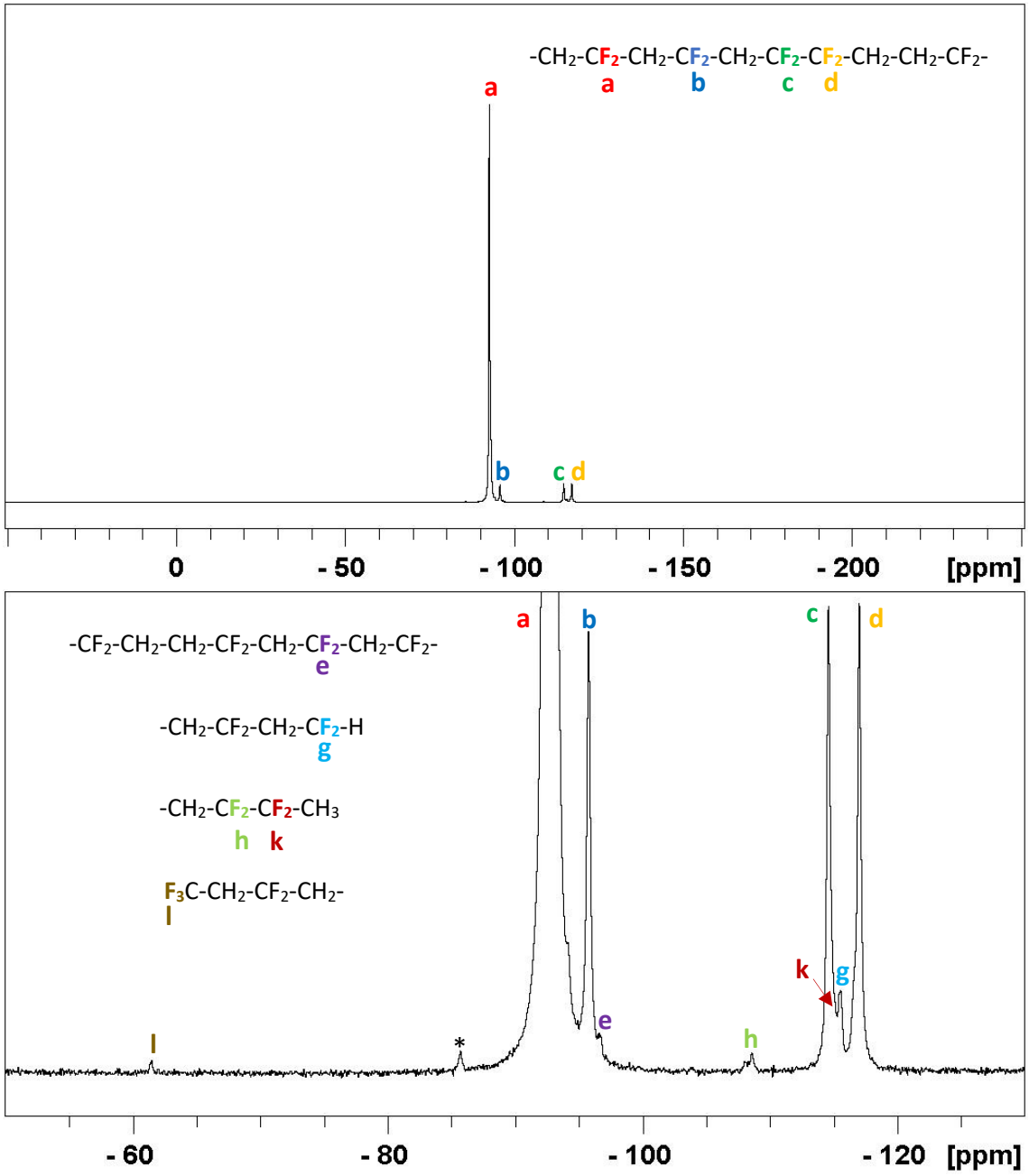

Figure 13. ^{19}F NMR spectrum (376.5 MHz, DMF-d_7) of the PVDF isolated from entry 12 of Table 3. Full spectrum above and expansion of the -120 to -80 ppm region below. The starred resonances could not be attributed to any expect signal of possible products.

The first-order kinetic plot represented in Figure 14 indicates that the polymerization occurs with a relatively constant radical concentration. Entry 11 has a conversion slightly lower than expected, maybe due to experimental errors since each point comes from a different Carius tube. The VDF concentrations were determined from the yields as shown previously in Equation 2 (Section 5.2.2.1).

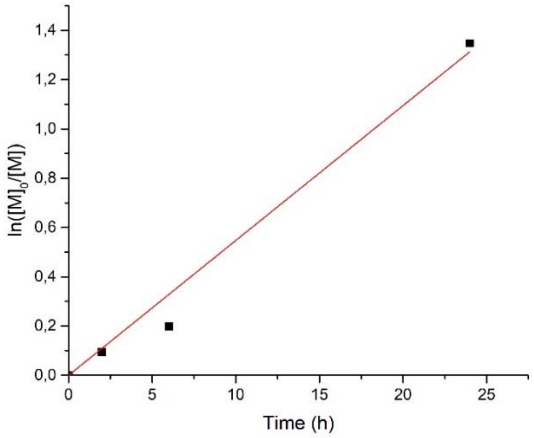

Figure 14. First-order kinetic plot for the polymerization of VDF initiated by UV irradiation (300 nm) in presence of [Mn(CO)$_5$(CF$_3$)].

The SEC traces of the crude polymers from entries 10 to 12 are represented in Figure 15. The number average molar mass increases during the reaction since at higher reaction times the polymer was perceived by refractive index detector at lower elution times.

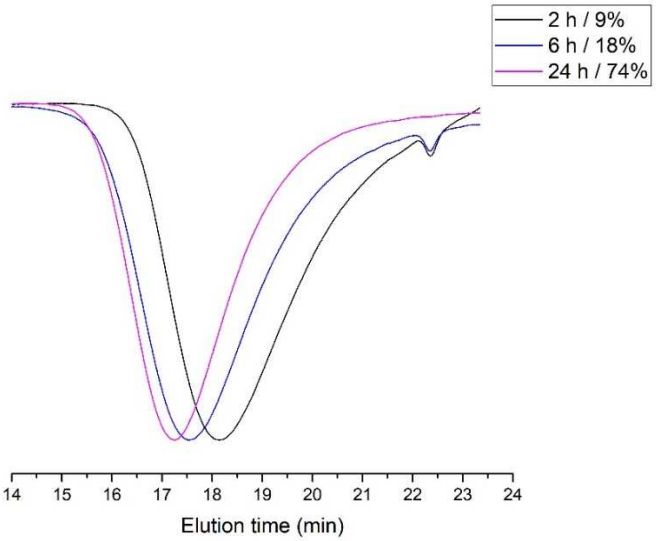

Figure 15. SEC traces of PVDF (entries 10 to 12 of Table 3) in DMF.

The graphical representation of the number average molar mass and dispersity versus conversion (Figure 16) clearly shows an increase of the molar mass and a decrease of dispersity during the polymerization. Both parameters evolve significantly at the beginning of the polymerization and then this evolution is less accentuated at the end. In addition, the initially present low molar mass population disappears gradually.

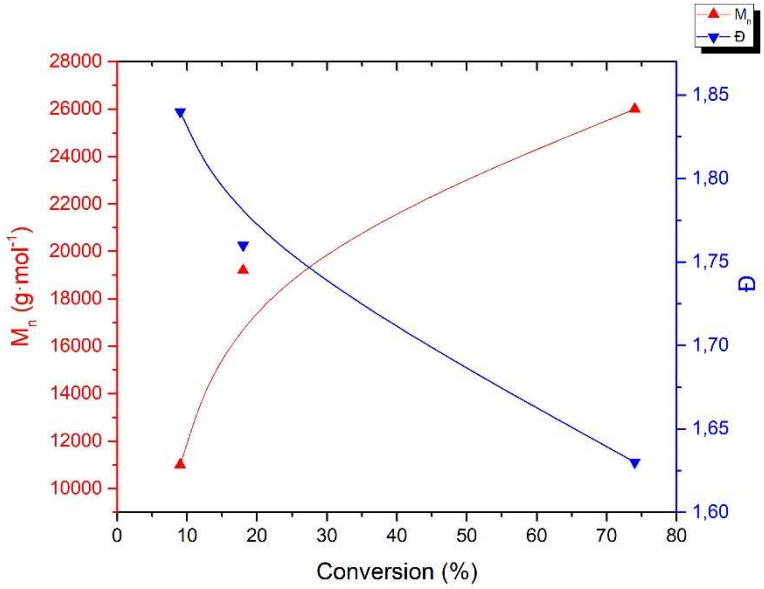

Figure 16. Plot of number average molar mass and dispersity vs conversion of VDF polymerization initiated by UV irradiation in presence of [Mn(CO)$_5$(CF$_3$)].

The observed trends in this polymerization are suggestive of a certain level control for an RDRP. However, the final polymer dispersity was relatively high the M_n is much higher than the expected value from the monomer/initiator ratio and the M_n growth and the dispersity drop were not linear, suggesting a certain control at least at the beginning of the polymerization.

Obtained solutions by different activations methods had different colors (Figure 17) after 24 h of reaction. Thermal activation led to a deep yellow solution, while the one activated by visible light led a cloudy white solution. Finally, activation by UV led to a very viscous, almost a solid, brown solution.

Figure 17. Carius tubes containing PVDF after 24 h of polymerization activated thermally (left), with visible light (center) and UV irradiation (right).

The SEC analyses of different activation methods (entries 5, 9 and 12 h, thermal, visible light and UV activation respectively after 24 h of polymerization) are represented in Figure 18. They reveal monomodal and relatively narrow molar mass distributions, since PVDF made under the same conditions by free radical polymerization typically show Đ > 2.1.[33] The highest molar mass product was obtained from the visible light activation experiment and the lowest one from the thermal activation experiment.

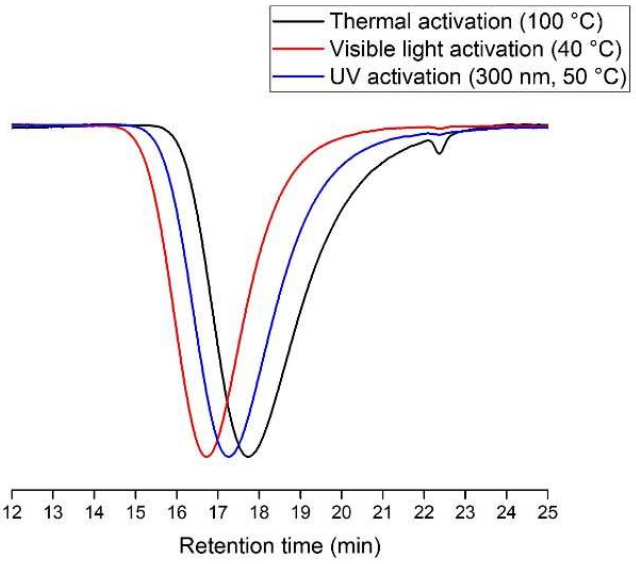

Figure 18. SEC traces of PVDF (entries 5, 9 and 12 of Table 1, 2 and 3 respectively) in DMF after 24 h of reaction by various initiation methods.

The high molar masses relative to the calculated values for an ideal controlled process show low initiator efficiencies (0.19, 0.08 and 0.13 for the thermal, visible and UV methods, respectively), indicating that the thermal activation method is the most efficient one. The initiator efficiencies were calculated with the following equation:

$$Initiator\ efficiency = \frac{M_{n,th}}{M_{n,exp}} \qquad \text{(Equation 3)}$$

5.2.3. VDF/[Mn(CO)$_5$(CHF$_2$)]

Compound **9** has a weaker Mn-C bond than compound **8** and even weaker than compound **10**, as confirmed by both the experimentally determined and the calculated BDEs, as shown in the previous chapter. Thus, the radical generation should require less energy compared to compound **8**. Therefore, 80 °C was chosen as the reaction temperature to initiate the polymerization by the thermal activation mode ($t_{½}$ ≈ 46 min and $t_{99\%}$ ≈ 5h in C_6D_6).

Table 4. Reaction conditions and yields obtained in the VDF polymerization initiated by compound **9**.

Entry	Activation method	Target DP	Time (h)	Yield [a] (%)
1	Thermal (80 °C)	50	24	0
2	hv (visible light)	50	24	2
3	hv (UV 300 nm)	50	24	5

[a] Determined from the weight of the isolated polymer.

The polymerization with thermal activation at 80 °C for 24 h (entry 1 in Table 4) led to a small amount of a brown-yellowish powder. However, this material does not contain any PVDF because no resonances were found in the ^{19}F NMR spectrum. These results may be explained by the nature of the solvent which affects the radical generation rate (BDE determination was achieved in C_6D_6 while polymerization was performed in DMC). Probably in the case of DMC the radical generation from **9** is slower.

For entries 2 and 3 there was indeed some PVDF formation, although only in very low yields, much lower than for compound **8** under the same conditions. The ^{19}F NMR spectra of the polymers recovered from entries 2 and 3 (Figure 19 and 20 respectively) clearly show the formation of PVDF.[37] Nevertheless, the residual compound **9** shows a much more intense resonance than the PVDF head-to-tail signal, indicating that the cleavage of the Mn-CHF_2 bond is very slow under visible light, contrary to the cleavage of the Mn-CF_3 bond in compound **8**. This behavior is completely unexpected because the Mn-CF_3 bond is much stronger than the Mn-CHF_2 bond. Additionally, a relatively intense resonance at δ -114.4 was attributed to the CHF_2 chain-end from the initiator or transfer from DMC onto PVDF macroradical. Relative integration of this signal in Figure 19 and of the main PVDF resonance indicates that the obtained product is in fact an oligomer with 8-9 monomers. Two more resonances were detected at δ -75.9 and -74.7. Despite their low intensities, they seem to be two AB systems. They may be attributed to a PVDF-$CH=CF_2$ chain-end (both fluorine atoms are non-equivalent), as previously reported in the literature,[45] probably formed by a β-H elimination from the PVDF-CH_2-CF_2-$Mn(CO)_5$ dormant chain (see Scheme 3). However, strangely this product was only observed in with these conditions. The polymer obtained by photochemical activation with UV irradiation, on the other hand, exhibits only a very small resonances from compound **9**, as expected because UV is a more energetic electromagnetic radiation compared to visible light. In this case, the formation of PVDF-$CH=CF_2$ was not observed, but a relatively intense signal from the CHF_2 chain-end was detected. The relative integration reveals that the DP is 6-7 in this case, even lower than that obtained with visible light activation.

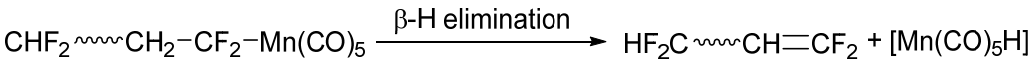

Scheme 3. Proposed reaction for the formation of PVDF-$CH=CF_2$ by β-H elimination.

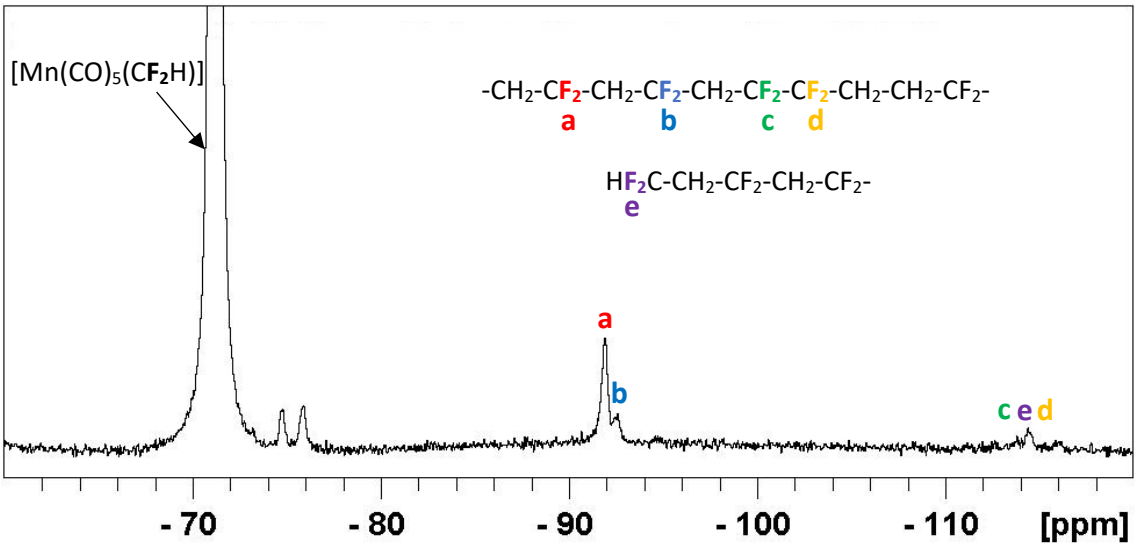

Figure 19. ^{19}F NMR spectrum (376.5 MHz, DMSO-d_6) of the crude polymer recovered from entry 2 of Table 4.

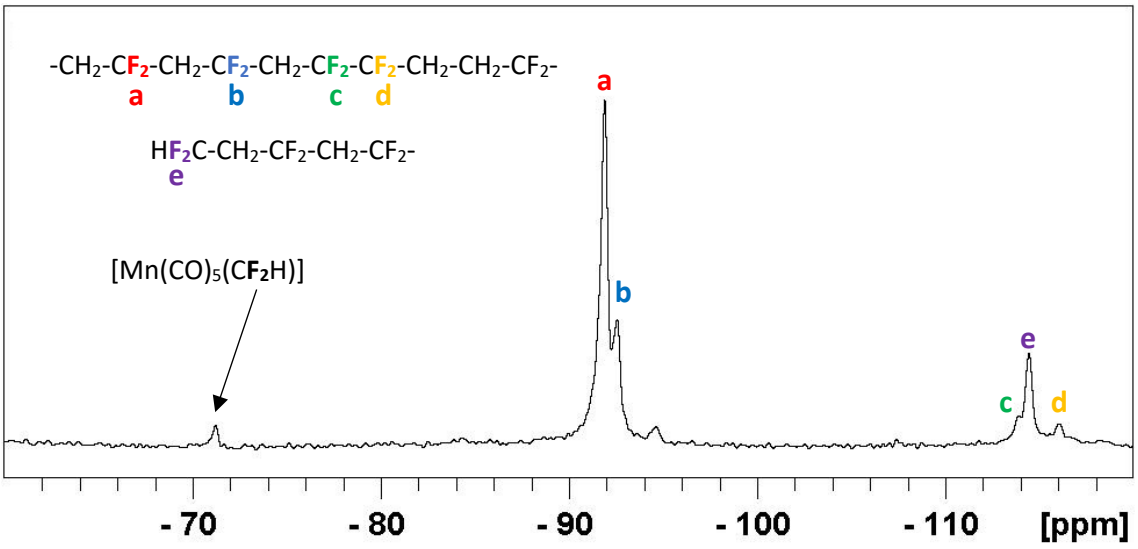

Figure 20. ^{19}F NMR spectrum (376.5 MHz, DMSO-d_6) of the crude polymer recovered from entry 3 of Table 4.

5.2.4. VDF/[Mn(CO)$_5$(CH$_2$CF$_3$)]

Three polymerizations were performed with thermal activation using compound **10** as initiator. The experimental studies described in Chapter 4 and the computational work indicate that this complex has a higher Mn-R_F BDE than compound **9** but lower than compound **8**. Hence, two reactions were carried out at 90 °C ($t_{½}$ ≈ 22 min and $t_{99\%}$ ≈ 2.4 h in C_6D_6) with different DP, and one at 100 °C. The experimental conditions and

the analytical data for the polymers recovered by precipitation in cold *n*-pentane are shown in Table 5.

Table 5. Experemintal conditions and results of the polymerization of VDF in presence of [Mn(CO)$_5$(CH$_2$CF$_3$)] initiated thermally (100 °C).

Entry	Target DP	Temperature (°C)	Reaction time (h)	Yield [a] (%)	M_n [b] (g·mol^{-1})	Đ	H-H [c] (%)
1	50	90	24	2	32200	1.11	3.5
2	100	90	24	3	32200	1.16	4.0
3	100	100	24	3	31600	1.15	4.2

[a] Determined from the weight of obtained polymer. [b] Calculated by SEC in DMF by refractive index (calibrated with PMMA standards). [c] Determined by relative integration of ^{19}F NMR spectrum.

In all experiments carried out with compound **10**, the reaction yields are surprisingly low (2-3%). Apparently, the target DP does not affect to the molar mass of the final polymer (entries 1 and 2). Indeed, the measured M_n values are equal in both cases and the dispersities are also quite similar. These values are also very close to those of the polymer obtained in entry 3. The ^{1}H and ^{19}F NMR spectrum (Figure 21 and 22 respectively) of the latter sample (Table 5, entry 3) shows the main resonances of PVDF as reported in the literature.[37]

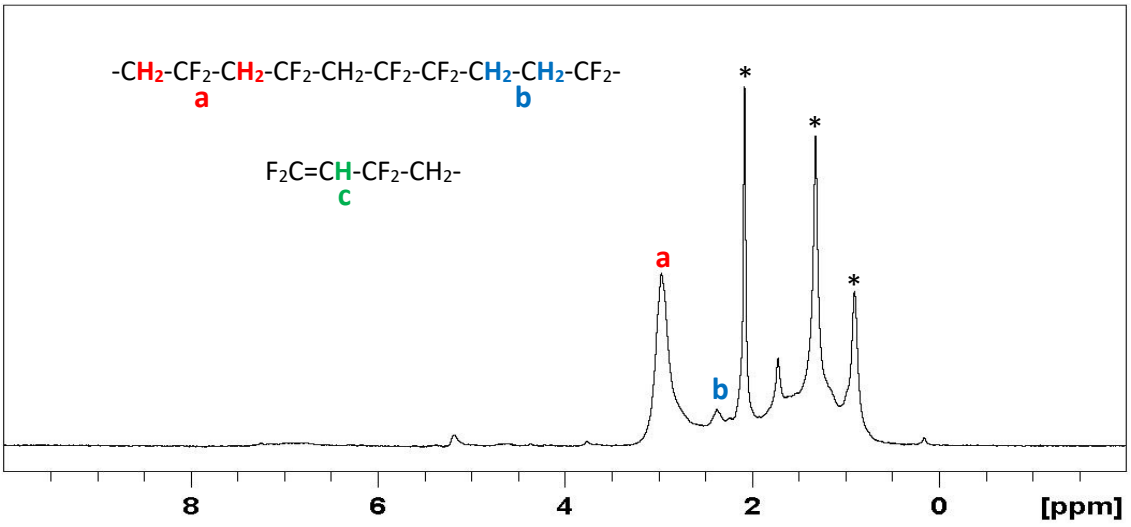

Figure 21. ^{1}H NMR spectrum (400 MHz, acetone-d_6) of the precipitated polymer isolated from entry 3 of Table 5. The starred resonance is due to the deuterated solvent and precipitation solvent (*n*-pentane).

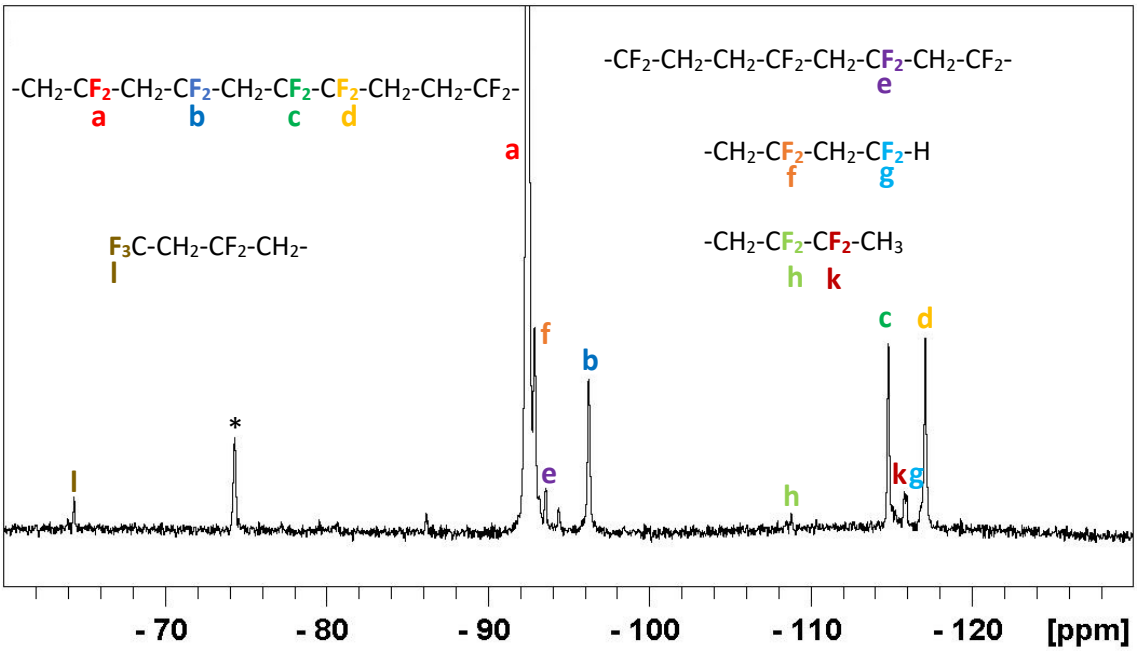

Figure 22. ^{19}F NMR spectrum (376.5 MHz, acetone-d_6) of the precipitated polymer isolated from entry 3 of Table 5. The starred resonances could not be attributed to any expect signal of possible products.

5.2.5. VDF/[Mn(CO)$_5$(COCF$_2$CH$_3$)]

As mentioned in Chapter 3, compound **11** could not be obtained in sufficient quantities and in a sufficiently pure state to use it as initiator in polymerization. Nevertheless, the synthesis of corresponding acyl complex (compound **7**) was achieved successfully. Therefore, polymerization of VDF were carry out with this complex, supposing that it should be decarbonyled *in-situ* under the conditions employed during the polymerization, followed by the Mn-C homolytic cleavage. Another possibility is the generation of the H$_3$C-CF$_2$-CO$^\bullet$ radical. However, the decarbonylation process should be favored.

5.2.5.1. Thermal activation

The calculated BDE for compound **11** is the lowest one among all fluoroalkylpentacarbonylmanganese(I) complexes synthesized in this work (46.0 kcal·mol^{-1}),[26] hence 80 °C should be sufficient for its thermal activation. In addition, this temperature is also sufficient to promote the decarbonylation of this complex as shown

in Chapter 3. The experimental conditions used and the results of the polymerizations are presented in Table 6.

Table 6. Experimental conditions and results of the polymerization of VDF in the presence of [Mn(CO)$_5$(COCF$_2$CH$_3$)] by thermal activation (80 °C).

Entry	Target DP	Temperature (°C)	Reaction time (h)	Yield [a] (%)	M_n [b] (g·mol^{-1})	Đ	H-H [c] (%)
1	50	80	4	1	-	-	-
2	50	80	8	1	-	-	-
3	50	80	12	2	-	-	-
4	50	80	24	7	16200	1.38	3.5

[a] Determined from the weight of obtained polymer. [b] Calculated by SEC in DMF with refractive index detection (calibrated with PMMA standards). [c] Determined by relative integration of the ^{19}F NMR spectrum.

The reaction yields are very low, even after 24 h, reaching only 7% in entry 4. Because of the low amount of polymer obtained in entries 1 to 3, a SEC analysis could not be performed for these samples. Despite the low conversion, the dispersity of the polymer obtained after 24 h of reaction at 80 °C (entry 4) is relatively low. ^{1}H NMR spectrum shows very broad peaks and it was not possible to identify any signal, maybe due to the presence of a manganese paramagnetic specie. ^{19}F NMR spectrum displays the characteristic resonances of PVDF[37] (Figure 23). However, two additional resonances from unidentified products are present at δ -148.2 and 136.0.

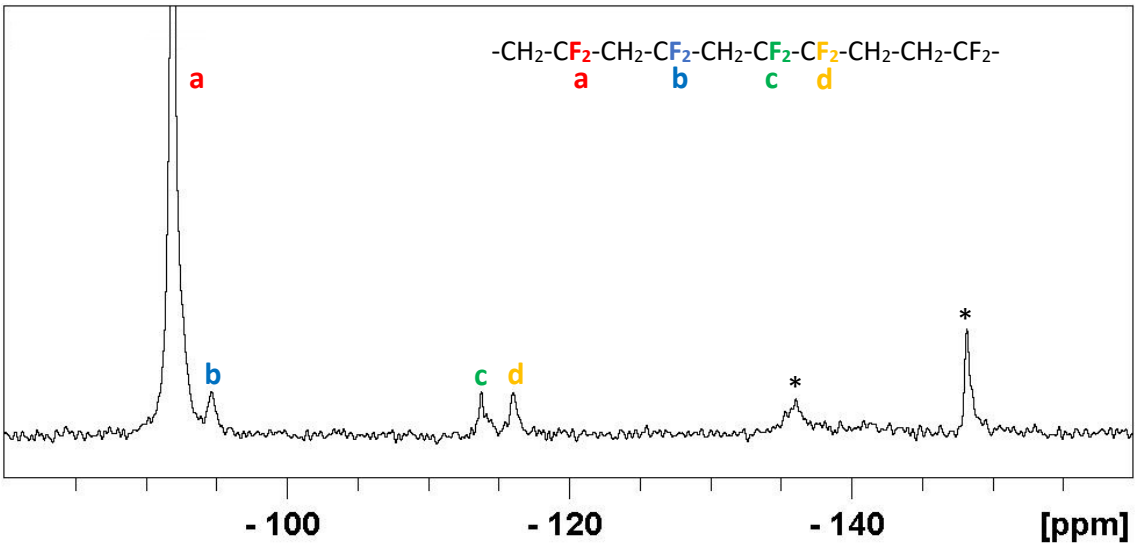

Figure 23. ^{19}F NMR spectrum (376.5 MHz, DMSO-d$_6$) of the polymer isolated from entry 4. The starred resonances could not be attributed to any expect signal of possible products.

The first-order kinetic plot of entries 1 to 4 is shown in Figure 24. Due to the low conversion and the number of data points, it is not possible to conclude with confidence about the kinetic behavior of this reaction.

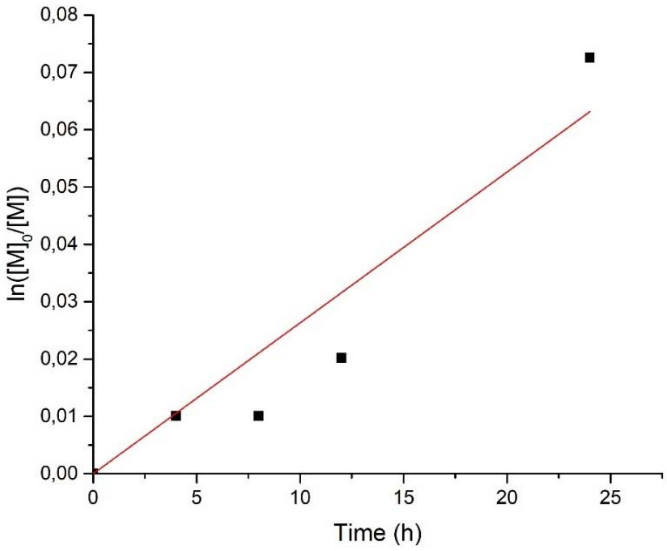

Figure 24. First-order kinetic plot for the polymerization of VDF initiated by thermal activation (80 °C) in presence of [Mn(CO)$_5$(COCF$_2$CH$_3$)].

5.2.5.2. Visible light activation

Compound **7** was also tested as initiator of VDF polymerization under visible light. The experimental conditions and the polymerization results are shown in Table 7. Surprisingly, the initiation by visible light works much better than the thermal initiation at 80 °C, reaching a 24% yield after 24 h (entry 8). Like for the polymerizations with all other tested complexes, the H-H percentage is as expected for a VDF polymerization.[35] The first-order kinetic plot (Figure 25) shows that all the data points are quite well aligned, suggesting that the radical concentration is approximately constant throughout the reaction. On the other hand, the molar mass increases at the beginning of the reaction (between entries 5 and 6), while the dispersity decreases slightly (Figure 27). Subsequently, both parameters remain constant and finally they show the opposite trend (Figure 26 and 27). However, small differences of molar masses and dipersities and the experimental and analytical errors do not allow to conclude clearly the trend of this parameters.

Table 7. Experimental conditions and results of the polymerization of VDF in the presence of [Mn(CO)$_5$(COCF$_2$CH$_3$)] initiated by visible light irradiation.

Entry	Target DP	Reaction time (h)	Yield [a] (%)	M_n [b] (g·mol^{-1})	Đ	H-H [c] (%)
5	50	4	3	12600	1.48	3.6
6	50	8	8	22500	1.44	3.7
7	50	12	13	24000	1.40	3.4
8	50	24	23	23000	1.45	3.6

[a] Determined from the weight of the isolated polymer. [b] Calculated by SEC in DMF with refractive index detection (calibrated with PMMA standards). [c] Determined by relative integration of the ^{19}F NMR spectrum.

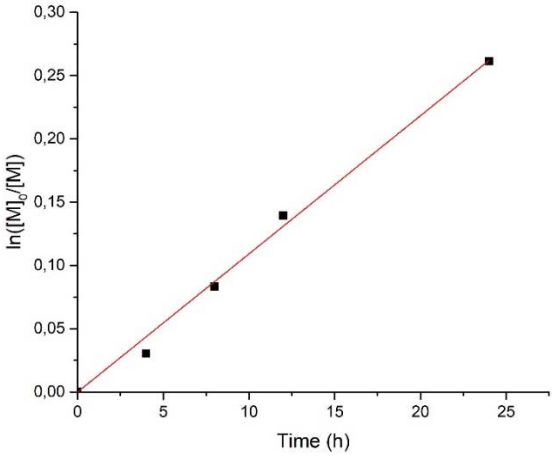

Figure 25. First-order kinetic plot for the polymerization of VDF in presence of [Mn(CO)$_5$(COCF$_2$CH$_3$)] initiated by thermal activation (100 °C) .

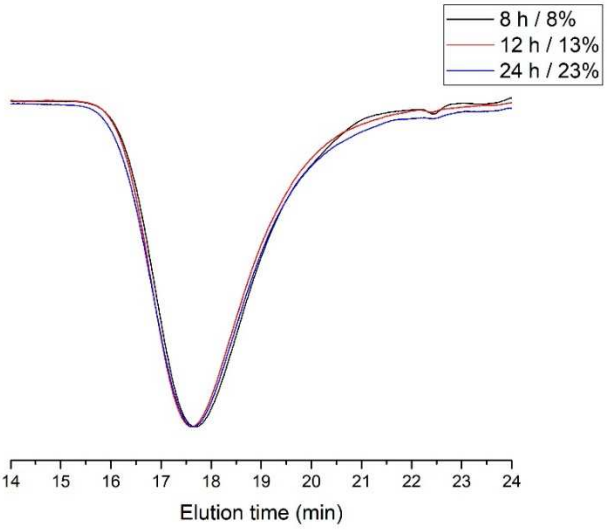

Figure 26. SEC traces of PVDF (entries 6, 7 and 8 of Table 7) in DMF.

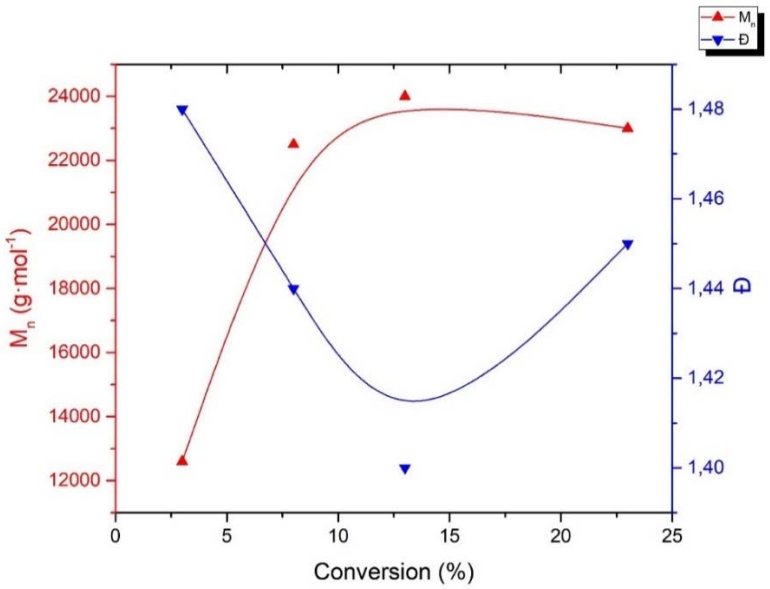

Figure 27. Number average molar mass and dispersity vs conversion of polymerization of VDF with complex **7** initiated photochemically (visible light).

5.2.5.3. UV activation

Four additional polymerizations of VDF were performed using compound **7** as initiator under UV irradiation (300 nm). Each reaction was stopped at a different time and the resulting polymers were analyzed (see Table 8). The yields are rather similar to those of the visible light activation. However, in this case the molar masses are lower than for any other VDF polymerization, except for compound **9** where only oligomers were obtained.

The first-order kinetic plot (Figure 28) indicates that in this case the polymerization rate slows down more than expected for a first-order reaction. The expected process is Mn-CF_2CH_3 bond cleavage just after the *in-situ* decarbonylation of compound **7**. However, the high energy of the UV irradiation may produce a side-reaction leading to the decomposition of compound **7** or **11** by another pathway that does not involve homolytic Mn-R_F bond cleavage.

Table 8. Experimental conditions and results of the VDF polymerization in the presence of $[Mn(CO)_5(COCF_2CH_3)]$ initiated by UV irradiation (300 nm).

Entry	Target DP	Reaction time (h)	Yield [a] (%)	M_n [b] ($g \cdot mol^{-1}$)	Đ	H-H [c] (%)
9	50	4	16	11100	1.57	3.6
10	50	8	18	10000	1.69	3.7
11	50	12	20	9500	1.81	3.4
12	50	24	21	7000	1.94	3.6

[a] Determined from the weight of isolated polymer. [b] Calculated by SEC in DMF with refractive index detection (calibrated with PMMA standards). [c] Determined by integration of the ^{19}F NMR spectrum.

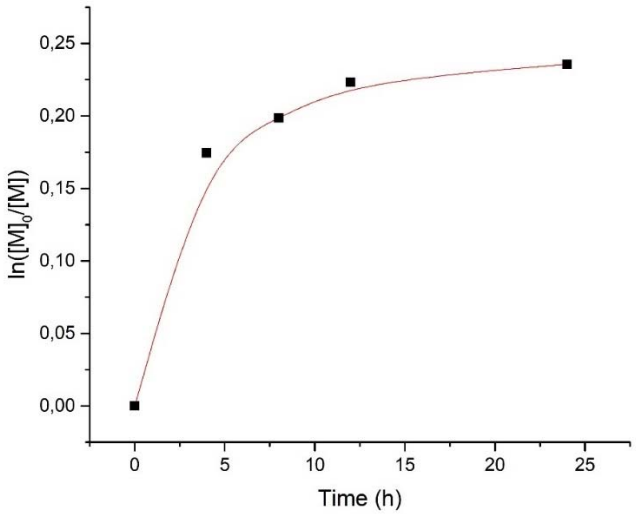

Figure 28. First-order kinetic plot for the polymerization of VDF in presence of $[Mn(CO)_5(COCF_2CH_3)]$ initiated by UV irradiation.

The size exclusion chromatograms of the recovered PVDF samples from entries 9 to 12 (Figure 29) shows a molar mass reduction along the reaction. In addition, the dispersity increased. Moreover, a second population with low molar masses increase along the reaction. This second population probably derives from the low molar mass oligomers. The trends of the number average molar mass and dispersity versus conversion (Figure 30) exhibits clearly that the behavior does not correspond to an RDRP, but rather a conventional radical polymerization.

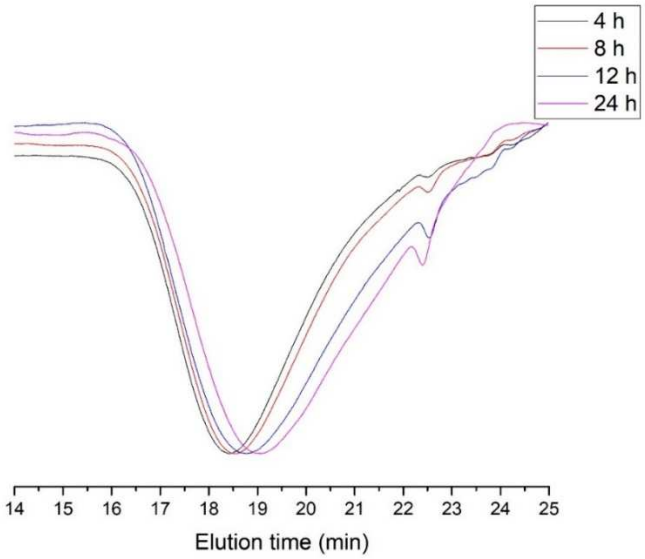

Figure 29. SEC traces of PVDF (entries 9, 10, 11 and 12 of Table 8) in DMF.

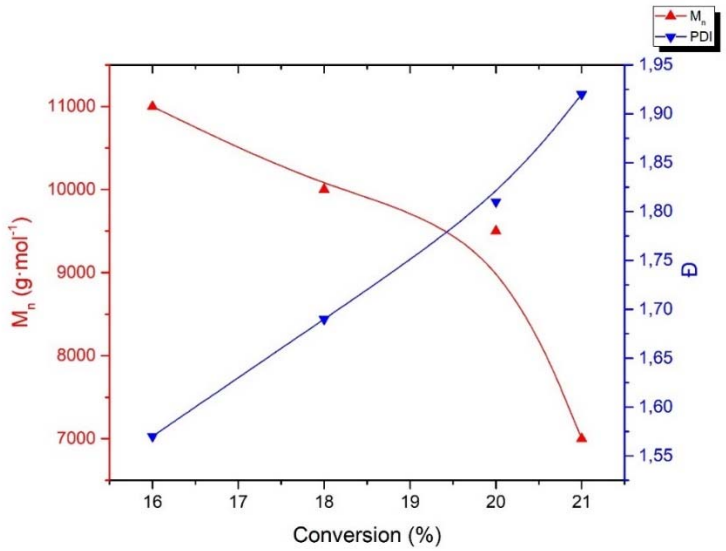

Figure 30. Number average molar mass and dispersity vs conversion for the VDF polymerization with complex **7** initiated photochemically (UV irradiation).

5.2.6. Thermal properties of PVDF synthesized by different activation methods

The thermal properties of a few PVDF samples obtained with $[Mn(CO)_5(CF_3)]$ and $[Mn(CO)_5(COCF_2CH_3)]$ and initiated by thermal or photochemical methods after 24 h of reaction were analyzed by thermogravimetric analysis (TGA) and by differential scanning

calorimetry (DSC). TGA allowed determining the loss of mass as a function of the temperature, showing the thermal stability of the polymer. Figure 31 shows the TGA analyses of five PVDF samples and Table 9 summarizes the results.

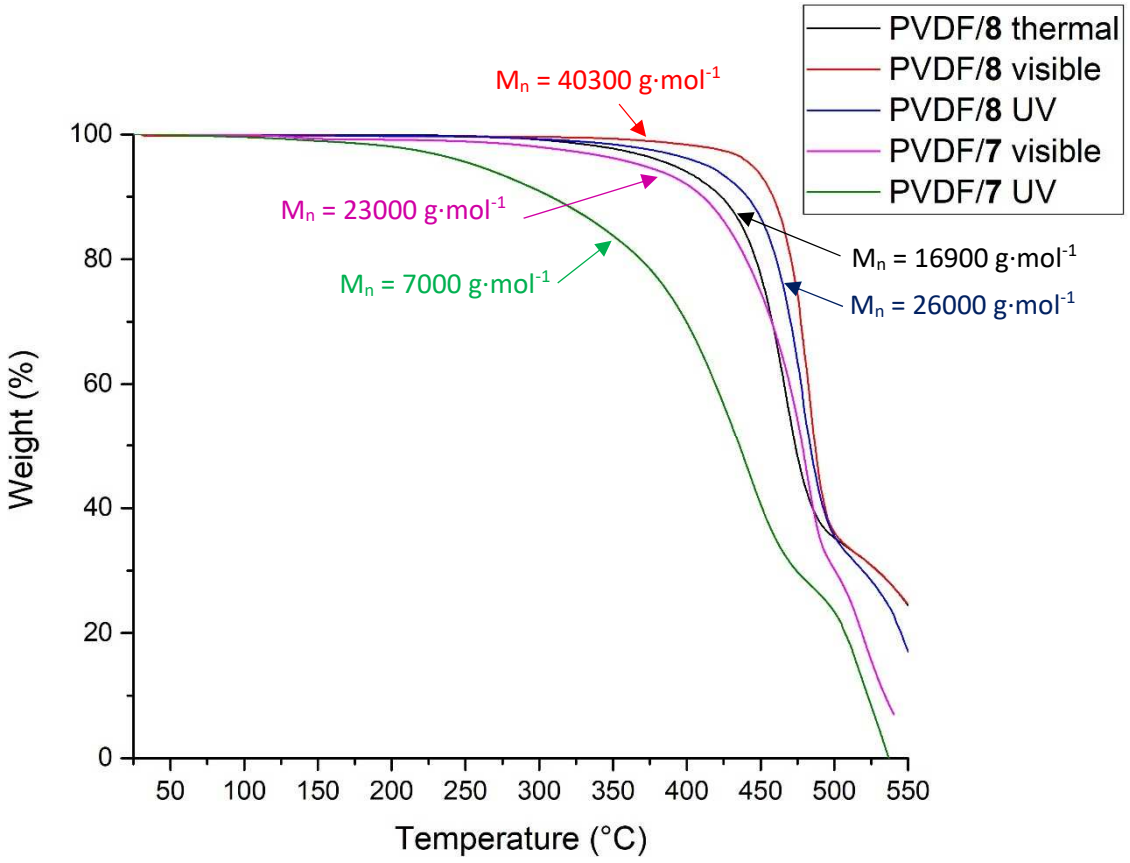

Figure 31. Thermograms of PVDF synthesized with compounds **7** and **8** after 24 h of reaction and initiated by different activation methods.

Table 9. Temperatures of decomposition of PVDF samples (98, 95 and 90%).

Complex	Activation method	M_n (g·mol^{-1})	$T_{98\%}$	$T_{95\%}$	$T_{90\%}$
8	Thermal (100 °C)	16900	343	391	424
8	Visible light	40300	412	444	459
8	UV (300 nm)	26000	364	414	441
7	Visible	23000	295	370	406
7	UV (300 nm)	7000	199	259	308

The decomposition temperature is higher for the higher molar masses, and it decreases for the lower molar masses as expected. For instance, the polymer for which the temperature corresponding to a 2% mass loss is the highest (412°C) is the one synthesized with compound **8** with visible light, while the one for which this temperature is the lowest (199 °C) is the one obtained with compound **7** by UV irradiation.

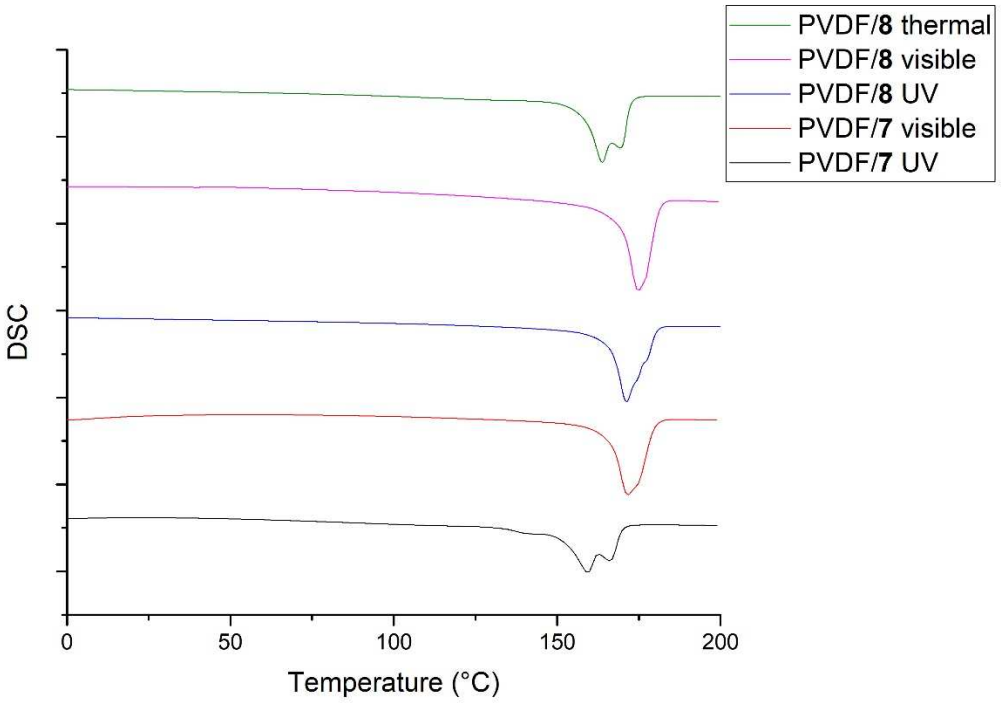

Figure 32. DSC thermograms of PVDF synthesized with different activation methods and initiators.

Table 10. Molar masses and thermal characteristics of PVDF obtained by polymerization of VDF in the presence of complexes 7 and 8 from different activation methods.

Complex	Activation method	M_n (g·mol^{-1})	Melting point (°C)	Enthalpy of fusion (J·g^{-1})	Degree of crystallinity (%)
8	Thermal (100 °C)	16900	164	-46.1	44
8	Visible light	40300	175	-55.3	53
8	UV (300 nm)	26000	171	-45.9	44
7	Visible	23000	172	-52.4	50
7	UV (300 nm)	7000	159	-45.8	44

As expected, the melting point of PVDF is higher for the higher molar masses (reaching 175 °C in good agreement with the literature).[46] In addition, the degree of crystallinity is similar for the PVDF synthesized by thermal or UV activation whatever the nature of the complex. However, is rather higher for the visible activation, reaching a 50-53%.

5.3. VAc/MAF-TBE copolymerization with [Mn(CO)$_5$R$_F$]

Four copolymerizations of VAc and MAF-TBE were carried out using compounds **5** and **10** as initiators (Scheme 4). This copolymer is already known, previously synthesized by OMRP using cobalt(II) acetylacetonate as controlling agent.[24] A perfectly alternating structure was demonstrated, in agreement to the measured reactivity ratios that are both essentially equal to zero.[47]

The remarkable properties of fluorinated homopolymers have already been described in this work, however alternating copolymers were not mentioned. They have been reported as a valuable tool to build copolymer with some degree of sequence control.[48] In addition, MAF and MAF-esters containing fluorinated copolymers are used for many applications such as electrolyte membranes for fuel cells and for Li-ion batteries. Nevertheless, the homopolymerization of MAF and MAF-esters, including MAF-TBE, can only be produced anionically since these monomers do not homopolymerize under radical conditions because of their strong electron acceptor character and the bulkiness of the CF_3 and COO-^{t}Bu groups.[49-51] However, hey can be copolymerized together with electron-donating monomers such as vinyl acetate[51] or vinyl ethers.

The aim of this study was to check the initiation capacity of the complexes which do not efficiently initiate the VDF polymerization, such as compound **9** and **10**, with more reactive monomers. However, in order to check the ability to generate radicals by

other acyl derivatives than compound **7**, complex **5** was also chosen instead of compound **9**.

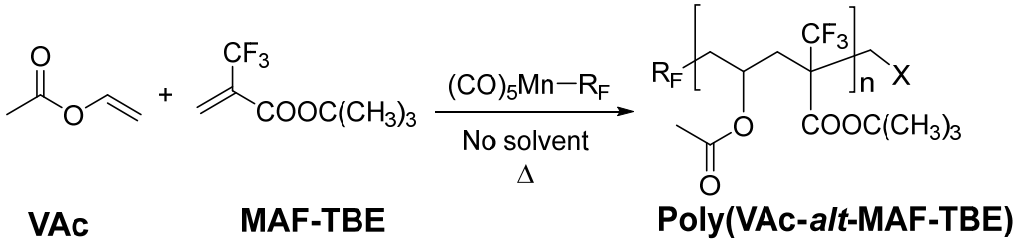

Scheme 4. Alternating copolymerization of VAc and MAF-TBE initiated by $[Mn(CO)_5R_F]$ complexes.

Table 11. Experimental conditions and results of the copolymerization of VAc and MAF-TBE.

Entry	$-R_F$	Temperature (°C)	Reaction time (h)	Yield (%)	M_n (g·mol^{-1})	Đ	Mn/VAc/MAF ratio
1	$-CO-CHF_2$	70	72	17	58300	1.53	1:50:50
2	$-CO-CHF_2$	85	3	38	41300	1.43	1:50:50
3	$-CH_2-CF_3$	70	72	21	7000	1.69	1:50:50
4	$-CH_2-CF_3$	80	18	83	76000	2.12	1:50:50

The VAc/MAF-TBE copolymerization initiated by compounds **5** and **10** led to the production of the copolymer in high yields (Table 11), proving that these compounds can indeed initiate a radical polymerization, indirectly suggesting that the low yields observed in the case of VDF are related to the low reactivity of the generated radicals (except $F_3C^{\bullet}$) with this monomer.

The ^1H and ^{19}F NMR spectra (Figures 33 and 34) of the isolated polymer show clearly the formation of VAc-*alt*-MAF-TBE. The perfect alternation is proved since the only monomer which can homopolymerize is the VAc, and no ^1H NMR signal at δ 4.9 (the typical chemical shift of VAc-VAc dyads) was observed.

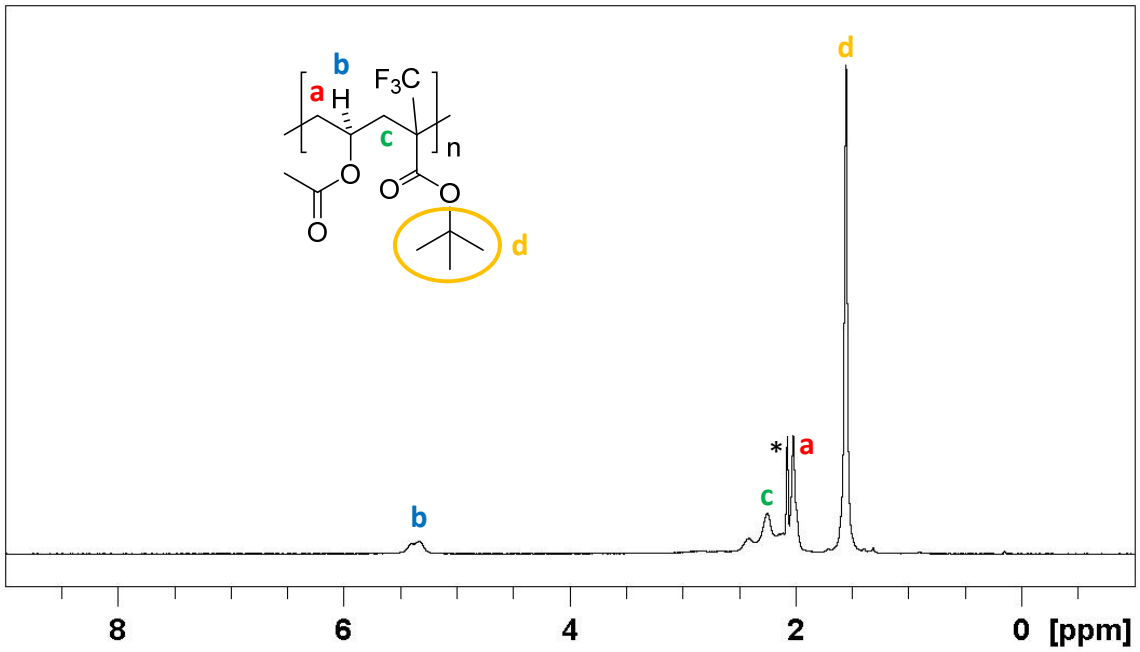

Figure 33. ^{1}H NMR spectrum (400 MHz, acetone-d_6) of the polymer isolated from entry 4 of Table 11. The starred resonance is due to the solvent.

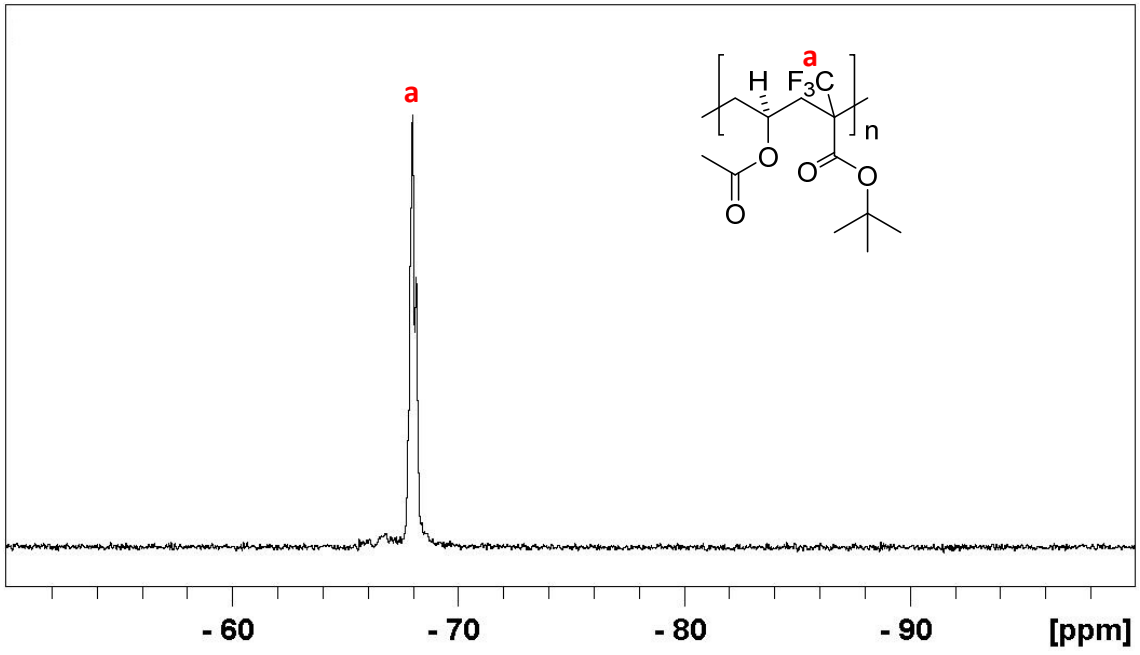

Figure 34. ^{19}F NMR spectrum (376.5 MHz, acetone-d_6) of the polymer isolated from entry 4 of Table 11.

5.4. Polymerization of methyl acrylate with [Mn(CO)$_5$(CH(CH$_3$)(COOCH$_3$))]

Initial polymerization tests of methyl acrylate (MA) using compound **1** as initiator were performed in bulk because compound **1** is perfectly soluble in MA. Three polymerizations were carried out at different temperatures (70, 50 and 30 °C) and different target DP (70, 30 and 20 respectively). However, these polymerization tests led to a very viscous solution and even to a solid after a short time (0.5-1 h), suggesting the formation of very high molar mass macromolecules and making it impossible to perform a detailed kinetic study.

Thus, subsequent polymerizations were performed in dilute solutions. C_6D_6 was chosen as a suitable solvent for this polymerization, since the monomer, the polymer and the complex are soluble in this solvent. In addition, no hydrogen transfer is possible from benzene because of the strength of the C-H (or in this case C-D) bond.

A kinetic study was carried out for the polymerization of methyl acrylate (MA) initiated by compound **1** in C_6D_6 and using 1,3,5-trioxane as internal standard (Scheme 5).

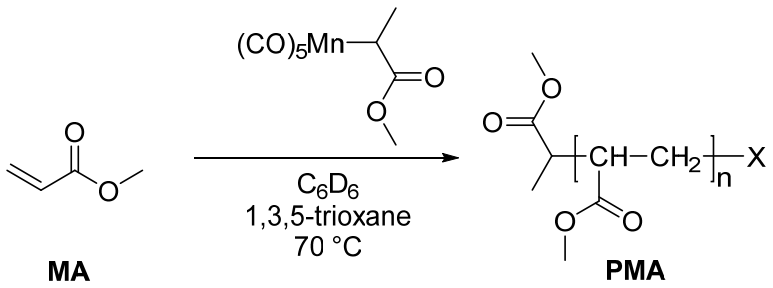

Scheme 5. Homopolymerization of methyl acrylate initiated by compound **1**.

A sample of the crude reaction mixture was taken each hour for the first 8 h. Then, two more samples were taken after 22 and 24 hours. All samples were analyzed by ^{1}H NMR and by SEC and the corresponding results are reported in Table 12. A polymer with very high molar mass was obtained after 1 h. However, the molar mass drops along the reaction while the dispersity raised.

Table 12. Experimental conditions and results of the MA polymerization in the presence of [Mn(CO)$_5$(CH(CH$_3$)(COOCH$_3$))] at 70 °C.

Entry	Reaction time (h)	Conversion [a] (%)	Yield [b] (%)	M_n [c] (g·mol^{-1})	Đ
1	1	2	7	210000	1.70
2	2	6	11	173000	1.80
3	3	9	12	172500	1.73
4	4	10	13	152500	1.98
5	5	12	13	148500	2.05
6	6	14	13	114000	2.57
7	7	15	14	99500	2.68
8	8	16	14	89000	2.97
9	22	18	16	67000	3.79
10	24	18	16	65000	3.86

[a] Determined by relative integration of the ^{1}H NMR spectrum. [b] Determined from the weight of the isolated polymer. [c] Calculated by SEC in THF with refractive index detection (calibrated with PMMA standards).

The ^{1}H NMR spectrum of the polymer isolated from entry 10 (Figure 35) shows the expected resonances of PMA and MA, plus those of 1,3,5-trioxane and benzene. At higher times, all these signals broadened, perhaps because of the formation of a manganese paramagnetic species.

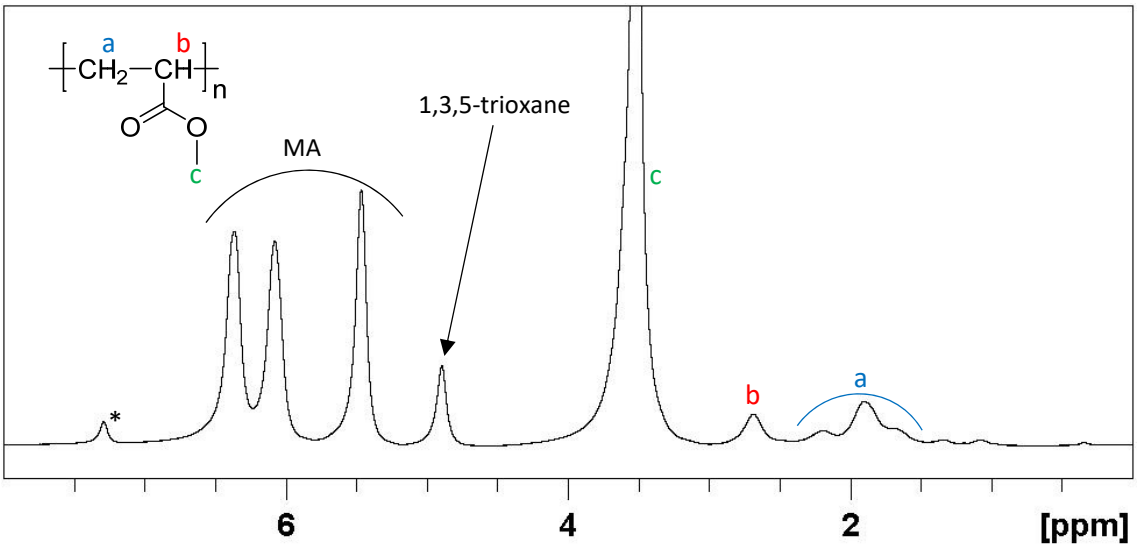

Figure 35. ^{1}H NMR spectrum (400 MHz, benzene-d_6) of entry 10. The starred resonance is due to the solvent.

The monomer conversion evolved more or less in agreement with a first-order behavior for the first 8 hours as shown in Figure 36, reaching a 16% of conversion (Entry 8). Then, the reaction rate decreased, achieving only a 18% conversion after 24 hours (Entry 10). This behavior can be explained by the life-time of compound **1** at 70 °C ($t_{½}$ = 58 min and $t_{99\%}$ = 6.4 h in C_6D_6) combined with transfer reactions that kill the active chain. The size exclusion chromatograms show that only the small molar masses evolve during the polymerization (Figure 37). In addition, the number average molar mass and dispersity vs conversion representation (Figure 38) exhibits a common behavior of a conventional radical polymerization since the molar mass decrease while the dispersity increase.

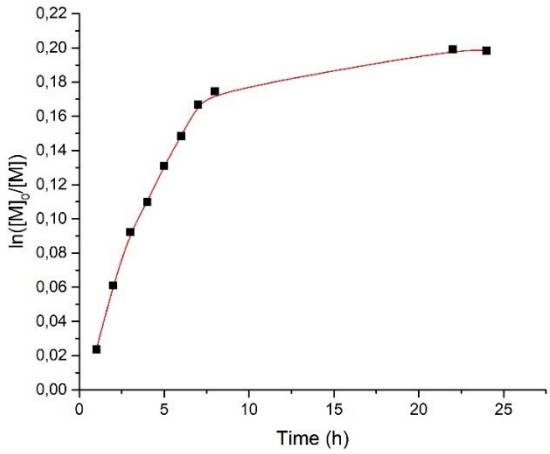

Figure 36. First-order kinetic plot for the polymerization of MA initiated by [Mn(CO)$_5$(CH(CH$_3$)(COOCH$_3$)].

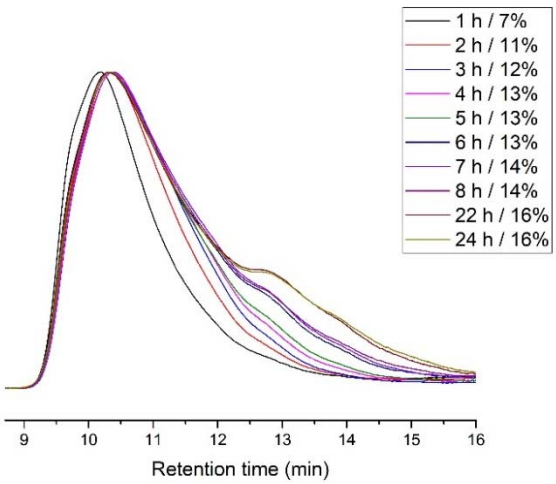

Figure 37. SEC traces of PMA (entries 1 to 10) in THF.

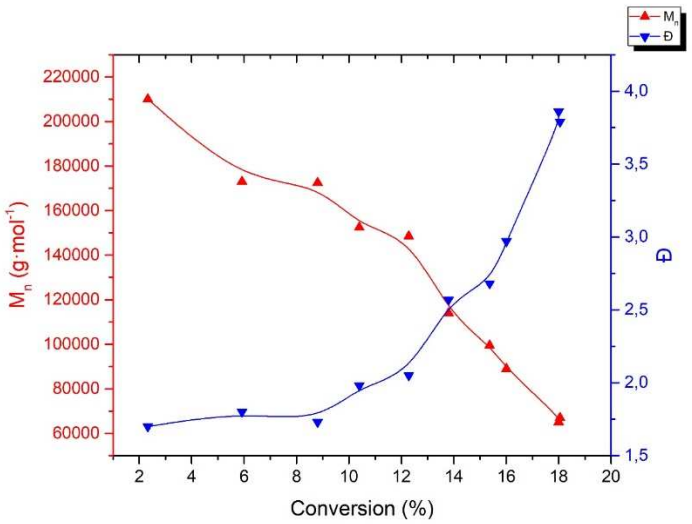

Figure 38 Number average molar mass and dispersity vs conversion of polymerization of MA initiated by compound **1**.

5.5. Polymerization of styrene with $[Mn(CO)_5(CH(CH_3)(C_6H_5))]$

The polymerization of styrene was carried out with compound **3**. However, this complex could not be obtained in a pure state. In fact, probably the complex used was the corresponding acyl complex due to spontaneous decomposition of **3** as observed Johnson *et al.*[52] by a dissociation of a CO ligand follow by a migratory insertion as proposed in Chapter 2. However, the corresponding acyl complex should be able to initiate the polymerization by a decarbonylation follow by the homolytic cleavage of the Mn-C bond. Two polymerization tests of styrene were carried out with the obtained compound, at 50 and 70 °C in bulk, because compound **3** (or its acyl complex) is soluble in styrene (Scheme 6). A little amount of mesitylene was added to each reaction as internal standard to monitor the relative amount of formed polymer and residual monomer.

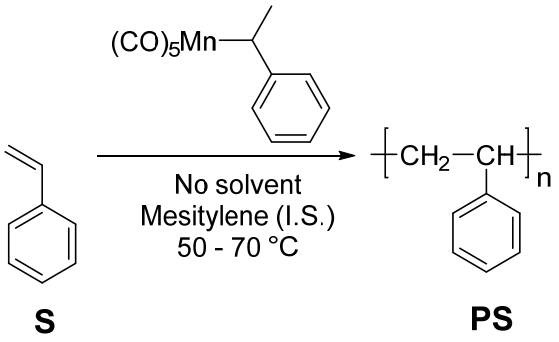

Scheme 6. General synthetic pathway employed to synthesize PS using compound **1** as initiator.

The first polymerization test, with a target DP of 80 and at 70°C, gave the polymer with a 43% of conversion after 18 h. Table 13 shows the results obtained for this polymerization at different reaction times. The conversion increases very rapidly at the beginning of the reaction to reach 33% after 2 h. Then, 15 h later it has only increased to 53%. On the other hand, the molar mass is high at the beginning of the polymerization, followed by a slight decrease after 1 h (entries 1 to 2) and then remains more or less constant during the polymerization (21000-22600 $g \cdot mol^{-1}$). In addition, the dispersity decreases between entries 1 and 2, then an increase is observed (entries 2 to 4). This behavior is maybe produced by experimental and analytical errors since the molar mass and dispersity have irregular trends.

Table 13. Results of the polymerization of VDF in presence of $[Mn(CO)_5(CH(CH_3)(C_6H_5))]$ at 70 °C

Entry	Reaction time (h)	Conversion (%)	M_n ($g \cdot mol^{-1}$)	Đ
1	1	15	21200	1.34
2	2	33	17400	1.26
3	17	43	22600	1.61
4	18	43	21000	1.54

The ^1H NMR spectrum of the polymer recovered from entry 4 (Figure 39) displays the expected resonances of PS and S, proving the initiation of the polymerization by compound **3** (or its corresponding acyl complex).

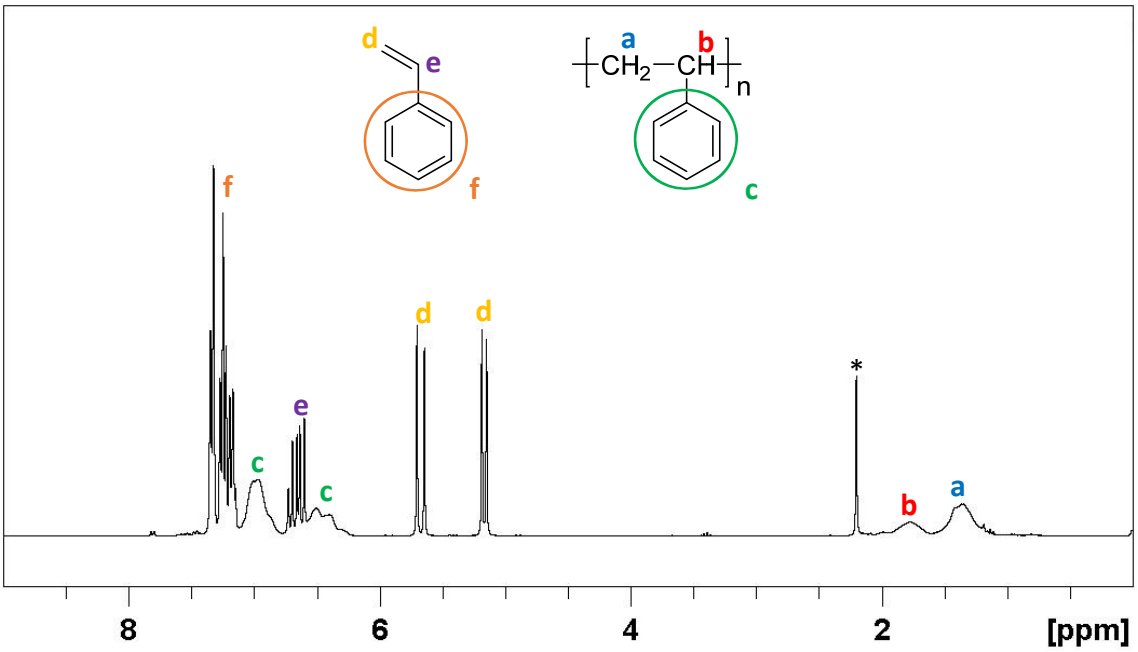

Figure 39. ^{1}H NMR spectrum (400 MHz, acetone-d_6) of entry 4. The starred resonance is due to the solvent.

The size exclusion chromatograms (Figure 40) show the increasing of the molar mass along the polymerization. However, several populations with different molar masses were observed, producing a raise in the dispersity as shown in Table 13.

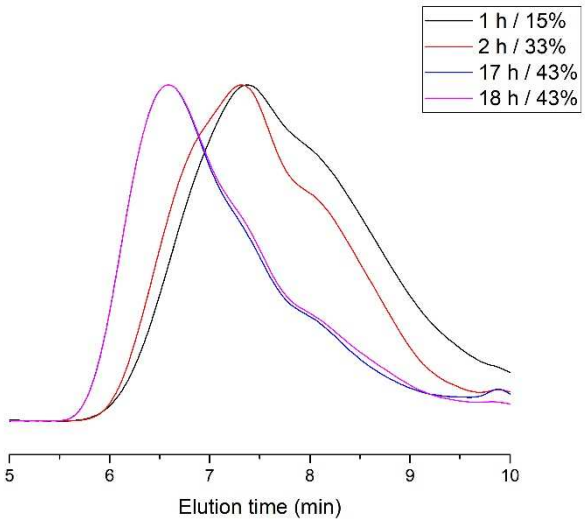

Figure 40. SEC traces of polystyrene (entries 1 to 4 of Table 10) in THF.

A second styrene polymerization was carried out at 50 °C, targeting the same molecular mass, with monitoring for 45 h. The results of this polymerization are presented in Table 14. The general observed behavior consists of a tendency to increase the molar mass along the polymerization (Figure 42), accompanied by a dispersity increase. In addition, the first-order kinetic plot shows a linear behavior (Figure 41).

Table 14. Results of the polymerization of styrene in presence of [Mn(CO)$_5$(CH(CH$_3$)(C$_6$H$_5$))] at 50 °C.

Entry	Reaction time (h)	Conversion (%)	M_n (g·mol^{-1})	Đ
5	0.75	10	21200	1.34
6	1.5	13	17400	1.26
7	3	15	22600	1.61
8	5	23	21000	1.54
9	6	28	26600	2.00
10	22	40	26600	1.96
11	27	56	37400	2.51
12	45	76	35400	1.95

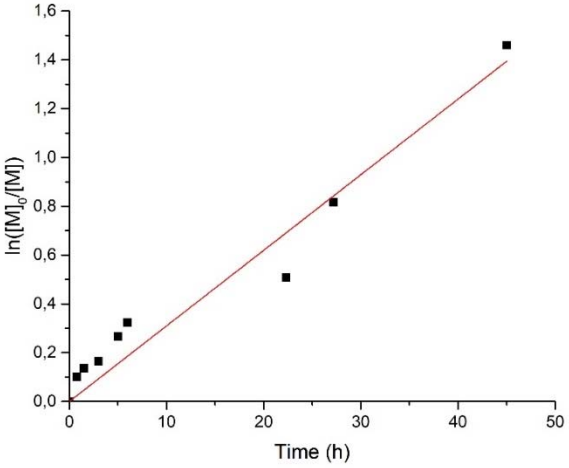

Figure 41. First-order kinetic plot for the polymerization of styrene at 50 °C in the presence of compound **3**.

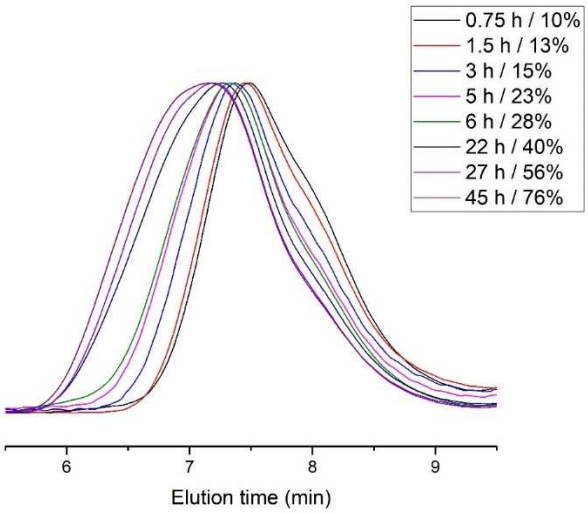

Figure 42. SEC traces of polystyrene (entries 5 to 12 of Table 11) in THF.

The representation of the number average molar mass *vs.* conversion (Figure 43) shows a point cloud, probably because of experimental and analytical errors. However, the general behavior seems to be an increase of both molar mass and dispersity, proving that the reaction is not well-controlled. The molar mass and dispersity increases are much accentuated at the beginning of the polymerization and less pronounced later.

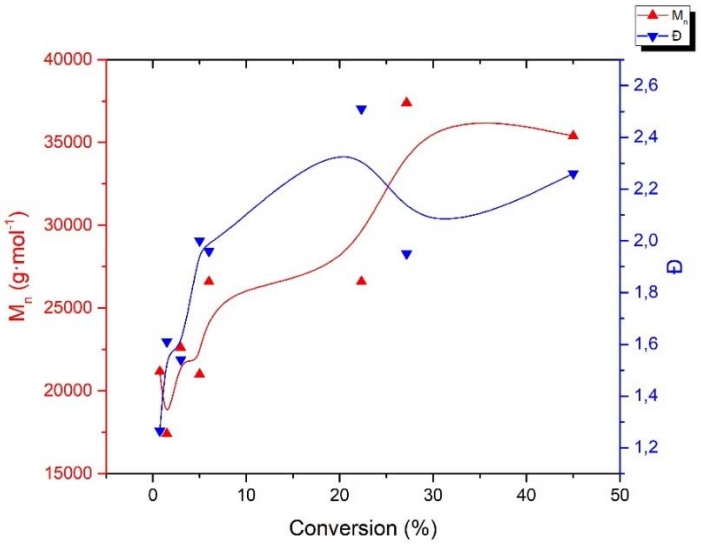

Figure 43. Number average molecular and dispersity vs conversion for the polymerization of PS initiated by compound **3**.

5.6. Conclusion

Alkyl and fluoroalkylpentacarbonylmanganese(I) complexes are able to initiate the polymerization of VDF and some hydrocarbon monomers by the homolytic bond cleavage of the Mn-R bond. In the case of VDF homopolymerization, the results are different depending on the nature of the R_F group and on the activation method, yielding PVDF in almost all the cases but with different conversions, molar masses and dispersities. The better results in terms of activation were obtained with $[Mn(CO)_5(CF_3)]$, obtaining up to 74% of yield with UV irradiation, in front of 68% by thermal activation or 60% by visible light activation. Even if this complex has the strongest BDE of the four fluoroalkylpentacarbonylmanganese(I) complexes as shown in Chapter 4, the generated radical is the least stable and thus the most reactive one. The second best results was

surprisingly obtained with [Mn(CO)$_5$(COCF$_2$CH$_3$)]. Despite the fact that its corresponding fluoroalkyl complex has the lowest predicted BDE, it can initiate the polymerization of VDF in relatively low yield under visible light and UV irradiation (21 and 23% respectively). Nevertheless, the thermal activation at 80 °C seems the worst one for this complexe since the obtained yield was only 7%. Conversely, [Mn(CO)$_5$(CHF$_2$)] and [Mn(CO)$_5$(CH$_2$CF$_3$)] are not efficient initiators in all the activation methods tested in this chapter. For both complexes, the best results were obtained by UV irradiation, reaching however only a 5% yield.

On the other hand, the alkylpentacarbonylmanganese(I) complexes tested in the polymerization of hydrocarbon monomers such as methyl acrylate or styrene gave good results in term of activation, yielding relatively high conversions in both cases. The bulk polymerization led to a very high conversion in a short time. The use of [Mn(CO)$_5$(CH(CH$_3$)(C$_6$H$_5$))] (or the corresponding acyl complex) in the homopolymerization of styrene without solvent led to polystyrene in high yields. However, in no case was the reaction well-controlled, since the dispersities increased along the polymerization.

5.7. Experimental section

Materials. VDF was kindly supplied by Arkema and used as received. MAF-TBE was kindly supplied by Tosho and used as received. Methyl acrylate (99%, Aldrich) was purified through a basic alumina column prior to use to remove the inhibitor (monomethyl ether hydroquinone). Styrene (ReagentPlus® grade, ≥99%, Sigma-Aldrich) was distilled under vacuum prior to use to remove the stabilizer (4-*tert*-butylcatechol). Compounds dimethyl carbonate (≥99%, Merck KGaA), acetone (VMR Chemicals), pentane (VMR Chemicals), dimethyl formamide (VMR Chemicals), 1,3,5-trioxane (99%, Fluorochem), mesitylene (98%, Sigma-Aldrich), benzene-d_6 (99.5%D, Euriso-top), acetone-d_6 (99.5%D, Euriso-top), DMSO-d_6 (99.5%D, Euriso-top) and DMF-d_7 (99.5%D, Euriso-top) were used as received.

Instrumentation. The Nuclear Magnetic Resonance (NMR) spectra were recorded on a Bruker Avance III HD 400 MHz spectrometer. The instrumental parameters for recording spectra were as follows: ^{1}H NMR: flip angle 30°, acquisition time 5.7 s, pulse delay 2 s, number of scans 64, and a pulse width of 3.05 µs; ^{19}F NMR: flip angle 30°, acquisition time 2 s, pulse delay 2 s, number of scans 64, and a pulse width of 3.76 µs; ^{13}C NMR: flip angle 30°, acquisition time 1.5 s, pulse delay 2 s, number of scans 10240, and a pulse width of 3.27 µs. The probe has a lower background ^{19}F signals compared to standard dual-channel probes. SEC with 0.1 M LiBr/DMF as the eluent, calibrated with poly(methyl methacrylate) standards from Polymer Laboratories, was run with a Varian Prostar (model 210) pump at a flow rate of 0.8 mL·min^{-1} using two 300 mm long, mixed-D PL-gel 5 µm columns (molar mass range: $2{\cdot}10^2$ – $4{\cdot}10^5$ g·mol^{-1} from Polymer Laboratories) thermostated at 70 °C, connected to a Shodex (model RI-101) refractometer detector. Typical sample concentration was 10 mg/mL.

VDF polymerizations with trifluoromethyl(pentacarbonyl)manganese. The radical polymerizations of VDF were carried out in thick-walled 12 mL Carius tubes in which the solvent (5 mL of dimethyl carbonate) and [Mn(CO)$_5$(CF$_3$)] (128 mg, 0.48 mmol) were added. The resulting solutions were then degassed by performing three freeze-pump-thaw cycles. Then, the gaseous VDF monomer (1.5 g, 23.4 mmol) was transferred into the Carius tube, which was cooled at the liquid nitrogen temperature, using a custom-made manifold that enables the accurate measurement of the gas quantity (using "pressure drop vs mass of monomer" calibration curves). The tube was then sealed under static vacuum at the liquid nitrogen temperature. For the thermal activation experiments, the tube was placed horizontally in a thermostatic shaking water bath. For the visible light activation experiment, the tube was placed horizontally in a tube roller shaker with 3 LED bulbs (Diall 1102270698, 14 W, 1521 lm), radiating from above, placed at 2 cm from the tube. The proximity of the bulbs caused the tube to warm up to 40 °C. For the UV activation experiment, the tube was equipped with a small magnetic stirring bar and stirred vertically in a Rayonet RPR-200 UV reactor equipped with sixteen 300

nm wavelength UV-lamps of 35 W each. Despite the fan placed inside the UV chamber, the heat generated by the UV lamps caused the tube to warm up to 50 °C. After 24 h, each tube was frozen into liquid nitrogen, opened, and the solvent was evaporated in a rotary evaporator. The resulting polymers were dissolved in DMF-d_7 or DMSO-d_6 or acetone-d_6 (depending on the solubility) and analyzed by ^{1}H and ^{19}F NMR spectroscopies. The molar masses and dispersities were determined by SEC in DMF (refractive index, calibrated with PMMA standards).

VAc/MAF-TBE copolymerization. The radical copolymerization of VAc and MAF-TBE were carried out in a Schlenk tube under an argon atmosphere. As a representative example, 93.3 mg of $[Mn(CO)_5(CH_2CF_3)]$ ($3.35 \cdot 10^{-1}$ mmol) were introduced in a Schlenk tube. Then, 1.554 g of VAc (18.1 mmol) and 3.324 g of MAF-TBE (16.9 mmol) were added to the Schlenk tube. The resulting solution was degassed by performing three freeze-pump-thaw cycles, and finally the Schlenk tube was refilled with argon. The solution was heated up to 80 °C for 18 h, and the resulting dark yellow solid was dissolved in 15 mL of acetone. The polymer was precipitated adding the solution dropwise to 200 mL of cold n-pentane, and then the precipitated was dried at 80 °C under vacuum for 16 h, yielding 4.053 g of a yellow-brownish solid (83% yield). The polymer was dissolved in acetone-d_6 and analyzed by ^{1}H and ^{19}F NMR spectroscopies. The molar masses and dispersities were determined by SEC in DMF (refractive index, calibrated with PMMA standards).

Methyl acrylate polymerization. The radical polymerization of MA was carried out in a Schlenk tube under an argon atmosphere. First, 165 mg of $[Mn(CO)_5(CH(CH_3)(COOCH_3))]$ ($5.85 \cdot 10^{-1}$ mmol) were introduced in a Schlenk tube. Then, 2.52 g of MA (29.3 mmol), 100 mg of 1,3,5-trioxane (1.11 mmol) and 3 mL of benzene-d_6 were added to the Schlenk tube. The resulting solution was degassed by performing three freeze-pump-thaw cycles, and finally the Schlenk tube was refilled with argon. The solution was heated up to 70 °C for 24 h, and some samples with 0.2 mL were taken to follow the polymerization evolution. The samples were introduced in a NMR tube and

0.3 mL of benzene-d_6 were added. They were analyzed by ^{1}H NMR spectroscopy and then the solvent was evaporated to dissolved the resulting solid in DMF. The molar masses and dispersities were determined by SEC in DMF (refractive index, calibrated with PMMA standards).

Styrene polymerization. The radical polymerizations of styrene were carried out in a Schlenk tube under an argon atmosphere. As a representative example, 358 mg of [$Mn(CO)_5(CH(CH_3)(C_6H_5))$] (1.19 mmol) were introduced in a Schlenk tube. Then, 10.0 g of styrene (96.0 mmol) and 259 mg of mesitylene (2.15 mmol) were added to the Schlenk tube. The resulting solution was degassed by performing three freeze-pump-thaw cycles, and finally the Schlenk tube was refilled with argon. The solution was heated up to 70 °C for 18 h, and some samples with 0.2 mL were taken to follow the polymerization evolution. The samples were introduced in a NMR tube and 0.3 mL of acetone-d_6 were added. They were analyzed by ^{1}H NMR spectroscopy and then the solvent was evaporated to dissolved the resulting solid in THF. The molar masses and dispersities were determined by SEC in DMF (refractive index, calibrated with PMMA standards).

5.8. References

[1] X. Ma; Z. Zuo; G. Liu; Z. Huang *ACS Omega* **2017**, *2*, 4688-4692.
[2] D. A. Valyaev; D. Wei; S. Elangovan; M. Cavailles; V. Dorcet; J.-B. Sortais; C. Darcel; N. Lugan *Organometallics* **2016**, *35*, 4090-4098.
[3] S. Vijjamarri; V. K. Chidara; G. Du *ACS Omega* **2017**, *2*, 582-591.
[4] N. Duc Hanh; X. Trivelli; F. Capet; J.-F. Paul; F. Dumeignil; R. M. Gauvin *ACS Catal.* **2017**, *7*, 2022-2032.
[5] B. Dutta; V. Sharma; N. Sassu; Y. Dang; C. Weerakkody; J. Macharia; R. Miao; A. R. Howell; S. L. Suib *Green Chem.* **2017**, *19*, 5350-5355.
[6] N. A. Espinosa-Jalapa; A. Kumar; G. Leitus; Y. Diskin-Posner; D. Milstein *J. Am. Chem. Soc.* **2017**, *139*, 11722-11725.
[7] W. Liu; L. Ackermann *ACS Catal.* **2016**, *6*, 3743-3752.
[8] D. Zell; U. Dhawa; V. Mueller; M. Bursch; S. Grimme; L. Ackermann *ACS Catal.* **2017**, *7*, 4209-4213.
[9] A. D. Asandei; O. I. Adebolu; C. P. Simpson *J. Am. Chem. Soc.* **2012**, *134*, 6080-6083.

[10] C. P. Simpson; O. I. Adebolu; J.-S. Kim; V. Vasu; A. D. Asandei *Macromolecules* **2015**, *48*, 6404-6420.
[11] M. Tatemoto *Int. Polym. Sci. Tech.* **1985**, *12*, 85-98.
[12] G. David; C. Boyer; J. Tonnar; B. Ameduri; P. Lacroix-Desmazes; B. Boutevin *Chem. Rev.* **2006**, *106*, 3936-3962.
[13] S. Banerjee; Y. Patil; T. Ono; B. Améduri *Macromolecules* **2017**, *50*, 203-214.
[14] M. A. Bachmann; W. L. Gordon; J. L. Koenig; J. B. Lando *Journal of Applied Physics* **1979**, *50*, 6106-6112.
[15] D. E. Mattern; F. T. Lin; D. M. Hercules *Analytical Chemistry* **1984**, *56*, 2762-2769.
[16] A. J. Lovinger; D. D. Davis; R. E. Cais; J. M. Kometani *Polymer* **1987**, *28*, 617-626.
[17] P. Pladis; A. H. Alexopoulos; C. Kiparissides *Ind. Engin. Chem. Res.* **2014**, *53*, 7352-7364.
[18] A. D. Asandei *Chem. Rev.* **2016**, *116*, 2244-2274.
[19] R. Poli *Angew. Chem. Int. Ed.* **2006**, *45*, 5058–5070.
[20] R. Poli In *Polymer Science: A Comprehensive Reference*; Matyjaszewski, K., Möller, M., Eds.; Elsevier BV: Amsterdam, 2012; Vol. 3, p 351–375.
[21] R. Poli *Chem. Eur. J.* **2015**, *21*, 6988-7001.
[22] J. Demarteau; B. Améduri; V. Ladmiral; M. A. Mees; R. Hoogenboom; A. Debuigne; C. Detrembleur *Macromolecules* **2017**, *50*, 3750-3760.
[23] S. Banerjee; E. V. Bellan; F. Gayet; A. Debuigne; C. Detrembleur; R. Poli; B. Améduri; V. Ladmiral *Polymers* **2017**, *9*, 702.
[24] S. Banerjee; V. Ladmiral; A. Debuigne; C. Detrembleur; S. M. W. Rahaman; R. Poli; B. Améduri *Macromol. Rapid Commun.* **2017**, *38*, 1700203.
[25] S. Banerjee; V. Ladmiral; A. Debuigne; C. Detrembleur; R. Poli; B. Améduri *Angew. Chem. Int. Ed.* **2018**, *57*, 2934–2937.
[26] R. Poli; S. M. W. Rahaman; V. Ladmiral; B. Ameduri *J. Organomet. Chem.* **2018**, *864*, 12-18.
[27] W. R. Dolbier *Chem. Rev.* **1996**, *96*, 1557-1584.
[28] D. F. McMillen; D. M. Golden *Annu. Rev. Phys. Chem.* **1982**, *33*, 493-532.
[29] J. M. Martell; R. J. Boyd; Z. Shi *J. Phys. Chem.* **1993**, *97*, 7208-7215.
[30] J. M. Tedder; J. C. Walton *Tetrahedron* **1980**, *36*, 701-707.
[31] J. M. Tedder *Angew. Chem. Int. Ed.* **1982**, *21*, 401-410.
[32] S. I. Serov; M. V. Zhuravlev; V. P. Sass; S. V. Sokolov *J. Org. Chem. USSR* **1981**, *17*, 48-52.
[33] M. Guerre; S. M. W. Rahaman; B. Ameduri; R. Poli; V. Ladmiral *Macromolecules* **2016**, *49*, 5386-5396.
[34] S. M. Aliwi; C. H. Bamford; S. U. Mullik *J. Polym. Sci., Polym. Symp.* **1975**, 33-50.
[35] D. E. Mattern; F. T. Lin; D. M. Hercules *Anal. Chem.* **1984**, *56*, 2762-2769.
[36] J. M. Tedder; J. C. Walton *Acc. Chem. Res.* **1976**, *9*, 183-191.
[37] M. Duc; B. Ameduri; B. Boutevin; M. Kharroubi; J. M. Sage *Macromol. Chem. Physic.* **1998**, *199*, 1271-1289.
[38] J. Guiot; B. Ameduri; B. Boutevin *Macromolecules* **2002**, *35*, 8694-8707.
[39] M. Guerre; B. Campagne; O. Gimello; K. Parra; B. Ameduri; V. Ladmiral *Macromolecules* **2015**, *48*, 7810-7822.
[40] B. Ameduri; C. Ladaviere; F. Delolme; B. Boutevin *Macromolecules* **2004**, *37*, 7602-7609.
[41] F. Boschet; T. Ono; B. Ameduri *Macromol. Rapid Commun.* **2012**, *33*, 302-308.
[42] M. Destarac; K. Matyjaszewski; E. Silverman; B. Améduri; B. Boutevin *Macromolecules* **2000**, *33*, 4613-4615.
[43] E. Girard; J. D. Marty; B. Améduri; M. Destarac *ACS Macro Lett.* **2012**, *1*, 270-274.
[44] N. Golzari; J. Adams; S. Beuermann *Polymers* **2017**, *9*.
[45] B. Otazaghine; L. Sauguet; B. Ameduri *J. Fluorine Chem.* **2005**, *126*, 1009-1016.

[46] J. T. Goldbach; R. Amin-Sanayei; W. He; J. Henry; W. Kosar; A. Lefebvre; G. O'Brien; D. Vaessen; K. Wood; S. Zerafati In *Fluorinated Polymers*; Ameduri, B., Sawada, H., Eds.; The Royal Society of Chemistry: 2017; Vol. 2, p 127-157.
[47] S. Banerjee; V. Ladmiral; C. Totee; B. Ameduri *European Polymer Journal* **2018**, *104*, 164-169.
[48] J. F. Lutz; M. Ouchi; D. R. Liu; M. Sawamoto *Science* **2013**, *341*, 628-+.
[49] H. Ito; B. Giese; R. Engelbrecht *Macromolecules* **1984**, *17*, 2204-2205.
[50] K. T. McElroy; S. T. Purrington; C. L. Bumgardner; J. P. Burgess *J. Fluorine Chem.* **1999**, *95*, 117-120.
[51] Y. Patil; B. Ameduri *Prog. Polym. Sci.* **2013**, *38*, 703-739.
[52] R. W. Johnson; R. G. Pearson *J. Chem. Soc., Chem. Commun.* **1970**, 986-987.

General conclusion

General conclusion

This work was carried out to evaluate the possible existence of PVDF-$Mn(CO)_5$ species in the iodine transfer polymerization of VDF, when this is run in the presence of the manganese pentacarbonyl radical. This radical is generated from addition of $[Mn_2(CO)_{10}]$ by irradiation with visible light and has the role to reactivate the more stable reverse dormant chains. For this purpose, several alkyl and fluoroalkylpentacarbonylmanganese(I) complexes modeling the dormant chains of PVDF and of other polymers have been synthesized and fully characterized. Specifically, three alkylpentacarbonylmanganese(I) complexes have been prepared from potassium pentacarbonyl manganate and the corresponding alkylbromide by nucleophilic substitution. $[Mn(CO)_5(COCH_2CH_2COOCH_3)]$ (**1**) was reported in the literature but only as a by-product. Its synthesis and characterization by ^1H NMR and FTIR spectroscopy are reported here for the first time. In contrast, $[Mn(CO)_5(COCH_2CH_2COOCH_3)]$ (**2**) has not been previously reported. In addition to the formation of the desired product, obtaining of several by-products, have also been investigated. Among them, the corresponding acyl (**2a**) complex has been isolated and fully characterized. $[Mn(CO)_5(CH(CH_3)(C_6H_5))]$ (**3**) was previously reported in the literature. However, it could not be isolated as a pure product because of its spontaneous decomposition, yielding the corresponding acyl complex among other products as previously reported. The present study also did not lead to the isolation of compound **3**, even when taking great precautions such as purification by column chromatography at -30 °C under an argon atmosphere, storage at -24 °C under an argon atmosphere, etc. The isolated product seems to correspond to the acyl complex (**3a**), as previously reported. Furthermore, the formation of 2-phenylpropanal has been observed during the decomposition of **3** and a mechanism leading to its formation is proposed.

Four fluoroalkylpentacarbonylmanganese(I) complexes have been prepared by decarbonylation of the corresponding acyl complexes, and fully characterized. The more direct nucleophilic substitution of halide by pentacarbonylmanganate anion from the corresponding fluoroalkyl halides does not lead to the expected products because of the

high electronegativity of the fluorine atoms. Two of the synthesized compounds, $[Mn(CO)_5(CF_3)]$ (**8**) and $[Mn(CO)_5(CHF_2)]$ (**9**), had been previously described in the literature. However, the full characterization of these complexes and their corresponding acyl complexes (**4** and **5**) have been disclosed in this contribution for the first time. Moreover, two new fluoroalkylpentacarbonylmanganese(I) complexes, $[Mn(CO)_5(CH_2CF_3)]$ (**10**) and $[Mn(CO)_5(CF_2CH_3)]$ (**11**) and their corresponding acyl complexes (**6** and **7**) have been prepared and studied. Compound **11** could not be obtained in a pure state, presumably because it decomposes during the synthesis *via* both thermal and photochemical decarbonylation processes. In addition, the FTIR properties of compounds **8**-**10** in *n*-pentane solution has been an in-depth studied, revealing the presence of several weak bands corresponding to the major $[Mn(^{12}CO)_5R_F]$ and minor $[Mn(^{12}CO)_4(eq\text{-}^{13}CO)R_F]$ and $[Mn(^{12}CO)_4(ax\text{-}^{13}CO)R_F]$ isotopomers. This study was supported by DFT calculations at an unprecedented level of detail.

In order to confirm the higher values of the Mn^I-R_F BDEs for compounds **8** and **9**, predicted by a recently published DFT article, relative to previously reported experimental data, a new and accurate experimental method to determine the metal-alkyl or fluoroalkyl BDEs has been set up for these two compounds and extended to other alkyl and fluoroalkylpentacarbonylmanganese(I) complexes (**1** and **10**). This method consists of a kinetic study of the Mn-R bond cleavage in the presence of an excess radical trap, tris(trimethylsilyl)silane (TTMSS). The Eyring's equation led to the $\Delta H^{\ddagger}$ parameter, a close approximation of the BDE. The obtained BDE values agree with the DFT calculations and show that the bond strength decreases in the following decreasing order: CF_3 (**8**) > CH_2CF_3 (**10**) > CHF_2 (**9**) > $CH(CH_3)(COOCH_3)$ (**1**), confirming that the presence of fluorine atoms in the alkyl chain strengthens the Mn-R bond. Interestingly, three fluorine atoms in the β-position (compound **10**), led to a higher BDE than two fluorine atoms in the α-position (compound **9**). In addition, the thermal decomposition of the fluoroalkylpentacarbonylmanganese(I) complexes in the presence of TTMSS was accompanied by side-reactions. The identification of a few by-products reveals an unprecedented reaction of the $[Mn(CO)_5R_F]$ complexes, the α-F elimination. A DFT study suggests that this process is only possible after creating a vacant coordination site on the Mn center by CO dissociation. Further studies will be necessary

to unveil the other decomposition pathways and to determine the BDEs of other complexes such as compounds **2**, **3** and **11**, once these will be obtained in a pure state.

A few VDF polymerization tests have been carried out using the $[Mn(CO)_5R_F]$ complexes produced in this work as initiators under thermal and photochemical conditions (visible light and UV). These tests show that the VDF polymerization is initiated by compounds **7** and **8**. However, compounds **9** and **10** led to very low yields and consequently they are not a good initiator for the polymerization of this monomer. On the other hand, the copolymerization of VAc with MAF-TBE can be thermally initiated with these complexes, proving that they are able to thermally generate radicals. Unfortunately, the resonance of the PVDF-$Mn(CO)_5$ chain ends could not be identified. No evidence of an RDRP process was found, except for the polymerization run in the presence of complex **8** activated by UV irradiation, which showed an increase of the molar mass and a decrease of the dispersity during the polymerization. However, deeper investigations on this system are required to confirm this behavior.

Polymerization experiments of a few non-fluorinated monomers such as methyl acrylate and styrene have been carried out by thermal initiation with $[Mn(CO)_5R]$. Compound **1** can initiate the polymerization of methyl acrylate, even at mild temperatures. Additionally, the polymerization of styrene using compound **3** (or from the corresponding acyl complex **3a**) led to polystyrene in high yields. However, the analyses of the obtained polymers do not agree with an RDRP process.

Deeper investigations are required to complete this study. First, additional VDF polymerizations initiated by $[Mn(CO)_5R_F]$ should be achieved to more firmly conclude about the kinetic behavior in all the cases. In addition, several tiny NMR resonances of the isolated PVDF products have remained unidentified. Deeper NMR investigations are necessary for the elucidation of these functions and for the mechanism of their formation. Moreover, the choice of other ligands to replace one or more carbonyl ligands in the $[Mn(CO)_5R_F]$ system, in addition to the smart choice of the fluoroalkyl chain, could modulate the Mn-R_F bond strength and even avoid the dimerization of the manganese radical, leading to a well-controlled OMRP process. Finally, studying the

behavior of these complexes or of other related alkyl or fluoroalkylpentacarbonyl-manganese(I) complexes with other ligands in the (co)polymerization of other fluorinated monomers promises to be a rewarding area of research.

Appendix

Appendix

A. Alkylpentacarbonylmanganese(I) complexes single-cristal X-ray structure data

A.1. Compound $[Mn(CO)_5(CH(CH_3)(OCOCH_3)]$, **2**

Table A.1.1. Crystal data and structure refinement for compound $[Mn(CO)_5(CH(CH_3)(OCOCH_3)]$ (**2**).

Empirical formula	$C_9H_7MnO_7$	
Formula weight	282.09	
Temperature	173(2) K	
Wavelength	0.71073 Å	
Crystal system	Triclinic	
Space group	P-1	
Unit cell dimensions	a = 6.5875(2) Å	α = 80.5360(10)°.
	b = 6.7920(2) Å	β = 78.298(2)°.
	c = 13.2813(5) Å	γ = 88.2430(10)°.
Volume	573.96(2) $Å^3$	
Z	2	
Density (calculated)	1.632 Mg/m3	
Absorption coefficient	1.169 mm^{-1}	
Crystal size	0.02 x 0.12 x 0.14 mm^3	
Reflections collected	44271	
Independent reflections	6893 [R(int) = 0.077]	
Max. and min. transmission	1 and 0.85	
Goodness-of-fit on F^2	0.9517	
Final R indices [I>2sigma(I)]	R1 = 0.0487, wR2 = 0.1173	
R indices (all data)	R1 = 0.0697, wR2 = 0.1460	
Largest diff. peak and hole	1.60 and -1.12 e.Å-3	

Table A.1.2. Bond lengths [Å] for compound $[Mn(CO)_5(CH(CH_3)(OCOCH_3)]$ (**2**).

Mn1—C2	1.8745 (18)	C6—O7	1.467 (2)
Mn1—C4	1.836 (2)	C6—C11	1.516 (3)
Mn1—C6	2.1717 (19)	O7—C8	1.336 (2)
Mn1—C12	1.8671 (19)	C8—O9	1.203 (2)
Mn1—C14	1.858 (2)	C8—C10	1.504 (3)
Mn1—C16	1.849 (2)	C12—O13	1.133 (2)
C2—O3	1.132 (2)	C14—O15	1.135 (3)
C4—O5	1.137 (3)	C16—O17	1.133 (3)

Table A.1.3. Bond angles [°] for compound $[Mn(CO)_5(CH(CH_3)(OCOCH_3)]$ (**2**).

C2—Mn1—C4	94.31 (9)	C14—Mn1—C16	88.41 (9)
C2—Mn1—C6	83.96 (7)	Mn1—C2—O3	178.13 (18)
C4—Mn1—C6	177.80 (8)	Mn1—C4—O5	178.2 (2)
C2—Mn1—C12	90.64 (8)	Mn1—C6—O7	108.07 (12)
C4—Mn1—C12	89.58 (9)	Mn1—C6—C11	116.12 (14)
C6—Mn1—C12	91.79 (8)	O7—C6—C11	106.28 (16)
C2—Mn1—C14	91.12 (8)	C6—O7—C8	119.13 (14)
C4—Mn1—C14	93.63 (10)	O7—C8—O9	124.58 (18)
C6—Mn1—C14	85.07 (8)	O7—C8—C10	111.11 (17)
C12—Mn1—C14	176.21 (9)	O9—C8—C10	124.3 (2)
C2—Mn1—C16	170.35 (9)	Mn1—C12—O13	175.89 (19)
C4—Mn1—C16	95.34 (10)	Mn1—C14—O15	177.8 (2)
C6—Mn1—C16	86.40 (9)	Mn1—C16—O17	178.3 (2)
C12—Mn1—C16	89.28 (9)		

A.2. Compound $[Mn(CO)_5(COCH(CH_3)(OCOCH_3)]$, **2a**

Table A.2.1 Crystal data and structure refinement for compound $[Mn(CO)_5(COCH(CH_3)(OCOCH_3)]$ (**2a**).

Empirical formula	C_{10} H_7 Mn O8	
Formula weight	310.10	
Temperature	173(2) K	
Wavelength	0.71073 Å	
Crystal system	Monoclinic	
Space group	P 21/n	
Unit cell dimensions	a = 6.4759(4) Å	α = 90°.
	b = 6.7177(4) Å	β = 90°.
	c = 29.242(4) Å	γ = 90°.
Volume	1272.1(2) $Å^3$	
Z	4	
Density (calculated)	1.619 Mg/m^3	
Absorption coefficient	1.069 mm^{-1}	
F(000)	624	
Crystal size	0.5 x 0.12 x 0.08 mm^3	
Theta range for data collection	3.146 to 26.370°.	
Reflections collected	7640	
Independent reflections	2545 [R(int) = 0.0581]	
Completeness to theta = 26.370°	99.9 %	
Absorption correction	Semi-empirical from equivalents	
Max. and min. transmission	1.0 and 0.814	
Refinement method	Full-matrix least-squares on F^2	
Data / restraints / parameters	2545 / 0 / 175	
Goodness-of-fit on F^2	1.054	
Final R indices [I>2sigma(I)]	R1 = 0.0589, wR2 = 0.1381	
R indices (all data)	R1 = 0.0716, wR2 = 0.1495	
Largest diff. peak and hole	0.531 and -0.849 e.Å-3	

Table A.2.2. Bond lengths [Å] for compound [$Mn(CO)_5(COCH(CH_3)(OCOCH_3)]$ (**2a**).

Mn(1)-C(1)	2.107(5)	Mn(1)-C(2)	1.859(7)
Mn(1)-C(3)	1.874(6)	Mn(1)-C(4)	1.864(7)
Mn(1)-C(5)	1.854(6)	Mn(1)-C(6)	1.862(7)
O(1)-C(1)	1.205(6)	O(2)-C(2)	1.118(8)
O(3)-C(3)	1.127(7)	O(4)-C(4)	1.139(8)
O(5)-C(5)	1.140(7)	O(6)-C(6)	1.121(7)
O(11)-C(13)	1.349(7)	C(1)-C(11)	1.531(8)
O(11)-C(11)	1.438(7)	C(11)-C(12)	1.525(8)
O(13)-C(13)	1.194(7)	C(13)-C(14)	1.484(9)

Table A.2.3. Bond angles [°] for compound [$Mn(CO)_5(COCH(CH_3)(OCOCH_3)]$ (**2a**).

C(2)-Mn(1)-C(1)	84.7(2)	C(3)-Mn(1)-C(1)	82.0(2)
C(4)-Mn(1)-C(1)	176.8(3)	C(5)-Mn(1)-C(1)	86.8(2)
C(6)-Mn(1)-C(1)	94.8(2)	C(2)-Mn(1)-C(3)	90.3(3)
C(2)-Mn(1)-C(4)	92.4(3)	C(5)-Mn(1)-C(2)	89.3(3)
C(2)-Mn(1)-C(6)	179.5(3)	C(4)-Mn(1)-C(3)	96.5(3)
C(5)-Mn(1)-C(3)	168.8(3)	C(6)-Mn(1)-C(3)	89.6(3)
C(5)-Mn(1)-C(4)	94.7(3)	C(6)-Mn(1)-C(4)	88.1(3)
C(5)-Mn(1)-C(6)	90.6(3)	C(11)-C(1)-Mn(1)	123.0(4)
O(1)-C(1)-Mn(1)	122.5(4)	O(2)-C(2)-Mn(1)	179.8(6)
O(3)-C(3)-Mn(1)	176.9(6)	O(4)-C(4)-Mn(1)	179.0(6)
O(5)-C(5)-Mn(1)	178.2(5)	O(6)-C(6)-Mn(1)	175.3(5)
C(13)-O(11)-C(11)	117.3(4)	C(12)-C(11)-C(1)	109.5(5)
O(1)-C(1)-C(11)	114.4(5)	O(13)-C(13)-O(11)	123.3(6)
O(11)-C(11)-C(12)	107.3(5)	O(13)-C(13)-C(14)	126.7(5)
O(11)-C(11)-C(1)	112.2(4)	O(11)-C(13)-C(14)	110.0(5)

B. Fluoroalkylpentacarbonylmanganese(I) complexes single-cristal X-ray structure data

B.1. Compound $[Mn(CO)_5(COCF_3)]$, **4**

Table B.1.1. Crystal data and structure refinement for compound $[Mn(CO)_5(COCF_3)]$ (**4**).

Empirical formula	$C_7F_3MnO_6$
Formula weight	292.01
Temperature, K	173(4)
Wavelength, Å	0.71073
Crystal system	Orthorhombic
Space group	$Pna2_1$
a, Å	14.4714(4)
b, Å	10.8047(4)
c, Å	6.3778(2)
α, °	90.0
β, °	90.0
γ, °	90.0
Volume, $Å^3$	997.23(6)
Z	4
Density (calc), Mg/m^3	1.945
Abs. coefficient, mm^{-1}	1.384
F(000)	568
Crystal size, mm^3	0.38 x 0.25 x 0.20
Theta range, °	3.389 to 26.342
Reflections collected	5749
Indpt reflections (R_{int})	2006 (0.0257)
Completeness, %	99.5
Absorption correction	Multi-scan
Max. / min. transmission	1.0 / 0.944
Refinement method	F^2
Data /restraints/parameters	2006 / 16 / 183
Goodness-of-fit on F^2	1.040
R1, wR2 [$I>2\sigma(I)$]	0.0235, 0.0506
R1, wR2 (all data)	0.0262, 0.0517
Flack's parameter	0.067(12)
Residual density, $e.Å^{-3}$	0.224 / -0.188

Table B.1.2. Bond lengths [Å] for compound $[Mn(CO)_5(COCF_3)]$ (**4**).

Mn(1)-C(1)	1.872(3)	Mn(1)-C(2)	1.862(3)
Mn(1)-C(3)	1.869(3)	Mn(1)-C(4)	1.863(3)
Mn(1)-C(5)	1.879(3)	Mn(1)-C(6)	2.051(3)
C(1)-O(1)	1.131(4)	C(4)-O(4)	1.132(4)
C(2)-O(2)	1.134(4)	C(5)-O(5)	1.125(4)
C(3)-O(3)	1.129(4)	C(6)-O(6)	1.212(4)
C(6)-C(7)	1.566(4)	C(7)-F(2)	1.292(6)
C(7)-F(1)	1.294(6)	C(7)-F(3)	1.335(6)

Table B.1.3. Bond angles [°] for compound $[Mn(CO)_5(COCF_3)]$ (**4**).

C(2)-Mn(1)-C(4)	88.87(14)	C(3)-Mn(1)-C(5)	91.37(14)
C(2)-Mn(1)-C(3)	90.28(14)	C(1)-Mn(1)-C(5)	91.20(14)
C(4)-Mn(1)-C(3)	93.43(14)	C(2)-Mn(1)-C(6)	93.01(13)
C(2)-Mn(1)-C(1)	89.98(14)	C(4)-Mn(1)-C(6)	84.07(13)
C(4)-Mn(1)-C(1)	174.14(14)	C(3)-Mn(1)-C(6)	175.83(14)
C(3)-Mn(1)-C(1)	92.32(15)	C(1)-Mn(1)-C(6)	90.25(14)
C(2)-Mn(1)-C(5)	177.93(15)	C(5)-Mn(1)-C(6)	85.28(13)
C(4)-Mn(1)-C(5)	89.79(13)	O(1)-C(1)-Mn(1)	179.6(3)
O(2)-C(2)-Mn(1)	177.4(3)	O(4)-C(4)-Mn(1)	177.2(3)
O(3)-C(3)-Mn(1)	178.5(3)	O(5)-C(5)-Mn(1)	178.9(3)
O(6)-C(6)-Mn(1)	125.2(2)	C(7)-C(6)-Mn(1)	122.4(2)
O(6)-C(6)-C(7)	112.4(3)	F(2)-C(7)-C(6)	109.8(4)
F(2)-C(7)-F(1)	109.9(5)	F(1)-C(7)-C(6)	114.6(3)
F(2)-C(7)-F(3)	104.8(4)	F(3)-C(7)-C(6)	112.6(3)
F(1)-C(7)-F(3)	104.6(5)		

B.2. Compound $[Mn(CO)_5(COCHF_2)]$, **5**

Table B.2.1. Crystal data and structure refinement for compound $[Mn(CO)_5(COCHF_2)]$ (**5**).

Empirical formula	$C_7HF_2MnO_6$
Formula weight	274.02
Temperature, K	180(2)
Wavelength, Å	0.71073
Crystal system	Orthorhombic
Space group	$Pna2_1$
a, Å	14.0916(7)
b, Å	10.8226(7)
c, Å	6.3265(3)
α, °	90.0
β, °	90.0
γ, °	90.0
Volume, $Å^3$	964.84(9)
Z	4
Density (calc), Mg/m^3	1.886
Abs. coefficient, mm^{-1}	1.409
F(000)	536
Crystal size, mm^3	0.32 x 0.25 x 0.14
Theta range, °	3.450 to 26.365
Reflections collected	5532
Indpt reflections (R_{int})	1777 (0.0326)
Completeness, %	99.1
Absorption correction	Multi-scan
Max. / min. transmission	1.0 and 0.669
Refinement method	F^2
Data /restraints/parameters	1777 / 1 / 145
Goodness-of-fit on F^2	1.119
R1, wR2 [$I>2\sigma(I)$]	0.0405, 0.1090
R1, wR2 (all data)	0.0419, 0.1107
Flack's parameter	0.01(3)
Residual density, $e.Å^{-3}$	0.947 / -0.853

Table B.2.2. Bond lengths [Å] for compound $[Mn(CO)_5(COCHF_2)]$ (**5**).

Mn(1)-C(1)	2.057(5)	Mn(1)-C(2)	1.875(6)
Mn(1)-C(3)	1.880(6)	Mn(1)-C(4)	1.869(6)
Mn(1)-C(5)	1.862(5)	Mn(1)-C(6)	1.858(6)
C(11A)-C(1)	1.551(8)	C(11B)-C(1)	1.551(8)
C(11A)-F(12A)	1.297(18)	C(11B)-F(12B)	1.327(13)
C(11A)-F(11A)	1.39(2)	C(11B)-F(11B)	1.360(12)
C(1)-O(11)	1.224(7)	C(2)-O(2)	1.135(7)
C(3)-O(3)	1.124(7)	C(4)-O(4)	1.124(7)
C(5)-O(5)	1.131(7)	C(6)-O(6)	1.132(7)

Table B.2.3. Bond angles [°] for compound $[Mn(CO)_5(COCHF_2)]$ (**5**).

C(6)-Mn(1)-C(5)	88.4(2)	C(5)-Mn(1)-C(2)	90.2(3)
C(6)-Mn(1)-C(4)	93.4(2)	C(4)-Mn(1)-C(2)	92.4(3)
C(5)-Mn(1)-C(4)	90.9(2)	C(6)-Mn(1)-C(3)	90.5(2)
C(6)-Mn(1)-C(2)	174.1(2)	C(5)-Mn(1)-C(3)	177.4(3)
C(4)-Mn(1)-C(1)	176.1(2)		
C(4)-Mn(1)-C(3)	91.5(2)	C(5)-Mn(1)-C(1)	91.9(2)
C(2)-Mn(1)-C(3)	90.7(3)	C(2)-Mn(1)-C(1)	90.3(2)
C(6)-Mn(1)-C(1)	84.1(2)	C(3)-Mn(1)-C(1)	85.6(2)
O(2)-C(2)-Mn(1)	179.5(6)	O(5)-C(5)-Mn(1)	176.7(5)
O(3)-C(3)-Mn(1)	178.6(5)	O(6)-C(6)-Mn(1)	177.4(5)
O(4)-C(4)-Mn(1)	177.8(5)	O(11)-C(1)-Mn(1)	124.3(4)
F(12A)-C(11A)-F(11A)	102.1(11)	F(12B)-C(11B)-F(11B)	100.2(8)
F(12A)-C(11A)-C(1)	108.4(8)	F(12B)-C(11B)-C(1)	108.2(5)
F(11A)-C(11A)-C(1)	112.6(7)	F(11B)-C(11B)-C(1)	114.4(6)
O(11)-C(1)-C(11A)	111.7(5)	O(11)-C(1)-C(11B)	111.7(5)
C(11A)-C(1)-Mn(1)	123.9(4)	C(11B)-C(1)-Mn(1)	123.9(4)

B.3. Compound $[Mn(CO)_5(COCF_2CH_3)]$, **7**

Table B.3.1. Crystal data and structure refinement for compound $[Mn(CO)_5(COCF_2CH_3)]$ (**7**).

Empirical formula	$C_8H_3F_2MnO_6$
Formula weight	288.04
Temperature, K	173(2)
Wavelength, Å	0.71073
Crystal system	Monoclinic
Space group	$P2_1/c$
a, Å	14.6140(10)
b, Å	6.2155(4)
c, Å	12.4305(9)
α, °	90.0
β, °	106.608(2)
γ, °	90.0
Volume, $Å^3$	1082.00(13)
Z	4
Density (calc), Mg/m^3	1.768
Abs. coefficient, mm^{-1}	1.261
F(000)	568
Crystal size, mm^3	0.20 x 0.12 x 0.05
Theta range, °	1.454 to 30.029
Reflections collected	27995
Indpt reflections (R_{int})	3169 (0.0317)
Completeness, %	100.0
Absorption correction	Multi-scan
Max. / min. transmission	0.7476 / 0.6021
Refinement method	F^2
Data /restraints/parameters	3169 / 0 / 155
Goodness-of-fit on F^2	1.159
R1, wR2 [$I>2\sigma(I)$]	0.0254, 0.0734
R1, wR2 (all data)	0.0301, 0.0869
Flack's parameter	
Residual density, $e.Å^{-3}$	0.686 / -0.450

Table B.3.2. Bond lengths [Å] for [$(CO)_5Mn(COCF_2CH_3)$] (**7**).

Mn(1)-C(1)	2.0748(14)	Mn(1)-C(2)	1.8562(15)
Mn(1)-C(3)	1.8809(14)	Mn(1)-C(4)	1.8617(14)
Mn(1)-C(5)	1.8566(14)	Mn(1)-C(6)	1.8697(14)
F(1)-C(11)	1.379(2)	F(2)-C(11)	1.357(2)
O(1)-C(1)	1.2072(18)	O(4)-C(4)	1.1318(18)
O(2)-C(2)	1.1369(18)	O(5)-C(5)	1.1306(18)
O(3)-C(3)	1.1258(18)	O(6)-C(6)	1.1297(18)
C(1)-C(11)	1.560(2)	C(11)-C(12)	1.491(2)

Table B.3.3. Bond angles [°] for [$(CO)_5Mn(COCF_2CH_3)$] (**7**).

C(2)-Mn(1)-C(5)	94.42(7)	C(4)-Mn(1)-C(6)	89.22(6)
C(2)-Mn(1)-C(4)	92.67(6)	C(2)-Mn(1)-C(3)	90.00(6)
C(5)-Mn(1)-C(4)	90.11(6)	C(5)-Mn(1)-C(3)	89.59(6)
C(2)-Mn(1)-C(6)	92.64(6)	C(6)-Mn(1)-C(3)	90.76(6)
C(5)-Mn(1)-C(6)	172.94(6)	C(4)-Mn(1)-C(3)	177.33(6)
C(2)-Mn(1)-C(1)	177.22(6)	C(5)-Mn(1)-C(1)	84.25(6)
C(4)-Mn(1)-C(1)	84.91(6)	C(6)-Mn(1)-C(1)	88.69(6)
C(3)-Mn(1)-C(1)	92.42(6)	O(1)-C(1)-C(11)	114.71(13)
O(1)-C(1)-Mn(1)	123.39(11)	O(3)-C(3)-Mn(1)	177.01(14)
C(11)-C(1)-Mn(1)	121.83(10)	O(4)-C(4)-Mn(1)	179.29(14)
O(2)-C(2)-Mn(1)	179.29(15)	O(5)-C(5)-Mn(1)	178.10(15)
O(6)-C(6)-Mn(1)	177.77(14)		
F(2)-C(11)-F(1)	104.11(15)	F(2)-C(11)-C(1)	109.42(14)
F(2)-C(11)-C(12)	111.00(16)	F(1)-C(11)-C(1)	104.68(14)
F(1)-C(11)-C(12)	110.04(17)	C(12)-C(11)-C(1)	116.69(15)

B.4. Compound $[Mn(CO)_5(CF_3)]$, **8**

Table B.4.1. Crystal data and structure refinement for compound $[Mn(CO)_5(CF_3)]$ (**8**).

Empirical formula	$C_6F_3MnO_5$
Formula weight	264.91
Temperature, K	173(2)
Wavelength, Å	0.71073
Crystal system	Monoclinic
Space group	P 2_1/m
a, Å	6.3579(4)
b, Å	11.0117(6)
c, Å	6.5655(4)
α, °	90.0
β, °	107.459(2)
γ, °	90.0
Volume, $Å^3$	438.48(5)
Z	2
Density (calc), Mg/m^3	2.006
Abs. coefficient, mm^{-1}	1.768
F(000)	258
Crystal size, mm^3	0.380 x 0.320 x 0.200
Theta range, °	3.253 to 27.103°.
Reflections collected	7025
Indpt reflections (R_{int})	1021 (0.0299)
Completeness, %	99.9
Absorption correction	Multi-scan
Max. / min. transmission	0.7461 / 0.5264
Refinement method	F^2
Data /restraints/parameters	1021 / 0 / 76
Goodness-of-fit on F^2	1.235
R1, wR2 [$I>2\sigma(I)$]	0.0304, 0.0895
R1, wR2 (all data)	0.0315, 0.0903
Residual density, $e.Å^{-3}$	0.555 / -0.608

Table B.4.2. Bond lengths [Å] for $[(CO)_5Mn(CF_3)]$ (**8**).

Mn(1)-C(1)	1.858(3)	Mn(1)-C(2)	1.873(2)
Mn(1)-C(3)	1.872(2)	Mn(1)-C(4)	2.067(3)
F(1)-C(4)	1.372(3)	F(2)-C(4)	1.371(2)
O(1)-C(1)	1.134(3)	O(2)-C(2)	1.130(3)
O(3)-C(3)	1.129(3)		

Table B.4.3. Bond angles [°] for $[(CO)_5Mn(CF_3)]$ (**8**).

C(1)-Mn(1)-C(2)	92.00(8)	C(2)-Mn(1)-C(2)#1	89.99(13)
C(1)-Mn(1)-C(3)	92.05(8)	C(3)-Mn(1)-C(4)	88.35(8)
C(3)#1-Mn(1)-C(3)	87.36(13)	C(2)-Mn(1)-C(4)	87.61(8)
C(3)#1-Mn(1)-C(2)	91.19(9)	C(1)-Mn(1)-C(4)	179.45(11)
C(3)-Mn(1)-C(2)	175.74(8)	O(1)-C(1)-Mn(1)	179.8(2)
O(2)-C(2)-Mn(1)	179.50(19)	O(3)-C(3)-Mn(1)	177.62(19)
F(2)-C(4)-F(2)#1	103.0(2)	F(2)-C(4)-Mn(1)	115.68(13)
F(2)-C(4)-F(1)	102.88(15)	F(1)-C(4)-Mn(1)	114.88(17)
C(1)-Mn(1)-C(2)	92.00(8)	C(2)-Mn(1)-C(2)#1	89.99(13)

Symmetry transformations used to generate equivalent atoms: #1 x,-y+1/2,z

B.5. Compound $[Mn(CO)_5(CHF_2)]$, **9**

Table B.5.1. Crystal data and structure refinement for compound $[Mn(CO)_5(CHF_2)]$ (**9**).

Empirical formula	$C_6HF_2MnO_5$
Formula weight	246.01
Temperature, K	173(2)
Wavelength, Å	0.71073
Crystal system	Orthorhombic
Space group	Pnma
a, Å	12.2397(3)
b, Å	10.7284(2)
c, Å	6.29540(10)
α, °	90.0
β, °	90.0
γ, °	90.0
Volume, $Å^3$	826.66(3)
Z	4
Density (calc), Mg/m^3	1.977
Abs. coefficient, mm^{-1}	1.623
F(000)	480
Crystal size, mm^3	0.37 x 0.32 x 0.2
Theta range, °	3.329 to 26.367
Reflections collected	9162
Indpt reflections (R_{int})	890 (0.0733)
Completeness, %	99.8
Absorption correction	Multi-scan
Max. / min. transmission	0.7457 / 0.6876
Refinement method	F^2
Data /restraints/parameters	890 / 0 / 88
Goodness-of-fit on F^2	1.145
R1, wR2 [$I>2\sigma(I)$]	0.0248, 0.0667
R1, wR2 (all data)	0.0254, 0.0674
Residual density, $e.Å^{-3}$	0.516 / -0.582

Table B.5.2. Bond lengths [Å] for compound [$(CO)_5Mn(CHF_2)$] (**9**).

Mn(1)-C(1)	1.861(2)	Mn(1)-C(2)	1.853(3)
Mn(1)-C(3)	1.859(3)	Mn(1)-C(4)	1.971(2)
F(11)-C(4)	1.372(3)	F(12)-C(4)	1.391(3)
O(1)-C(1)	1.134(3)	O(2)-C(2)	1.126(4)
O(3)-C(3)	1.136(4)	O(4)-C(4)	1.062(4)

Table B.5.3. Bond angles [°] for compound [$(CO)_5Mn(CHF_2)$] (**9**).

C(2)-Mn(1)-C(3)	174.60(12)	C(1)#1-Mn(1)-C(4)#1	176.94(8)
C(2)-Mn(1)-C(1)	91.29(9)	C(1)-Mn(1)-C(4)#1	90.16(9)
C(3)-Mn(1)-C(1)	92.44(8)	C(2)-Mn(1)-C(4)	87.98(9)
C(1)#1-Mn(1)-C(1)	92.83(12)	C(3)-Mn(1)-C(4)	88.10(9)
C(1)-Mn(1)-C(4)	176.94(8)	C(4)#1-Mn(1)-C(4)	86.84(12)
O(1)-C(1)-Mn(1)	178.71(18)	O(3)-C(3)-Mn(1)	176.3(2)
O(2)-C(2)-Mn(1)	180.0(3)	O(4)-C(4)-Mn(1)	170.7(3)
F(11)-C(4)-Mn(1)	118.96(18)	F(12)-C(4)-Mn(1)	118.02(18)
F(11)-C(4)-F(12)	104.1(2)		

Symmetry transformations used to generate equivalent atoms: #1 x,-y+1/2,z

B.6. Compound $[Mn(CO)_5(CH_2CF_3)]$, **10**

Table B.6.1. Crystal data and structure refinement for compound $[Mn(CO)_5(CH_2CF_3)]$ (**10**).

Empirical formula	$C_7H_2F_3MnO_5$
Formula weight	278.03
Temperature, K	173(2)
Wavelength, Å	0.71073
Crystal system	Monoclinic
Space group	$P2_1/n$
a, Å	11.6543(7)
b, Å	6.8405(4)
c, Å	24.2843(14)
α, °	90.0
β, °	96.288(5)
γ, °	90.0
Volume, $Å^3$	1924.3(2)
Z	8
Density (calc), Mg/m^3	1.919
Abs. coefficient, mm^{-1}	1.421
F(000)	1088
Crystal size, mm^3	0.500 x 0.250 x 0.130
Theta range, °	3.095 to 26.372
Reflections collected	10468
Indpt reflections (R_{int})	3934 (0.0232)
Completeness, %	99.4
Absorption correction	Multi-scan
Max. / min. transmission	1.0 / 0.787
Refinement method	F^2
Data /restraints/parameters	3934 / 0 / 289
Goodness-of-fit on F^2	1.092
R1, wR2 [$I>2\sigma(I)$]	0.0279, 0.0630
R1, wR2 (all data)	0.0341, 0.0662
Residual density, $e.Å^{-3}$	0.323 / -0.279

Table B.6.2. Bond lengths [Å] for compound $[(CO)_5Mn(CH_2CF_3)]$ (**10**).

Molecule A		Molecule B	
Mn(1)-C(12)	1.834(2)	Mn(2)-C(22)	1.842(2)
Mn(1)-C(14)	1.860(2)	Mn(2)-C(24)	1.865(2)
Mn(1)-C(15)	1.869(2)	Mn(2)-C(25)	1.868(2)
Mn(1)-C(16)	1.870(2)	Mn(2)-C(23)	1.869(2)
Mn(1)-C(13)	1.871(2)	Mn(2)-C(26)	1.870(2)
Mn(1)-C(11)	2.167(2)	Mn(2)-C(21)	2.162(2)
F(11)-C(111)	1.349(2)	F(21)-C(211)	1.348(3)
F(12)-C(111)	1.354(2)	F(22)-C(211)	1.356(3)
F(13)-C(111)	1.353(2)	F(23)-C(211)	1.357(2)
O(12)-C(12)	1.138(2)	O(22)-C(22)	1.137(2)
O(13)-C(13)	1.129(2)	O(23)-C(23)	1.131(2)
O(14)-C(14)	1.136(2)	O(24)-C(24)	1.135(2)
O(15)-C(15)	1.130(2)	O(25)-C(25)	1.127(2)
O(16)-C(16)	1.131(2)	O(26)-C(26)	1.133(2)
C(11)-C(111)	1.469(3)	C(21)-C(211)	1.478(3)

Table B.6.3. Bond angles [°] for $[(CO)_5Mn(CH_2CF_3)]$ (**10**).

C(12)-Mn(1)-C(14)	90.79(8)	C(22)-Mn(2)-C(24)	94.16(8)
C(12)-Mn(1)-C(15)	92.90(9)	C(22)-Mn(2)-C(25)	91.83(9)
C(14)-Mn(1)-C(15)	88.88(8)	C(24)-Mn(2)-C(25)	89.06(8)
C(12)-Mn(1)-C(16)	93.75(9)	C(22)-Mn(2)-C(23)	93.39(8)
C(14)-Mn(1)-C(16)	89.88(8)	C(24)-Mn(2)-C(23)	172.44(8)
C(15)-Mn(1)-C(16)	173.25(9)	C(25)-Mn(2)-C(23)	91.02(8)
C(12)-Mn(1)-C(13)	91.58(9)	C(22)-Mn(2)-C(26)	91.59(9)
C(14)-Mn(1)-C(13)	177.50(9)	C(24)-Mn(2)-C(26)	89.78(8)
C(15)-Mn(1)-C(13)	90.19(9)	C(25)-Mn(2)-C(26)	176.46(9)
C(16)-Mn(1)-C(13)	90.78(8)	C(23)-Mn(2)-C(26)	89.70(8)
C(12)-Mn(1)-C(11)	176.25(8)	C(22)-Mn(2)-C(21)	175.28(9)
C(14)-Mn(1)-C(11)	92.90(8)	C(24)-Mn(2)-C(21)	86.25(8)
C(15)-Mn(1)-C(11)	86.53(8)	C(25)-Mn(2)-C(21)	83.48(8)
C(16)-Mn(1)-C(11)	86.91(8)	C(23)-Mn(2)-C(21)	86.24(8)
C(13)-Mn(1)-C(11)	84.72(8)	C(26)-Mn(2)-C(21)	93.11(9)
C(111)-C(11)-Mn(1)	118.63(13)	C(211)-C(21)-Mn(2)	118.53(14)
O(12)-C(12)-Mn(1)	179.6(2)	O(22)-C(22)-Mn(2)	179.06(19)
O(13)-C(13)-Mn(1)	179.5(2)	O(23)-C(23)-Mn(2)	179.05(19)
O(14)-C(14)-Mn(1)	177.51(17)	O(24)-C(24)-Mn(2)	178.06(18)
O(15)-C(15)-Mn(1)	178.8(2)	O(25)-C(25)-Mn(2)	178.16(18)
O(16)-C(16)-Mn(1)	178.93(17)	O(26)-C(26)-Mn(2)	178.3(2)
F(11)-C(111)-F(13)	104.46(15)	F(21)-C(211)-F(22)	105.23(18)
F(11)-C(111)-F(12)	105.56(15)	F(21)-C(211)-F(23)	105.24(18)
F(13)-C(111)-F(12)	104.47(16)	F(22)-C(211)-F(23)	104.93(18)
F(11)-C(111)-C(11)	113.83(17)	F(21)-C(211)-C(21)	113.99(19)
F(13)-C(111)-C(11)	113.71(16)	F(22)-C(211)-C(21)	113.24(18)
F(12)-C(111)-C(11)	113.82(17)	F(23)-C(211)-C(21)	113.32(18)

B.7. Compound $[Mn(CO)_5(SCOCF_2CH_3)]$, **12**

Table B.7.1. Crystal data and structure refinement for compound $[Mn(CO)_5(SCOCF_2CH_3)]$ (**12**).

Empirical formula	$C_8H_3F2MnO_6S$
Formula weight	320.10
Temperature, K	173(2) K
Wavelength, Å	0.71073 Å
Crystal system	Monoclinic
Space group	P 21/c
a, Å	6.3503(4) Å
b, Å	14.9583(9) Å
c, Å	12.3127(9) Å
α, °	90.0
β, °	97.149(3)
γ, °	90.0
Volume, $Å^3$	1160.49(13)
Z	4
Density (calc), Mg/m^3	1.832
Abs. coefficient, mm^{-1}	1.359
F(000)	632
Crystal size, mm^3	0.4 x 0.26 x 0.05
Theta range, °	2.723 to 29.130
Reflections collected	50232
Indpt reflections (R_{int})	3131 (0.0466)
Completeness, %	100.0 %
Absorption correction	Semi-empirical from equivalents
Max. / min. transmission	0.7462 / 0.6211
Refinement method	Full-matrix least-squares on F2
Data /restraints/parameters	3131 / 0 / 164
Goodness-of-fit on F^2	1.063
R1, wR2 [$I>2\sigma(I)$]	0.0346, 0.0852
R1, wR2 (all data)	0.0431, 0.0908
Residual density, $e.Å^{-3}$	1.206 / -0.764

Table B.7.2. Bond lengths [Å] for compound $[Mn(CO)_5(SCOCF_2CH_3)]$ (**12**).

Mn(1)-C(11)	1.836(2)	Mn(1)-C(12)	1.883(2)
Mn(1)-C(13)	1.873(2)	Mn(1)-C(14)	1.866(2)
Mn(1)-C(15)	1.886(2)	Mn(1)-S(1)	2.3772(6)
F(1)-C(2)	1.326(3)	F(2)-C(2)	1.380(3)
S(1)-C(1)	1.725(2)	O(2)-C(1)	1.209(3)
C(1)-C(2)	1.546(3)	C(2)-C(22)	1.460(4)
O(11)-C(11)	1.132(3)	O(12)-C(12)	1.124(3)
O(13)-C(13)	1.125(3)	O(14)-C(14)	1.125(3)
O(15)-C(15)	1.120(3)		

Table B.7.3. Bond angles [°] for $[Mn(CO)_5(SCOCF_2CH_3)]$ (**12**).

C(11)-Mn(1)-C(12)	91.05(9)	C(11)-Mn(1)-C(14)	90.44(10)
C(11)-Mn(1)-C(13)	90.72(9)	C(11)-Mn(1)-C(15)	94.27(9)
C(13)-Mn(1)-C(12)	91.08(10)	C(14)-Mn(1)-C(12)	177.58(10)
C(12)-Mn(1)-C(15)	88.01(9)	C(14)-Mn(1)-C(13)	90.81(10)
C(13)-Mn(1)-C(15)	174.93(9)	C(14)-Mn(1)-C(15)	89.97(10)
C(11)-Mn(1)-S(1)	176.47(7)	C(12)-Mn(1)-S(1)	92.47(7)
C(13)-Mn(1)-S(1)	88.90(7)	C(14)-Mn(1)-S(1)	86.06(7)
C(15)-Mn(1)-S(1)	86.16(7)	C(1)-S(1)-Mn(1)	106.25(8)
O(11)-C(11)-Mn(1)	176.7(2)	O(12)-C(12)-Mn(1)	175.7(2)
O(13)-C(13)-Mn(1)	178.0(2)	O(14)-C(14)-Mn(1)	179.2(2)
O(15)-C(15)-Mn(1)	177.4(2)	O(2)-C(1)-C(2)	117.0(2)
C(2)-C(1)-S(1)	116.08(17)	O(2)-C(1)-S(1)	126.91(17)
F(1)-C(2)-F(2)	104.7(3)	F(1)-C(2)-C(1)	110.8(2)
F(1)-C(2)-C(22)	112.2(3)	F(2)-C(2)-C(1)	107.0(2)
F(2)-C(2)-C(22)	107.4(3)	C(22)-C(2)-C(1)	114.0(2)

C. DFT investigation of the homolytic cleavage and the side

All attempts to locate a transition state $\mathbf{TS_{GD}}$ (or related intermediate) led to expulsion of $SiFH_3$ and optimization of a local minimum corresponding to the oxacyclopropyl derivative **I** (Scheme S.B1), a 16-electron species characterized by an α-agostic interaction. A rotamer of this complex where the open coordination site is stabilized by donation from an F lone pair (**J**) is found at slightly lower energy (see Figure S.B1). Starting from either **I** or **J**, relaxed scans along the H···C distance, leading to complex $[(CO)_4Mn(COCHF_2)]$ (**E**), yielded geometries with energy > 50 kcal/mol from **A**, excluding this as the operating the H/F exchange pathway.

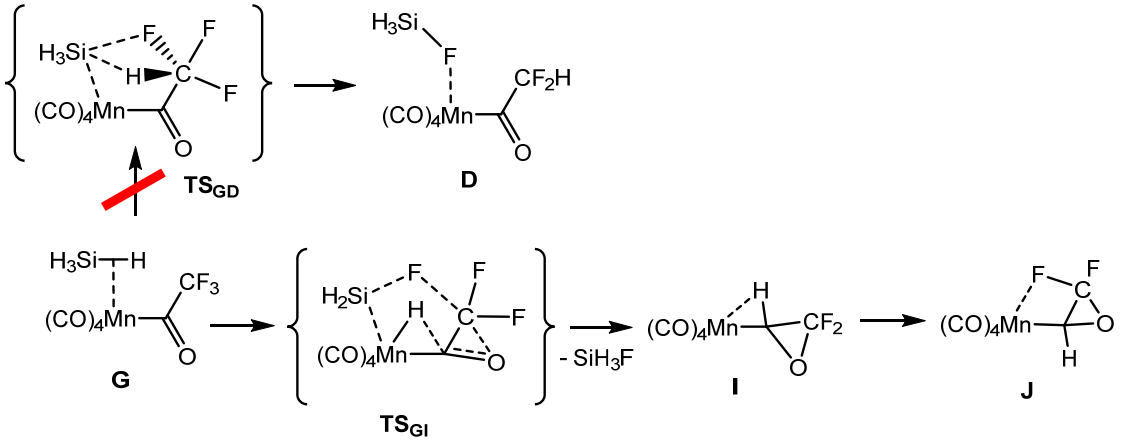

Scheme C.1. Pathway leading from intermediate **G** to the oxacyclopropyl derivatives **I** and **J**.

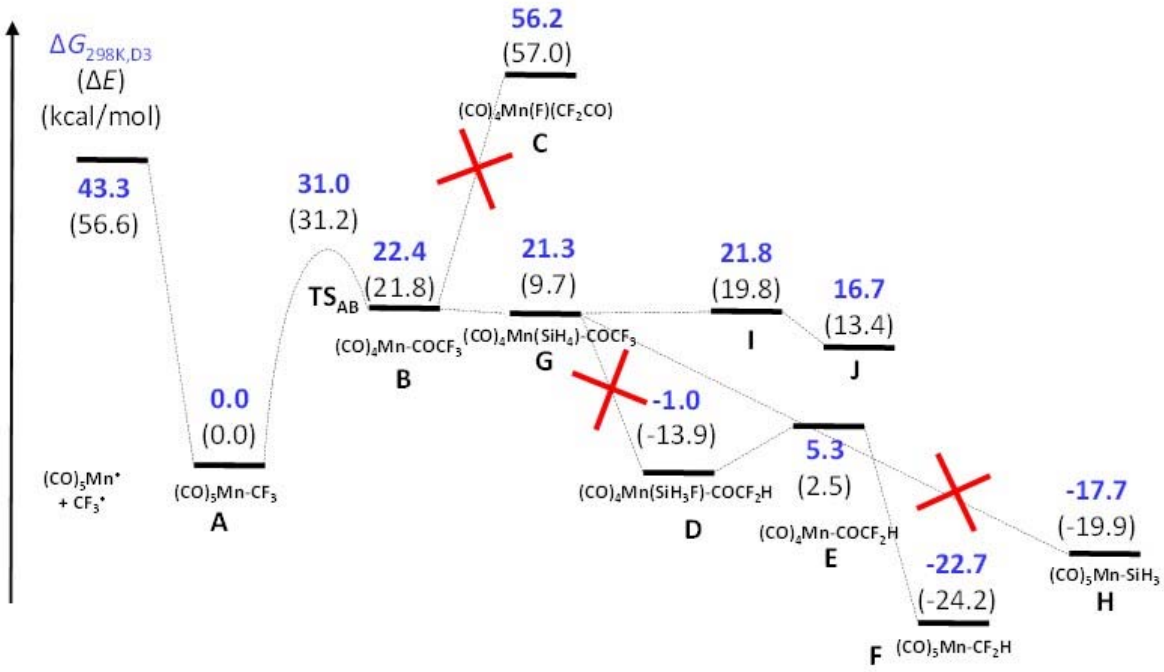

Figure C.1. Energy profile (relative D3-corrected G_{298} values as bold blue figures and electronic energy values in parentheses, in kcal/mol) for the pathways illustrated in Schemes 3 (Chapter 4) and C.1.

A relaxed scan, starting from structure **G**, on the H···C, in search for an alternative pathway of CHF_3 formation, gave the result shown in Figure C.2.

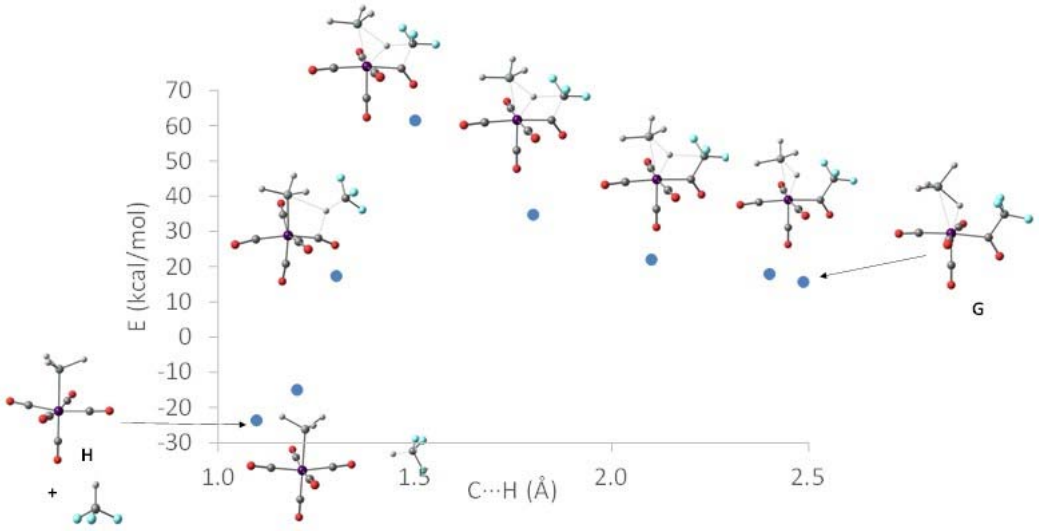

Figure C.2. Relaxed scan on the H···C coordinate, leading from **G** to the combination of **H** and CHF_3. Energies are reported relative to **A** + SiH_4.

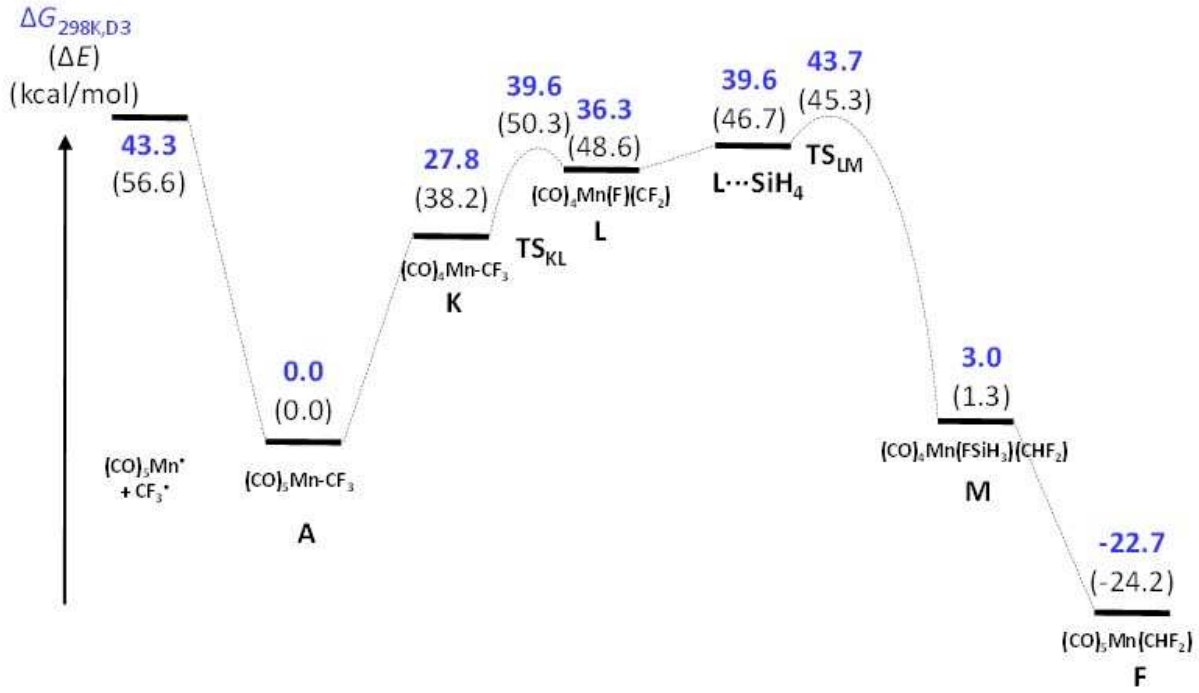

Figure C.3. Energy profile (relative D3-corrected G_{298} values as bold blue figures and electronic energy values in parentheses, in kcal/mol) for the H/F scrambling pathway illustrated in Chapter 4 Scheme 6.

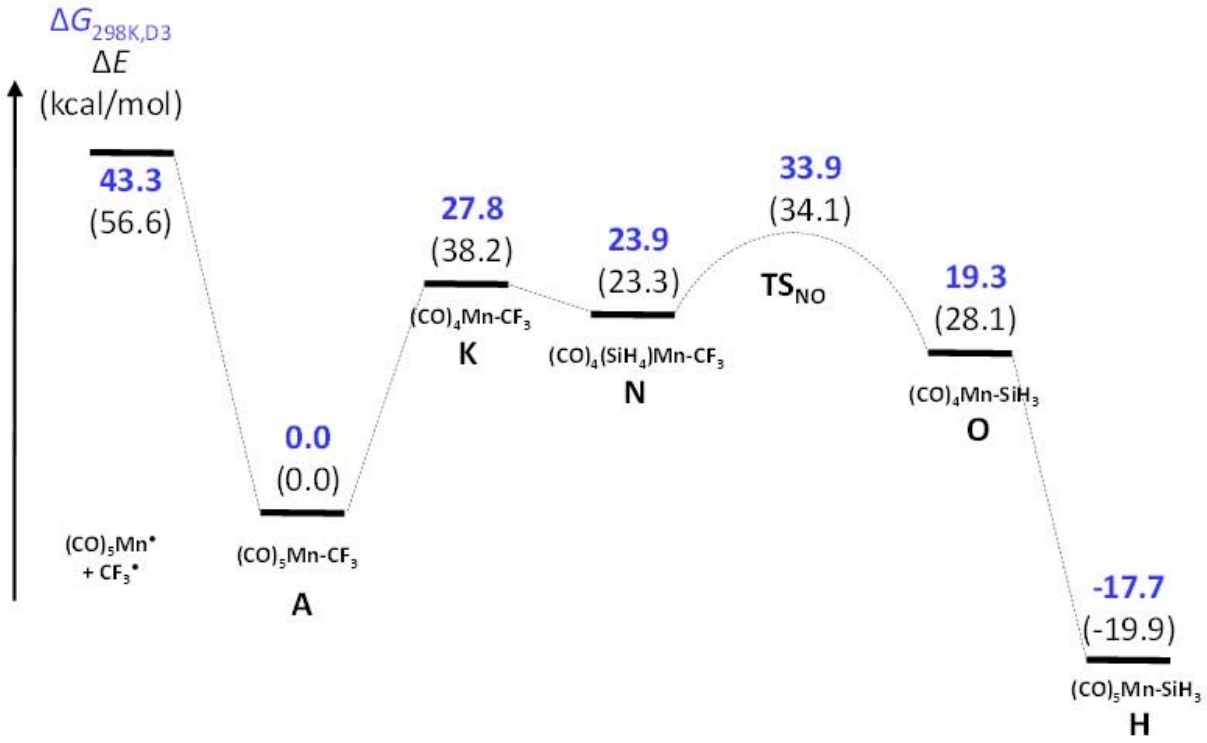

Figure C.4. Energy profile (relative D3-corrected G_{298} values as bold blue figures and electronic energy values in parentheses, in kcal/mol) for the CHF_3 formation pathway shown in Chapter 4 Scheme 6.

Table C.1. Calculated D3-corrected *H* and *G* data for key molecules and fragments related to the homolytic Mn-R_F bond cleavage and silane-assisted R_FH formation at 298 and 373K.

System	H_{298} (hartrees)	H_{373} (hartrees)	G_{298} (hartrees)	G_{373} (hartrees)
$CF_3^\bullet$	-337.257701	-337.255986	-337.285810	-337.2937907
$CHF_2^\bullet$	-238.083033	-238.0815921	-238.109111	-238.116555
$CH_2CF_3^\bullet$	-376.515939	-376.5131423	-376.547919	-376.5569764
$[(CO)_5Mn^\bullet]$	-670.485416	-670.4796461	-670.535262	-670.5491023
$[(CO)_5Mn(CF_3)]$	-1007.830866	-1007.822981	-1007.890037	-1007.906424
$[(CO)_5Mn(CHF_2)]$	-908.644980	-908.6374875	-908.703306	-908.7194436
$[(CO)_5Mn(CH_2CF_3)]$	-1047.081880	-1047.073275	-1047.143540	-1047.160621
CO	-113.188767	-113.1878236	-113.208203	-113.2139319
SiH_4	-291.709512	-291.707999	-291.732104	-291.738679
TS_{NO} **($R_F = CF_3$)**	-1186.299261	-1186.290771	-1186.359984	-1186.376819
TS_{NO} **($R_F = CHF_2$)**	-1087.118729	-1087.110629	-1087.177297	-1087.193552
TS_{NO} **($R_F = CH_2CF_3$)**	-1225.560842	-1225.551627	-1225.623792	-1225.641253

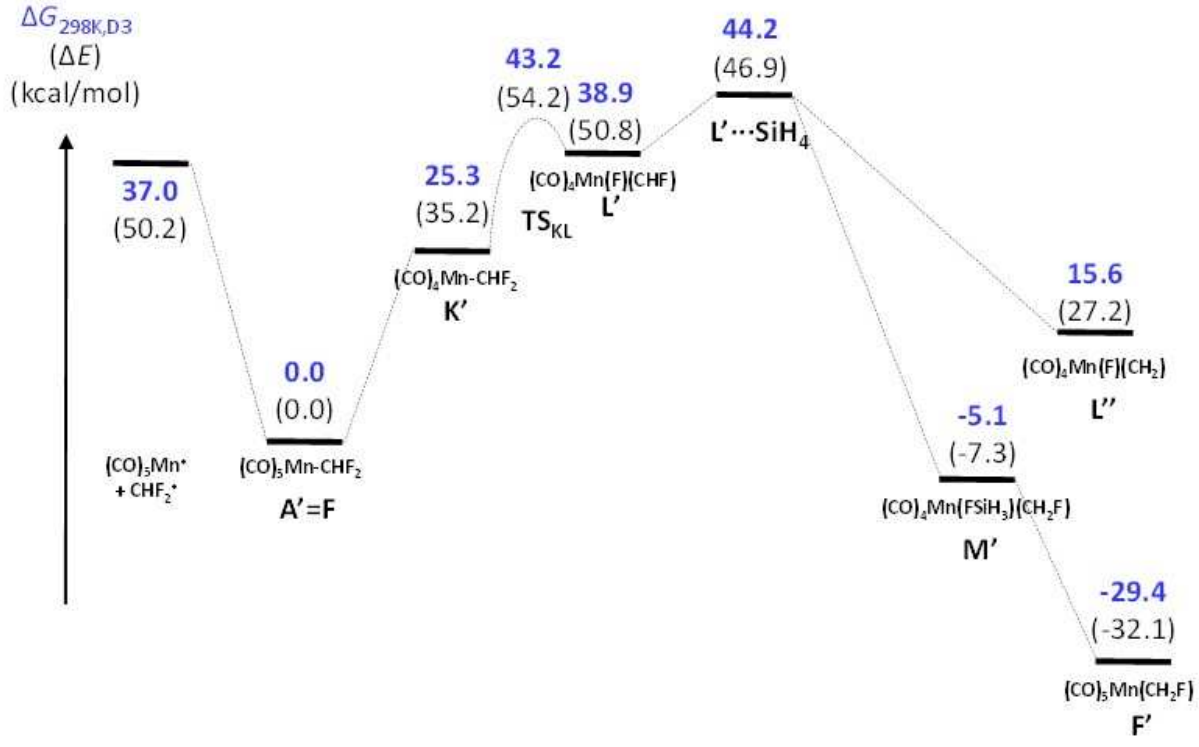

Figure C.5. Energy profile (relative D3-corrected G_{298} values as bold blue figures and electronic energy values in parentheses, in kcal/mol) for the H/F scrambling pathway illustrated in Chapter 4 Scheme 7.

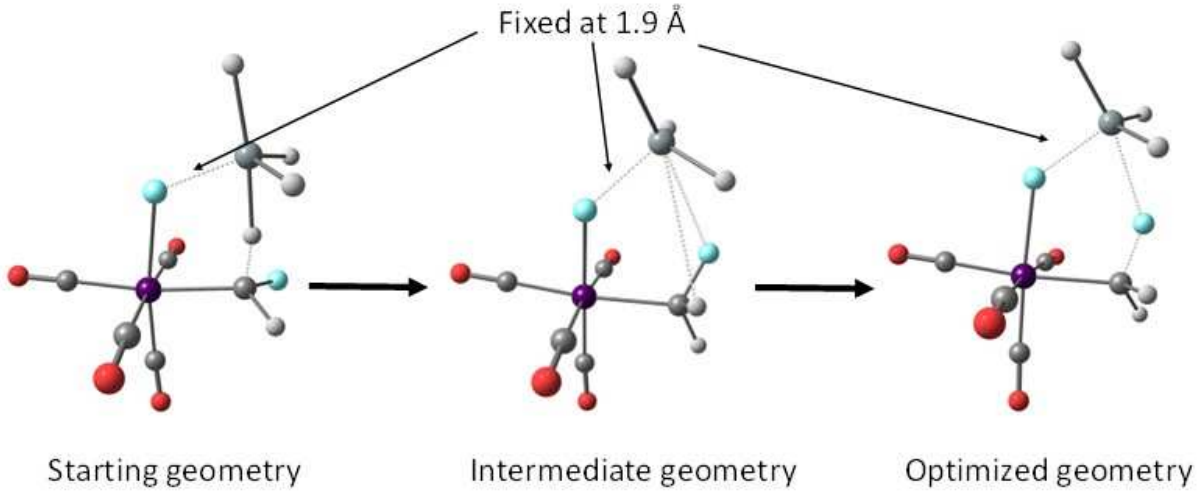

Figure C.6. Result of one partial optimization, searching for **$TS_{K'L'}$**, with the Si···F distance fixed at 1.9 Å, showing the tendency of Si in SiH_4 to abstract the F on the alkylidene rather than the F on the Mn atom.

Table C.2. Calculated D3-corrected *H* and *G* data for key molecules and fragments related to the H/F exchange pathway for compounds **8** and **9** at 298 and 373K. [a]

System	H_{298} (hartrees)	H_{373} (hartrees)	G_{298} (hartrees)	G_{373} (hartrees)
TS_{LM} **(8)**	-1186.282055	-1186.273425	-1186.344245	-1186.361463
L'···SiH_4 **(9)**	-1087.093172	-1087.084578	-1087.156826	-1087.174408

[a] For the relevant data of compounds **8**, **9**, CO and SiH_4, see Table C.1.

RESUME

Les polymères fluorés sont des matériaux possédant des propriétés remarquables, ce qui donne lieu à des nombreuses applications. Cependant, même si la polymérisation radicalaire contrôlée (PRC ou RDRP) a connu un grand développement dès le milieu des années 90, l'obtention de polymères de taille et de structure bien définies pour certains monomères fluorés reste encore un réel défi. C'est le cas du fluorure de vinylidène (VDF), $H_2C=CF_2$, qui lors de la polymérisation radicalaire peut conduire à une addition normale (tête-queue) ou des additions inverses (tête-tête et queue-queue). Ces défauts d'enchainement provoquent la formation d'espèces dormantes peu réactives lors d'une PRC. Ceci entraine l'accumulation de chaînes dormantes difficiles à réactiver qui conduit à une perte de contrôle et à l'augmentation de la polymolécularité. Des études récentes ont montré que l'utilisation de complexes organométalliques peut minimiser ce problème en rééquilibrant les énergies nécessaires pour réactiver les deux différentes chaînes dormantes. D'autre part, des calculs théoriques ont montré que les complexes de manganèse pentacarbonyle alkyle et fluoroalkyle, $[Mn(CO)_5R]$ et $[Mn(CO)_5R_F]$ respectivement, peuvent former des espèces dormantes normales et inverses dont les énergies d'activation sont proches. Ceci pourrait entrainer un certain degré de contrôle de la polymérisation. Dans cette étude, plusieurs complexes de manganèse du type $[Mn(CO)_5R]$ et $[Mn(CO)_5R_F]$ (R = $CH(CH_3)(COOCH_3)$, $CH(CH_3)(OCOCH_3)$ et $CH(CH_3)(C_6H_5)$; R_F = CF_3, CHF_2, CH_2CF_3 et CF_2CH_3) ont été synthétisés et parfaitement caractérisés, puis ont été utilisés comme amorceurs de polymérisation de divers monomères et comme modèles de bouts de chaîne en PRC par des complexes organométalliques (OMRP). Pour cela, des mesures expérimentales de l'enthalpie de dissociation homolytique de la liaison Mn-C ont été réalisées par des méthodes cinétiques. De plus, une étude plus approfondie sur la formation de certains sous-produits lors de la décomposition thermique de complexes de manganèse fluoroalkyle en présence du tris(trimethylsilyl)silane en tant que piégeur de radicaux a été réalisée et soutenue par des calculs théoriques. Ces complexes ont également été testés en polymérisation du VDF et d'autres monomères non-fluorés.

Mots clés : chimie organométallique · complexes de manganèse · fluorure de vinylidene · polymérisation radicalaire contrôlée · réactivité radicalaire

SUMMARY

Fluoropolymers are materials characterized by remarkable properties and are involved in many applications. However, although controlled radical polymerization (CRP or RDRP) has been extraordinarily developed since the mid-90s, synthesizing well-defined polymers of certain fluorinated monomers still remains a crucial challenge. This is the case of vinylidene fluoride (VDF), $H_2C=CF_2$, which under radical polymerization can undergo normal additions (head to tail) or reverse additions (head to head and tail to tail). These chain defects cause the formation of less reactive dormant species during a CRP. This favors an accumulation of less reactive dormant chains and leads to a loss of the control as well as to an increase of the dispersity. Recent studies have concluded that the use of organometallic complexes can minimize this problem by equilibrating the energies needed to reactivate both types of dormant chains. On the other hand, theoretical calculations have shown that alkyl and fluoroalkyl manganese pentacarbonyl complexes, $[Mn(CO)_5R]$ and $[Mn(CO)_5R_F]$ respectively, are able to lead to normal and inverse dormant species with a similar activation energy. This could afford some degree of controlled polymerization. In this study, several manganese complexes ($[Mn(CO)_5R]$ and $[Mn(CO)_5R_F]$, where R = $CH(CH_3)(COOCH_3)$, $CH(CH_3)(OCOCH_3)$ and $CH(CH_3)(C_6H_5)$; R_F = CF_3, CHF_2, CH_2CF_3 and CF_2CH_3) have been synthesized and fully characterized. They were then used as original initiators for the polymerization of various monomers and as chain-end models in CRP mediated by organometallic complexes (OMRP). Experimental measurements of the dissociation enthalpy of the Mn-C bond were carried out by kinetic methods. In addition, a deeper study of the formation of certain by-products during the thermal decomposition of the fluoroalkylpentacarbonylmanganese(I) complexes in the presence of tris(trimethylsilyl)silane as a radical trap was carried out and supported by theoretical calculations. These complexes were also tested in the polymerization of VDF and of other non-fluorinated monomers.

Keywords: controlled radical polymerization · manganese complexes · organometallic chemistry · radical reactivity · vinylidene fluoride